METAL ION RELEASE AND SIGNALING IN MOLECULAR LOGIC GATE DESIGN

A DISSERTATION SUBMITTED TO

THE GRADUATE SCHOOL OF ENGINEERING AND SCIENCE

OF BILKENT UNIVERSITY

IN PARTIAL FULFILLMENT OF THE REQUIREMENTS FOR

THE DEGREE OF

DOCTOR OF PHILOSOPHY

IN

MATERIALS SCIENCE AND NANOTECHNOLOGY

By

TAHA BİLAL UYAR

October, 2016

METAL ION RELEASE AND SIGNALING IN MOLECULAR LOGIC GATE DESIGN

By Taha Bilal Uyar

October, 2016

We certify that we have read this dissertation and that in our opinion it is fully adequate, in scope and in quality, as a thesis of the degree of Doctor of Philosophy.

Engin Umut Akkaya (Principal Advisor)

Dönüş Tuncel

Salih Özçubukçu

Bilge Baytekin

Emrullah Görkem Günbaş

Approved for the Graduate School of Engineering and Science:

Ezhan Karaşan
Director of the Graduate School

ABSTRACT

METAL ION RELEASE AND SIGNALING IN MOLECULAR LOGIC GATE DESIGN

Taha Bilal Uyar
Ph.D. in Materials Science and Nanotechnology
Supervisor: Engin Umut Akkaya
October, 2016

Mimicking the biological structures is one of the main goals of the natural sciences, because processes are well-organized in nature despite its amazing complexity. On account of this, releasing metal ions at molecular level is a crucial topic owing to similar process in living organisms. In this thesis, we designed novel cage compounds for this purpose. Our novel cage molecule is activated with near-IR light while almost all of the cage compounds in the previous literature function in the UV region. Consequently, it is appropriate for using in biological systems. Release of zinc ions that has critical roles in human body successfully achieved by our novel compound in Part 2 of the thesis work.

Molecular logic concept is one of the promising areas of chemistry. Today, electronic devices consists of silicon based circuits that process information by using binary logic. Molecular logic offers alternative for silicon based devices. Using molecules to process data is a promising idea in the fields from electronics to biotechnology. In part 3, we proposed AND gate whose inputs are pH and glutathione while the response is singlet oxygen which can be used to destroy cancer cells. It is possible to process much complicated information by combining more than one logic gate. In first part of the thesis study, we designed modular molecular logic gates by cascading of three logic gates via metal ion signals.

In the last part, a fluorescent chemosensor was proposed for dopamine molecule, which is crucial in a number of biological processes at the human body.

Keywords: molecular logic gate, cage compounds, fluorescence, glutathione, photosensitizer, metal ion release, BODIPY, dopamine.

ÖZET

METAL İYONU SALIMI ve MOLEKÜLER MANTIK DEVRELERİNDE SİNYALİZASYON

Taha Bilal Uyar
Malzeme Bilimi ve Nanoteknoloji, Doktora
Tez Danışmanı: Engin Umut Akkaya
Ekim, 2016

Biyolojik yapıların taklit edilmesi doğa bilimlerinin temel hedeflerinden bir tanesidir çünkü doğanın inanılmaz karmaşık yapısına rağmen çok düzenli bir işleyişi vardır. Bundan dolayı, canlı sistemlerde de gerçekleşen metal iyonu salımının moleküler seviyede gerçekleştirilmesi çok önemli bir konudur. Bu tezde, biz de bu amaca yönelik yeni kafes bileşikler tasarladık. Literatürdeki hemen hemen tüm kafes bileşikleri UV bölgesinde çalışıyorken, bizim yeni tasarladığımız kafes molekülü yakın IR ışığıyla aktif hale geliyor. Bu sebeple de biyolojik sistemlerde kullanımı uygundur. 2. Bölümde, insan vücudunda kritik rollerde bulunan çinko iyonunun salımı bizim yeni molekülümüzle başarılı bir şekilde gerçekleştirildi.

Moleküler mantık devreleri kimyanın gelecek vadeden alanlarından bir tanesidir. Günümüzde, elektronik cihazlar ikili sisteme göre işlem yapan silikon bazlı devrelerden oluşurlar. Moleküler mantık kapıları, fiziksel ve teknolojik bariyerlerden dolayı gelişiminin neredeyse sonuna gelmiş olan silikon bazlı cihazlara bir alternatif sunmaktadır. Elektronik alanından biyoteknolojiye kadar, bilgiyi işlemek için moleküllerin kullanılması ilham verici bir fikirdir. 3. Bölümde, pH ve glutatyon girdileriyle kanser hücrelerini yok etmek için kullanılan singlet oksijen üreten bir VE mantık kapısı tasarladık. Birden fazla mantık kapısını birleştirerek çok daha karmaşık işlemler yapmak da mümkündür. Tezin ilk kısmında, üç tane mantık kapısını metal iyonu vasıtasıyla birleştirerek modüler bir moleküler mantık kapsısı tasarladık.

Son kısımda ise insan vücudundaki birçok biyolojik olayda çok kritik öneme sahip olan dopamin molekülü için bir floresans kemosensör tasarlandı.

Anahtar kelimeler: moleküler mantık kapısı, kafes bileşikler, floresans, glutatyon, ışık duyarlandırıcı, metal iyonu salımı, BODIPY, dopamin.

ACKNOWLEDGEMENT

I would like to express my hearty gratitude to my supervisor Engin Umut Akkaya for his deep insight, intense knowledge and support throughout my graduate studies. I am also grateful to him for teaching us how to become a good scientist. I will never forget his support throughout my life.

I am sincerely grateful to Ruslan Guliyev, Ahmet Atılgan, Sündüs Erbaş-Çakmak, Tuğba Özdemir-Kütük Yusuf Çakmak, Safacan Kölemen, Bilal Kılıç and Nisa Yeşilgül for their patience, great friendship and all their valuable contributions to the projects that we worked on together.

I would like to thank former and present group members of the Akkaya group Özlem Seven, Abdurrahman Türksoy, Seylan Ayan, Deniz Yıldız, Dilek Işık-Taşgın, Cansu Kaya, Serdal Kaya, Ceren Çamur, Darika Okeeva, Esra Tanrıverdi, Fazlı Sözmen, İlke Şimşek-Turan, José Luis Bila, Hale Atılgan, Tuğçe Karataş, Murat Işık, Ziya Köstereli, Onur Büyükçakır and rest of our group for their valuable support and friendship.

I would like to gratefully acknowledge my Thesis Committee Members, Assoc. Prof. Dr. Dönüş Tuncel and Assist. Prof. Dr. Salih Özçubukçu for their encouraging and fruitful discussions and advices for four years. Also, I would like to thank Assist. Prof. Dr. Bilge Baytekin and Assist. Prof. Görkem Günbaş for participating the dissertation committee.

I would like to thank to TÜBİTAK (The Scientific and Technological Research Council of Turkey) for financial support.

I also would like to thank all members of UNAM for facilities and multidisciplinary research atmospher.

Most importantly, I would like to thank my family for their love, support, and understanding.

LIST OF ABBREVIATIONS

BODIPY	**:**	Boradiazaindacene
AcOH	**:**	Acetic Acid
$CHCl_3$	**:**	Chloroform
DDQ	**:**	Dichlorodicyanoquinone
DMF	**:**	Dimethylformamide
TFA	**:**	Trifluoroacetic Acid
THF	**:**	Tetrahydrofuran
Et_3N	**:**	Triethylamine
TLC	**:**	Thin Layer Chromotography
ICT	**:**	Internal Charge Transfer
PET	**:**	Photoinduced Electron Transfer
ET	**:**	Energy Transfer
FRET	**:**	Förster Resonance Energy Transfer
HOMO	**:**	Highest Occupied Molecular Orbital
LUMO	**:**	Lowest Unoccupied Molecular Orbital
HRMS	**:**	High Resolution Mass Spectroscopy
NMR	**:**	Nuclear Magnetic Resonance

TABLE OF CONTENTS

LIST OF FIGURES

LIST OF TABLES

CHAPTER 1

1. Introduction

1.1. What is Supramolecular Chemistry?

Jean-Marie Lehn won the Nobel Prize in 1987 for his work in young research area, which is called “supramolecular chemistry” [1]. He defined this area as the “chemistry of molecular assemblies and of the intermolecular bond” [2]. In addition, there are some other expressions such as “chemistry beyond the molecule”, “the chemistry of the non-covalent bond” and “non-molecular chemistry”. In the supramolecular chemistry, there are host and guest molecules that stand together by non-covalent interactions that is illustrated in the figure 1 below.

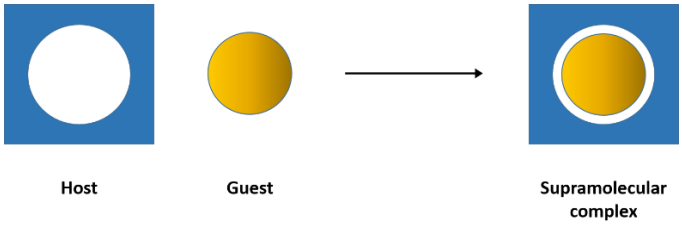

Figure 1. Conformity of host and guest in supramolecular chemistry.

The supramolecular chemistry is relatively young discipline and it has been studied since the late 1960s. However, it began with Emil Fischer almost a hundred years ago. He defined the term “lock and key principle” that explain structural fit of enzyme-substrate long time ago [3]. Then, this ‘structural fit’ has been expressed with this model for long time. This concept is based on molecular recognition that an enzyme interact with only particular substrate. Almost in the same time with Fischer, Alfred Werner conducted his research in coordination chemistry, which stands on also non-covalent interactions [4]. Then in 1937, Wolf described the “übermolecül” term for self-associated carboxylic acid structures by hydrogen bonding [5]. Watson and Crick

solved the double helix structure of DNA in 1953 [6]. In 1967, crown ethers were discovered incidentally by Charles Pederson [7]. First “supramolecular” term is used by Jean-Marie Lehn in the late 1970s: “Just as there is a field of molecular chemistry based on the covalent bond, there is a field of supramolecular chemistry, the chemistry of molecular assemblies and of the intermolecular bond”.

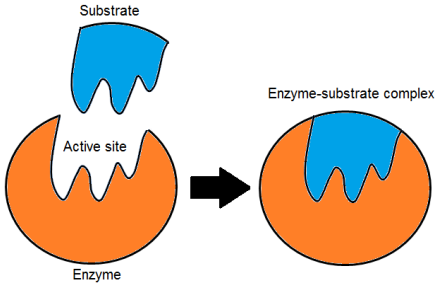

Figure 2. Lock and key model for enzyme-substrate conformity.

Supramolecular chemistry mainly includes two categories, which are host-guest chemistry and self-assembly. The type of structure is determined according to size and shape. In the host-guest chemistry, host molecules are remarkably bigger than guest molecules. In these model, guest molecules are surrounded by host molecules. In the self-assembly model, size of two molecules relatively close to each other [8]. In the nature, there are several examples for both host-guest and self-assembly models. For instance, enzymes and their substrates are example of host-guest complexes. A substrate binds to binding site of an enzyme. A binding site is a region that has proper size, geometry and chemical environment to interact to some specific molecule or ion. It is important concept in the especially in biochemistry. Another example for host-guest interaction is the coordination chemistry. Metal ion is guest for the large ligands that especially macrocyclic compounds. The self-assembly model also has several examples from the nature. Non-covalent interaction, which is hydrogen bond between the chains of DNA is one of the most known examples of self-assembly structure. In the self-assembly structures, there is an equilibrium between two or more species that are building blocks of the main structure. The self-assembly process is usually spontaneous and reversible.

Supramolecular chemistry is used in wide range. Its application areas are catalysis [9], molecular recognition [10], molecular devices [11], light harvesting systems [12], solar cells [13], and molecular logic gates [14]. It is still growing and popularity of supramolecular chemistry is increasing rapidly every day.

1.1.1. Basic Supramolecular Interactions

Supramolecular chemistry is built by non-covalent interactions. Supramolecular structures are hold by these interactions, which are weaker than chemical bonds. The energy in a single bond of these interactions is between 2 kj mol^{-1} to 200 kj mol^{-1} but they are uncommonly has the energy greater than 100 kj mol^{-1}. One of the most significant features of these weak interactions is being reversible, which plays a vital role in the existing of life. These supramolecular interactions are electrostatic interactions, hydrogen bonding, Van der Waals forces, π interactions and hydrophobic effect.

1.1.1.1. Electrostatic Interactions

Electrostatic interactions based on attraction forces between positive and negative charges such as metal ions, polar molecules, etc. Electrostatic interactions split into three categories, which are (i) ion-ion interactions, (ii) ion-dipole interactions, and (iii) dipole-dipole interactions. Ion-ion interaction is the strongest one and it is called ionic bond, which is the one of the chemical bonds. It is non-directional interaction different from the other two electrostatic interactions. Ion-dipole interaction is stronger than dipole-dipole because ion has more charge than polar molecule, which has partial charge only. For example, NaCl solution has ion-dipole interaction that is between polar water molecule and sodium or chloride ions. Dipole-dipole interaction is found between two polar molecules and relatively weak interaction. The example for the dipole-dipole is interaction between acetone molecules.

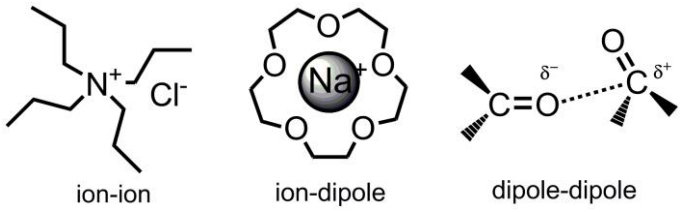

Figure 3. Examples for different types of electrostatic interactions.

1.1.1.2. Hydrogen Bonding

When hydrogen atom binds to electronegative atom with covalent bond, electron of hydrogen withdraw by this atom and hydrogen atom has strong partial positive charge anymore. In this situation, hydrogen atom which is positively charged interacts with other electron rich atoms and that is called hydrogen bonding. For hydrogen bonding, hydrogen atom must covalently connect to most electronegative atoms, which are fluorine, oxygen, and nitrogen. Hydrogen bonding is the strongest intermolecular interaction according to experimental results. For example, HF molecule has higher boiling point than HI molecule, although HI is much heavier. Hydrogen bonding is specific form of dipole-dipole interaction, but it is considerably stronger than others because positively charged hydrogen atom is so small that results much stronger interaction. In the nature, there are many examples for hydrogen bonding in vital part of biological systems. The interaction between the chains of DNA is the one of the most known example. There are two hydrogen bonds between adenine and thymine and three between guanine and cytosine and these hydrogen bonds hold the chains together.

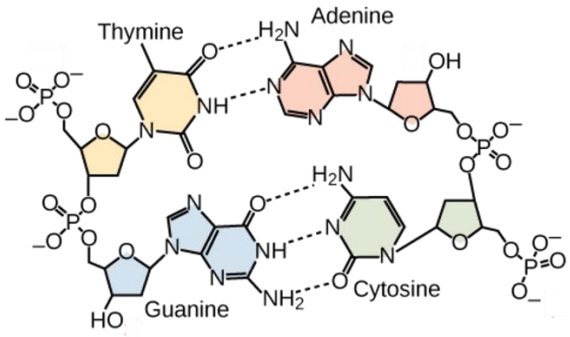

Figure 4. Hydrogen bonding in DNA.

1.1.1.3. Van der Waals Forces

Van der Waals forces are the common name of all of the intermolecular interactions that includes dipole-dipole, dipole-induced dipole, and induced dipole-induced dipole. A molecule which has even no permanent dipole can have instant dipole because of the non-homogeneous distribution of electrons of molecule. That instant dipole causes polarization of neighboring atoms or molecules and that is named London dispersion forces which is weakest intermolecular interaction. All of atoms or molecules have London dispersion forces which is also known as induced dipole-induced dipole interactions. Almost all of hydrocarbons are good example of the molecules which have no polarity so majority of hydrocarbon molecules have only London dispersion forces.

1.1.1.4. Π Interactions

π interactions consist of three main group π- π interaction, cation- π interaction and anion- π interaction. The most known is π- π stacking interaction which is because of the interaction between p orbitals. π- π interaction divided into two types which are face-to-face and edge-to-face interactions. π stacking interactions of nucleobases contribute to stabilizing of DNA double helix structure. Another example is that organic compounds which have aromatic ring are dissolved better in benzene on account of π stacking interactions. Cation- π interactions are very strong as hydrogen bonding as, so it is used for sensing of some cations. Na ion-benzene interaction is example for this interaction.

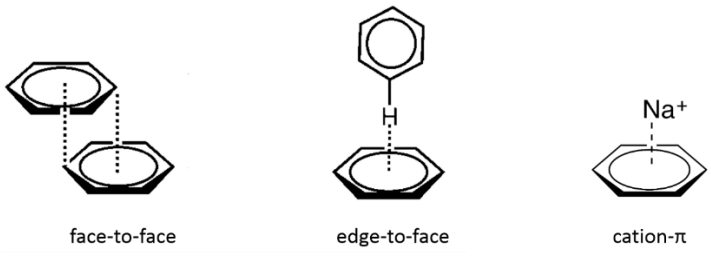

Figure 5. Examples for π- π interactions types.

1.1.1.5. Hydrophobic Effect

Like dissolves like is simple rule in the general chemistry. Polar solvents dissolve in polar compounds and non-polar dissolves non-polar. Non-polar molecules aggregate in polar solvents owing to the desire of decreasing surface of touching area. Hydrophobic effect splits into two type with respect to energy; enthalpic and entropic hydrophobic effects. Hydrophobic effect is used in biochemistry to study some biological facts such as protein folding.

1.2. Luminescence

Mostly, particles are in their ground states at room temperatures. These particles absorb the energy when they are exposed to a radiation. A particle, which is absorbed photon is called excited. Emission of ultraviolet, visible or infrared photons from this excited particle is defined "luminescence". In Latin, lumen means light and 'luminescenz' was used for the first time by Eilhardt Wiedemann in 1888. There are many types of luminescence such as photoluminescence, electroluminescence, chemiluminescence, etc. Photoluminescence is a kind of luminescence and excitation occurs with light. Photoluminescence is composed of fluorescence and phosphorescence which are particular type of luminescence. There are many other de-excitation (returning ground state) pathways for an excited molecule which are internal conversion, energy transfer, excimer formation, intersystem crossing, etc. (Figure 6) [15]. These processes are explained in following paragraph.

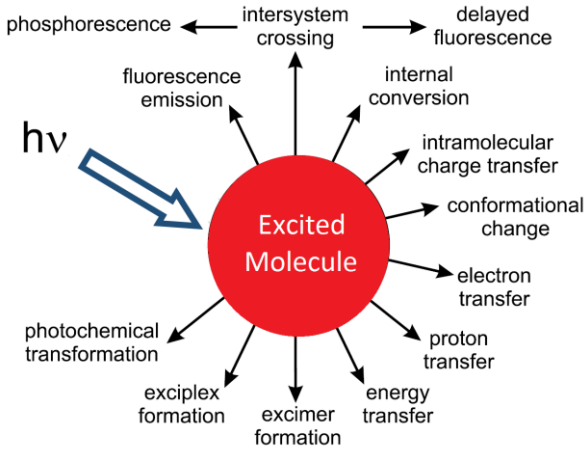

Figure 6. Energy releasing processes of an excited molecule.

The Perrin-Jablonski diagram [16] uses to show absorption and de-excitation processes in simple way. S and T letters represent the singlet and triplet energy states. The difference between them is spin of the electron. Energy levels which are between the singlet or triplet energy states are vibrational levels.

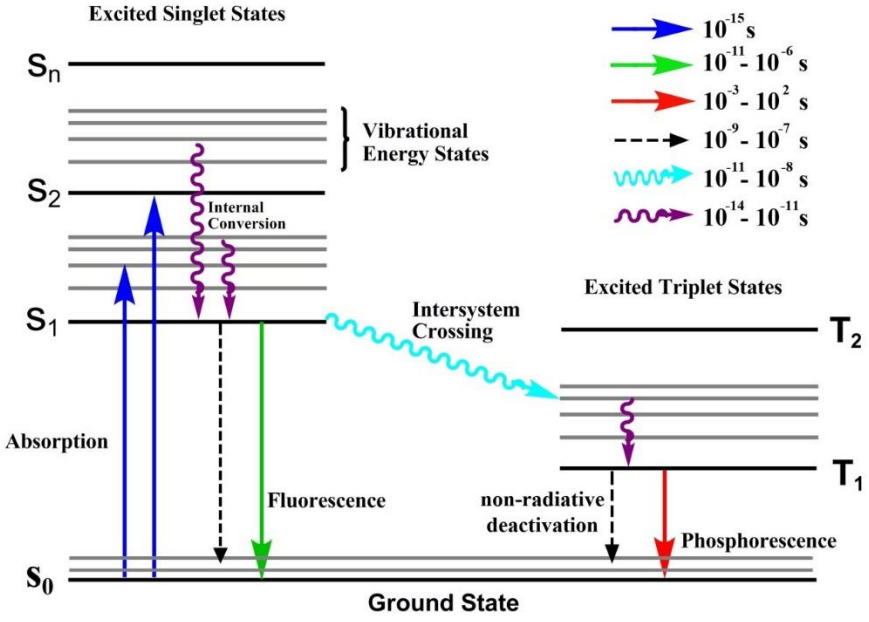

Figure 7. The Perrin-Jablonski diagram.

The first process is absorption, which is the fastest process in the all of them. After the absorption process, the molecule is excited and there are several de-excitation ways to

ground state. Internal conversion is non-radiative vibrational relaxation between vibrational levels, which have same spin multiplicity. It is not efficient way for transition from S_1 to S_0 or T_1 to T_0, so probably fluorescence or phosphorescence can be observed in this situation. Fluorescence is radiative process which electron passes away S_1 to S_0. Actually emission is fast process as much as absorption but some cases that staying in S_1 or other non-radiative processes can be reason for delay. Another way for de-excitation is intersystem crossing which is the transition singlet to triplet energy state. Intersystem crossing is non-radiative process and takes place between the vibrational levels, which have same energy. Although transition between states that have different multiplicity is forbidden, large spin-orbit coupling makes possible this replacement. Phosphorescence, which is radiative way for relaxation is slow transition T_1 to S_0. De-excitation non-radiative relaxation is usually preponderant to phosphorescence due to T_1 to S_0 transition is forbidden. Phosphorescence can be observed mostly in low temperatures.

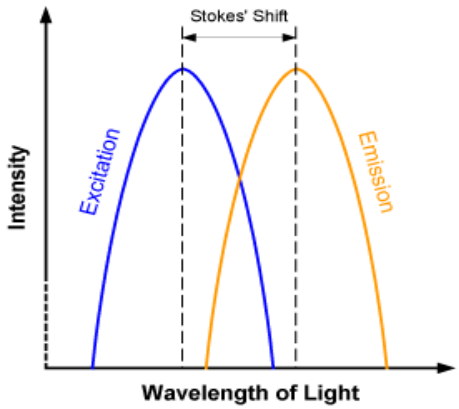

Figure 8. Stokes' shift.

In most cases, absorption and fluorescence wavelengths are different from each other and fluorescence wavelength is the longer one. The reason of this situation is that rapid vibrational relaxation of excited electron to lower energy levels in non-radiative way. The difference between absorption and fluorescence wavelength is named as Stokes' shift [17]. Fluorescence wavelength is independent from the absorption wavelength

because of the reason mentioned above. This cases is called Kasha's Rule [18]. Today, it is known that there are exceptions for Kasha's Rule.

1.3. Fluorescent Dyes

Working principle of fluorescent dyes are completely different from the traditional ones. In traditional dyes, dye absorbs the particular wavelengths of white light then the complementary color left behind is seen. For example, an orange dye means that blue light is absorbed and remaining orange color is observed. Process of fluorescent dyes are explained before. Fluorescent organic dyes, which have emission in ultraviolet (UV), visible (VIS), infrared (IR) and near-infrared (NIR) regions have many application areas from medicine to nanotechnology. The figure shows that dyes that are commonly used in the applications [19].

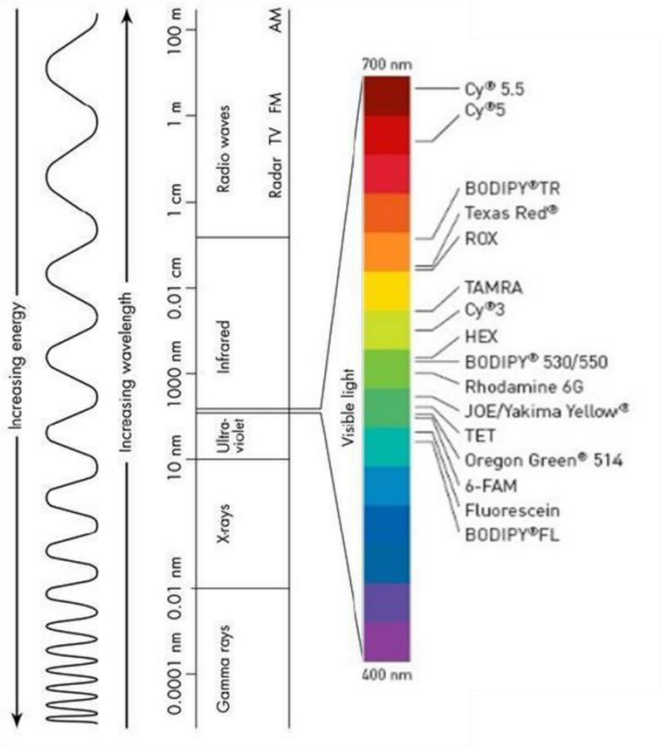

Figure 9. Common fluorescent dyes in visible region.

Almost all of the visible region is covered by the organic dyes, which have some advantages in different aspects. Naphthalene, pyrene and coumarin based dyes are

usually found in UV region. On the other hand, IR dyes are consist of fluorescein, rhodamine, bodipy, and cyanine derivatives. All of these dyes are different from each other according to their properties, which are photochemical features, structures, spectral features and chemical characteristics. All of the dye families have both advantages and disadvantages in many aspects. For instance, fluorescein is one the most used organic dyes in biological applications because of good water solubility, high quantum yield and molar coefficient. However, it has also some disadvantages in the aspects of self-quenching, photobleaching and pH sensitivity [20]–[22].

1.4. Molecular Sensors

In common definition, a sensor is a matter that detect changes in a particular place or medium and supply an output. An ideal chemosensor should be selective for a particular ion, molecule or particle in addition to determine quantity of analyte. They have very wide application areas from medicine to environment. A couple of examples for using areas of chemosensors are that detection of a toxic compound in body and measurement of heavy metal amount in drinking water [23].

Importance of molecular sensor is increasing in recent days because of high costs and low detection limits of other sensing methods. Molecular sensors are highly interdisciplinary area and they many types in respect of analyte type, sensing mechanism, etc.

Optical sensors is one of the most known and used types of molecular sensors. Their working principle is based on interaction with light. Fluorescent sensors are a common type of optical sensors on account of properties that high sensitivity, low cost and fast response. The difference between wavelength of absorbed and emitted lights provides an advantage for fluorescent molecular sensors. Fluorescence is different from absorbance in aspect of the ratio between signal intensity and concentration. Fluorescence signal intensity can be increased by incident beam power on the other absorbance signal is proportional to concentration of sample essentially. Therefore, fluorescent sensors can detect picomolar levels while micromolar levels can be

measured with absorbance. Moreover, fluorescent sensors are reliable since there is only a stable molecule and light interaction [15].

Today, fluorescent sensors are widely used by scientist in many application areas from biological studies to nantechnological applications. For example, the fluorescent sensor, which is according to Lee *et. al*. is capable to sense both cation and anion (Figure **10**). Binding of Pb (II) causes conformational changes that quench excimer fluorescence. There is also F- anion moiety, which is triazacrown by hydrogen bonding. Interaction with F- anion results in PET which is quenching of fluorescence [24].

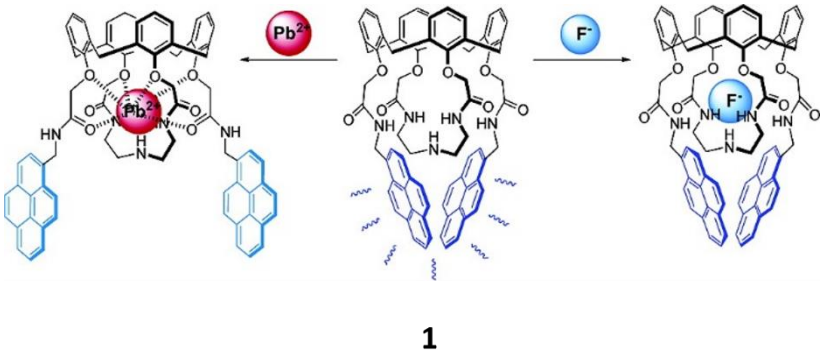

Figure 10. Bifunctional sensor for both cation and anion.

1.5. Photophysical Aspect of Fluorescent Chemosensors

A fluorescent probes consist of two main group, which are receptor and fluorophore parts. These parts are recognition and signaling moieties. Receptor part is very important in terms of sensitivity and selectivity [25]. Receptor should have good and selective affinity for target particle and not influenced from environmental effects such as temperature, pH, etc. The fluorophore that gives optical output is as significant as receptor part. Purpose of fluorophore is that converting chemical inputs to optical output such as fluorescence emission. Fluorescent probe can be designed in two types. In first type, receptor is attached directly to fluorophore and it is part of conjugation

system of fluorophore. Other type of fluorescent senor have also spacer part which can be aryl group to separate receptor from π conjugation system of fluorescent dye [26].

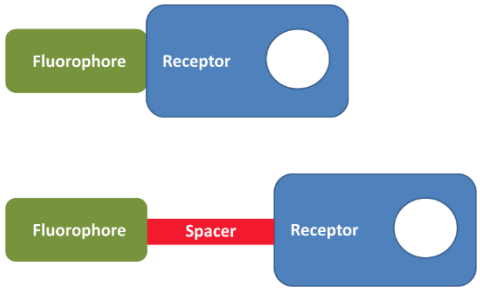

Figure 11. Schematic representations of fluorescent chemosensors.

1.5.1. Photoinduced Electron Transfer (PET)

Photoinduced electron transfer (PET) is observed in the fluorescent probe whose structure is fluorophore-spacer-receptor type. In this type of fluorescent sensor, receptor is not part of conjugation because of the spacer, however still they are close enough for electronic interaction [27].

Figure **12** shows that working mechanism of PET. At the beginning, fluorophore absorbs a photon which excites electron from highest occupied molecular orbital (HOMO) to lowest unoccupied molecular orbital (LUMO). Receptor's donor atom that is commonly nitrogen atom has HOMO whose energy level is between the molecular orbitals mentioned before. After excitation, an electron of donor atom's HOMO moves to empty positon in fluorophore's HOMO. That transfer of electron prevents the returning of excited electrons. All of these events result in quenching of emission.

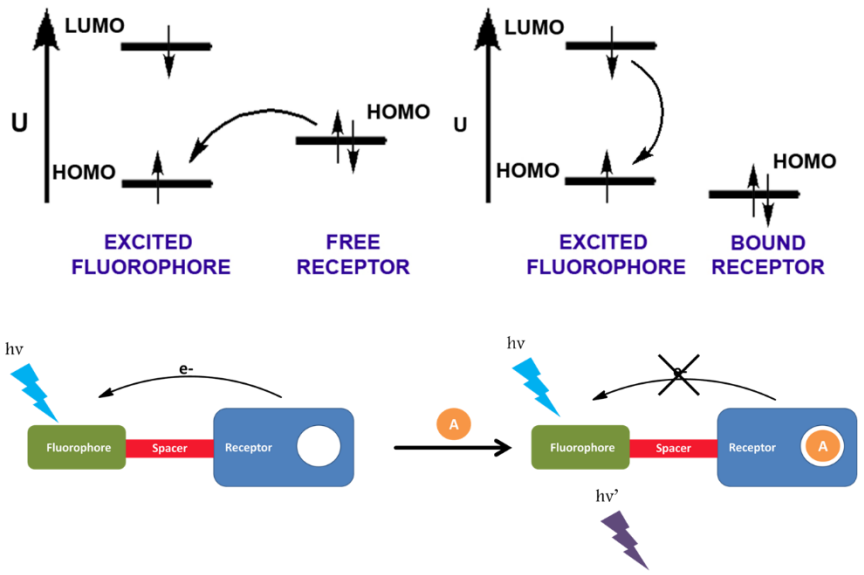

Figure 12. Schematic representation and mechanism of PET.

There are many examples for PET based fluorescent chemosensors in the literature [28]–[30]. The figure **13** shows that different PET based molecular sensors for various metal ions. Compound **2** [31] is very simple example for aza-crown ether based fluorescent probe whose fluorophore is anthracene. In other examples, cryptand [32] and podand [33] is attached as receptor. In this fluorescent sensors, binding of some alkali or transition metal ions prevents the quenching of emission.

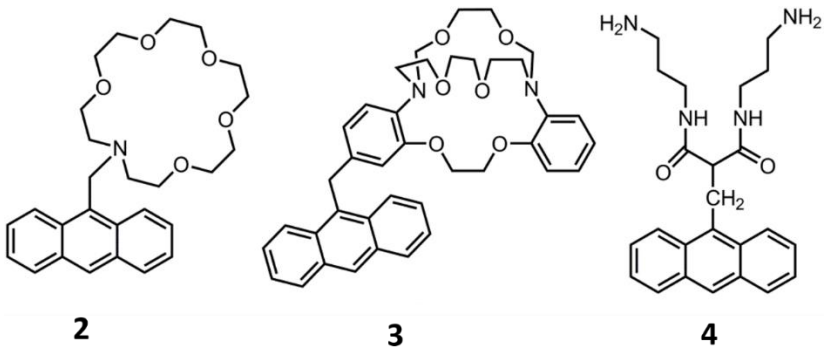

Figure 13. Example compounds for PET based chemosensors.

On the other hand, there are reverse PET based fluorescent chemosensors too. In this probes, binding of analyte causes quenching of emission. The figure shows mechanism

of reverse PET. Binding of analyte decrease the LUMO of donor atom and then excited electron moves the vacancy on the LUMO, so emission is quenched.

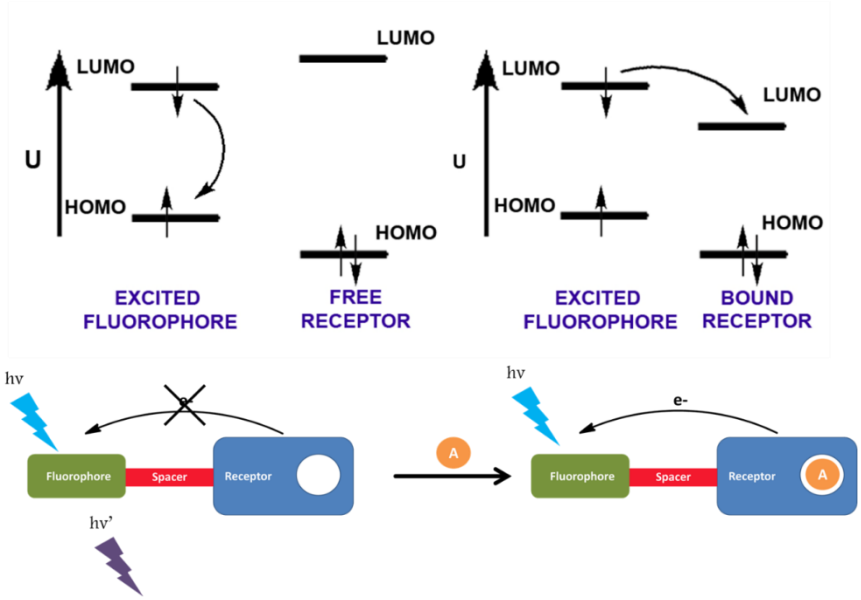

Figure 14. Schematic representation and mechanism of reverse PET.

An example for the reverse PET is compound **5**, which is designed and synthesized by Akkaya group. Fluorophore is BODIPY that will be explained at next section. Binding Zn (II) ion to bipyridine receptor quench the emission by oxidative PET [34].

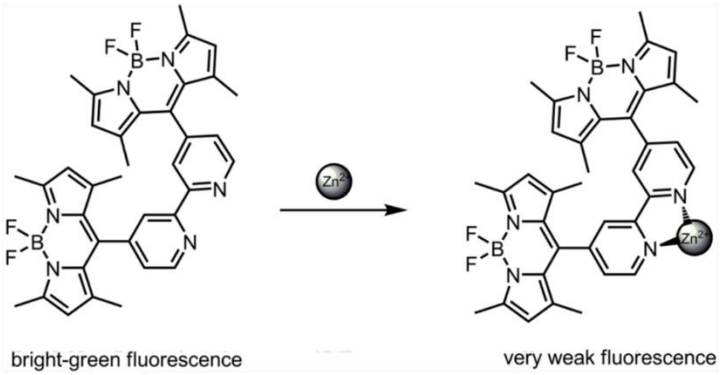

Figure 15. An example molecular sensor for reverse PET.

1.5.2. Internal Charge Transfer (ICT)

When receptor is attached to fluorophore directly, it becomes a part of conjugation too. In this type of fluorescent probes, binding of analyte changes in dipole moment that causes Stokes shift by intramolecular charge transfer from donor to acceptor. The positive or negative effect to excited state dipole results in changes of not only emission spectrum but also absorption spectrum [35].

ICT based fluorescent sensors split into two type. First one is that an electron donor group, which can be amino group is attached to fluorophore. Binding of cation to receptor decreases electron density of electron donor group that means less conjugation. As a result, blues shift in absorbance and fluorescence spectrums is observed. That can be explained also charge-dipole interaction. In the excited state, electron donor group is positively charged, therefore binding of a cation results in interaction between two positively charged particles. In this case, destabilization of excited state is higher than ground state, so energy gap between HOMO and LUMO increases which means blue shift [36].

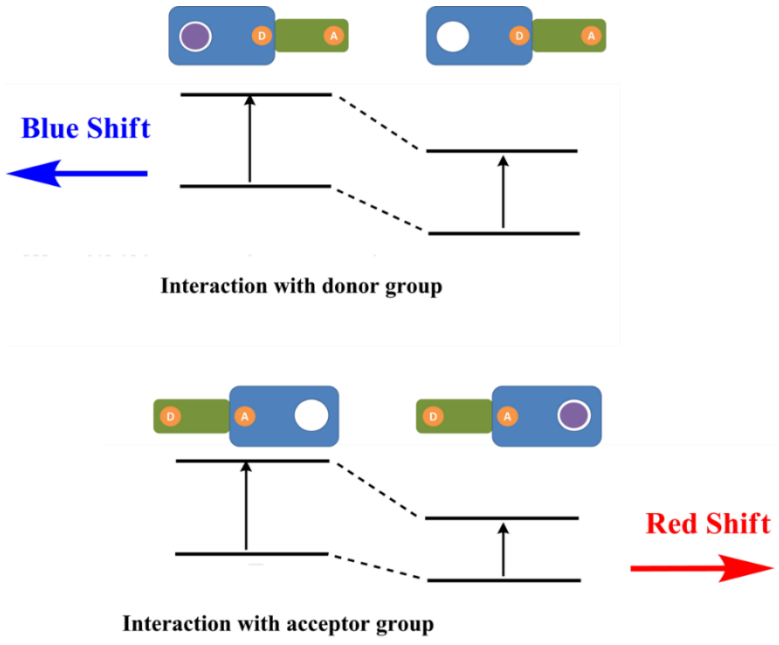

Figure 16. Red and blue shifts according to energy gap between HOMO and LUMO in ICT based chemosensors.

On the contrary, second type of ICT based probes indicates red shift in the fluorescence. Electron with drawing group like carbonyl is connected to fluorophore changes the result completely. Interaction between the cation and electron withdrawing group improve the electron withdrawing ability of this group. Stabilization and broader conjugation occurs with gaining of more electron for fluorophore by binding of analyte. A cation stabilize the electron withdrawing group, which is negatively charged in the excited states. Therefore, energy of excited states reduce more than ground states that results in decreasing the energy gap between HOMO and LUMO. In conclusion, red shift is observed in both absorbance and fluorescence spectrums [37].

There are many examples for ICT based fluorescent sensors. When metal ion is bound to compound **6** [38] and **7** [39], blue shift is observed. Receptor moiety is crown in these probes.

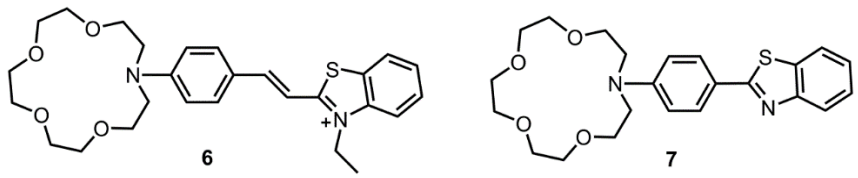

Figure 17. Examples for ICT based sensor which has crown ether as receptor.

Although they have similar structures, the shift in their absorbance and fluorescence spectrums is completely different for compounds which are shown in figure **18** [40]. Because their receptor parts are different that one of them electron donating aniline group the other one is electron withdrawing pyridine. As a result, these two compounds exhibit opposite spectral shift upon proton binding.

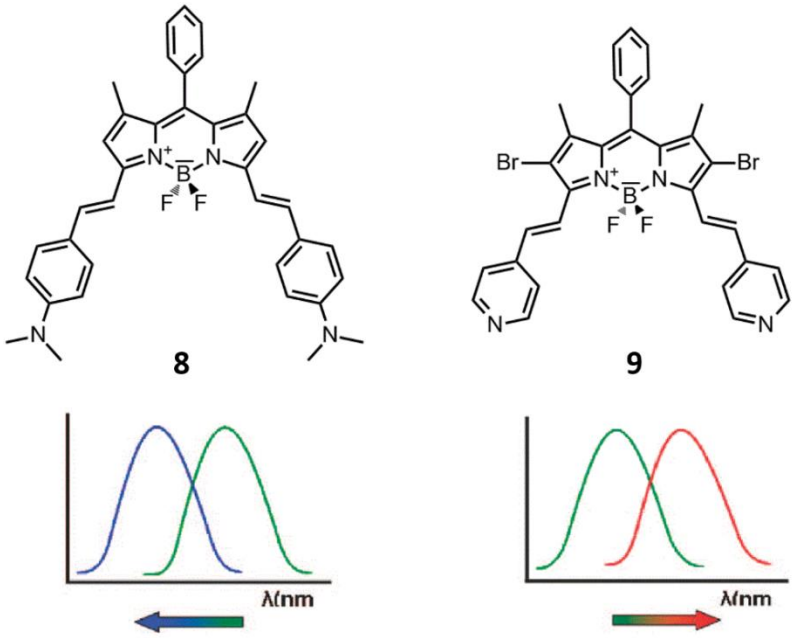

Figure 18. The fluorescent sensors that have similar structures show different responds in the presence of H^+.

1.5.3. Energy Transfer (ET)

Light-harvesting antenna system is used many phenomena in nature [41]. For example, green plants have light-harvesting mechanism to gather more sunlight from different wavelengths in photosynthesis. A wide scale of sunlight is collected by only one photosynthetic reaction center alone by the help of light-harvesting complexes. Inspired by these examples from the nature, many scientists try light-harvesting mimicking applications [42]. In supramolecular chemistry, designing and synthesis of artificial light-harvesting systems is the research area, whose popularity increases rapidly in recent years.

Donor and acceptor fluorophores are required to make energy transfer system. It can be explained simply that donor fluorophore is excited with light then the emission from acceptor part is observed [43]. There are two types of energy transfer mechanism that Förster and Dexter energy transfers (Figure **19**).

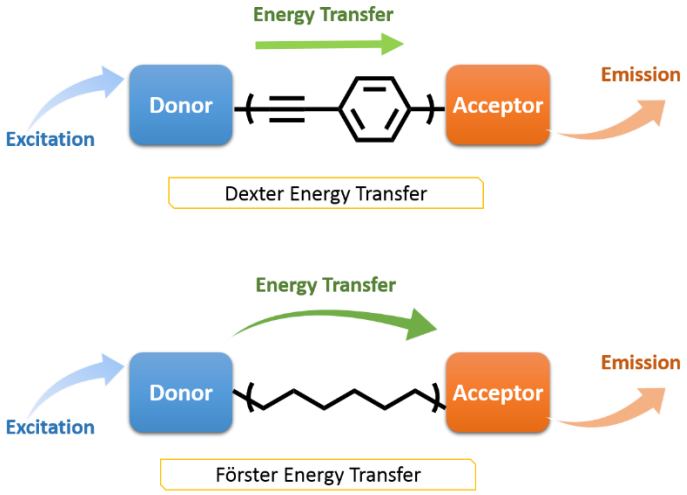

Figure 19. Schematic representation of Förster and Dexter energy transfers.

Characterization of energy transferred can be performed by tracking of parameters, which are lifetime, quantum yields, decreasing of donor emission and increasing of acceptor emission. Moreover, it is related to rate of deactivation of excited system. The requiring time of energy transfer must be less than lifetime of excited donor to carry out energy transfer successfully [44].

1.5.3.1. Dexter Type Energy Transfer

In Dexter type, energy is transferred by electron exchange. Orbital overlapping is required for electron transfer, so fluorophores are connected to each other by conjugated bridge. Because of that reason it is also named through-bond energy transfer. In this type of energy transfer, electron moves from HOMO of donor to LUMO of acceptor [45].

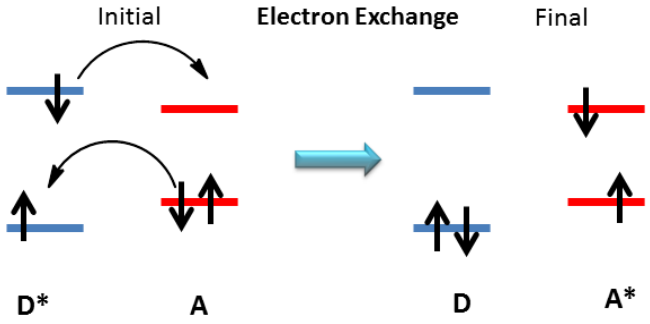

Figure 20. Schematic illustration of Dexter electron exchange mechanism.

There is an equation which shows rate constant for Dexter type energy transfer.

$$K_{dexter} = K\ J\ exp(-2R_{DA} / L)$$

In this equation K symbolizes orbital interaction, *J* is normalized integral of spectral overlapping, R_{DA} is space between donor and acceptor, and L is Van der Waals radii [44].

According to equation, Dexter energy transfer is much dependent on the distance between donor and acceptor. Energy transfer yield increases exponentially with increasing distance. Therefore, they have to very close to each other for efficient energy transfer. Dexter energy transfer is also named as 'short range energy transfer'.

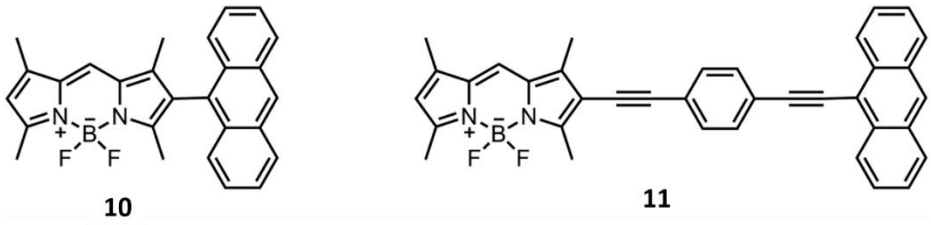

Figure 21. Examples for Dexter type energy transfer.

Figure **21** [46] shows that examples for through bond energy transfer. Anthracene-BODIPY cassettes are designed to understand effect of distance in Dexter type energy transfer that is published by Burgress et al. Results are interesting because compound **11** has more efficient energy transfer unlike compound **10**. The reason is that steric

hindrance in compound **10** disturbs the conjugation, so energy transfer efficiency decreases.

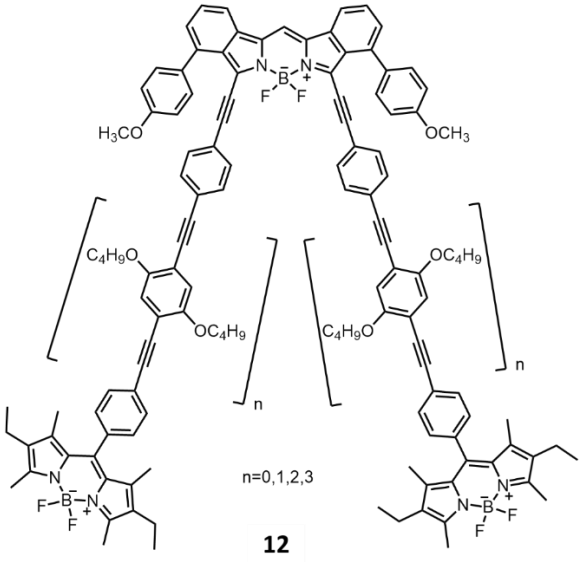

Figure 22. Another example for Dexter type energy transfer.

Another example for Dexter type energy transfer is shown in figure **22** [47]. It consists of three BODIPY units two of them are donors and the other one is acceptor that they are linked to each other with conjugated bridge. It is clarified that through bond energy transfer decreases with distance.

1.5.3.2. Förster Type Energy Transfer

In Dexter energy transfer, orbital interaction is required, on the other hand Fluorescence (Förster) energy transfer (FRET) becomes in case of spectral overlapping. Energy is transferred from donor fluorophore to acceptor non-radiatively. It was introduced by Förster first time in 1948 [48] and today it has many applications in the fields from biotechnology to electrochemistry. The scientists need FRET since in some cases Stokes' shift of a fluorophore is not enough to distinguish the difference.

Förster energy transfer depends on several factors. It is similar to Dexter type, FRET is also much dependent on distance between donor and acceptor fluorophores. Energy transfer efficiency is inversely proportional to sixth power of distance. The other

significant factor for efficiency is spectral overlap of donor's emission and acceptor's absorbance [49].

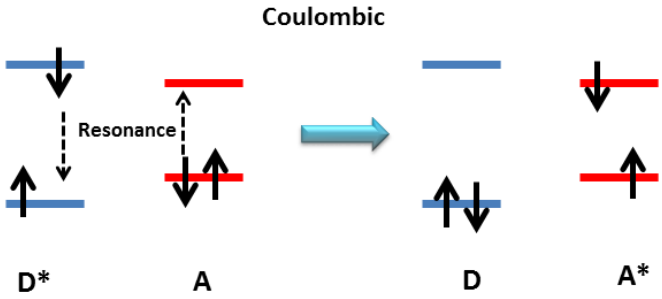

Figure 23. Schematic illustration of Förster electron exchange mechanism.

The electronical mechanism of FRET is shown in figure x. After the excitation of donor, excited donor transfer its energy to acceptor in non-radiative way which is called resonance. Then excited electron of acceptor moves to ground state by emitting light.

The rate equation of FRET is given below:

$$k_{ET} = \frac{1}{\tau_D}\left(\frac{R_c}{d}\right)^6$$

Where τ_D represents excited state lifetime of donor in the lack of acceptor, d is the distance between donor and acceptor and Rc is critical radius which is the distance when k_{ET} equals to real decay rate of donor. The equation of Rc is given below:

$$R_c^6 = \frac{9000(\ln 10)K^2\Phi_D}{128\pi^5 N n^4}J$$

Where Φ_D symbolizes the emission quantum yield in the lack of acceptor, K is orientation factor and n represents refractive index of solvent, N is Avogadro's number and *J* is the integral of spectral overlap [50].

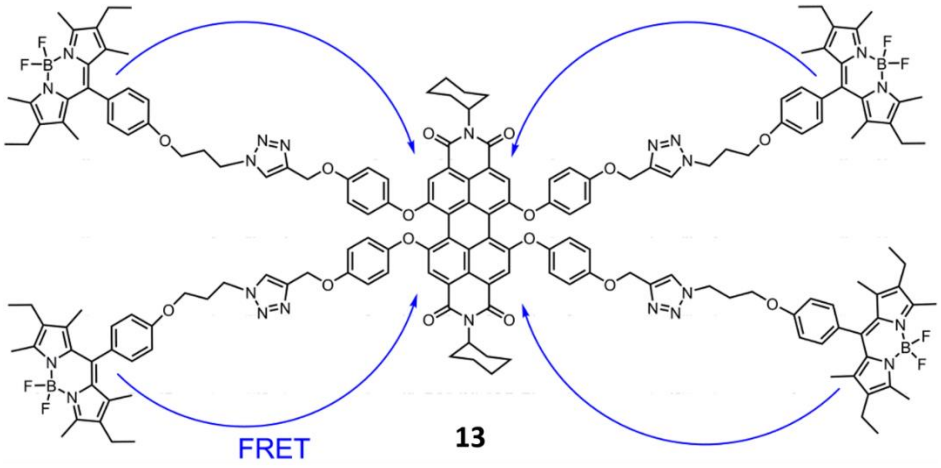

Figure 24. A literature example for BODIPY based Föster type energy transfer.

In the figure **24** [51], one of the most known example is shown. In this example, BODIPY fluorophores as donors are attached to perylene based acceptor unit. Click chemistry is used to bind donors to acceptor in this study. FRET efficiency is calculated as 99% that is satisfying result.

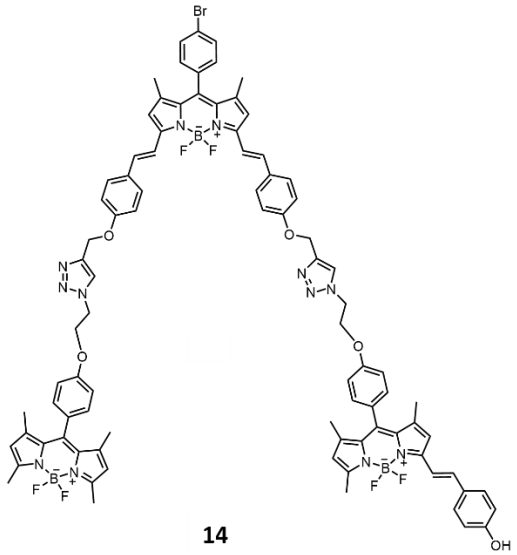

Figure 25. Another example for Föster type energy transfer.

Another example is compound **14** [52] that three BODIPY units are covalently attached each other via click reaction. Excitation wavelengths are 501 nm and 572 nm

and emission wavelength is 662 nm that there is huge difference between them. Energy transfer yield is 99% for both donors.

1.6. Sensing of Particular Ions or Compounds

1.6.1. Metal Ions

Metal ions participate in several important biological processes from muscle contraction to nerve impulses. Moreover, catalytic amount of cations are involved in binding site of many enzymes. Not only lack of some metal ions but also overdose of them are the reasons of various diseases directly or indirectly. There are many examples for relation between ion levels and some illnesses. For example, control of lithium is considerable in the treatment of manic depression and also potassium amount in high blood pressure [53]–[56].

Transition metals have critical roles in environmental pollution and biological metabolism [57]. Therefore, observing and tracking of their concentration is important for understanding of their toxic and pollutant effects. These metal ions are especially Pb (II), Cd (II), Hg (II), etc. that have many negative effects on the balance of nature.

Selectivity is still challenge to design a good receptor, which has affinity for only one cation relatively. Because of that reason, many types of receptor synthesized and this field is very comprehensive. For example, majorly oxygen atoms containing crown ethers derivatives can be used to sense alkali or alkali earth metals that are hard metals relatively. According hard and soft acid and bases (HSAB) theory, hard acids interact with hard bases better and soft prefers soft also because of charge to size ratio. Another example is that usually Hg (II) receptors consist of Sulphur containing crown ethers due to HSAB again. Besides HSAB, size also important itself only that size compatibility between ion and moiety is required. In the figure **26**, there are examples for different metal chemosensors. Compound **15** is sodium selective fluoroionophore [58]. Compounds **16,17** and **18** are capable to sense Hg(II) ions [59]–[61].

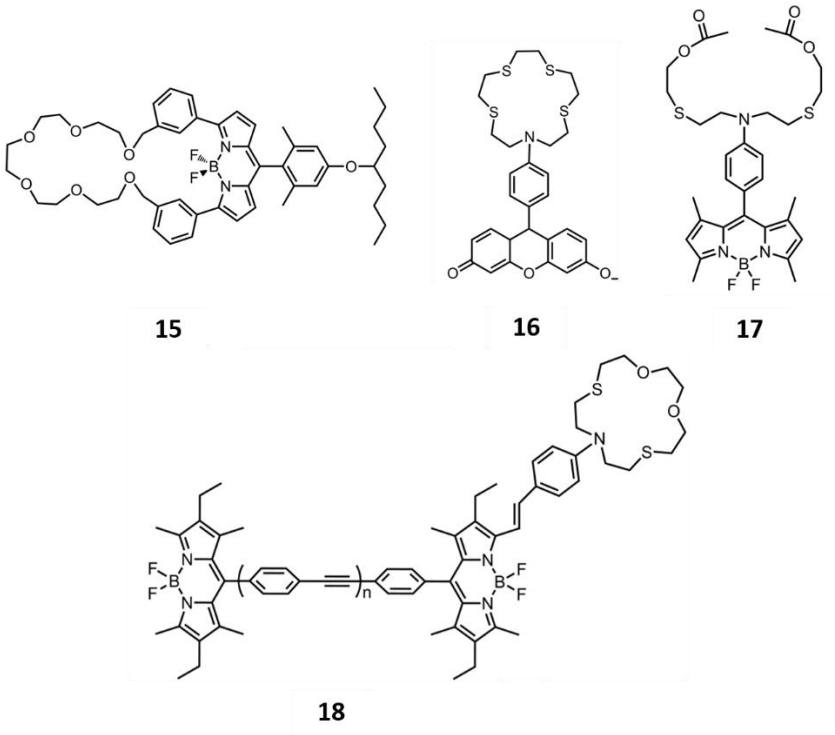

Figure 26. Literature examples for metal ion sensors.

1.6.1.1. Zinc (II) Ion Sensors

Zinc (II) ion is the second most abundant transition metal ion in the brain and also it participates as main component in many biological processes. Major amount of zinc presents as tightly bound to proteins, on the other hand minority is in the mobile form as intracellular zinc ions which are existing in the tissues, brain, intestine, pancreas, and retina, however the exact function is still obscure in the many biological processes. Moreover zinc ions, which are coming from intracellular metalloproteins have a role in programmed cell death called 'apoptosis'. Zinc ion is very critical in the several disorders such as Alzheimer's disease, epilepsy, Parkinson's disease, ischemic stroke and infantile diarrhea. In spite of intensive research on role of zinc ion in these processes, a lot uncertain points about its function should be clarify. Therefore, it is still challenge to design new receptors to monitor quantity of zinc ions [62]–[64].

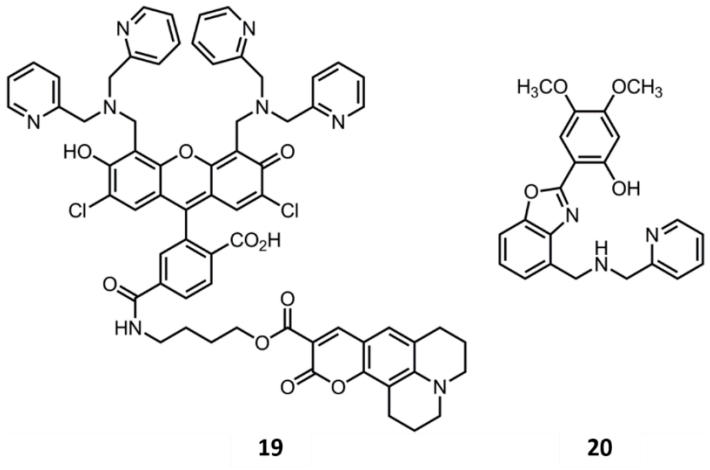

Figure 27. Some literature examples for Zn (II) ion sensors.

There are many examples of fluorescent sensors for zinc ions. Compound **19** [65], which is shown in the figure **27** is the example of ratiometric sensor for intracellular zinc ion. There is ester linkage between coumazin group and fluorescein and that is hydrolyzed by esterase enzyme in the cell. After leaving of coumazin, fluorescein that emits at 534 nm is sensitive to zinc concentration. Compound **20** [66] is another example that is developed O`Halloran et al. It is water soluble and very selective to zinc ion. Intracellular zinc ion can be monitored by emission of this molecule.

1.6.2. Biological Thiols

Cysteine (Cys), homocysteine (Hcy) and glutathione (GSH) are biological thiols, which are very important roles in enzyme functionality and preservation of redox states because of the good nucleophilic properties. The change in amount of biological thiols is related with many diseases such as occlusive vascular, premature arteriosclerosis, leukemia, diabetes, etc. [67]–[69].

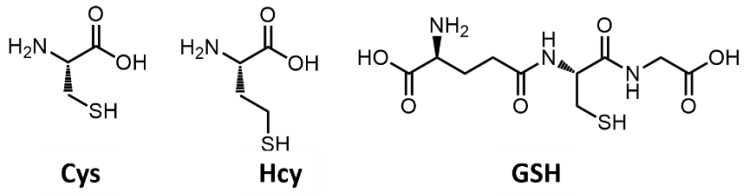

Figure 28. The chemical structure of Cysteine (Cys), homocysteine (Hcy) and glutathione (GSH).

Glutathione (GSH) is tripeptide, which consists of glutamate, glycine and cysteine. In the synthesis of GSH, the enzymes that γ-glutamylcysteine synthetase and glutathione synthetase participate as catalyzer. In the tumor cells GSH concentration is more than normal cells 1000-fold. GSH takes part in antioxidant response, cell proliferation, regulation of gene expression, etc. Lack of GSH causes the diseases, which are Parkinson's disease, AIDS, Alzheimer's disease, cancer and heart attack [70], [71].

1.6.2.1. Detection of Thiols

Detection of the thiols that are Cysteine (Cys), homocysteine (Hcy) and especially glutathione (GSH) is certainly significant because of their properties mentioned before [72], [73]. Two characteristic of thiols are helpful for sensing of them. These two properties that they are good nucleophiles and they have affinity to metal ions are very beneficial to design fluorescent-based thiol probes. Many reactions and methods, which are Michael addition, cyclization, metal complex formation, redox reactions and disulfide bond cleavage are used in sensing of thiols. pH of medium is also important in sensing because of the acidity of thiol derivatives [74], [75].

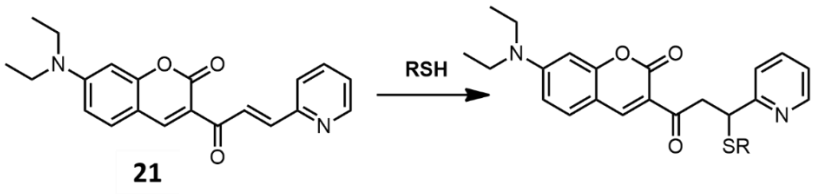

Figure 29. Example for thiol sensor based on Michael addition.

Compound **21** [76] is example for Michael addition based fluorescent probes. The coumarin that includes α, β-unsaturated ketone derivative has no emission. After binding of thiol derivative, it starts to give emission. This PET based thiol sensor is shown in the figure **29**.

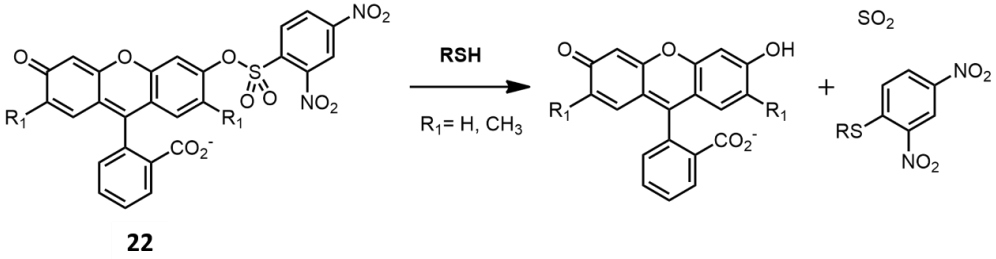

Figure 30. Thiol probe based on PET mechanism.

In the figure **30**, there is another thiol sensor example. This example based on cleavage of sulfonamide and sulfonate. Thiol derivative attacks to electron deficient 2,4-dinitrophenyl sulfonyl part of compound **22** and that results in turning on the emission of fluorescein because of de-sulfonylation [77].

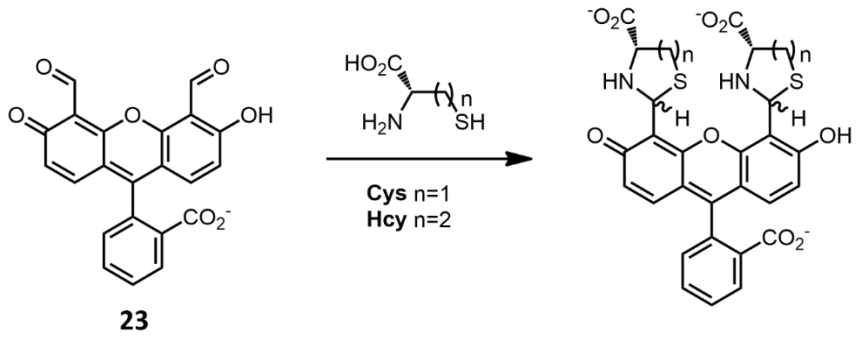

Figure 31. Thiol sensor based on cyclization of aldehydes.

Compound **23** [78] is a successful example for sensing of thiols by cyclization of aldehydes. The reaction between bisaldehyde and cysteine or homocysteine causes the shift of absorption maximum to longer wavelength. Monoaldehyde derivative of compound **23** is more selective for Cys. The reason is related with formation five-membered ring at end of reaction.

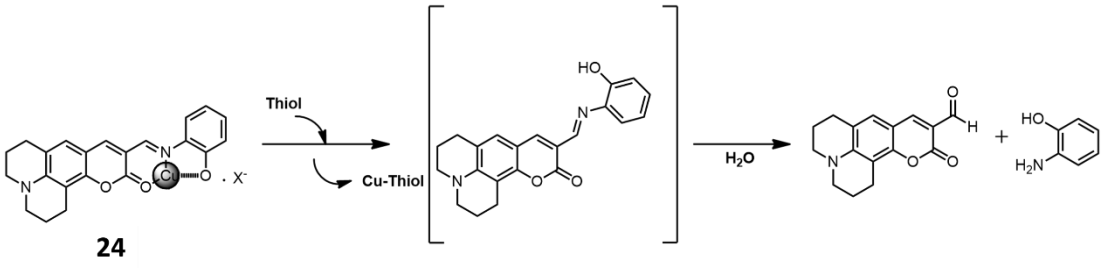

Figure 32. Thiol probe based on metal ions.

Another method to sense thiols is using their high affinity to metal ions. Kim *et. al.* were used iminocoumarin which includes Cu (II) ion for sensing thiols at pH 7.4. Adding of thiol to compound **24** [79] results in coumarinaldehyde, which has high emission as distinct from the initial non-emissive metal complex. Compound **24** is another example for PET based turn-on fluorescent sensor for thiols.

1.6.2.2. Disulfide Bond Cleavage

Thiols are strong reducing agents and by this way they can break the disulfide bonds. First example is compound **25** [80] which consists of coumarin and porphyrin derivatives that are connected with disulfide bond. Coumarin is donor and porphyrin is acceptor part of the structure and there is fluorescence resonance energy transfer (FRET) between them. In the presence of thiols, disulfide bond is cleaved, therefore FRET is over at this point. Emission shifts from red to blue color. By this way, thiols can be sensed easily and detected by naked eye.

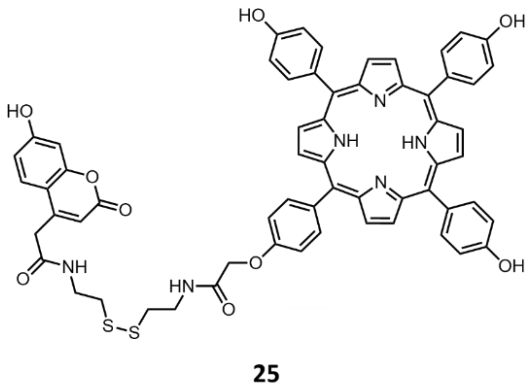

Figure 33. Thiol sensor based on disulfide bond cleavage.

Another example for disulfide bond cleavage is compound **26** [81] as shown in figure **34**. There are three main parts in this structure, which are rhodamine, BODIPY and folate that is folic acid receptor. Aim of folate is targeting of folic acid that is found more in some type of cancer cells. In this structure, BODIPY and rhodamine fluorophores are donor and acceptor respectively. There is FRET in lack of GSH. Concentration of GSH in tumor cells is more than normal cells almost 1000 times. In the presence of GSH, disulfide bond is broken and emission wavelength is changed from 595 nm to 520 nm.

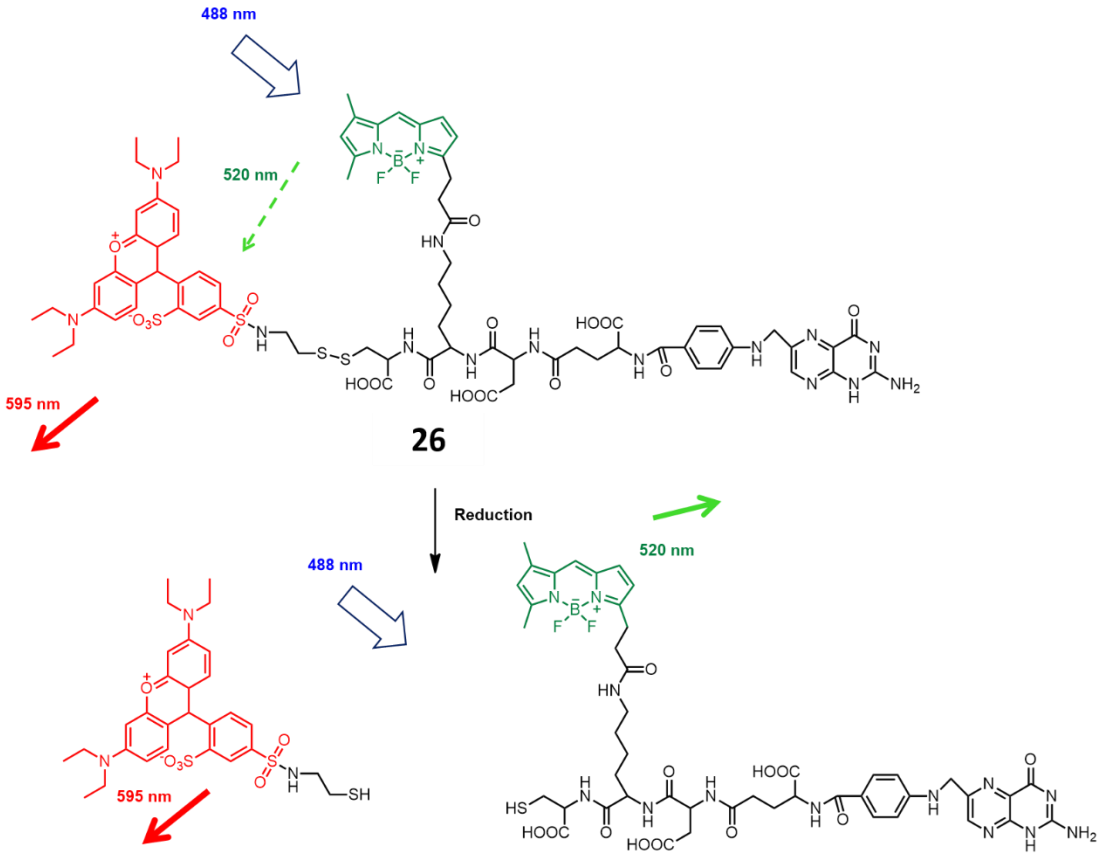

Figure 34. Disulfide bond cleavage based FRET.

1.7. BODIPY Dyes

4,4-difluoro-4- borata-3a, 4a-diaza-s-indacene which is abbreviated as BODIPY was first discovered accidentally by Treibs and Kreuzer in 1968 [82]. They used acetic anhydride to acylate the 2,4-dimethylpyrrole in the presence of $BF_3 \cdot OEt_2$. Dipyrrin

compound was synthesized by acid catalyzed then dipyrrin formed complex with borontrifluoride to yield BODIPY (Figure **35**). Almost 20 years later, Haugland and Kang explored the fluorescence properties of BODIPY in 1988 [83], [84]. After the recognition of BODIPY as a fluorophore, it has been used in many applications in the areas from molecular sensors to biomedical materials. There are many reaction sites on BODIPY which can be modified by nucleophilic and electrophilic substations.

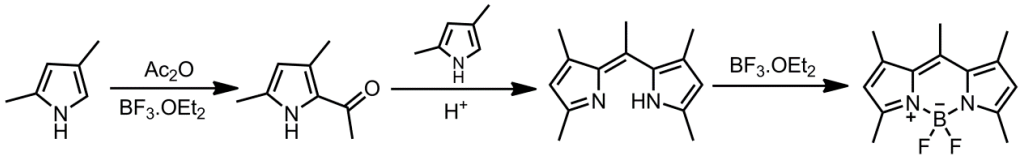

Figure 35. First synthesis of BODIPY dye.

BODIPY has many excellent properties against the other fluorescent dyes. For instance, BODIPY dyes absorbs and emits strongly in the fields from visible to near-IR. Not only quantum yields but also absorption coefficients of BODIPY dyes are quite high [85]. Furthermore, they have thermal and photostability in different types of mediums and solubility in organic solvents is very good. They are usually neutral molecules, therefore insensitive to pH and polarity of solvents [86].

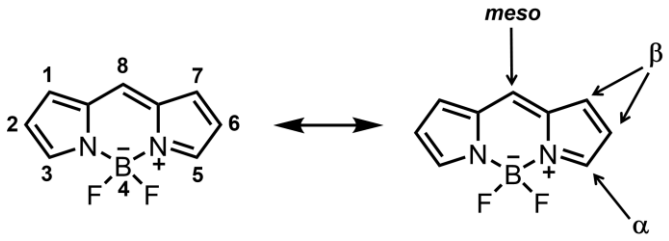

Figure 36. Structure and numbering of BODIPY core.

The most significant characteristic of BODIPY dyes is probably easy chemistry. It possible to functionalize almost all positions on BODIPY and the yields of reactions are satisfactory. BODIPY family gains new members with each of this modification that every new member has different chemical and photophysical features [87].

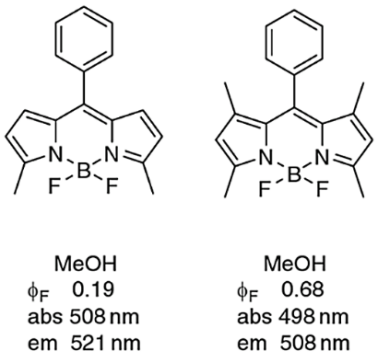

Figure 37. Quantum yields of BODIPY dyes that one them has methyl group at 1, 7 positions.

Every positon effects different property of BODIPY dye that is mentioned before [88]–[91]. For instance, quantum yield of BODIPY is influenced remarkably with aromatic substation on meso positon. In the figure **37**, the difference between fluorescence quantum efficiencies of two BODIPY dyes are very large while their structures are very similar. In phenyl-BODIPY (without methyl groups), possible conjugation between phenyl group and BODIPY core causes quenching of emission. Presence of methyl groups at 1 and 7 positions keeps the phenyl group at perpendicular to BODIPY core. Methyl groups prevent the free rotation because of steric hindrance. As a result of that structural change, the fluorescent quantum yield increases enormously.

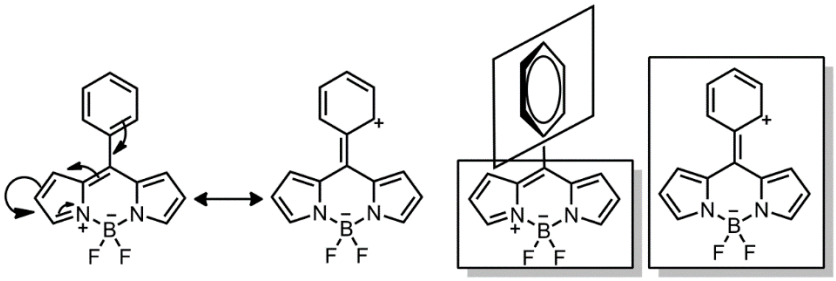

Figure 38. Free rotation of phenyl group that is attached to meso position of BODIPY.

Modification of meso position is realized with acid-catalyzed in the synthesis part. Water-soluble groups, receptors for particular ions or molecules and donor-acceptor moieties can be attached to meso position.

2 and 6 positon of BODIPY is less positive, so electrophilic reactions are preferred instead nucleophilic. Sulfonation, nitration, halogenation and formylation of these positions can be possible because of the electron rich characteristic. Binding of heavy atoms like bromine and iodine causes intersystem crossing, by this way fluorescence of BODIPY decreases. This substation makes possible producing singlet oxygen, which is very important for photodynamic therapy.

Modification of 1, 3, 5 and 7 positions allows several additional functions to BODIPY [86], [92]. The most used reaction to functionalize especially 3 and 5 positions is Knoevenagel condensation [93]. In this reaction, Dean-Stark apparatus [94] is used for to get rid of water, which forms as product. By using this reaction, several types of electron donor and withdrawing aldehydes can be attached to these positons. They cause red shift in absorption and emission spectrum [95] so that it can be proper for biological applications.

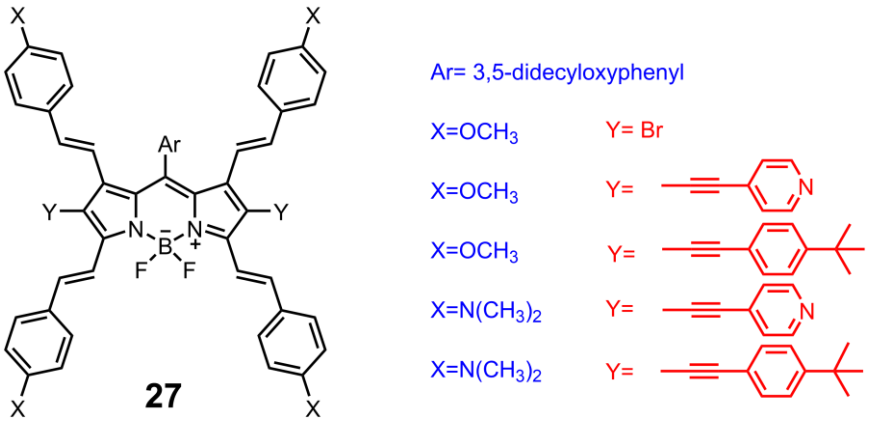

Figure 39. Structures of the tetra-styryl BODIPY derivatives.

Akkaya group stated that 1 and 7 positions are also reactive as 3 and 5 positions [96]. Tetra-styryl BODIPY dyes were synthesized by Akkya group in 2009 (Figure **39**). Then, Ziessel et al reported the tetra-styryl BODIPY whose absorption wavelength is 720 nm and emission wavelength is 800 nm (Figure **40**) [97]. Also both of two groups, which have many study on BODIPY show that 3 and 5 positions are more acidic than 1 and 7 positions. Modification of BODIPY with some groups such as dimethyl amino

and pyridine makes possible pH sensitive applications in the area from sensors to drug delivery.

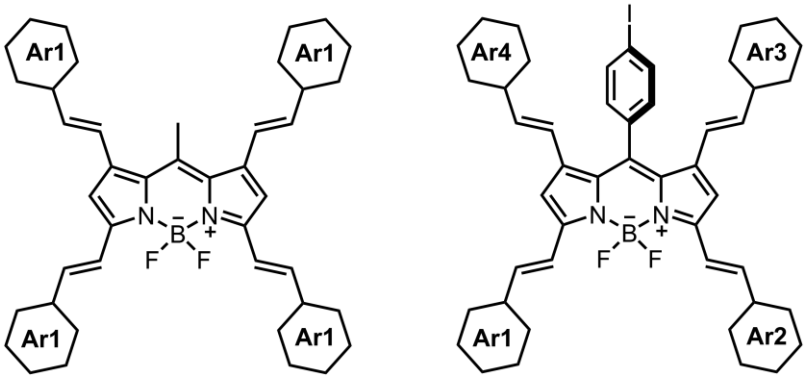

Figure 40. Schematic representation of 1, 3, 5, 7-tetrastyryl BODIPY derivatives.

1.7.1. Applications of BODIPY

BODIPY dyes has many significant properties which are mentioned before. Because of that adorable features, it has wide application area from sensing to solar cells. The figure shows the application areas of BODIPY.

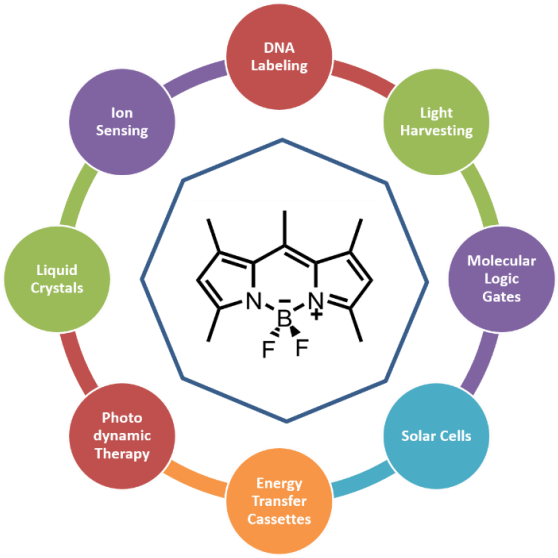

Figure 41. Applications of BODIPY.

There are many examples in the literature for BODIPY based chemosensors because of the properties such as easy modification, photostability and thermal stability, high

fluorescence quantum efficiency, etc. Daub and Rurack synthesized BODIPY based chemosensor first time in 1997 [98]. In the figure **42**, some examples for PET and ICT based BODIPY sensors for particular ions are given. In compound **28** [92], aniline group is attached to meso postion and that is for sensing of proton. Compound **29** [99] and **30** [100], which are dipicolylamine substituted BODIPYs sense in order of zinc and cadmium ions. In compound **31** [34] and **32** [101], receptor moieties are bipyridine and terpyridine groups respectively.

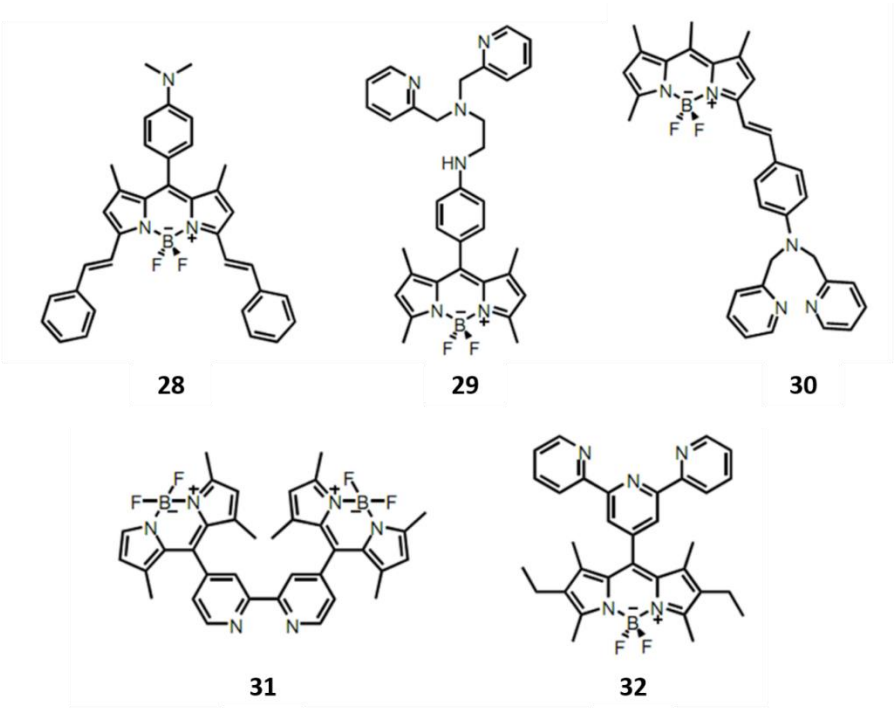

Figure 42. Examples for BODIPY based chemosensors.

Another application area of BODIPY dyes is photodynamic therapy (PDT) which will be explained in detailed later. PDT is cancer treatment method that photosensitizer in the tissue produce singlet oxygen in the case irradiation with light. Singlet oxygen, which is produced by photosensitizer destroys the cancer cells. IR and Near-IR photosensitizers are more proper for PDT because penetration of these lights to human skin is better. PDT is used especially in the treatment of skin cancer. BODIPY based dyes, which has often heavy atoms on 2 and 6 positons are used as photosensitizers. There are examples for BODIPY based PDT agents in the figure **43**. For example,

water soluble groups attached to compound **33** [102] to increase solubility in water because these molecules must work in aqueous media to destroy cancer cells. Also substitution on 3 and 5 positions increases conjugation that ensures longer wavelengths. Compound **34** [89] has very low fluorescence quantum yield that means better intersystem crossing. It is designed by Nagano et al and works in organic solvents. Compound **35** [103] and **36** [104] are another examples for water soluble BODIPY based photosensitizers by the help of sulfonate and carboxylic groups.

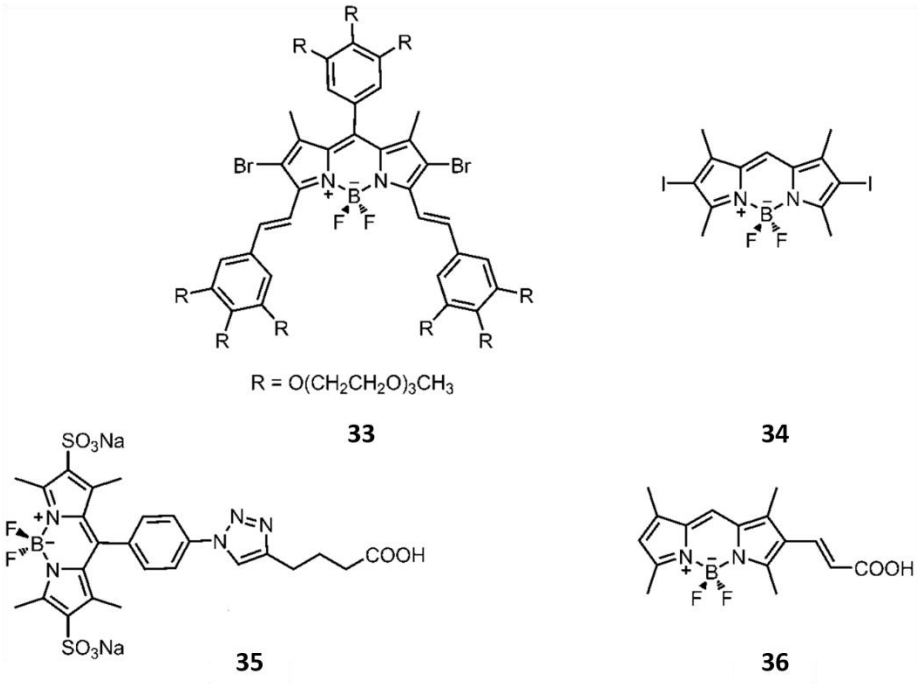

Figure 43. BODIPY based photosensitizers for photodynamic therapy.

Popularity of dye-sensitized solar cells (DSSCs) increases rapidly similar to other alternative energy sources nowadays. Many scientist conduct research on DSSCs to increase efficiency. BODIPY dyes are also used in this field and Nagono is leading scientist which used BODIPY in DSSCs first time. Usually carboxylic group (-COOH) is used for attaching dye to TiO_2 surface. In the figure **44**, compound **37** [105] was designed by Akkaya et al. for DSSCs. Conversion efficiency of this BODIPY based photosensitizer is reported as 1,66%.

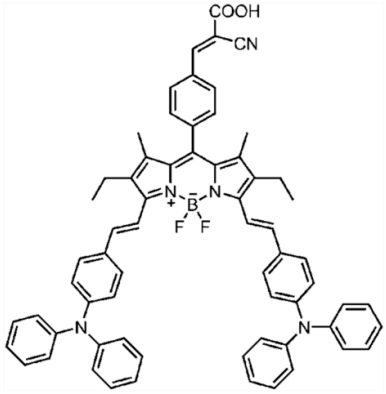

37

Figure 44. Example for BODIPY based photosensitizer that used in solar cells.

1.8. Photodynamic Therapy (PDT)

Photodynamic therapy (PDT) is very young cancer treatment method whose importance is increasing rapidly in recent days [106]–[109]. PDT consists of three main parts, which are photosensitizer, light and oxygen molecule. In the existence of O_2, photosensitizer is irradiated with light and by this way triplet oxygen molecule is excited indirectly. Unlike chemotherapy and radiotherapy, PDT is non-toxic and submissive treatment method. There are plenty of benefits against to radiotherapy and chemotherapy. First, side effects are very low because of the local application and it can be performed many times to same location due to it has almost no harmful effect and toxic properties. Another advantage is that functionalization of photosensitizer is possible with respect to types of cell, cancer, treatment and light. Disadvantage of PDT is difficulty in penetration of light, which can be furthest 5-10 mm. PDT is applicable usually skin cancer because of the penetration problem [110].

1.8.1. Photophysical Background of PDT

Photosensitizers are usually the organic dyes that have conjugated systems. In photosensitizer, the electron at ground state is excited with light to excited singlet state. The electron at excited singlet state is short-lived and it has different relaxation pathways such as fluorescence, interval conversion, intersystem crossing, etc. the spin

of excited electron changes with intersystem crossing from singlet to triplet state which has longer life time. The reason of long life time is that triplet-singlet transition called phosphorescence is forbidden transition. There is also another possible transition which is spin allowed between excited triplet photosensitizer and triplet oxygen that in at ground state. By this transition, highly reactive singlet oxygen species form [111]. The process is shown in the figure **45** [112].

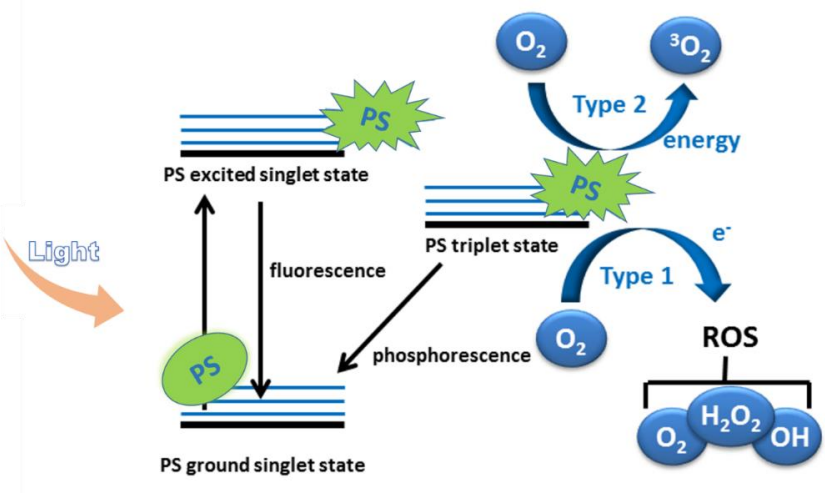

Figure 45. Photophysical processes in PDT.

1.8.2. Photosensitizers and Importance of Light

Photosensitizers that absorb visible and near-IR light have wide range of application fields. The distinctive feature of a PS is that it not only absorbs light in the traditional sense, but it can also transfer this resulting energy to the molecular oxygen to generate highly reactive singlet oxygen molecule [113]. The most common PSs are shown in Figure **46**.

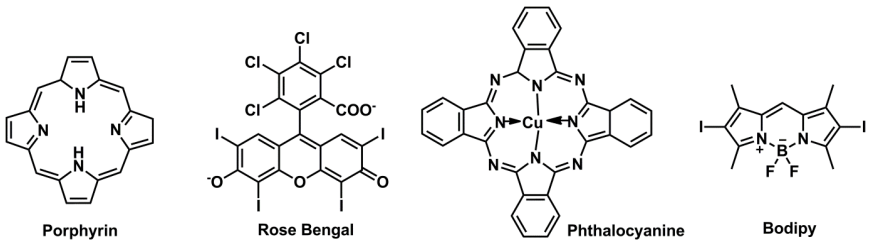

Figure 46. Common photosensitizers in PDT.

Porphyrins and Roze Bengal are common singlet oxygen generating compounds, however do not have strong absorption in the therapeutic window of the body. Phthalocyanine related sensitizers are more promising in terms of absorption profiles. Although the Boradiazaindacene (BODIPY) derivative depicted in figure **46** has an absorption maxima at 540 nm, its near-IR absorbing derivatives was easily synthesized and reported in the literature. Below, in figure 10, three different BODIPY based near-IR absorbing PSs are illustrated. All, absorb light in the 650-700 nm range, which is compatible with the therapeutic window of the body. While compound **38** [114] was introduced by Killoran et al., photosensitizers **39** [102] and **40** [115] were reported by the Akkaya group.

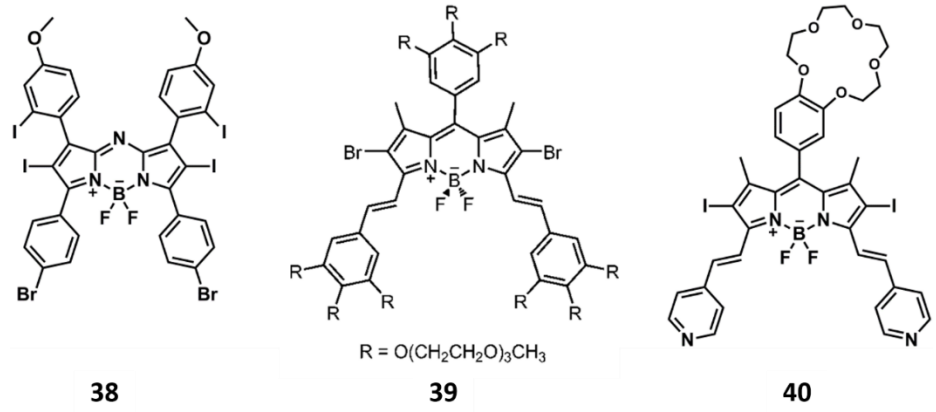

Figure 47. Literature examples for BODIPY based photosensitizers.

In PDT, wavelength of the light is important as characteristic of photosensitizers. Light must penetrate deeply to tissue to excite photosensitizer. Some compounds and structures in tissue such as macromolecules, organelles, cell layer, hemoglobin, and water interact with light in aspect of not only scattering but also absorption. The best penetration into tissue is possible between IR and near IR wavelengths [116]. For example, penetration of light whose wavelength is 700-850 nm is almost two times of 600 nm whose penetration depth is 1-3 mm [117].

1.8.3. Reaction of Singlet Oxygen with Olefins

Singlet oxygen has 1,2-cycloaddition reaction with unsaturated organic compounds [118], therefore this reaction between singlet oxygen and unsaturated compounds has many application areas from drug delivery to caged compounds.

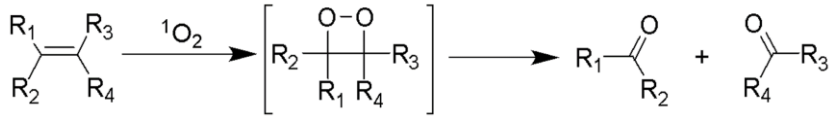

Figure 48. The reaction of singlet oxygen with unsaturated organic compounds.

Using singlet oxygen for cleavage of olefinic linker has many advantages against to other methods. First, designing of proper photosensitizer makes possible to controlled release of substrate according to pH, temperature, light, etc. Another advantage is that low energy is required, therefore IR light can used. There are some bond cleavage reactions which is activated by UV light, so they are not proper to use in biological systems because of the harmful effect of UV light to DNA. Additionally, there is one more negative effect of UV light that is penetration problem mentioned before. Third advantage is bond cleavage reaction with singlet oxygen is rapid and there is no side products.

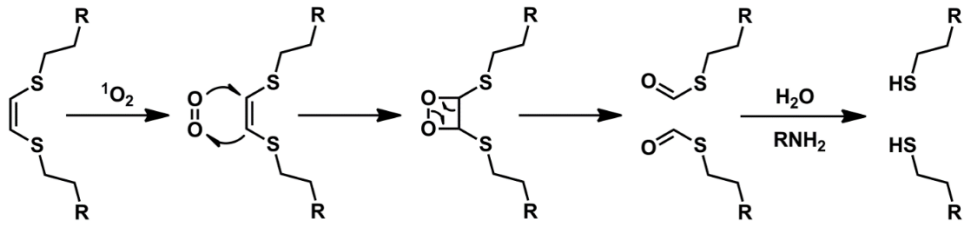

Figure 49. The reaction of singlet oxygen with unsaturated organic dithioethenyl bond.

Dithioethenyl bond is one of the olefin linkers. After the initial addition of singlet oxygen to the double bond of the dithioethenyl bridge, an unstable dioxoethane is formed, which spontaneously decomposes to produce S-alkyl methanethioate [119]. In aqueous solutions with the presence of amines, this compound easily hydrolyzes to the corresponding thiols (Figure **49**). In literature, there are some examples for using

dithioethenyl bond cleavage to release some molecules or particles. In the figure **50**, β-cyclodextrin and zinc phthalocyanine form a complex which is soluble in water [120]. Irradiation with light in the existence of oxygen molecule, dithioethenyl bond is broken. Zinc phthalocyanine separates from the β-cyclodextrin since the interaction weakens that changes from dimeric binding to monomeric binding.

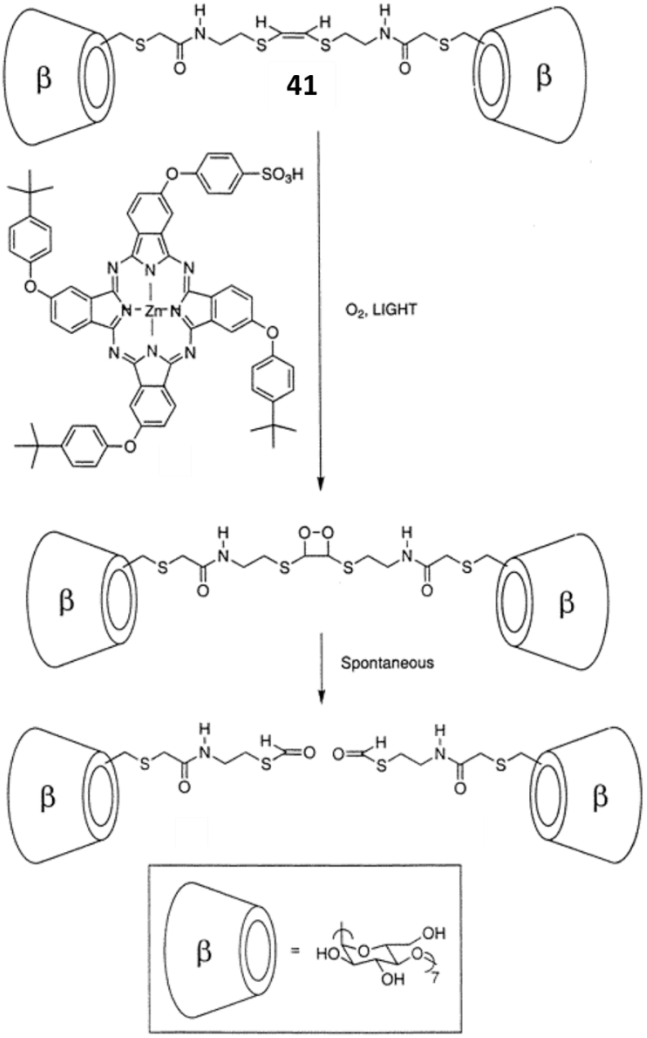

Figure 50. Cleavage of dithioethenyl bond results formation of monomeric structures from dimers.

1.9. Caged Compounds

Caged organic compounds and caged ions [121]–[125], which release their covalently bound payload in response to an external stimulus, have proven useful in the elucidation of a large number of biochemical processes. While some are used as

fluorescent probes, others are useful for the controlled release of drugs and bioactive agents. This control enables concentration of the released molecules to be manipulated in biological media. Caged organic compounds or caged ions that release in response to light attract the most attention, because light offers high spatiotemporal control and also does not influence normal cellular processes. Thus, the current research trend focuses on the phototriggered release of caged compounds in biological environments. Several excellent reviews have covered synthetic [126], biochemical [127], neurobiological [122] and biomedicinal [128] applications of photoresponsive caged compounds during the past decade.

Phototriggered release of biomolecules through caged compounds was first shown by Kaplan et al. in 1973 by the synthesis of a photolabile 2-Nitrobenzyl-protected ATP [129]. The protected phosphate tail effectively hinders any enzymatic ATP hydrolysis until its photorelease induced by 340 nm light (Figure **51**). After this ground-breaking work, 2-Nitrobenzyl derivatives have become the most common photolabile protecting groups in synthetic biochemistry. Over 40 nitrobenzyl protected biochemicals are now commercially available.

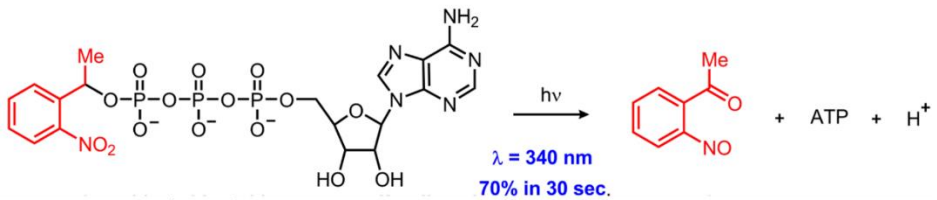

42

Figure 51. Photolysis reaction of nitrobenzyl-Caged ATP.

Commercially available Nitrobenzyl based caged calcium compounds are the most known phototriggers in the literature. Calcium is an important regulatory ion in physiological chemistry, playing important roles in signal transduction. Photolabile chelators that release Ca^{2+} upon irradiation are used to elucidate the role of this important second messenger in cellular processes such as muscle contraction and synaptic transmission [130]. When the commercial complex NP-EGTA Ca^{2+} is irradiated with UV light, the complex affinity to calcium ion decreases by 12,500 fold.

Another complex, DMNP-EDTA, demonstrates a 600,000-fold lower affinity (Figure **52**) [131].

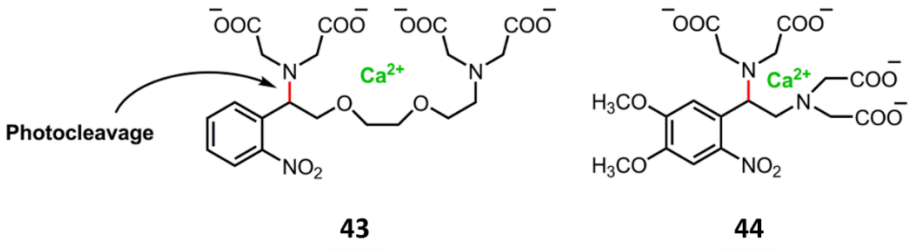

Figure 52. Commercial caged Ca(II) probes: NP-EGTA (left), DMNP-EDTA (right).

Recent developments in cell biology indicate that zinc ions also play a role as second messengers. Yamasaki et al. reported that the release of free zinc for intracellular signaling is controlled by modulating length of the time and intensity of immunoglobin E receptor-based signaling, which demonstrates its role as a second messenger [132]. The desire to probe the biological functions of zinc ions has guided the design of caged zinc ion compounds which provide spatiotemporal control of zinc release in different physiological conditions. One representative example was introduced by Burdette et al. [133], where the photolabile Nitrobenzyl derivative is used to study the release profile of Zn (II) ions (Figure **53**).

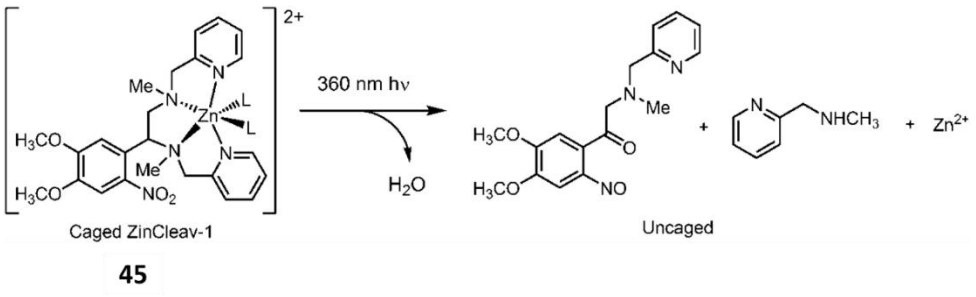

Figure 53. Photolabile caged Zn(II) ion compound ZinCleave-1.

These compounds, all still require high energy excitation at 360 nm or shorter wavelengths for the cleavage of covalent unit. However, the known fact that UV light induces DNA damage, limits the potential biological applications for these caged compounds, especially in the case of in vivo studies.

As an alternative to Nitrobenzyl based photoresponsive groups, coumarin derivatives have been used as photolabile protecting agents. These coumarin based cages can be cleaved by visible irradiation (400-450nm) [134], and their absorptions can be tuned by installing appropriate substituents on the coumarin skeleton. However, especially during in vivo studies, incident radiation within the red to near IR range (660-900nm) is most desired, because light in 660-900 nm range better penetrates into tissue [135] which is mentioned also previous chapter. New methods that use less detrimental, lower energy light in this range would be powerful tools in the development of caged compounds for in vivo studies.

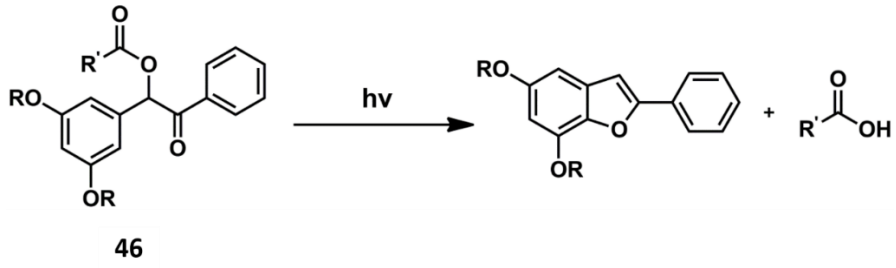

46

Figure 54. Photolysis and release of caged species from the typical 3',5'-dialkoxybenzoin structure to yield 2-phenylbenzofuran derivative and a carboxylic acid. Alcohols, amines, phospates and carbonates can also be liberated using this approach.

Recently, multiphoton excitation with near-IR light has been presented as a practical solution to the aforementioned issues [136]. While this technique seems to be very promising in terms of in vivo applications, unfortunately, many caging molecules do not have sufficient multiphoton absorption cross sections to be susceptible to near-IR pulsed lasers. This brings specific limitations to the successful use of this technique on photocleavable caged compounds. One illustrative example is the 3', 5'-dialkoxybenzoin cage, which is one of the most commonly utilized classes of multiphoton active photocages (Figure **54**) [137]. All esters, carbonates, and phosphates can be employed for photorelease from this caging unit. An efficient release (>95%) usually observed when subjected to short laser pulses. More importantly, the photorelease does not generally lead to side reactions, 5, 7-dialkoxy-2-phenylbenzofuran is the only generated species apart from the liberated species.

1.10. Molecular Logic Gates

1.10.1. Boolean Algebra

In 1847, the book whose name is "The Mathematical Analysis of Logic" was published by George Boole [138]. "Boolean Algebra" which is called also Boolean logic first introduced within this writing. It is a branch of algebra and the variables are true and false, which are represented with 1 and 0. George Boole said in 1854 [139], almost 125 years ago from today: "I am fully assured, that no general method for the solution of questions in the theory of probabilities can be established which does not explicitly recognize, not only the special numerical bases of the science, but also those universal laws of thought which are the basis of all reasoning, and which, whatever they may be as to their essence, are at least mathematical as to their form."

Today, Boolean logic is basic for the digital electronics and programming languages. The device, which perform Boolean logics is called a logic gate. A computer includes integrated circuits (ICs), which are built up by logic gates. A logic gate operates data by using Boolean functions and forms an output from one or more inputs. In an electronic devices, binary logic is used to process electronical signals that carry information. Every input and output must be true (1) or false (0) in binary logics which means electronically high or low voltage. Simply, a computer consists of silicon circuitry, binary logic to operate information and data, which consists of ones and zeros [140].

Boolean logic functions are formed by 16 operations. The most common functions are AND, OR, XOR, NAND, NOR, and XNOR in digital systems. NOR, NAND and XNOR reverse functions of OR, AND and XOR respectively.

INPUTS		OUTPUTS					
A	**B**	**OR**	**AND**	**XOR**	**NOR**	**NAND**	**XNOR**
0	0	0	0	0	1	1	1
1	0	1	0	1	0	1	0
0	1	1	0	1	0	1	0
1	1	1	1	0	0	0	1

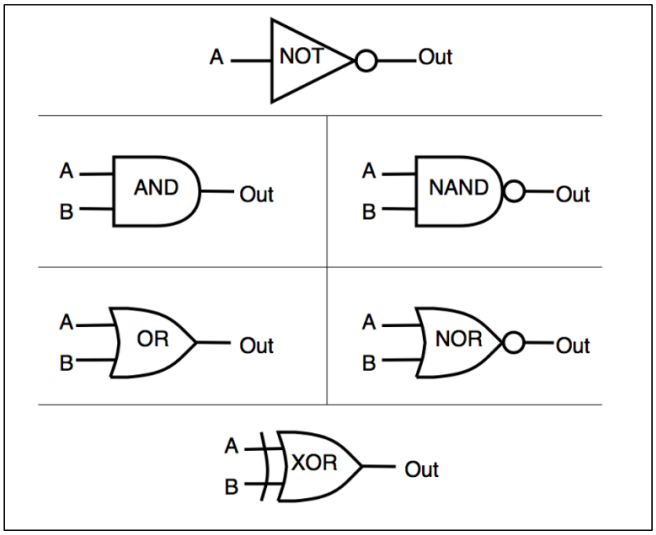

Figure 55. Schematic drawings and truth tables for common logic gates.

AND logic gate states that the output is 1, only in the case of both input is 1, otherwise output is 0. If at least one of the input is 1, the output is 1 in the OR gate. For the XOR gate, same inputs give 0 as the output, otherwise the output is 1. In the NAND, NOR and XNOR gates, the results are reverse of the AND, OR and XOR logic gates.

A basic logic gate can operate a simple function but very complex applications are being performed in the digital devices today. The question is how can they do it? By the integration of these 16 logic gates, many complex operations can be carried out in the devices. For example, a calculator which is almost the simplest device can perform many complex mathematical operations such as logarithm, taking derivative, integral, etc.

In electronic devices, most critical component is a semiconductor material which is called a transistor. Transistor can amplify or reduce the electrical signals and by this way it determines the output as 1 or 0 [141]. There are so many transistor which are

connected each other particularly in a computer chip. These chips conduct hard-core processes such as computer games which are massively detailed programs.

1.10.2. Molecular Logic Gates

A chip consists of millions of transistor and a computer includes a lot chips, therefore miniaturization, which means making on smaller scale is very important in recent days. Miniaturization makes the digital devices better in terms of performance, cost and size. However, it will not continue forever because of the physical and technological barriers. According to Moore's Law [142] which was defined by Intel co-founder Gordon Moore, miniaturization comes to an end in around 2020. Therefore, alternative possibilities are required to develop the technological devices. Recently, scientists considered alternative ways for digital information operating.

It is discussed in in previous chapter that, traditional data processing consists of silicon circuitry, binary logic for information processing and data transported with electrical signals. However, the inputs can be different from the electrical signals. Chemical and optical inputs are possible to be operated in binary logic. Today, designed molecules that is called "molecular logic gates" can operate the inputs like a logic gate. Molecular logic gates have a significant superiority against the silicon based logic gates, the advantage is they are significantly smaller. Therefore, molecular logic gates are up-and-coming alternatives to developed silicon based digital device.

The short history of molecular logic started with de Silva in 1993 [27]. He reported a molecule which operates inputs as AND gate. Compound **47** has two receptor parts which are selective for Na^+ ion and proton. This molecule is fluorescent only in the case of binding with not only Na^+ cation but also a proton, otherwise, the fluorescence is quenched by PET mechanism. That molecule is AND logic gate whose inputs are Na^+ ion and proton, the output is fluorescence emission.

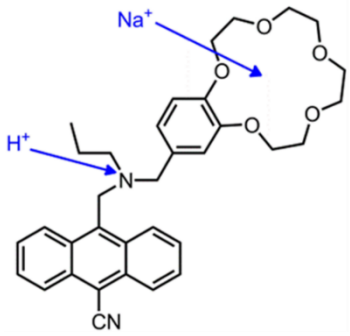

47

In1 (Na^+)	In2 (H^+)	Output (F. Intensity)	Q. Yield	F. Enhancement
0	0	0	0.011	1.0
1	0	0	0.020	1.8
0	1	0	0.013	1.2
1	1	1	0.068	6.2

Figure 56. Literature example for AND molecular logic gate.

Another example is again molecular AND gate by de Silva [143]. In this example, two PET based receptor is attached fluorophore which is anthracene. The output emitted light is above the threshold only in the presence of both H^+ and Na^+ ions (Figure **57**).

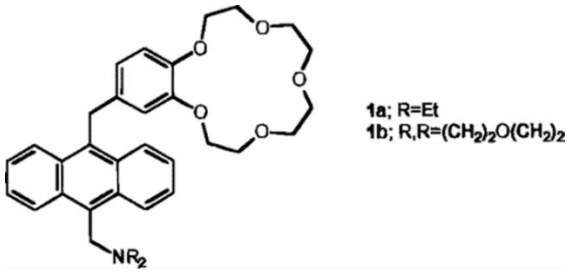

48

Figure 57. The example of AND logic gate by de Silva et al.

Compound **49** [144] is example for XNOR logic gate. In the molecule, there are two recognition sites which cause the ICT. One of them is selective for Ca^{+2} ions and other one catches the protons. The output in this molecular logic gate is an emission at 390 nm. Binding of Ca^{+2} ion causes the blue shift, on the other hand red shift is observed in the existence of H^+ ion. In the presence of both of them, the emission wavelength almost doesn't change. This molecule is also example of XOR logic gate when the output is defined as transmittance at 390 nm.

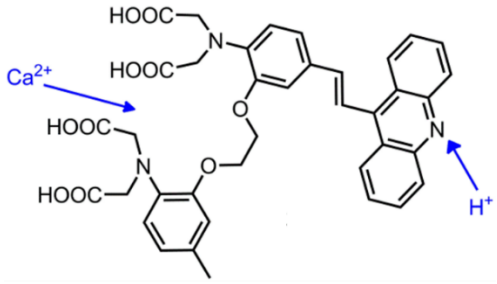

49

Figure 58. An example for XNOR and XOR molecular logic gates.

1.10.3. Higher Functions with Molecular Logic

As it is mentioned before, it is possible to make very complex logic gates by integration of them such as an output of one logic gate can be an input for another. The same situation is available also in molecular logic gates. Combining of several molecular logic gates consist of a logic gate that has higher function such as half adder, full adder, sequential logic, etc.

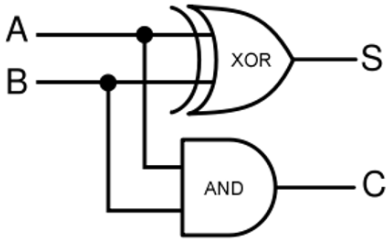

Inputs		Outputs	
A	B	Sum	Carry
0	0	0	0
0	1	1	0
1	0	1	0
1	1	0	1

Figure 59. Half-adder logic gate and its truth table.

Half-adder consist of AND gate and XOR gate which are working simultaneously and it is capable to add two bits. Its structure and truth table is shown in figure **59**. First example for half-adder was designed by Silva [145] who can be described as the "father of the molecular logic". Then, Shanzer et al. published a simple molecule which is mimicking of half-adder logic in 2005 [146]. However, different from their many colleagues, they did in a single molecule. Protonation of fluorescein step by step, brings out the fluorescein molecules which are charged differently and their

spectral properties are also different. In this study, absorption spectrum of fluorescein acts as XOR gate at 447 nm and AND gate at 501 nm (Figure **60**).

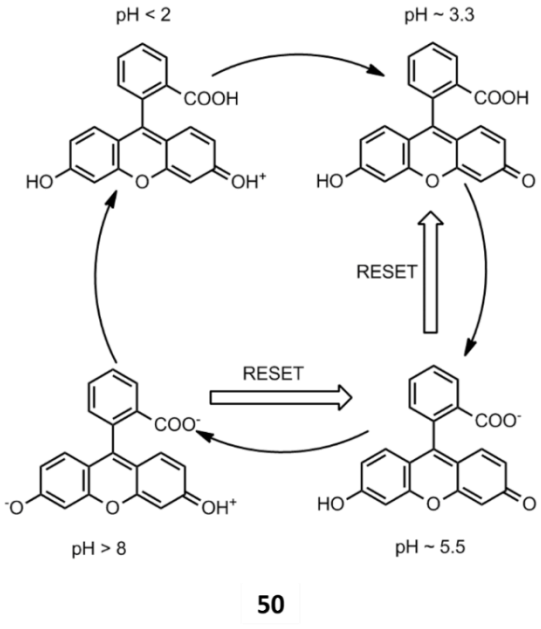

Figure 60. Literature example for half-adder molecular logic gate.

CHAPTER 2

2. Modular Logic Gates: Cascading Independent Logic Gates via Metal Ion Signals

This work is partially described in the following publication which was featured on the front cover of Dalton Trans.:

E. T. Ecik, A. Atilgan, R. Guliyev, **T. B. Uyar**, A. Gumus, E. U. Akkaya, *Dalt. Trans.* **2014**, *43*, 67–70.

2.1. Objective

Systematic cascading of molecular logic gates is an important issue to be addressed for advancing research in this field. We have demonstrated that photochemically triggered metal ion signals can be utilized towards this goal. Thus, independent logic gates were shown to work together while keeping their identity in more complex logic designs. Communication through the intermediacy of ion signals is clearly inspired from biological processes modulated by such signals, and implemented here with ion responsive molecules.

2.2. Introduction

The field of molecular logic gates continue to flourish since the original conception by de Silva [27]. Basic Boolean operators now have a large number of molecular equivalents [147]–[156] with various kinds of inputs and outputs. In addition to combinatorial logic, a few examples of sequential logic appeared as well [157]–[161]. However, some important questions remain and affects the work done in this field. Many in the field are convinced of potential niche applications, most likely in the medical (therapeutic) context [115], [162]–[164]. Even so, advanced functions require advanced level of logic gate cascading. In the digital electronic elements, cascading of gates can be easily handled as the inputs and outputs are both electrical. In chemical logic gates, the input/output heterogeneity is a major problem towards cascading gates. On the other hand, there are many examples of biological signal cascades [165], [166], with messenger molecules, ion signals and metabolic pathways. Thus, it makes most sense to make use of similar intermediary species to link or cascade independent molecular logic gates. Photochemical and reversible H^+ generation has already been applied in a cascading scheme [167].

Metal ion signaling seems especially enticing, considering a multitude of literature examples [121], [125], [133], [168] for "caged" metal ions, and the large variety of possible interactions and diverse set of photonic or chemical signals to be produced as outputs. Such compounds are typically metal ion complexes, which on irradiation with

short wavelength light, undergo a photochemical cleavage reaction, releasing metal ions. The release is due to reduced affinity of the cleaved pieces of the ligand for the metal ions in question. Thus, depending on the factors such as the fluence rate of the irradiation, quantum yield of the photochemical reaction, relative affinities of the ligand and the degradation products for the metal ion, a reproducible ion signal can be generated. Molecular logic gates, even in their earliest conception, were mostly chosen among ion responsive molecules, and their response was typically a change in emission intensity or wavelength.

2.3. Results and Discussion

In a recent work, we reported cascading of logic gates by a chemical reaction [169]. However, for a broadly applicable cascading scheme, the use of metal ions signals looks more promising. Thus, our first cascaded logic gates comprised of the caged zinc (II) compound **1** and dipicolyamine (DPA) substituted Bodipy dye **2**. The ligand used in compound **1**, has minor substitution differences with the previously reported compound [133] (and was synthesized in 6 steps from simpler precursors essentially following the literature procedure [133]). The Bodipy derivative **2** was also synthesized following established protocols [86], [87], [170]–[174] for Bodipy synthesis.

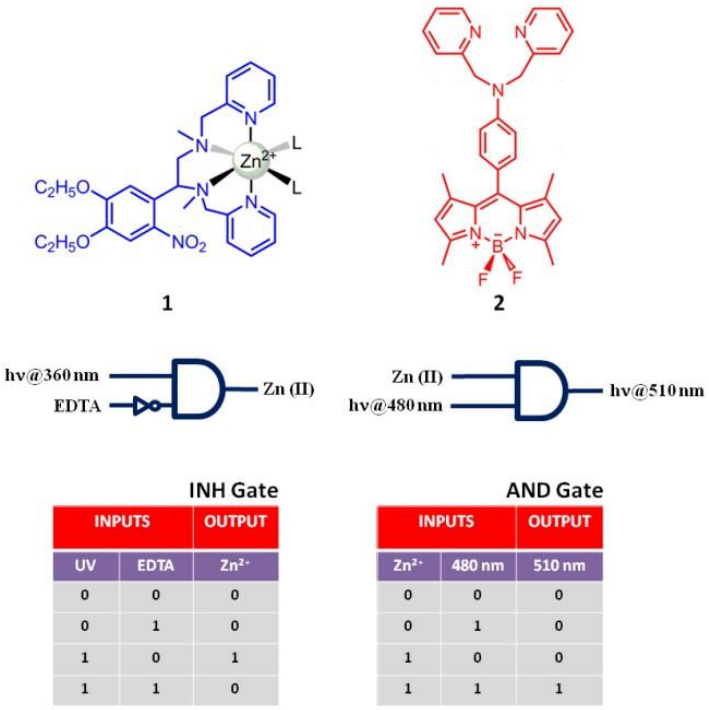

INH Gate

INPUTS		OUTPUT
UV	EDTA	Zn^{2+}
0	0	0
0	1	0
1	0	1
1	1	0

AND Gate

INPUTS		OUTPUT
Zn^{2+}	480 nm	510 nm
0	0	0
0	1	0
1	0	0
1	1	1

Figure 61. Independent INH and AND logic gates. Irradiation of the 10.0 μM solutions of compound 1 in acetonitrile solutions release Zn(II) ions, which are chelated by 2 to generate emission signal.

The Bodipy derivative **2** is weakly fluorescent in acetonitrile solutions. The quenching is widely ascribed to PeT process from the electron rich *meso* substituent [175]–[179]; however in polar solvents, a dark ICT state may play a role as well [26], [180], [181]. Ion binding enhances the emission intensity at 510 nm. On the other hand, EDTA is a non-selective chelator for many metal ions in aqueous and organic solutions.

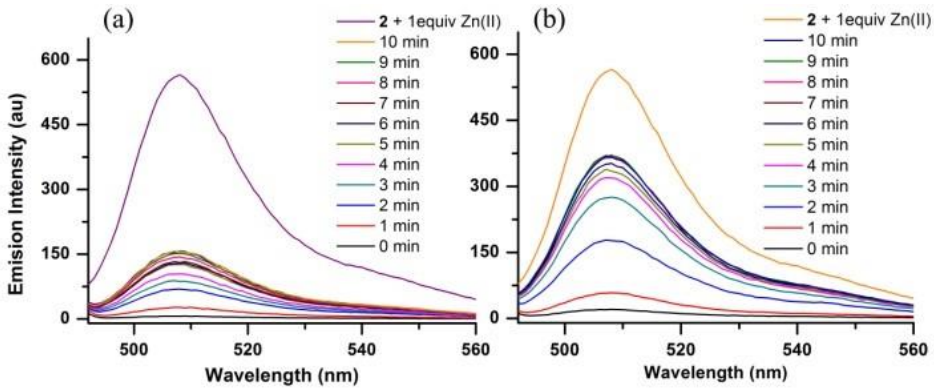

Figure 62. Fluorescence response of compound 2 upon uncaging of (a) 1 equivalent (b) 2 equivalents of cage compound 1 (5.0 μM each) recorded in acetonitrile. Initially compound 2 exhibits no

fluorescence (quenched due to the active PET process), irradiation of the solution at 360 nm resulted in the complete photolysis of 1 which can be followed by the enhanced emission spectrum of compound 2. Highest intensity curves (a-purple, b-orange) represent the maximum emission intensities of 2 which were obtained by the addition of 1.0 equivalent of zinc(II) cations in the form of triflate salt (λ_{ex}=480 nm, slit width=5-2.5).

Using EDTA as an input, we can devise an INH logic gate in a straightforward way (Figure **61**). Here is how that gate works: Irradiation at 360 (input1=1) results in a Zn(II) signal only when EDTA is not present (input2=0) That defines an independently functioning INH gate. Bodipy dye **2**, produces photonic output (emission at 510 nm) only if there are sufficient free Zn(II) ions in solution and if the compound is excited at 480 nm. When the two modular molecular logic gates designed this way are placed in the same solution, the two gates are cascaded, i.e., the output Zn(II) is taken up by the dipicolyl-bodipy which in turn generates green emission if it is also excited separately at 480 nm. Actual implementation is more successful if instead of 1:1 equivalency, more (2 equivalents) caged Zn(II) compound is added (Figure **62**). When both **1** and **2** were added at 5.0 μM concentrations, even at full degradation of the cage, the emission due to **2** is low, this is due to lower amount of Zn(II) release on degradation. At 2 equivalents of the cage compound under the same conditions almost 70% of the fully complexed **2** emission was obtained.

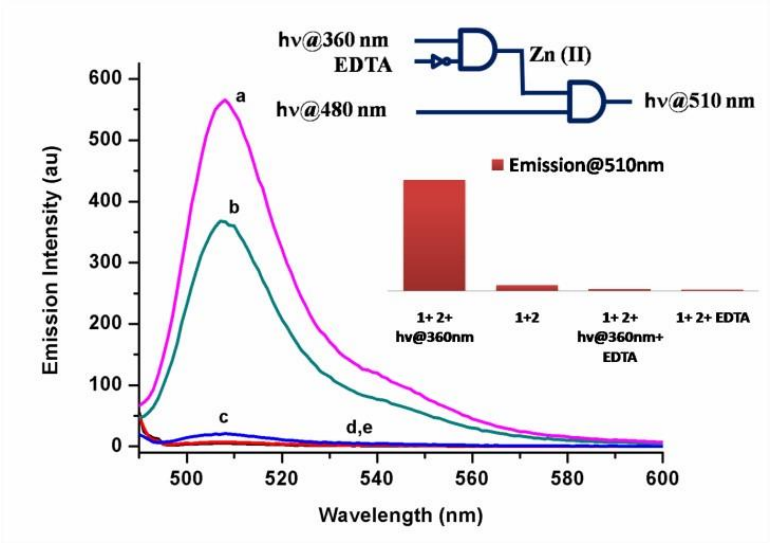

Figure 63. Cascading of the two independent gates INH and AND logic gates. a) The maximum emission intensity of 2 is obtained by the addition of 1 equivalent of zinc(II) triflate salt; b) Irradiation of the 10.0 μM solutions of compound 1 in acetonitrile solutions with 360 nm light releases Zn(II) ions, which are chelated by 2 (5.0 μM) to generate a very strong emission at 510 nm when irradiated at 480 nm; c) 1+2; d) 1+2+EDTA; e) The presence of EDTA (5.0 μM), reduces the available free Zn(II) significantly, with an expected result of negligible emission from the Bodipy dye.

Thus, in the optimal implementation of cascaded INH-AND logic modules, the solution initially contains 10.0 μM cage-compound **1** (INH module), 5.0 μM compound **2** (AND module). The cascaded gate response is strong, with a very large increase in the emission intensity at 510 nm (Figure **63**).

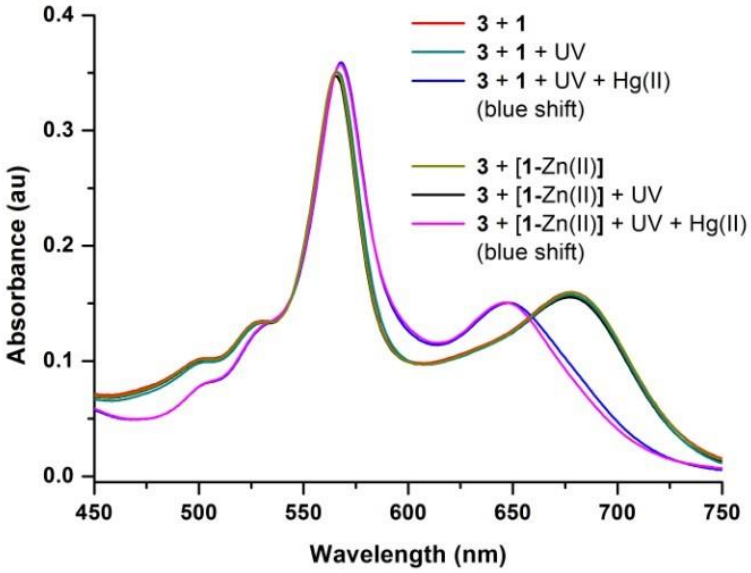

Figure 64. Absorbance spectra of compound 3 (3.0 μM) recorded in acetonitrile, in the presence of compound 1 and Hg(II) cations (3.0 μM, 18.0 μM, respectively). Also note that [1-Zn(II)] refers to the caging ligand alone, i.e., without the Zn(II) ions.

Encouraged by the success of the logic gate implementation, we wanted to demonstrate that higher order cascading is also possible (Figure **65**). We previously reported a through space energy transfer coupled AND logic gates [169]. The energy transfer, at the concentrations used in the study becomes possible only if the two AND logic gate modules are chemically tethered. This is to say that compound **3** can be viewed as two AND logic gates cascaded by chemical reaction. As the primary AND gate module in compound **3** is a dipicolylamine-derivative, we wanted to couple this AND-AND cascade which was shown to function independently previously, with photochemically released Zn(II) signal. The energy transfer between the AND-AND module is only possible when Hg(II) ions are added as well; this causes a blue shift in the absorbance spectrum increasing the spectral overlap, and hence the efficiency of through space energy transfer (Figure **64**). The absorbance band of the distyryl-Bodipy compound shows a hypsochromic shift of 40 nm on binding of the mercuric ions. Strong red emission from the AND-AND cascade also contingent upon the release of Zn(II), which blocks the PeT quenching operational in the meso-dipicolyaminophenyl substituted Bodipy unit.

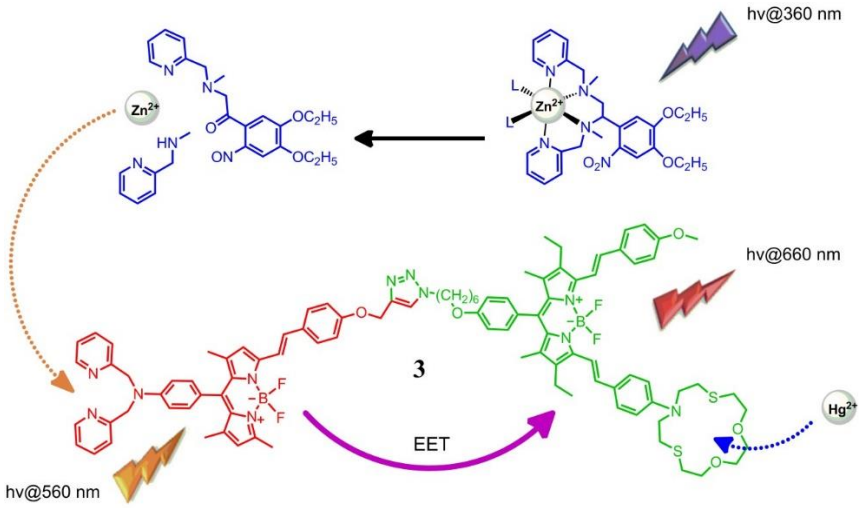

Figure 65. Cascaded logic modules.

In the figure 65, the Bodipy dye on the left is weakly emissive due to PeT. On Zn(II) ion complexation, one or more non-radiative pathways become inoperative. Excited state energy is then transferred to the longer wavelength distyryl-Bodipy. This dye becomes strongly emissive only if the energy transfer is possible and Hg(II), in addition to Zn(II) is made available in the solution, The result is AND-AND cascade. Photochemical generation of zinc ions in turn, incorporate the first gate as well, resulting in INH-AND-AND cascade.

The use of selective ligands minimize any chances for crosstalk between the gate inputs in solution. Thus, 3.0 μM solutions of compound **1** and compound **3**, when excited at 360 nm light, set off a sequence of events, which are in accordance with cascaded INH-AND-AND gates.

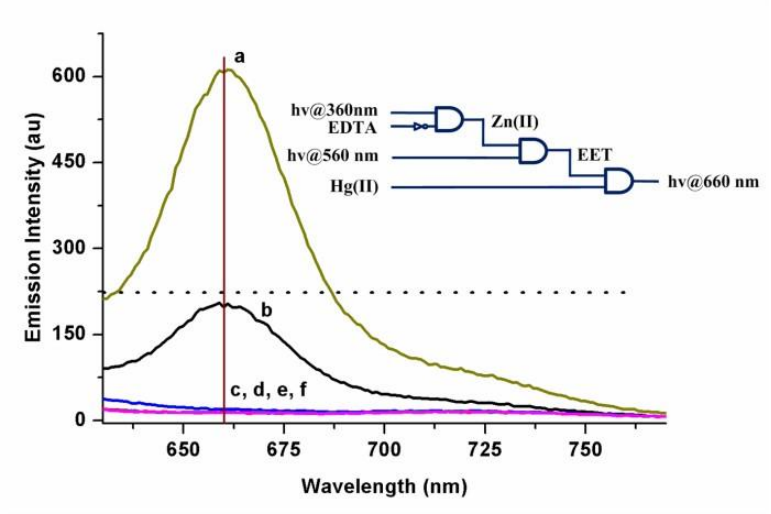

Figure 66. Spectral response of the cascaded INH-AND-AND logic modules: a) Emission spectra of 3 (3.0 μM) in acetonitrile in the presence of 1 and Hg(II) ions (3.0 μM, 18.0 μM, respectively); b) 3+[1-Zn(II)]+Hg(II)+hv@360 nm; c) 3+1+hv@360 nm; d)3+1; e) 3+[1-Zn(II)]+hv@360 nm; f) 3+[1-Zn(II)]. Also note that [1-Zn(II)] refers to the caging ligand alone, i.e., without the Zn(II) ions.

2.4. Conclusion

While we are cognizant of the fact that, chemical analogues of the electronic logic gates do not need follow the same developmental stages, it is clear that advanced information processing at the molecular level will require a set of modular logic gates, which can talk to each other by exchanging inputs and outputs. Some homogeneity in the choice of inputs and outputs will certainly help establishing the modularity of the logic gates. Metal ion signals may be a promising choice. In biological systems, ion signals together with small molecule fluxes, are to a great extent responsible for generating and maintaining nothing less than life itself. Thus, we feel cautiously optimistic that controlled ion fluxes may indeed play an important role in modular assembly of molecular information processors designed and implemented for a particular task in mind.

2.5. Experimental Details

All chemicals and solvents purchased from Sigma-Aldrich were used without further purification. Spectra of ^{1}H NMR and ^{13}C NMR were recorded using a Bruker DPX-400 in $CDCl_3$ with TMS as internal reference. Splitting in the spectra are shown as s (singlet), d (doublet), t (triplet), q (quartet), m (multiplet), dd (doublet of doublet), and br (broad).

Absorption spectrometry was performed using a Varian spectrophotometer. Steady state fluorescence measurements were conducted using a Varian Eclipse spectrofluorometer. Column chromatography of all products was performed using Merck Silica Gel 60 (particle size: 0.040–0.063 mm, 230–400 mesh ASTM). Reactions were monitored by thin layer chromatography using fluorescent coated aluminum sheets. Solvents used for spectroscopy experiments were spectrophotometric grade. Mass spectra were recorded on Agilent Technologies 6530 Accurate-Mass Q-TOF LC/MS. All other reagents and solvents were purchased from Aldrich and used without further purification.

Compounds **1** [182], **2** [183], **16** [148] and **17** [169] were synthesized according to literature.

Synthetic Pathway:

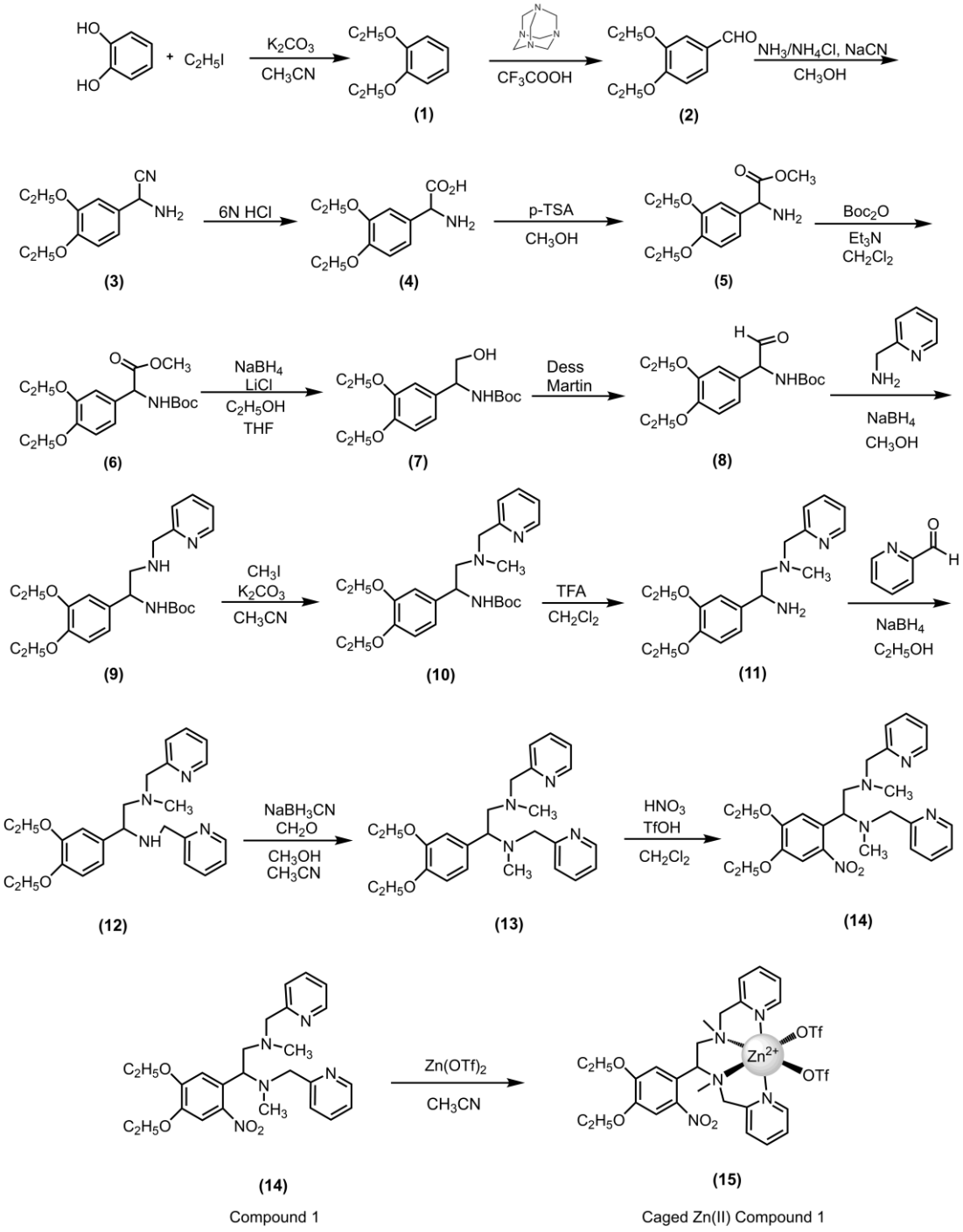

Synthesis of Compound 1

Catechol (10 g, 90 mmol) and ethyl iodide (22 mL, 43 g, 273 mmol) were dissolved in CH_3CN (150 mL) in a 500 mL round-bottomed flask. K_2CO_3 (37.6 g, 273 mmol) and a few crystals of 18-crown-6 were added. The reaction mixture was refluxed for 18 h and followed by TLC (hexane-ethyl acetate 8:1). The reaction mixture was filtered and the CH_3CN was evaporated in vacuo. The crude product was purified by silica gel column chromatography (hexane-ethyl acetate 8:1). Fractions containing compound **1** were collected then the solvent was removed to give white solid (11.5 g, 69.2 mmol, 76%).

^{1}H NMR (400 MHz, $CDCl_3$): δ_H 6.92 (s, 4H), 4.12 (q, J = 7.0 Hz, 4H), 1.47 (t, J = 7.0 Hz, 6H) ppm.

^{13}C NMR (100 MHz, $CDCl_3$): δ_C 148.9, 121.0, 113.9, 64.6, 14.9 ppm.

Synthesis of Compound 2

Compound **1** (10 g, 60 mmol) was dissolved in trifluoroacetic acid (20 mL) in a 100 mL round-bottomed flask. Hexamethylenetetramine (12.6 g, 89.9 mmol) was added. The reaction mixture was refluxed for 12 h and followed by TLC (hexane-ethyl acetate 5:1). Then, the mixture was treated with water and extracted with ethyl acetate. Organic layer was dried with Na_2SO_4 and the solvent was evaporated in vacuo. The crude product was purified by silica gel column chromatography (hexane-EtOAc 5:1) to get brown solid (5.8 g, 30 mmol, 50%).

^{1}H NMR (400 MHz, $CDCl_3$): δ_H 9.82 (s, 1H), 7.44-7.21 (m, 2H), 6.98 (d, J = 8.2 Hz, 1H), 4.25 – 4.05 (m, 4H), 1.50 (dt, J = 9.0, 7.0 Hz, 6H) ppm.

^{13}C NMR (100 MHz, $CDCl_3$): δ_C δ 190.5, 154.0, 148.8, 129.7, 126.22, 111.5, 110.5, 64.3, 64.2, 14.4, 14.4 ppm.

Synthesis of Compound 3 and 4

Compound **2** (5.0 g, 25.8 mmol) were dissolved in MeOH (15 mL) in a 250 mL round-bottomed flask. Sodium cyanide (1.9 g, 38.6 mmol) and ammonium chloride (2.10 g, 38.6 mmol) in NH_4OH (30 mL, 30% w/v) were added to the reaction mixture in a dropwise manner and the reaction mixture was stirred for 23 h at room temperature. The reaction mixture was filtered and the methanol was evaporated in vacuo. Then, it was washed with water and extracted with ethyl acetate. Organic layer was dried with Na_2SO_4 and the solvent was evaporated in vacuo to give brown solid. Crude product (**3**) was used in the next step without further purification. Compound **3** in 6 M HCl (60 mL) was refluxed for 4 h. The solution was concentrated in vacuo. Filtration of the resulting yellow suspension gave compound **4** as a yellow crystalline solid (4.0 g, 17 mmol, 82%).

^{1}H NMR (400 MHz, DMSO-d_6): δ_H 8.71 (s,3H), 7.05 (s, 1H), 6.90 (s, 2H),4.87 (s, 1H), 4.00 – 3.85 (m, 4H), 1.23 (q, J = 7.0 Hz, 6H) ppm.

^{13}C NMR (100 MHz, DMSO-d_6): δ_C 170.4, 149.4, 148.6, 125.71, 121.3, 113.7, 113.6, 64.4, 64.3, 55.7, 15.1, 15.1 ppm.

Synthesis of Compound 5

Compound **4** (4.0 g, 17 mmol) and p-toluenesulfonic acid monohydrate (6.40 g, 33.5 mmol) were dissolved in methanol (50 mL) in 250 mL round-bottomed flask and refluxed for 24 h. The solvent was removed and crude product was dissolved in NH_4OH (30 mL, 30% w/v) then extracted with CH_2Cl_2. Organic layer was dried with Na_2SO_4 and the solvent was evaporated in vacuo. The crude product was purified by silica gel column chromatography (CH_2Cl_2:CH_3OH 100:4). Corresponding fractions were combined then the solvent was evaporated under reduced pressure to yield white solid (3.1 g, 12 mmol, 73%).

^{1}H NMR (400 MHz, $CDCl_3$): δ_H 6.85 – 6.70 (m, 3H), 4.44 (s, 1H), 4.01 – 3.89 (m, 4H), 3.60 (s, 3H), 1.85 (b, 2H), 1.34 (td, J = 7.0, 3.2 Hz, 6H) ppm.

^{13}C NMR (100 MHz, $CDCl_3$): δ_C 174.6, 148.9, 148.6, 132.9, 119.2, 113.5, 112.1, 64.6, 64.6, 58.4, 52.3 ppm.

Synthesis of Compound 6 and 7

Compound **5** (3.1 g, 12 mmol) was dissolved in CH_2Cl_2 (60 mL) in 250 mL round-bottomed flask and triethylamine (1.8 mL, 1.3 g, 13 mmol) and di-tert-butyl dicarbonate (2.8 g, 13 mmol) were added. The reaction mixture was stirred for 23 h at room temperature and followed by TLC using CH_2Cl_2:CH_3OH (100:4). Then, it was washed sequentially with HCl (1 M, 20 mL), sat. $NaHCO_3$ solution (20 mL) and water (20 mL). Organic layer containing compound **6** was dried with Na_2SO_4 and the solvent was evaporated under reduced pressure. Compound **6** (4.0 g, 11 mmol, yellow solid) was used in the next step without further purification.

Compound **6** (4.0 g, 11 mmol) was dissolved in THF (30 mL) in 250 mL round-bottomed flask. After reducing the temperature of the reaction mixture to 0 ^oC, $NaBH_4$ (0.86 g, 22 mmol), LiCl (0.96 g, 22 mmol) and ethanol (20 mL) were added. The reaction mixture was stirred for 23 h at room temperature and followed by TLC using CH_2Cl_2:CH_3OH (100:4). The solvent mixture was evaporated in vacuo and the product was treated with water then extracted with CH_2Cl_2. Organic layer was dried with Na_2SO_4 and the solvent was evaporated in vacuo. The crude product was purified by silica gel column chromatography (CH_2Cl_2:CH_3OH 100:4) to obtain white solid (2.6 g, 8.0 mmol, 70%).

^{1}H NMR (400 MHz, $CDCl_3$): δ_H 6.75 – 6.61 (m, 3H), 5.38 (b, 1H), 4.51 (b, 1H), 4.04 – 3.81 (m, 4H), 3.6 (d, J = 5.8 Hz, 2H), 3.28 (t, J = 5.9 Hz, 1H), 1.28 (t, J = 7.0 Hz, 15H) ppm.

^{13}C NMR (100 MHz, $CDCl_3$): δ_H 156.2, 148.8, 148.1, 132.6, 118.9, 113.7, 112.4, 79.7, 66.3, 64.6, 56.4, 28.3, 14.8 ppm.

Synthesis of Compound 8

To round-bottomed flask containing argon-degassed CH_2Cl_2 (120 mL) were added Dess-Martin periodinane (4.90 g, 11.5 mmol) and Compound **7** (2.5 g, 7.7 mmol). The reaction mixture was stirred for 23 h at room temperature and followed by TLC (CH_2Cl_2:CH_3OH 100:4). The resulting reaction mixture was quenched by adding solution of saturated sodium thiosulfate. Then, it was extracted with CH_2Cl_2. The crude product was purified by silica gel column chromatography (CH_2Cl_2:CH_3OH 100:4). Corresponding fractions were collected then the solvent was removed under reduced pressure to yield yellow solid (2.3 g, 7.1 mmol, 93%).

^{1}H NMR (400 MHz, $CDCl_3$): δ_H 9.43 (s, 1H), 6.85 – 6.64 (m, 3H), 5.65 (b, 1H), 5.14 (s, 1H), 4.11 – 3.92 (m, 4H), 1.35 (t, J = 6.8 Hz, 15H) ppm.

^{13}C NMR (100 MHz, $CDCl_3$): δ_C 195.2, 155.0, 149.4, 149.1, 120.5, 113.8, 112.7, 64.6, 64.5, 64.3, 55.3, 28.3, 14.8, 14.7 ppm.

Synthesis of Compound 9

Compound **8** (2.2 g, 6.8 mmol) and 2-picolylamine (0.9 g, 8.3 mmol) were dissolved in methanol (50 mL) in 100 mL round-bottomed flask and stirred for 6 h at room temperature. After reducing the temperature of the reaction mixture to 0 ^oC, $NaBH_4$ (0. 51 g, 13.6 mmol) was added and the resulting mixture was stirred for 18 h at room temperature. The methanol was evaporated in vacuo. Then, crude product was treated with water and extracted with CH_2Cl_2. Organic layer was dried with Na_2SO_4 and the solvent was evaporated in vacuo. The crude product was purified by silica gel column chromatography (CH_2Cl_2:CH_3OH 100:6). Fractions containing compound **9** were collected and the solvent was removed to give yellow solid (1.7 g, 4.1 mmol, 60%).

^{1}H NMR (400 MHz, $CDCl_3$): δ_H 8.53 (d, J = 4.9 Hz, 1H), 7.63 (td, J = 7.7, 1.8 Hz, 1H), 7.24 (d, J = 7.8 Hz, 1H), 7.16 (ddd, J = 7.6, 5.0, 1.2 Hz, 1H), 6.90 – 6.62 (m, 3H), 5.60 (b, 1H), 4.73 (b, 1H), 4.15 (qd, J = 7.0, 1.8 Hz, 1H), 4.08 (q, J = 4.0 Hz, 4H), 3.88 (d, J = 2.4 Hz, 2H), 2.91 (m, 2H), 1.51 – 1.26 (m, 15H) ppm.

^{13}C NMR (100 MHz, $CDCl_3$): δ_C 159.5, 149.3, 148.8, 147.9, 136.5, 122.2, 121.9, 120.2, 118.5, 113.7, 112.8, 111.9, 64.6, 64.6, 64.5, 54.8, 54.4, 28.4, 11.9, 14.9 ppm.

HRMS (TOF-ESI): m/z calcd for $C_{23}H_{34}N_3O_4^+$: 416.52582 $[M+H]^+$, Found: 416.26336 $[M+H]^+$, Δ=-21.5 ppm.

Synthesis of Compound 10

Compound **9** (1.6 g, 3.9 mmol) and K_2CO_3 (0.8 g, 5.8 mmol) were dissolved in CH_3CN (40 mL) in a 100 mL round-bottomed flask. Methyl iodide (0.55 g, 3.9 mmol) was added to the reaction mixture in a dropwise manner. The reaction mixture was stirred for 5 h at room temperature and followed by TLC (CH_2Cl_2:CH_3OH 100:6). The mixture was filtered and the CH_3CN was evaporated in vacuo. The crude product was purified by silica gel column chromatography (CH_2Cl_2:CH_3OH 100:6) to yield brown solid (1.1 g, 2.6 mmol, 67%).

^{1}H NMR (400 MHz, $CDCl_3$): δ_H 8.59 (d, *J* = 2.3 Hz, 1H), 7.66 (td, *J* = 7.7, 1.8 Hz, 1H), 7.32 (d, *J* = 7.9 Hz, 1H), 7.19 (ddd, *J* = 7.5, 4.9, 1.2 Hz, 1H), 6.88 – 6.65 (m, 3H), 5.90 (b, 1H), 4.62 (b, 1H), 4.07 (qd, *J* = 7.0, 1.6 Hz, 4H), 3.80 (d, *J* = 14.2 Hz, 1H), 3.65 (d, *J* = 14.2 Hz, 1H), 2.73 – 2.50 (m, 2H), 2.34 (s, 3H), 1.43 (td, *J* = 7.0, 2.3 Hz, 15H) ppm.

HRMS (TOF-ESI): m/z calcd for $C_{24}H_{36}N_3O_4^+$: 430.26276 $[M+H]^+$, Found: 430.27953 $[M+H]^+$, Δ=-22.1 ppm.

Synthesis of Compound 11

Trifluoroacetic acid (3.0 mL, 4.8 g, 39 mmol) was added to a solution of **10** (1.0 g, 2.3 mmol) in CH_2Cl_2 (30 mL) and stirred at for 23 h at room temperature. After removing the solvent, saturated K_2CO_3 was added to the reaction mixture, and the product was extracted with CH_2Cl_2. Organic layer containing compound **11** was dried with Na_2SO_4 and the solvent was removed. No further purification was required and brown solid was obtained (0.73 g, 2.2 mmol, 95%).

^{1}H NMR (400 MHz, $CDCl_3$): δ_H 8.54 (b, 1H), 7.66 (t, *J* = 7.7 Hz, 1H), 7.43 (d, *J* = 7.8 Hz, 1H), 7.17 (t, *J* = 6.2 Hz, 1H), 6.95 (s, 1H), 6.91 – 6.75 (m, 2H), 4.08 (q, *J* = 7.0 Hz, 5H), 3.82 (d, *J* = 14.0 Hz, 1H), 3.68 (d, *J* = 14.2 Hz, 1H), 2.79 – 2.42 (m, 2H), 2.34 (s, 3H), 2.13 (b, 2H), 1.44 (t, *J* = 7.0 Hz, 6H) ppm.

^{13}C NMR (100 MHz, $CDCl_3$): δ_C δ 159.4, 149.0, 148.8, 147.9, 136.9, 136.4, 122.9, 121.9, 118.9, 113.6, 112.2, 66.5, 64.7, 64.6, 64.2, 53.0, 42.7, 14.9 ppm.

HRMS (TOF-ESI): m/z calcd for $C_{19}H_{28}N_3O_2^+$: 330.21033 $[M+H]^+$, Found: 330.22473 $[M+H]^+$, Δ=-21.6 ppm.

Synthesis of Compound 12

Compound **11** (600 mg, 1.80 mmol) and 2-pyridinecarboxaldehyde (0.20 mL, 0.23 g 2.2 mmol) were dissolved in methanol (50 mL) in 100 mL round-bottomed flask and refluxed for 2 h at room temperature. After reducing the temperature of the reaction mixture to 0 ^{o}C, $NaBH_4$ (140 mg, 3.6 mmol) was added and the resulting mixture was stirred for 18 h at room temperature. The methanol was evaporated in vacuo. Then, crude product was treated with water and extracted with CH_2Cl_2. Organic layer was dried with Na_2SO_4. The crude product was purified by basic alumina column chromatography (CH_2Cl_2:CH_3OH 100:2). Corresponding fractions were collected then the solvent was evaporated in vacuo to get brown solid (0.46 g, 1.1 mmol, 60%).

^{1}H NMR (400 MHz, $CDCl_3$): δ_H 8.59 – 8.39 (m, 2H), 7.67 (td, *J* = 7.6, 1.8 Hz, 1H), 7.63 – 7.52 (m, 2H), 7.21 – 7.08 (m, 3H), 6.99 (s, 1H), 6.86 – 6.81 (m, 2H), 4.18 – 3.98 (m, 5H), 3.90 – 3.51 (m, 4H), 2.76 (dd, *J* = 12.4, 10.6 Hz, 1H), 2.47 (dd, *J* = 12.4, 3.6 Hz, 1H), 2.25 (s, 3H), 1.44 (td, *J* = 7.0, 4.2 Hz, 6H) ppm.

^{13}C NMR (100 MHz, $CDCl_3$) δ_C 160.2, 159.6, 149.3, 148.9, 148.8, 147.9, 136.4, 136.1, 135.0, 123.0, 122.5, 121.9, 121.7, 120.1, 113.4, 112.6, 65.6, 64.6, 64.5, 63.9, 59.7, 52.7, 42.6, 14.9, 14.9 ppm.

HRMS(TOF-ESI): m/z calcd for $C_{25}H_{33}N_4O_2^+$: 421.25253 $[M+H]^+$, Found: 421.26430 $[M+H]^+$, Δ=-10.3 ppm.

Synthesis of Compound 13

Compound **12** (400 mg, 0.95 mmol) was dissolved in CH_3CN/CH_3OH (15/15 mL) in a 100 mL round-bottomed flask. Formaldehyde (37% in water, 3.1 mL, 3.4 g), $NaBH_3CN$ (180 mg, 2.90 mmol), AcOH (1.2 mL, 1.3 g, 31 mmol) were added and the reaction mixture was stirred for 18 h at room temperature. After the solvent was removed, saturated $NaHCO_3$ solution (10 mL) was added, and the mixture was extracted with CH_2Cl_2. Organic layer was dried with Na_2SO_4 then the solvent was evaporated in vacuo. The crude product was purified by basic alumina column chromatography (CH_2Cl_2:CH_3OH 100:4) to yield brown solid (0.29 g 0.67 mmol, 70%).

^{1}H NMR (400 MHz, $CDCl_3$): δ_H 8.60 – 8.39 (m, 2H), 7.62 (td, *J* = 7.5, 1.9 Hz, 1H), 7.56 – 7.41 (m, 2H), 7.20 (d, *J* = 7.8 Hz, 1H), 7.15 – 7.08 (m, 2H), 6.91 – 6.69 (m, 3H), 4.22 – 3.99 (m, 4H), 3.92 (s, 1H), 3.84 – 3.52 (m, 4H), 3.09 – 2.97 (m, 1H), 2.93 – 2.81 (m, 1H), 2.28 (s, 3H), 2.18 (s, 3H), 1.44 (dt, *J* = 8.6, 7.0 Hz, 6H) ppm.

^{13}C NMR (100 MHz, $CDCl_3$) δ_C 160.5, 159.8, 148.9, 148.3, 147.9, 136.3, 136.3, 132.3, 123.1, 122.8, 121.8, 121.7, 121.4, 114.5, 113.0, 66.0, 64.6, 64.5, 60.6, 60.3, 55.9, 43.1, 39.0, 14.9, 14.9 ppm.

HRMS(TOF-ESI): m/z calcd for $C_{26}H_{35}N_4O_2^+$: 435.26818 $[M+H]^+$, Found: 435.27529 $[M+H]^+$, Δ=0.37 ppm.

Synthesis of Compound 14 (**Compound 1-Zn (II)**)

Trifluoromethanesulfonic acid (0.26 mL, 0.44 g, 2.96 mmol) was dissolved in CH_2Cl_2 (10 mL) and anhydrous HNO_3 (0.080 mL, 0.12 g, 1.5 mmol) was added, which caused a white crystalline solid to precipitate in the solution. After reducing the temperature of the reaction mixture to 0 ^{o}C, Compound **13** (0.16 g, 0.37 mmol) dissolved in CH_2Cl_2 (2 mL) was added in one portion. The reaction mixture was stirred at to 0 ^{o}C, for 2 h and then quickly poured onto 1 g of crushed ice. A saturated solution of $NaHCO_3$ solution (10 mL) was added, and the reaction mixture was extracted with CH_2Cl_2.

Organic layer was dried over anhydrous Na_2SO_4 and the solvent was evaporated in vacuo. The crude product was purified by basic alumina column chromatography (CH_2Cl_2:CH_3OH 100:1). Corresponding fractions were gathered then the solvent was removed to get brown solid (44 mg, 0.090 mmol, 25%).

^{1}H NMR (400 MHz, $CDCl_3$): δ_H 8.61 – 8.33 (m, 2H), 7.62 (td, *J* = 7.7, 1.9 Hz, 1H), 7.51 (td, *J* = 7.7, 1.9 Hz, 1H), 7.40 (s, 1H), 7.34 (d, *J* = 7.8 Hz, 1H), 7.16 – 7.02 (m, 4H), 4.81 (dd, *J* = 8.6, 5.3 Hz, 1H), 4.21 – 4.11 (m, 2H), 4.10 – 3.96 (m, 2H), 3.86 – 3.51 (m, 4H), 2.98 (dd, *J* = 12.7, 5.3 Hz, 1H), 2.80 (dd, *J* = 12.8, 8.5 Hz, 1H), 2.32 (s, 3H), 2.25 (s, 3H), 1.50 (t, *J* = 7.0 Hz, 3H), 1.44 (t, *J* = 7.0 Hz, 3H) ppm.

^{13}C NMR (100 MHz, $CDCl_3$) δ_C 159.9, 159.3, 151.8, 148.9, 148.7, 146.8, 143.5, 136.4, 136.2, 131.3, 123.1, 122.4, 121.8, 111.9, 109.129, 64.9, 64.7, 60.8, 60.1, 59.4, 43.2, 39.6, 29.7, 14.6, 14.6 ppm.

HRMS(TOF-ESI): m/z calcd for $C_{26}H_{34}N_5O_4^+$: 480.25325 $[M+H]^+$, Found: 480.25847 $[M+H]^+$, Δ=4.25 ppm.

Preparation of Compound 15 (Caged Zn compound 1)

Zinc triflate (3.6 mg, 0.010 mmol) and Compound **14** (4.8 mg, 0.010 mmol) were dissolved in CH_3CN (5 mL) and the reaction mixture was stirred for 12 hours at room temperature.

2.5.1. Additional Information

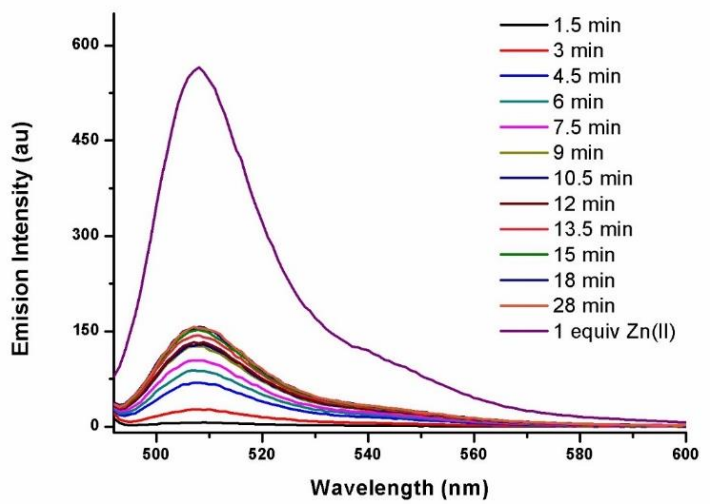

Figure 67. Fluorescence response of compound **16 (Bodipy dye 2**) upon uncaging of cage compound **15 (Caged Zn compound 1) (**5 μM each) recorded in acetonitrile. Initially compound **16** exhibits no fluorescence (quenched due to the active PET process), irradiation of the solution at 360 nm with a 450 W Xe-lamp resulted in the complete photolysis of **15** which can be followed by the enhanced emission spectrum of compound **16**. Purple line represents the maximum emission intensity of **16** which was obtained by the addition of 1 equivalent of zinc(II) triflate cations. (λex=480 nm, slit width=5-2.5).

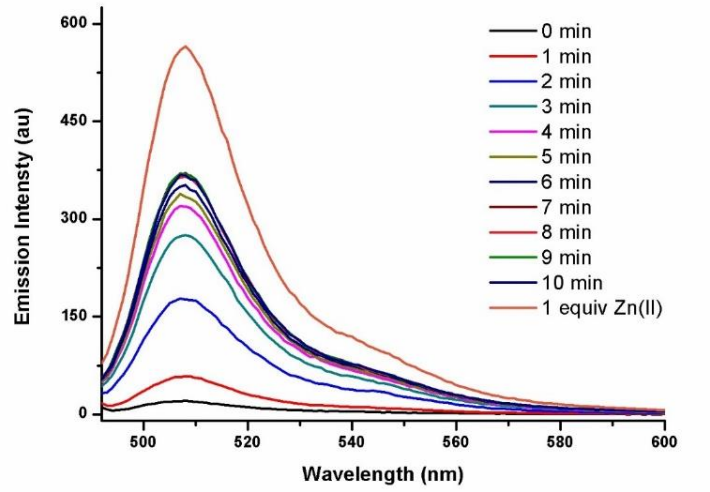

Figure 68. Fluorescence response of compound **16 (Bodipy dye 2**) upon uncaging of 2 equivalents of compound **15 (Caged Zn compound 1),** recorded in acetonitrile. Again orange line represents the maximum emission intensity of **16** which was obtained by the addition of 1 equivalent of zinc(II) triflate cations. (λex=480 nm, slit width=5-2.5).

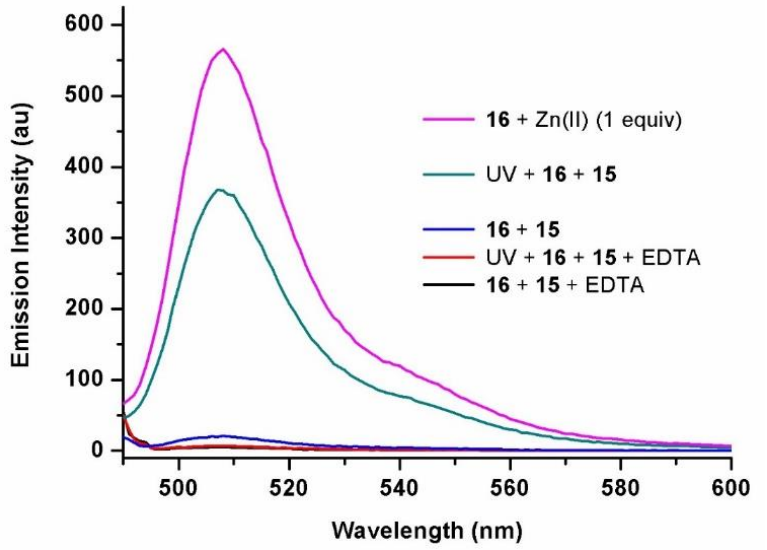

Figure 69. Fluorescence response of compound **16 (Bodipy dye 2**) upon uncaging of 2 equivalents of compound **15 (Caged Zn compound 1)** in the presence of **EDTA** (1 equiv) in acetonitrile solution. (λex=480 nm, slit width=5-2.5).

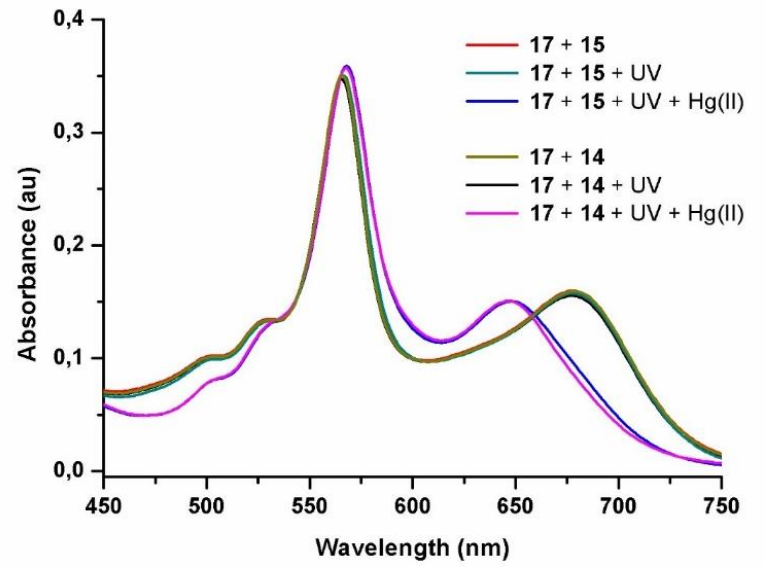

Figure 70. Absorbance spectra of Compound **17 (Compound 3)** (3.0 μM) recorded in acetonitrile, in the presence of compound **15 (Caged Zn compound 1)** and Hg(II) cations (3.0 μM, 18.0 μM, respectively).

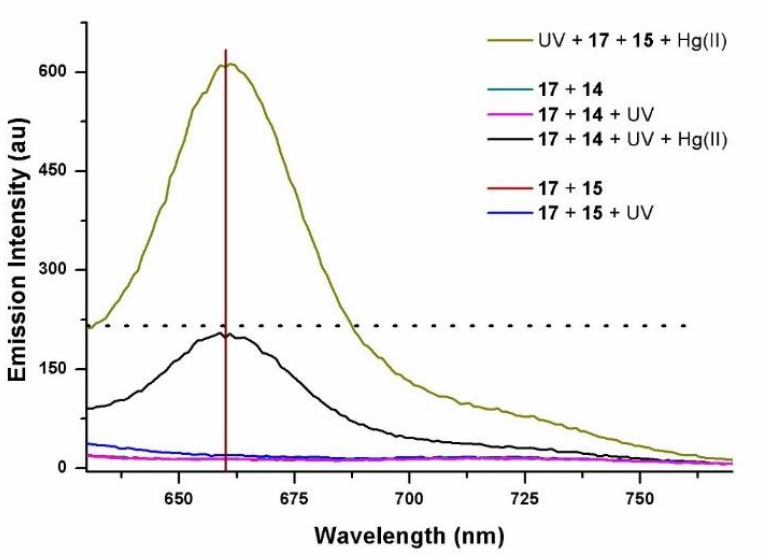

Figure 71. Emission spectra of Compound **17 (Compound 3)** (3.0 μM) in acetonitrile in the presence of compound **15 (Caged Zn compound 1)** and Hg(II) cations (3.0 μM, 18.0 μM, respectively, λex=560 nm, slit width=5-2.5)

CHAPTER 3

3. Near IR Triggered, Remote Controlled Release of Metal Ions: A Novel Strategy for Caged Ions

This work is partially described in the following publication:

A. Atilgan, E. Tanriverdi Eçik, R. Guliyev, T. B. Uyar, S. Erbas-Cakmak, E. U. Akkaya, *Angew. Chemie - Int. Ed.* **2014**, *53*, 10678–10681.

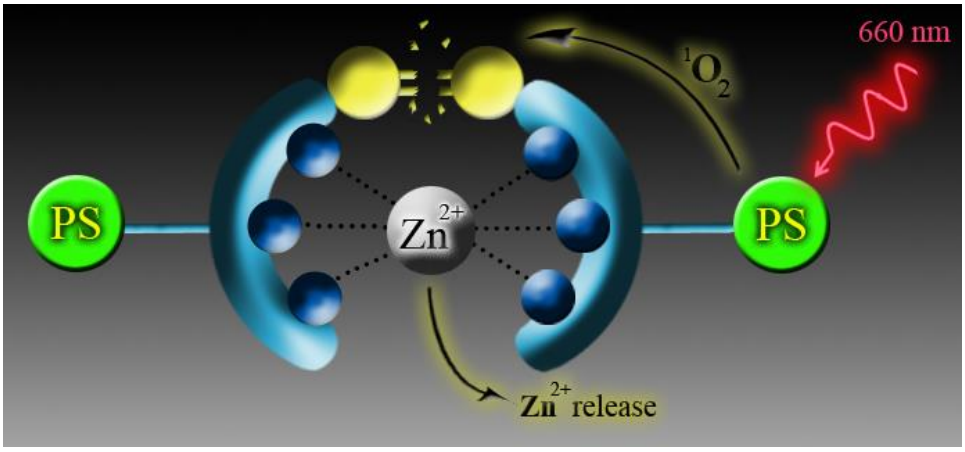

3.1. Objective

A ligand incorporating dithioethenyl moiety is cleaved into fragments of lower metal ion-affinity, on irradiation with low energy red/near IR light. The cleavage is a result of singlet oxygen generation on excitation of the photosensitizer modules. The method has many tunable elements that could make it a satisfactory caging strategy for metal ions.

3.2. Introduction

Remote manipulation of molecular or ionic concentrations at will, especially in well-defined compartments like cells or organelles or even *in vivo* in tissues is very important, as it provides an unparalleled capability to control biochemical processes [132], [184]–[187]. Caged compounds, in principle, carry such a potential [122], [130], [188]–[190]. However, as most uncaging processes involve a covalent bond breaking, there is a very constraining lower limit for the photonic energy of the light to be used for photochemical uncaging [121], [125]. For nitrobenzyl and related moieties it is around 360 nm, for a few others the lower energy/larger wavelength limit can be pushed back to 400-450 nm, with of course a penalty in the form of much reduced reaction quantum yields and diminished conversion efficiencies [133], [191], [192]. Unfortunately, the need for UV or blue light excitations limits the applicability severely, due to potential damage of the light to cells, high scatter and absorption of the light in biological media resulting very poor tissue penetration [193]. The problem can be circumvented by a few techniques; such as two photon excitation, x-ray photolysis or by incorporating upconverting nanoparticles [194]–[202]. All three, have advantages and disadvantages, however it looks like these techniques offer palliative solutions, which may introduce newer limitations/problems of their own (such as toxicity for UCNP, redesign of the cages and limited focal region for the two-photon techniques).

In recent years, a type of cleavage reaction which is dependent on the generation of singlet oxygen through photosensitization of dissolved molecular oxygen is gaining

hold [203], [204]. The process has some common elements with photodynamic action, with one difference, generated singlet oxygen reacts with an electron rich alkene (dialkylthio- or dialkoxy- substituted) in the designed microenvironment, resulting in the cleavage of molecule into two fragments at the location of the electron rich alkene within the molecule [119], [120], [205], [206]. The reaction is known to be efficient, and more to the point, can be driven by light of very low energy in the range of 650-900 nm [207], [208].This can be a tremendous advantage if/when the fragmentation event is to be linked to a biological process.

3.3. Results and Discussion

In our design, we wanted make use of low energy radiation to remotely release biologically relevant metal ions on demand. Zn (II) is a relevant target for caging, as changing concentrations of labile zinc ions are clearly involved in a number of pathological conditions, including the development of prostate cancer and Alzheimer's disease [185], [209]–[211]. However, we wanted to make our design modular so that with minimal changes in the modules, one could change the type of the metal ion to be caged/released and the wavelength of the excitation, all with relatively little price to be paid in terms of synthetic effort.

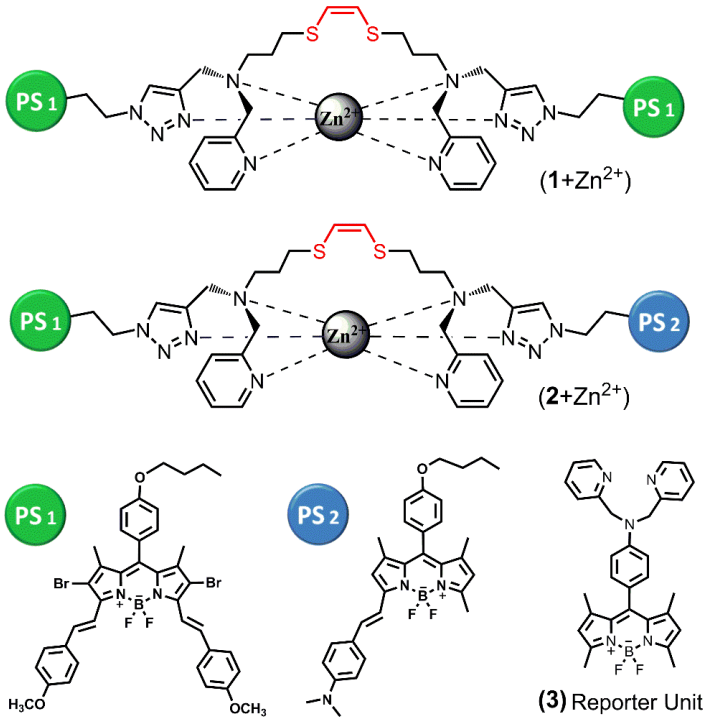

Figure 72. Structures of proposed caged Zn (II) compounds (1 and 2) and the reporter molecule (3). PS denotes the photosensitizer modules.

Our proof of principle design is shown in Figure **72**. We made abundant use of symmetry in the design to make the synthesis as minimally demanding as possible. Thus, brominated di-styryl Bodipy modules with red absorbtion maxima and *meso* azido substituents were prepared. These can be clicked on the specially crafted alkynyl substituted dithioethenyl unit. Zn(II) is expected to preferentially coordinate to the nitrogen donor atoms rather than sulphur donors of the "labile" linker, and the click reaction itself potentially contributes two new N-donor atoms on both sides of the linker (Figure **73**). Here, we have to note that due to the strong inactivation of Cu(I) catalyst by the ligand, standard click reaction conditions proved ineffective. A special Cu(I)-complex developed by Ozcubukcu et al. [212] for such troublesome cases were used with satisfactory results.

In our design, the photosensitizer is an integral part of the cage molecule, not to be added as an external agent. The advantage is obvious in terms of reaction efficiency. In addition, modular design allows freedom in choosing the sensitizer that could

absorb in any region of the spectrum, especially near IR. This choice is independent of the ligand choice and design, which is additional flexibility (Figure **73**).

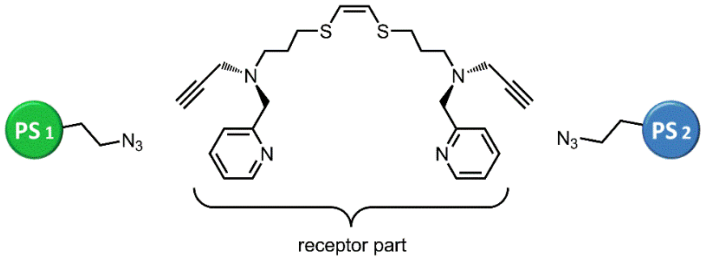

Figure 73. Modular design of the proposed caged compounds.

The ligand, in principle can be designed in different ways, by placing other donor groups, chelators, even carboxylate moieties for alkaline and alkaline-earth cations on the thiol substituents. The current design is expected to work optimally at 660 nm excitation (PS_1). In order to follow the progress of uncaging reaction, or the release of Zn(II) ions, we chose to employ a Bodipy-based fluorescent reporter of zinc (II), with a dipicolylamine ligand (**3**). We have been using this reporter molecule due to its rapid and strong response to increasing zinc concentrations with increasing emission intensity [169]. The strength of the binding of compounds **1** and **2** to Zn(II), and the binding stoichiometry was studied with isothermal titration calorimetry (ITC) by using compound **13** as a model compound. The model compound clearly shows a 1:1 binding stoichiometry, and a binding constant of $2.6x10^5$ M^{-1}. In addition, +2 charged species with the correct e/z ratio was identified for the 1:1 Zn(II) complex (Figure **74**).

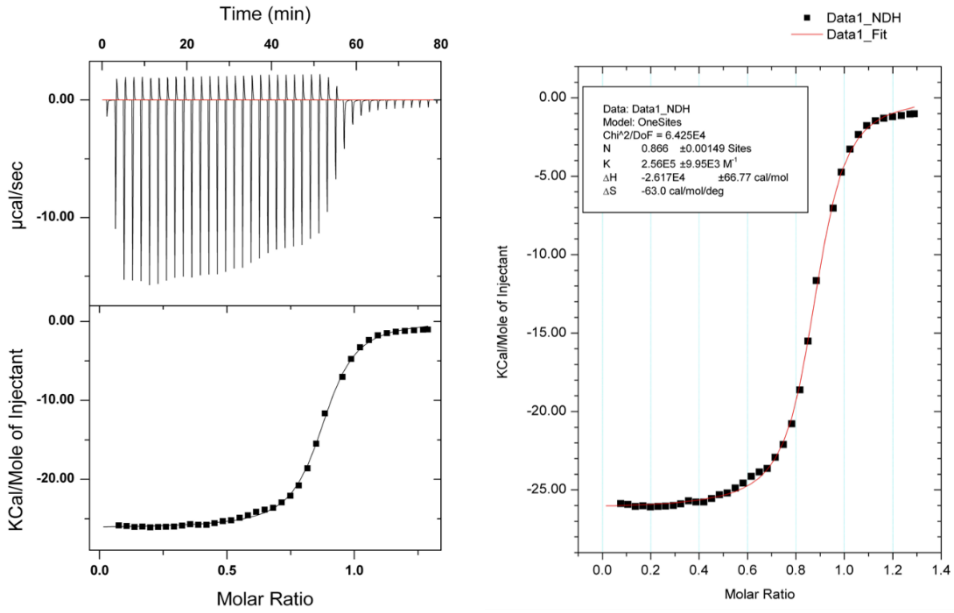

Figure 74. ITC titration curve of compound **13** in acetonitrile shows a clear 1-1 binding to Zn(II). Left: Final figure illustrating the titration of 0.9 mM compound 13 with 5.0 mM $Zn(OTf)_2$, Right: Thermodynamic parameters of interactions are summarized on the inset.

The zinc(II) release process (Figure **75**) starts by the absorption of a photon, in this case, it is a photon of red light (660 nm irradiation). Excited state photosensitizer, due to the presence of intersystem crossing facilitator heavy atoms (in this case, two bromine atoms) rapidly accesses the triplet state. Energy transfer to the dissolved molecular oxygen follows, generating singlet oxygen, which undergoes addition to the double bond creating a reactive dioxetane ring. Thermal opening at room temperature results in the cleavage products. The ligand itself is cleaved into two pieces which will have significantly lower affinity for Zn(II) ions. The net result is a release of metal ions.

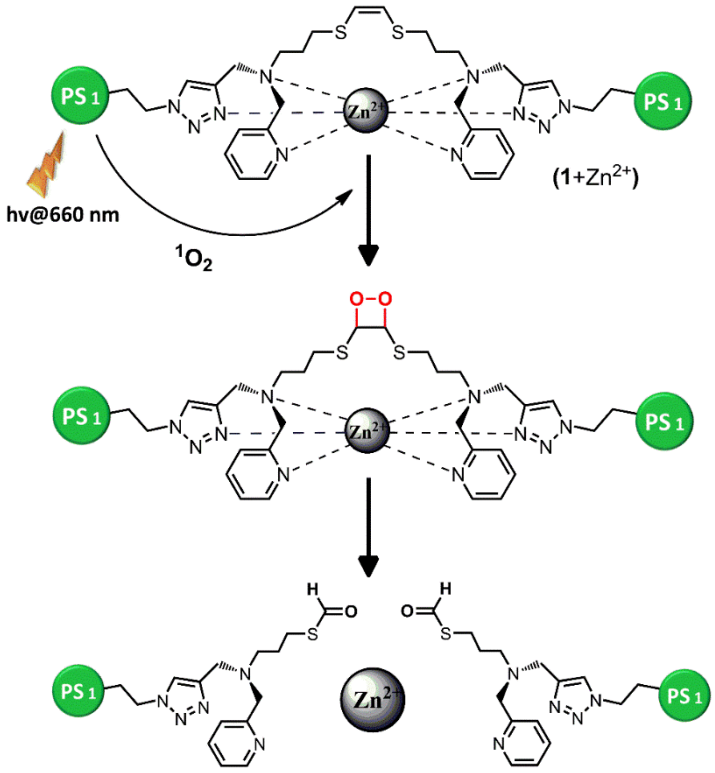

Figure 75. Working principle of the caged Zn(II) compound which can be activated by light of any chosen spectral region; PS: Photosensitizer, hν: Light absorbed by the PS.

Based on the above strategy, the uncaging experiment was then carried out by the irradiation of the caged Zn(II) (prepared by the addition of one equivalent of Zn(II) to the solution of (**1**) in the presence of the reporter molecule (**3**). As the light (filtered broad band white light to remove wavelengths shorter than 400 nm) shines over the solution aliquots were taken at four minute intervals, and the fluorescence of the Zn(II) reporter molecule was determined (Figure **76**).

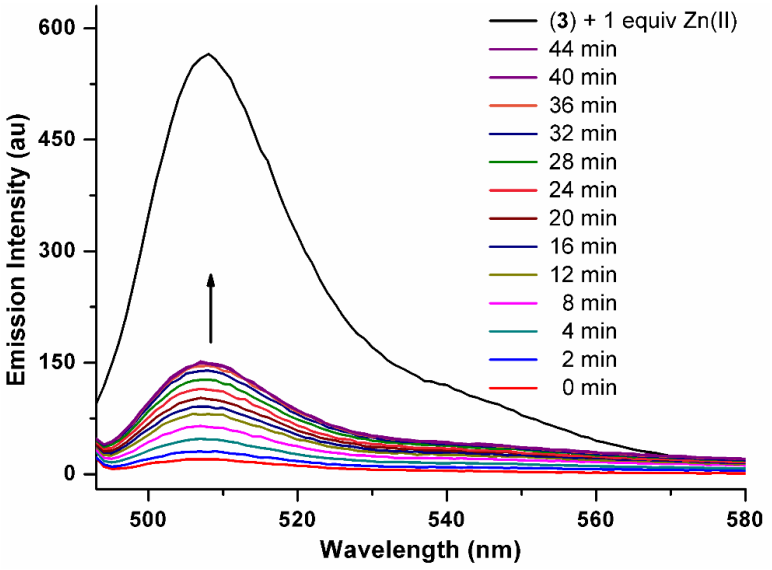

Figure 76. Fluorescence response of compound 3 (DPA-BOD) upon uncaging of 1+Zn(II) (5.0 μM each) in acetonitrile. Irradiation of the solution with the Xe-lamp (λ<400 nm is filtered out) resulted in the photolysis of Zn(II) complex of 1 which can be followed by the increase in the emission intensity due to 3-Zn(II) complex. (λ_{ex}=490 nm). Highest intensity curve represents the maximum emission intensity of 3 (DPA-Bod) which was obtained by the addition of 1.0 equivalent of zinc(II) cations in the form of triflate salt. Time values indicated, correspond to the duration of irradiation with the Xe lamp.

The emission intensity of the probe increased steadily, demonstrating the release of Zn(II) from the cage. Other alternative possibilities that might lead to emission increase at 530 nm were experimentally tested, and eliminated; for example, without irradiation, no change in the emission intensity of the probe is observed, when mixed with the caged Zn(II), attesting to higher affinity of the cage for Zn(II) ions compared to DPA-Bodipy (**3**). Without the probe as well, no emission change around 500 nm was observed when the cage compound was irradiated at 660 nm. Additional control experiments also proved that the singlet oxygen produced on excitation, does not interfere with the generated signal on Zn(II) binding to the reporter compound.

The singlet oxygen quantum yield of the PS_1 was determined to be 0.14, however even this photosensitizer of modest efficiency resulted in impressive uncaging. Replacing this chromophore with a more efficient photosensitizer is clearly expected to generate more effective uncaging cleavage.

We next sought to demonstrate the ability of an energy transfer cassette to affect the uncaging process. To that end, asymmetric compound **2** was synthesized (Figure **72**). Here, shorter wavelength dye, PS_2, with the absorption maxima at 600 nm and larger extinction coefficient is the primary excitation target, and since it does not contain heavy atoms, it is not expected have high intersystem crossing efficiency, but excited state energy transfer (EET) is possible [213]–[216]. When EET takes place to the other chromophore module, because of the bromines on the Bodipy core, singlet oxygen generation takes place. This again leads to the cleavage of the alkene, releasing to lower binding affinity fragments of the orginal ligand, which means uncaging of the Zn(II) to be reported then by the repoter compound **3** (Figure **77**). Using a broadband excitation source, we were able to excite the photosensitizer both directly and through energy transfer, which is expected to yield a higher efficiency in the uncaging process. The proportional increase in emission intensity is higher under these conditions demonstrating that Zn(II) release can be coupled to intramolecular energy transfer, demonstrating that antenna effect can be utilized for more effective uncaging and metal ion release.

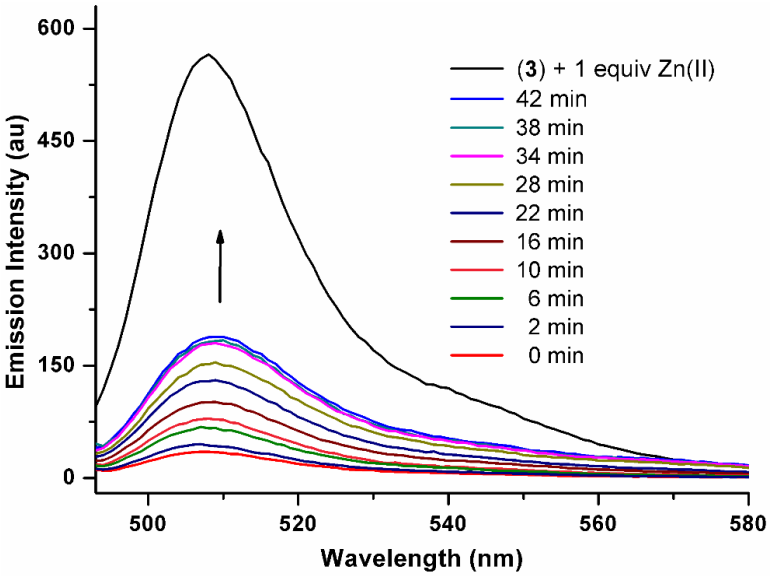

Figure 77. Fluorescence response of compound 3 (DPA-BOD) upon uncaging of 2+Zn(II) (5.0 μM each) recorded in acetonitrile. Initially 3 exhibits low fluorescence (quenched due to the active PET process), irradiation of the solution with the broadband Xe-lamp (λ<400 nm is filtered) resulted in the photolysis of Zn(II) complex of 2 which can be followed by the enhanced emission spectrum of 3

(λ_{ex}=490 nm). Highest intensity curve represents the maximum emission intensity of 3 (DPA-BOD) which was obtained by the addition of 1.0 equivalent of zinc(II) ions in the form of triflate salt. Time values indicated, correspond to the duration of irradiation with the Xe lamp.

The efficiency of the uncaging process was then compared with an established o-nitrobenzyl-containing caged Zn(II) compound [217] (which is structurally similar to a well-studied cage ligand [133]) under the same conditions. When excited at 360 nm, the o-nitrobenzyl caged compounds results in same signal enhancement in the reporter molecule as the symmetric cage (**1+Zn(II)**), but less than the compound **2+Zn(II)** (Figure **78**). In other words, we observed better results in terms of percent Zn(II) release under lower energy irradiation (660 nm), when compared to that of *o*-nitrobenzyl cages under UV irradiation. Percent release, following irradiation can be quantified. The emission peak area for the one equivalent Zn(II) in the presence of the reporter can be set to correspond to 100% free Zn(II) ions. Then, the ratios of the emission peak areas will yield the relative amounts of Zn(II) release. Thus, compound **1+Zn(II)** leads to 31% release, whereas **2+Zn(II)** leads to 40% free Zn(II). Under comparable conditions, that is, when the emission intensity increase has leveled off in acetonitrile, 29% of the o-nitrobenzyl caged zinc compound (Figure **77**) releases its bound Zn(II) ions which are reported by the fluorescent Zn(II) probe. These values do not imply incomplete reactions as some fraction of the Zn(II) may not be available to the reporter compound, due to residual affinity of the cleaved fragments to Zn(II) ions.

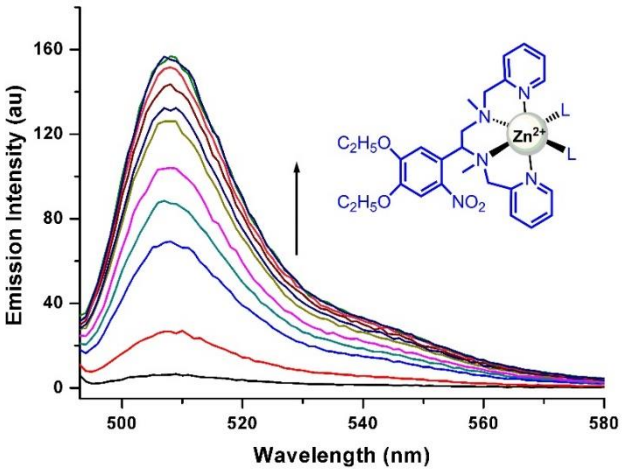

Figure 78. Fluorescence response of compound 3 upon uncaging of one equivalent o-nitrobenzyl Zn(II)-cage (5.0 μM each) recorded in acetonitrile. Initially compound 3 (DPA-BOD) exhibits no fluorescence (quenched due to the active PET process). As the solution was irradiated at 360 nm (for 10 minutes) the increase in the emission intensity levels off, which can be interpreted as the completion of photolysis of the Zn(II)-cage compound.

3.4. Conclusion

In conclusion, we report a novel modular design for caging ligands and red to near-IR triggered uncaging of Zn(II) ions from that cage. This is the first example of metal ion uncaging using more penetrating lower energy red to near IR light without resorting to upconversion, X-rays or two-photon techniques. The potential for biological systems including, model organisms (*in vivo*) is substantial. Further work along that direction may be even expected to yield designer cages for therapeutic applications as well.

3.5. Experimental Details

Isothermal titration calorimetry experiments were performed on iTC-200 microcalorimeter (Microcal Inc., Northampton, MA). All solutions were prepared in spectroscopic grade acetonitrile.

Compounds **1** [119], **2** [218], **5** [172], **Cu-catalyst** [212] and **DPA-Bod dye** [148] were synthesized according to literature.

Synthesis of Compound 1

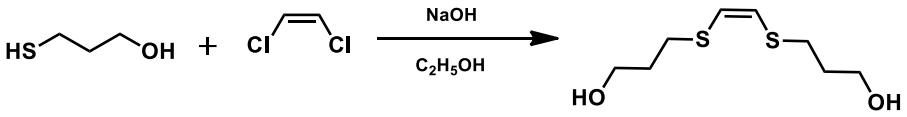

(1)

3-mercaptopropanol (1.8 g, 0.020 mol) and NaOH (0.8 g, 0.02 mol) were dissolved in ethanol (10 mL) was stirred at 0 °C for 30 min. Solution of cis-1,2-dichloroethylene (1 g, 0.01 mol) in EtOH (2 mL) was added dropwise and the reaction mixture was heated at 80 °C for 18 h. Then, it was treated with water and extracted with diethyl ether. Organic layer was dried with Na_2SO_4 and the solvent was evaporated in vacuo. The crude product was purified by silica gel column chromatography (hexane-ethyl acetate 1:4). Fractions containing compound **1** were collected then the solvent was removed to give light yellow liquid (1.5 g, 7.2 mmol, 72%).

^{1}H NMR (400 MHz, $CDCl_3$) δ_H 6.1 (s, 2H), 3.8 (t, J = 6.0 Hz, 4H), 2.8 (t, J = 7.0 Hz, 4H), 2.3 (s, 2H), 1.9 (tt, J = 7.0, 6.0 Hz, 4H) ppm.

^{13}C NMR (100 MHz, $CDCl_3$) δ_C 123.9, 60.9, 32.6, 30.8 ppm.

Synthesis of Compound 2

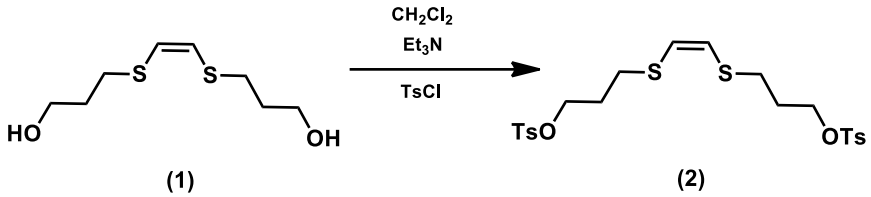

Compound **1** (750 mg, 3.61 mmol) was dissolved in CH_2Cl_2 (15 mL) in 100 mL round-bottomed flask. After, reaction was cooled to 0 ^oC, triethylamine (1.5 mL, 1.1 g, 10.8 mmol) and solution of p-toluene sulfonyl chloride (2.0 g, 11 mmol) in CH_2Cl_2 (5 mL) was added dropwise. The reaction mixture was stirred for 12 h at room temperature. After the extraction, organic layer was dried with Na_2SO_4 and the solvent was evaporated in vacuo. The crude product was purified by silica gel column chromatography (hexane-ethyl acetate 1:1) to yield white solid (1.4 g, 2.7 mmol, 75%).

^1H NMR (400 MHz, $CDCl_3$) δ_H 7.8 (d, J = 8.3 Hz, 4H), 7.4 (d, J = 8.1 Hz, 4H), 5.9 (s, 2H), 4.2 (t, J = 5.9 Hz, 4H), 2.8 (t, J = 6.9 Hz, 4H), 2.5 (s, 6H), 1.9 (m, 4H) ppm.

^{13}C NMR (100 MHz, $CDCl_3$) δ_C 144.9, 132.9, 129.9, 127.9, 123.9, 68.3, 29.9, 29.6, 21.7 ppm.

Synthesis of Compound 3

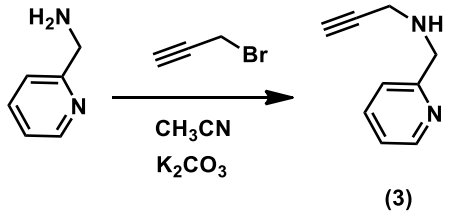

2-picolylamine (1.2 mL, 1.3 g, 12 mmol) and K_2CO_3 (1.6 g, 12 mmol) were dissolved in CH_3CN (10 mL) and stirred for 10 min. Solution of propargyl bromide (0.7g, 6 mmol) in CH_3CN (50 mL) was added dropwise and the reaction mixture was stirred for 12 h at room temperature. Then, the reaction mixture was filtered and the CH_3CN was removed in vacuo. The crude product was purified by silica gel column chromatography (CH_2Cl_2:CH_3OH:Et_3N 100:5:1). Corresponding fractions were

collected then the solvent was evaporated under reduced pressure to give brown solid (0.45 g ,3.1 mmol, 41%).

^{1}H NMR (400 MHz, $CDCl_3$) δ_H 8.5 (d, J = 3.9 Hz, 1H), 7.6 (td, J = 7.7, 1.8 Hz, 1H), 7.3 (d, J = 8.4 Hz, 1H), 7.1 (dd, J = 7.5, 4.9 Hz, 1H), 3.9 (s, 2H), 3.4 (s, 2H), 2.3 (s, 1H), 2.2 (t, J = 2.4 Hz, 1H) ppm.

^{13}C NMR (100 MHz, $CDCl_3$) δ_C 158.9, 149.3, 136.4, 122.4, 122.0, 81.7, 71.7, 53.5, 37.7 ppm.

HRMS (TOF-ESI): m/z calcd for $C_9H_{11}N_2^+$ 147.08785 $[M+H]^+$, Found: 147.08976 $[M+H]^+$, Δ= 13.02 ppm.

Synthesis of Compound 4

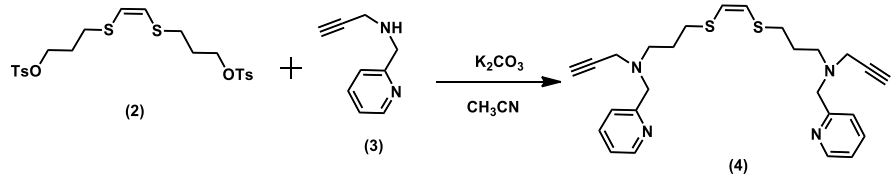

Compound **2** (600 mg, 1.16 mmol) were dissolved in CH_3CN (20 mL) in a 100 mL round-bottomed flask. Compound **3** (375 mg, 2.56 mmol) and K_2CO_3 (450 mg, 4.65 mmol) were added to the reaction mixture and the reaction mixture was refluxed for 18 h. Then, the reaction mixture was filtered and the CH_3CN was evaporated in vacuo. The crude product was purified by silica gel column chromatography (CH_2Cl_2:CH_3OH:Et_3N 100:5:1). Fractions containing compound **4** were collected then the solvent was removed to get brown solid (0.30 g, 0.65 mmol, 56%).

^{1}H NMR (400 MHz, $CDCl_3$) δ_H 8.5 (m, 2H), 7.6 (td, J = 7.6, 1.8 Hz, 2H), 7.4 (d, J = 7.7 Hz, 2H), 7.1 (m, 2H), 6.0 (s, 2H), 3.8 (s, 4H), 3.4 (d, J = 2.4 Hz, 4H), 2.7 (t, J = 7.3 Hz, 4H), 2.6 (t, J = 6.9 Hz, 4H), 2.2 (t, J = 2.3 Hz, 2H), 1.8 (p, J = 7.1 Hz, 4H) ppm.

^{13}C NMR (100 MHz, $CDCl_3$) δ_C 158.9, 149.3, 136.4, 123.5, 123.0, 122.1, 78.3, 73.3, 59.7, 51.9, 42.2, 31.9, 28.1 ppm.

HRMS (TOF-ESI): m/z calcd for $C_{26}H_{33}N_4S_2^+$ 465.2068 $[M+H]^+$, Found: 465.2094 $[M+H]^+$, Δ= 10.07 ppm.

Synthesis of Compound 6

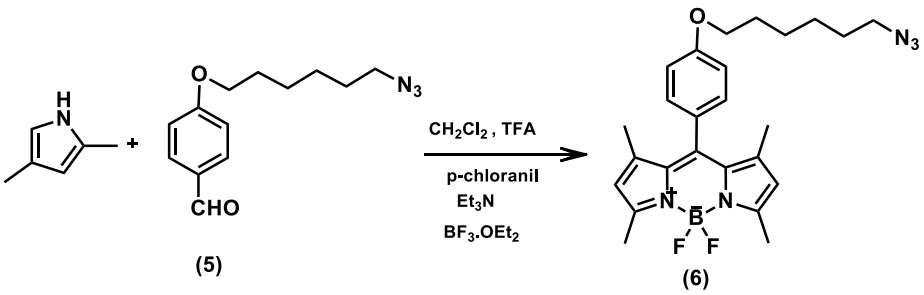

CH_2Cl_2 (300 mL) was purged with Ar for 30 min. 2,4-dimethyl pyrrole (0.46 g, 4.8 mmol) and compound **5** [218] (0.55 g, 2.2 mmol) were added. The color of the solution turned into red after the addition of 3 drops of trifluoroacetic acid. The reaction mixture was stirred at room temperature for 12 h. Then, p-chloranil (0.54 g, 2.2 mmol) was added and the reaction mixture was stirred at room temperature for 45 min. Then triethyl amine (6 mL) and boron trifluoride diethyl etherate (6 mL) were added sequentially. After stirring at room temperature for 30 min, it was washed with water. Organic layer was dried with Na_2SO_4 and the solvent was evaporated under reduced pressure. The crude product was purified by silica gel column chromatography using *n*-hexane-CH_2Cl_2 (1:2) to yield dark red solid (0.31 g, 0.67 mmol, 53%).

^{1}H NMR (400 MHz, $CDCl_3$) δ_H 7.1 (d, J = 8.3 Hz, 2H), 6.9 (d, J = 8.3 Hz, 2H), 5.9 (s, 2H), 3.9 (t, J = 6.4 Hz, 2H), 3.2 (t, J = 6.8 Hz, 2H), 2.5 (s, 6H), 1.8 – 1.7 (m, 2H), 1.6 (p, J = 7.0 Hz, 2H), 1.5 – 1.4 (m, 4H), 1.4 (s, 6H) ppm.

^{13}C NMR (100 MHz, $CDCl_3$) δ_C 159.6, 155.2, 143.1, 141.9, 131.8, 129.2, 126.9, 121.07, 115.0, 67.9, 51.4, 29.1, 28.8, 26.6, 25.7, 14.6, 14.6 ppm.

HRMS(TOF-ESI): m/z calcd for $C_{25}H_{31}BF_2N_5O^+$ 466.34641 $[M+H]^+$, Found: 466.25188 $[M+H]^+$, Δ= 16.21 ppm.

Synthesis of Compound 7

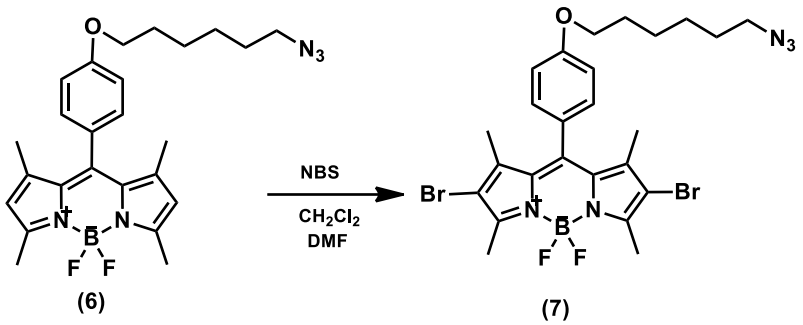

Compound **6** (0.37 g, 0.80 mmol) was dissolved in CH_2Cl_2:DMF (10:2 mL) was stirred for 10 min. Solution of NBS (N-boromosuccinimide) (283 mg, 1.60 mmol) in CH_2Cl_2 (10 mL) was added dropwise and the reaction mixture was stirred for 2 h at room temperature. After the extraction, organic layer was dried with Na_2SO_4 and the solvent was evaporated in vacuo. The crude product was purified by silica gel column chromatography (hexane-CH_2Cl_2 1:1). Corresponding fractions were combined and the solvent was removed to give red solid (0.20 g, 0.32 mmol, 40%).

^{1}H NMR (400 MHz, $CDCl_3$) δ_H 7.1 (d, J = 8.5 Hz, 2H), 7.0 (d, J = 8.5 Hz, 2H), 4.0 (t, J = 6.4 Hz, 2H), 3.3 (t, J = 6.8 Hz, 2H), 2.6 (s, 6H),), 1.9 – 1.8 (m, 2H), 1.7-1.6 (m, 2H), 1.5 – 1.4 (m, 4H), 1.4 (s, 6H).

^{13}C NMR (100 MHz, $CDCl_3$) δ_C 160.1, 153.7, 142.4, 140.6, 130.8, 129.1, 126.2, 115.3, 111.63, 68.0, 51.4, 29.7, 29.1, 28.8, 26.6, 25.7, 13.9, 13.6 ppm.

HRMS (TOF-ESI): m/z calcd for $C_{25}H_{28}BBr_2F_2N_5O^+$ 619.06853 [M^+], Found: 619.07808 $[M]^+$, Δ= -15.43 ppm.

Synthesis of Compound 8

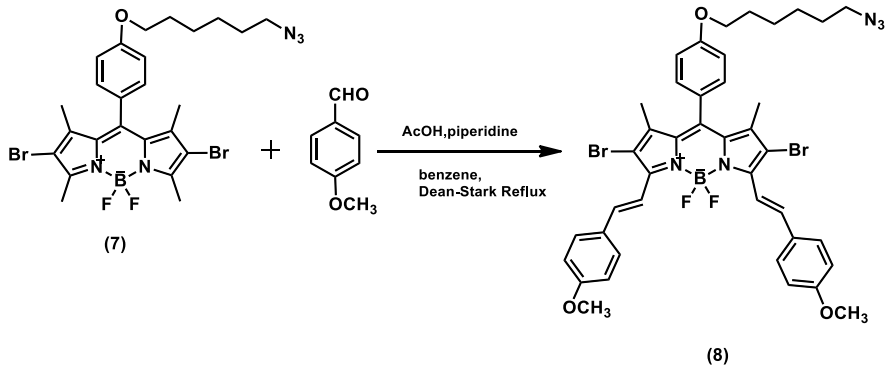

4-methoxybenzaldehyde (61 mg, 0.44 mmol) and Compound **7** (110 mg, 0.180 mmol) were dissolved in benzene (30 mL). Piperidine (300μL) and acetic acid (300μL) were added. The reaction mixture was reflux using Dean-Stark apparatus until all aldehyde was consumed. Then, crude product was treated with water and extracted with CH_2Cl_2. Organic layer was dried with Na_2SO_4 and the solvent was evaporated in vacuo. The crude product was purified by silica gel column chromatography (hexane-CH_2Cl_2 1:2) to obtain purple solid (0.18 g, 0.20 mmol, 42%).

^{1}H NMR (400 MHz, $CDCl_3$) δ_H 8.1 (d, J = 16.6 Hz, 2H), 7.7 – 7.6 (m, 6H), 7.2-7.1 (m, 2H), 7.1 – 7.0 (m, 2H), 6.9 (d, J = 8.8 Hz, 4H), 4.1 (t, J = 6.5 Hz, 2H), 3.9 (s, 6H), 3.3 (t, J = 6.9 Hz, 2H), 1.8-17 (m, 2H), 1.7 (q, J = 7.2 Hz, 2H), 1.6-1.5 (m, 4H), 1.5 (s, 6H).

^{13}C NMR (100 MHz, $CDCl_3$) δ_C 160.8, 160.0, 148.4, 140.9, 139.1, 138.7, 132.4, 129.8, 129.6, 129.3, 126.8, 116.2, 115.3, 114.3, 110.1, 67.9, 55.4, 51.4, 29.7, 29.1, 28.8, 26.6, 25.7, 13.9 ppm.

Synthesis of Compound 9

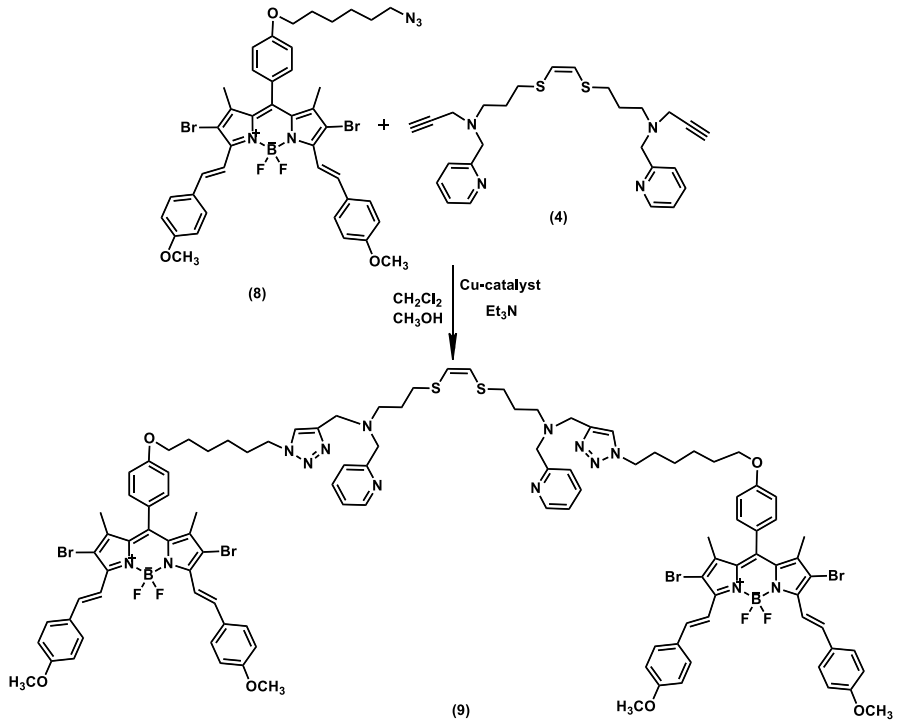

Compound **4** (12 mg, 0.026 mmol) and Compound **8** (50 mg, 0.057 mmol) were dissolved in CH_2Cl_2:MeOH (5:1 mL). Flask was covered with aluminum folio to avoid light and reaction mixture was bubbled with Ar for 15 min. Triethylamine (100 μL) and Cu-catalyst [212] (1%, 0.3 mg) were added and the reaction mixture was stirred for 12 h at room temperature. After the extraction with dichloromethane, organic layer was dried with Na_2SO_4. The crude product was purified by silica gel column chromatography (CH_2Cl_2:MeOH 100:8). Fractions containing compound **9** were collected and the solvent was removed in vacuo to get purple solid (20 mg, 0.0092 mmol, 32%).

^{1}H NMR (400 MHz, $CDCl_3$) δ_H 8.6 – 8.5 (m, 2H), 8.1 (d, J = 16.6 Hz, 4H), 7.7 – 7.4 (m, 16H), 7.5 (d, J = 7.9 Hz, 2H), 7.2 m, 6H), 7.1 – 7.0 (m, 4H), 7.0 – 6.9 (m, 8H), 6.0 (s, 2H), 4.4 (t, J = 7.2 Hz, 4H), 4.0 (t, J = 6.3 Hz, 4H), 3.9 (s, 12H), 3.8 (s, 4H), 3.7 (s, 4H), 2.8 (t, J = 7.3 Hz, 4H), 2.7 (m, 4H), 2.6-2.5 (m, 4H), 2.0-1.9 (m, 4H), 1.9-1.8 (m, 4H), 1.6-1.5 (m, 4H), 1.5 (s, 12H), 1.5 – 1.4 (m, 4H) ppm.

^{13}C NMR (100 MHz, $CDCl_3$) δ_C 160.8, 159.9, 149.3, 149.08, 148.3, 143.9, 141.0, 1389.0, 138.7, 136.5, 136.5, 132.4, 129.8, 129.6, 129.3, 126.8, 123.6, 123.3, 122.1, 116.1, 115.3, 114.3, 110.0, 73.4, 67.9, 59.6, 55.4, 52.2, 50.2, 48.5, 42.2, 31.9, 30.3, 29.0, 26.4, 25.6, 13.9 ppm.

Synthesis of Compound 10

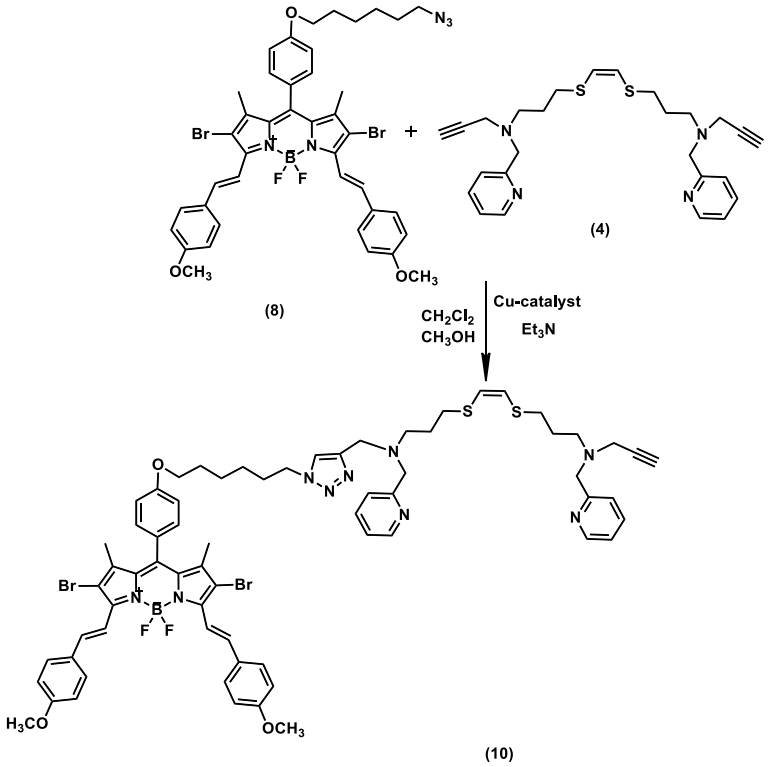

Compound **8** (50 mg, 0.057 mmol) and Compound **4** (265 mg, 0.571 mmol) were dissolved in CH_2Cl_2:MeOH (5:1 mL). Flask was covered with aluminium folio to avoid light and Ar was purged for 15 min. Triethylamine (100 μL) and Cu-catalyst [212] (1%, 3 mg) were added and the reaction mixture was stirred for 48 h at room temperature. After the extraction, organic layer was dried with Na_2SO_4 and the solvent was evaporated in vacuo. The crude product was purified by silica gel column chromatography (CH_2Cl_2:MeOH 100:4) to yield dark blue solid (30 mg, 0.023 mmol, 40%).

^{1}H NMR (400 MHz, $CDCl_3$) δ_H 8.6 (m, 2H), 8.1 (d, J = 16.6 Hz, 2H), 7.7 – 7.6 (m, 8H), 7.5 (d, J = 8.2, 1H), 7.4 (d, J = 7.9, 1H), 7.3 (s, 1H), 7.2 – 7.1 (m, 4H), 7.1– 7.0

(m, 2H), 7.0 – 6.9 (m, 4H), 6.1 (s, 1H), 6.0 (s, 1H), 4.4 (t, *J* = 7.2 Hz, 2H), 4.0 (t, *J* = 6.3 Hz, 2H), 3.9 (s, 6H), 3.8 (s, 4H), 3.4 (d, *J* = 2.4 Hz, 2H), 2.8 (td, *J* = 7.1, 5.8 Hz, 4H), 2.7 (t, *J* = 7.0 Hz, 4H), 2.3 (t, *J* = 2.2 Hz, 1H), 2.0 – 1.9 (m, 2H), 1.9 – 1.8 (m, 8H), 1.7 – 1.5 (m, 2H), 1.5 (s, 6H), 1.4 (m, 2H).

^{13}C NMR (100 MHz, $CDCl_3$) δ_C 160.7, 159.9, 158.9, 149.3, 149.1, 148.3, 140.9, 138.9, 138.7, 136.6, 136.5, 132.4, 129.8, 129.6, 129.3, 129.1, 128.2, 126.8, 123.1, 122.1, 116.1, 115.2, 114.3, 110.0, 78.3, 73.4, 73.3, 67.9, 59.8, 59.7, 55.4, 52.0, 50.2, 48.5, 42.2, 31.9, 30.2, 29.7, 29.1, 28.2, 26.4, 25.6, 13.9 ppm.

Synthesis of Compound 11

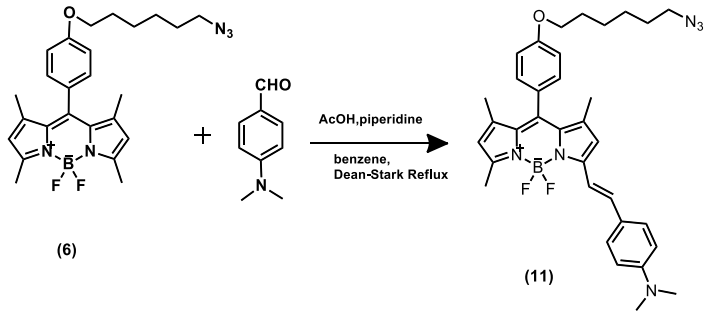

Compound **6** (125 mg, 0.272 mmol) and 4-methoxybenzaldehyde (36 mg, 0.24 mmol) were dissolved in benzene (50 mL). Piperidine (150µL) and acetic acid (150µL) were added. The reaction mixture was refluxed at 110 ^{0}C by using Dean-Stark apparatus until all aldehyde was consumed. Then, crude product was treated with water and extracted with CH_2Cl_2. Organic layer was dried with Na_2SO_4 and the solvent was evaporated in vacuo. The crude product was purified by silica gel column chromatography (hexane-CH_2Cl_2 1:3). Corresponding fractions were collected then the solvent was removed to give blue solid (40 mg, 0.067 mmol, 25%).

^{1}H NMR (400 MHz, $CDCl_3$) δ_H 7.5 (d, *J* = 8.8 Hz, 2H), 7.3 (d, *J* = 14.4 Hz, 2H), 7.2 (d, *J* = 8.5 Hz, 2H), 7.0 (d, *J* = 8.6 Hz, 2H), 6.7 (d, *J* = 8.7 Hz, 2H), 6.6 (s, 1H), 6.0 (s, 1H), 4.0 (t, *J* = 6.4 Hz, 2H), 3.3 (t, *J* = 6.8 Hz, 2H), 3.0 (s, 6H), 2.6 (s, 3H), 1.9 – 1.8 (m, 2H), 1.7 (p, *J* = 7.0 Hz, 2H), 1.6 – 1.5 (m, 4H), 1.50 (s, 3H), 1.46 (s, 3H) ppm.

^{13}C NMR (100 MHz, $CDCl_3$) δ_C 159.5, 154.6, 152.7, 151.0, 142.9, 140.8, 139.1, 137.6, 133.5, 130.6, 129.6, 129.2, 127.3, 124.7, 120.3, 117.6, 114.9, 114.5, 112.0, 67.8, 51.4, 40.2, 29.2, 28.8, 26.6, 25.7, 14.9, 14.6, 14.5 ppm.

HRMS(TOF-ESI): m/z calcd for $C_{34}H_{39}BF_2N_6O^+$ 596.3246 [M^+], Found: 596.3250 $[M]^+$, Δ= -0.67 ppm.

Synthesis of Compound 12

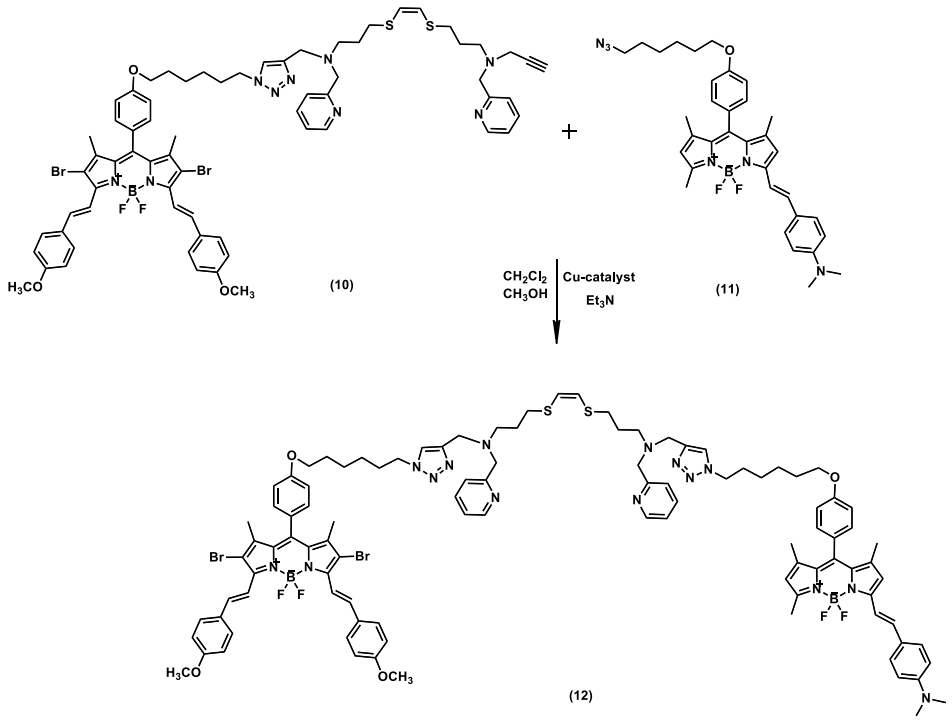

Compound **10** (30 mg, 0.023 mmol) and Compound **11** (20 mg, 0.034 mmol) and were dissolved in CH_2Cl_2:Methanol (5:1 mL). Flask was covered with aluminium folio to avoid light and Ar was purged for 15 min. Triethylamine (100 μL) and Cu-catalyst [212] (0.3 mg) were added and the reaction mixture was stirred for 48 h at room temperature. After the washing with water, organic layer was dried with Na_2SO_4 and the solvent was evaporated in vacuo. The crude product was purified by silica gel column chromatography (CH_2Cl_2:Methanol 100:7) to obtain dark purple solid (23 mg, 53%).

^{1}H NMR (400 MHz, $CDCl_3$) δ_H 8.6 – 8.5 (m, 2H), 8.1 (d, *J* = 16.6 Hz, 2H), 7.7– 7.6 (m, 9H), 7.5 – 7.4 (m, 6H), 7.3 (d, *J* = 16.7 Hz, 2H), 7.2 – 7.1 (m, 6H), 7.1 – 7.0 (m, 2H), 7.0-6.9 (m, 6H), 6.7 (d, *J* = 8.4 Hz, 2H), 6.6 (s, 1H), 6.0 (s, 1H), 5.9 (s, 1H), 4.4 (q, *J* = 6.9 Hz, 4H), 4.0 (m, 4H), 3.9 (s, 6H), 3.8 (s, 4H), 3.7 (s, 4H), 3.0 (s, 6H), 2.8 (t, *J* = 7.2 Hz, 4H), 2.7 (d, *J* = 6.6 Hz, 4H), 2.6 (s, 4H), 2.0-1.8 (m, 12H), 1.6– 1.5 (m, 4H), 1.48 (s, 9H), 1.44 (s, 6H) ppm.

^{13}C NMR (100 MHz, $CDCl_3$) δ_C 160.7, 159.9, 159.4, 154.6, 152.7, 151.0, 149.1, 148.3, 142.9, 141.0, 140.8, 139.0, 138.7, 137.6, 136.5, 133.5, 132.4, 131.6, 130.6, 129.8, 129.6, 129.6, 129.5, 129.3, 129.2, 129.1, 128.7, 128.2, 127.3, 126.8, 124.7, 123.4, 123.3, 122.7, 122.1, 120.3, 117.6, 116.1, 115.2, 114.9, 114.4, 114.3, 114.1, 112.0, 110.0, 67.9, 67.8, 59.7, 55.4, 54.3, 53.4, 52.2, 50.2, 48.4, 40.2, 31.9, 30.3, 29.7, 29.1, 29.0, 27.8, 26.4, 26.3, 25.6, 14.9, 14.6, 14.5, 14.0 ppm.

Synthesis of the reference Compound 13

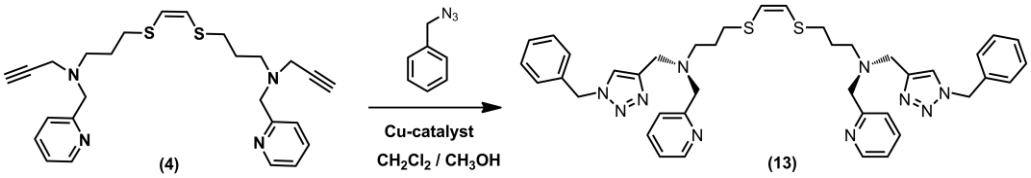

Compound **4** (46 mg, 0.11 mmol) and benzyl azide (29 mg, 0.22 mmol) were dissolved in CH_2Cl_2:Methanol (5:1 mL). Flask was covered with aluminum folio to avoid light and Ar was purged for 15 min. Triethylamine (100 μL) and Cu-catalyst [212] (1%) were added and the reaction mixture was stirred for 12 h at room temperature. After the washing with water, organic layer was dried with Na_2SO_4. The crude product was purified by silica gel column chromatography (CH_2Cl_2:Methanol 93:7). Fractions containing compound **13** were collected then the solvent was evaporated in vacuo to yield brown solid (42 mg, 0.058 mmol, 57%).

^{1}H NMR (400 MHz, $CDCl_3$) δ_H 8.5 (m, 2H), 7.6 (td, *J* = 7.6, 1.8 Hz, 2H), 7.43 (s, 2H), 7.36 (d, *J* = 7.7 Hz, 2H), 7.3-7.2 (m, 6H), 7.2-7.1 (m, 4H) 7.1 (m, 2H), 6.0 (s, 2H), 5.5 (s, 4H), 3.8 (s, 4H), 3.7 (s, 4H), 2.7 (t, *J* = 7.3 Hz, 4H), 2.6 (t, *J* = 6.9 Hz, 4H), 1.8 (p, *J* = 7.1 Hz, 4H) ppm.

^{13}C NMR (100 MHz, $CDCl_3$) δ_C 159.3, 148.9, 144.8, 136.4, 134.9, 129.0, 128.6, 127.9, 123.1, 122.8, 122.0, 59.8, 54.0, 52.2, 48.6, 31.9, 27.9 ppm.

HRMS (TOF-ESI): m/z calcd for $C_{40}H_{46}N_{10}S_2$ $[M+Na]^+$ 753.3241, Found: 753.3204 $[M+Na]^+$, Δ= 4.78 ppm.

Preparation of Zn complex of Compound 4

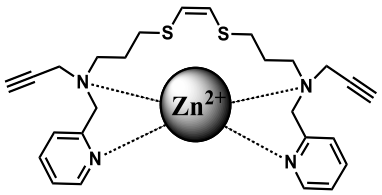

Zinc triflate (3.65 mg, 0.01 mmol) and compound **4** (4.7 mg, 0.01 mmol) were dissolved in CH_3CN (5 mL) and the reaction mixture was stirred for 12 hours at room temperature.

HRMS (TOF-ESI): m/z calcd for $C_{28}H_{33}F_6N_4O_6S_4Zn^+$ (with two counter ions, i.e., 2 triflates) 827.040 $[M+H]^+$, Found: 827.0554 $[M+H]^+$, Δ= -9.83 ppm.

Preparation of Zn complex of Compound 13

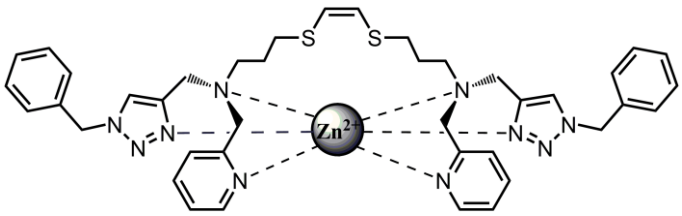

Zinc triflate (3.65 mg, 0.01 mmol) and compound **13** (7.3 mg, 0.01 mmol) were dissolved in CH_3CN (5 mL) and the reaction mixture was stirred for 1 hour at room temperature.

HRMS (TOF-ESI): m/z calcd for $C_{40}H_{46}N_{10}S_2Zn^{2+}$ 397.1314 $[M^{+2}]$, Found: 397.1384 $[M^{2+}]$, Δ= -17.42 ppm.

Preparation of Zn Compound 1

Zinc triflate (0.74 mg, 0.002 mmol) and compound **9** (4.4 mg, 0.002 mmol) were dissolved in CH_2Cl_2 (10 mL) and the reaction mixture was stirred for 12 hours at room temperature.

Preparation of Zn Compound 2

Zinc triflate (0.74 mg, 0.002 mmol) and compound **12** (3.9 mg, 0.002 mmol) were dissolved in CH_2Cl_2 (10 mL) and the reaction mixture was stirred for 12 hours at room temperature.

3.5.1. Additional Information

Singlet Oxygen Measurements:

Singlet oxygen quantum yields (φ_Δ) were calculated according to the literature [219], [220]. The relative quantum yields were calculated with reference to methylene blue (MB) in dichloromethane as 0.57 [220]. Air satutared DCM was obtained by bubbling air for 15 minutes. The absorbance of DPBF was adjusted around 1.0 a.u. in air saturated dichloromethane. Then, the photosensitizer **(8)** was added to cuvette and photosentizer's absorbance was adjusted around 0.1 After, taking some measurements in dark, we exposed the cuvette to monochromatic light at the peak absorption wavelength for 3 minute. Absorbance was measured for several times after each irradiation. The graphics recorded are shown below; Figures 2 to 5. Then, slope of absorbance maxima of DPBF at 414 nm versus time graph for each photosensitizer were calculated. Singlet oxygen quantum yield were calculated according to the equation:

$$\varphi_\Delta (\mathbf{8}) = \varphi_\Delta (\text{ref}) \times [m (\mathbf{8})/m(\text{ref})] \times [F(\text{ref})/F(\mathbf{8})] \times [PF(\text{ref})/PF(\mathbf{8})]$$

where **8** and ref designate 'compound **8**' and 'methylene blue' respectively. m is the slope of difference in change in absorbance of DPBF (414 nm) with the irradiation

time, F is the absorption correction factor, which is given by $F = 1 - 10^{-OD}$(OD at the irradiation wavelength), and PF is absorbed photonic flux (μEinstein dm^{-3} s^{-1}).

φ_{Δ} (**8**) = φ_{Δ} (ref) ×[m (**8**)/m(ref)]×[F(ref)/F(**8**)]×[PF(ref)/PF(**8**)]

φ_{Δ} (**8**) = 0.57 ×[-0.02905/-0.22956]×[1-$10^{-0.1}$)/1-$10^{-0.05}$]×[1)]

φ_{Δ} (8) =0.14

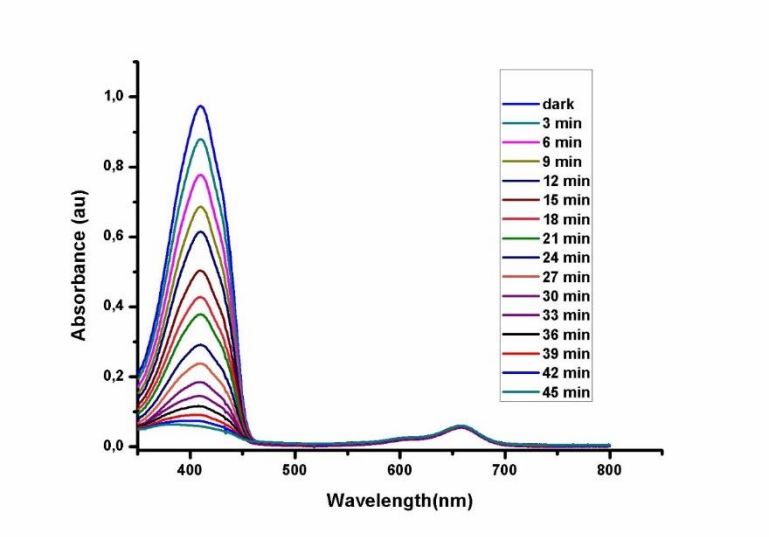

Figure 79. Decrease in absorbance spectrum of trap molecule DBPF in the presence of compound **8** (3μM) in dichloromethane. (λex=660 nm, slit width=14-14, Xe-lamp).

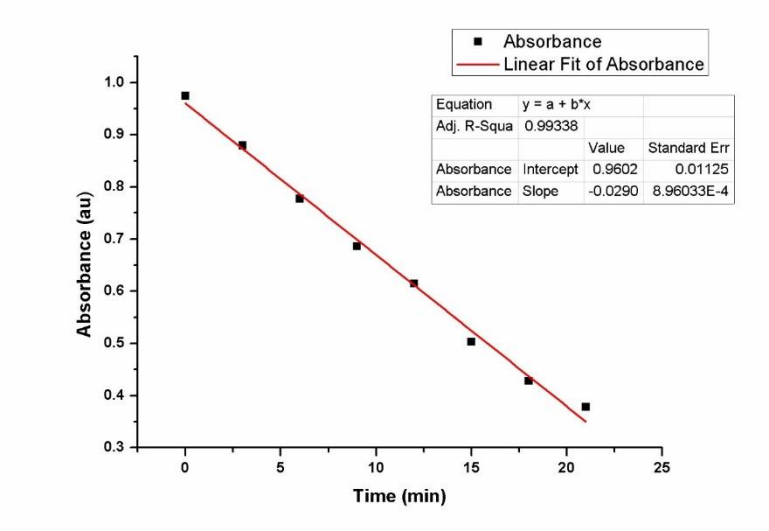

Figure 80. Absorbance decrease of DPBF at 414 nm with time in dichloromethane in the presence of compound **8**.

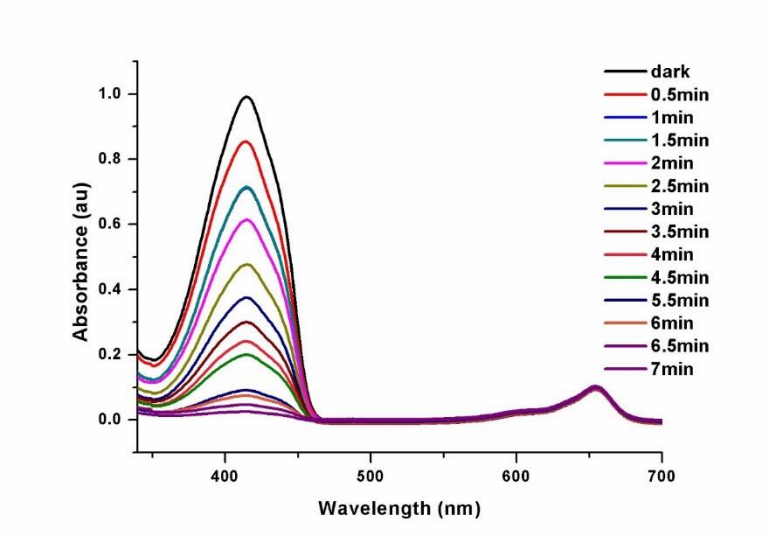

Figure 81. Decrease in absorbance spectrum of trap molecule DBPF in the presence of methylene blue (1µM) in dichloromethane (λex=660 nm, slit width=14-14, Xe-lamp).

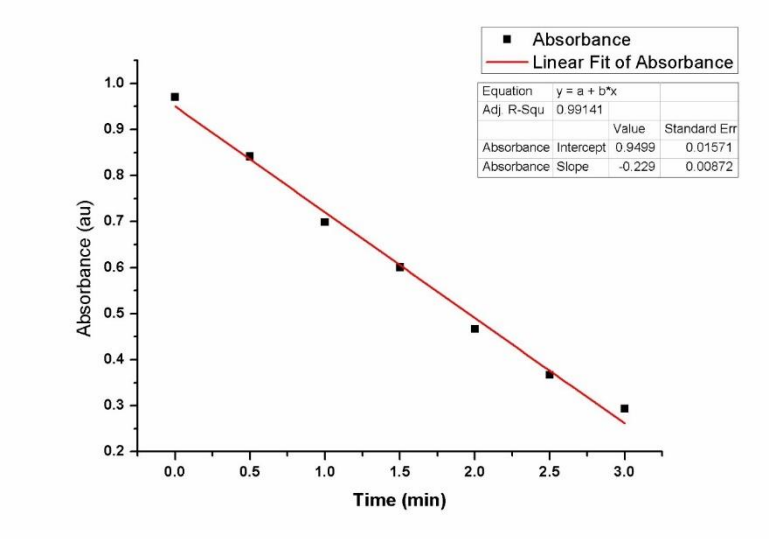

Figure 82. Absorbance decrease of DPBF at 414 nm with time in dichloromethane in the presence of methylene blue (reference).

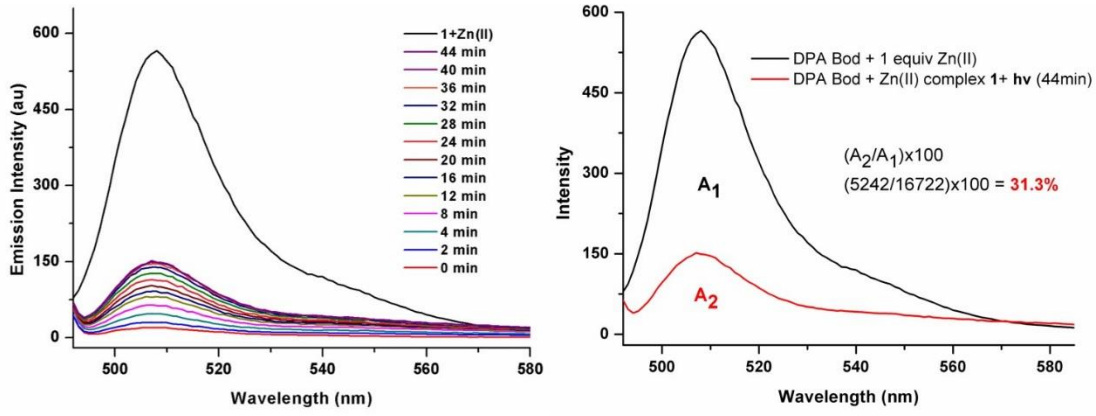

Figure 83. Fluorescence response of compound DPA-BOD upon uncaging of Zn complex **1** (5.0 μM each) recorded in acetonitrile. Initially DPA-BOD exhibits low fluorescence (quenched due to the active PET process), irradiation of the solution with the broadband 450 W Xe-lamp (λ<550 nm is filtered) resulted in the photolysis of Zn complex **1** which can be followed by the enhanced emission spectrum of DPA-BOD (λex=490 nm, slit width=5-2.5). Highest intensity curve represent the maximum emission intensitie of DPA-BOD which was obtained by the addition of 1.0 equivalent of zinc(II) cations in the form of triflate salt. (λex=490 nm, slit width=5-2.5).

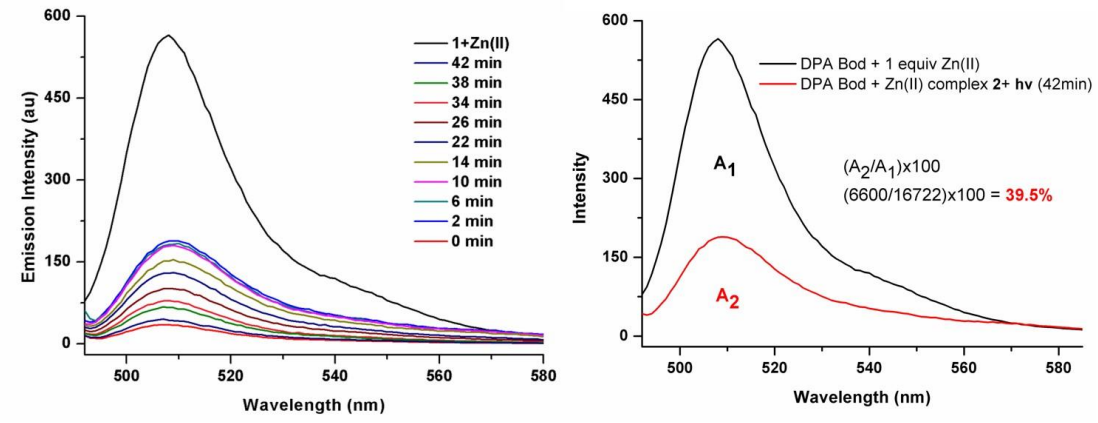

Figure 84. Fluorescence response of compound DPA-BOD upon uncaging of Zn complex **2** (5.0 μM each) recorded in acetonitrile. Initially DPA-BOD exhibits low fluorescence (quenched due to the active PET process), irradiation of the solution with the broadband 450 W Xe-lamp (λ<550 nm is filtered) resulted in the photolysis of Zn complex **2** which can be followed by the enhanced emission spectrum of DPA-BOD (λex=490 nm, slit width=5-2.5). Highest intensity curve represent the maximum emission intensitie of DPA-BOD which was obtained by the addition of 1.0 equivalent of zinc(II) cations in the form of triflate salt. (λex=490 nm, slit width=5-2.5).

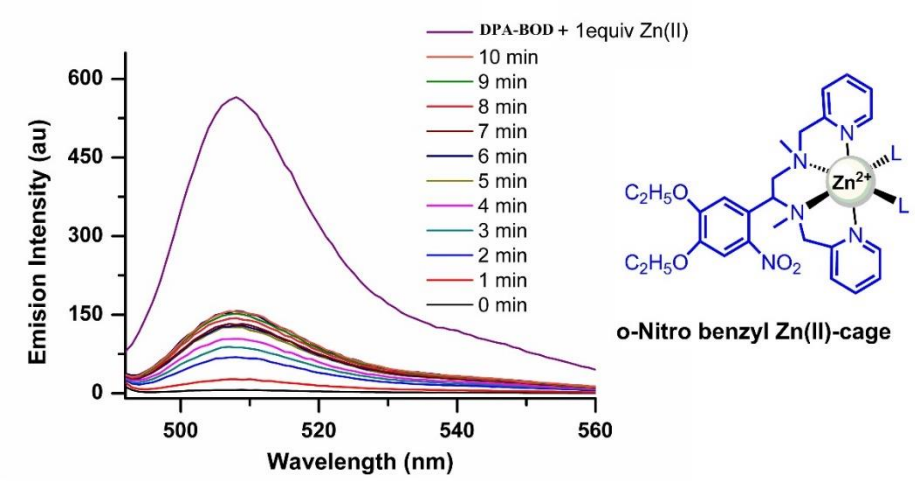

Figure 85. Fluorescence response of compound **DPA-BOD** upon uncaging of 1 equivalent **Zn(II)-cage** (5.0 μM each) recorded in acetonitrile. Initially compound **DPA-BOD** exhibits no fluorescence (quenched due to the active PET process), irradiation of the solution at 360 nm resulted in the complete photolysis of **Zn(II)-cage** which can be followed by the enhanced emission spectrum of compound **DPA-BOD**. Highest intensity curve (purple) represents the maximum emission intensity of **DPA-BOD** which were obtained by the addition of 1.0 equivalent of zinc(II) cations in the form of triflate salt[7] (λ_{ex}=490 nm, slit width=5-2.5).

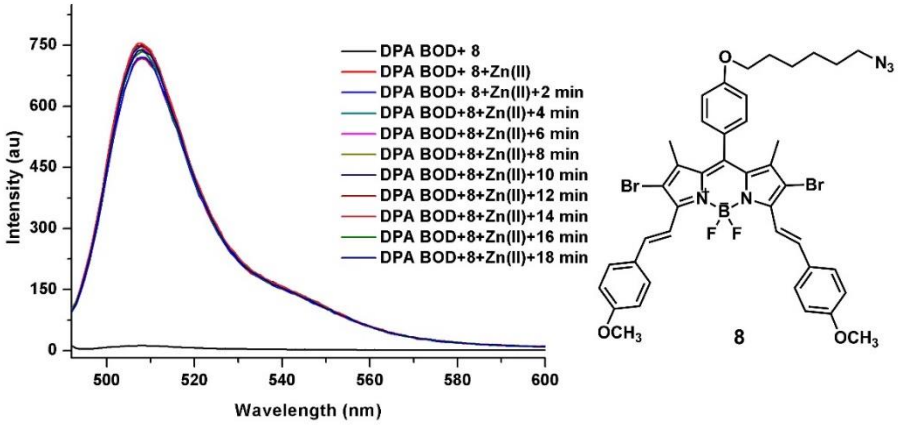

Figure 86. Control experiment of DPA-BOD: Singlet oxygen generated from the irradiation of compound 8 does not change the fluorescence profile of Zn-DPA BOD complex.

CHAPTER 4

4. Selective Photosensitization through AND Logic Response: Optimization of pH and Glutathione Response of Activatable Photosensitizers

This work is partially described in the following publication:

S. Erbas-Cakmak, F. P. Cakmak, S. D. Topel, T. B. Uyar, E. U. Akkaya, *Chem. Commun.* **2015**, *51*, 12258–61.

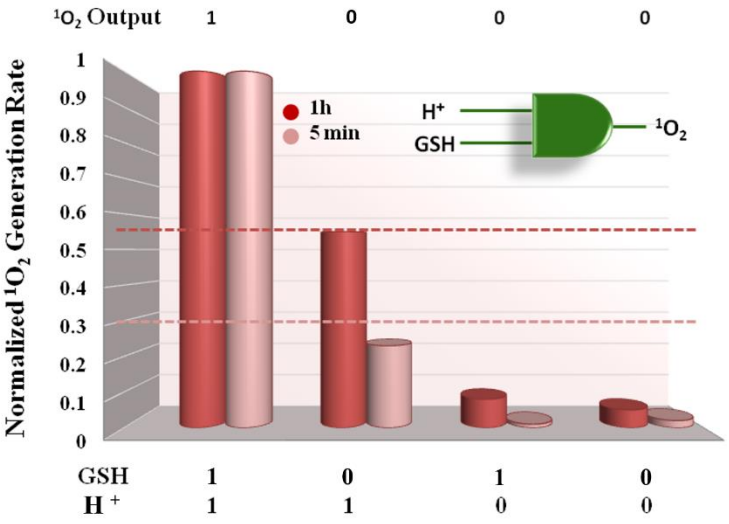

4.1. Objective

A series of pH and glutathione (GSH) responsive photosensitizers were designed and synthesized. pK_a values were optimized by adjusting the inductive contribution of substituents to reach a pH range (6.0-7.4) relevant to tumour microenvironment. pH-activatable behaviour and redox mediated release of the quencher from the PS by GSH allows the construction of an AND logic operator for selective photodynamic action in aqueous solutions.

4.2. Introduction

The research in molecular logic gates, which was initiated by the seminal work by A. P. de Silva [27] blossomed in the two decades that followed [147], [149], [153], [162], [221], [222]. In addition, the limitations and the potential of this approach has become clearer. A particularly promising application of molecular logic gates may be in the field of information processing therapeutic agents. Incorporation of Boolean logic ideas in the function of therapeutic agents would be very valuable, if the same results cannot be achieved by random optimization studies. Previously, our group and others provided the early examples of the work in that direction [115], [163], [164], [208], [223]–[230]. Our first proof of principle work which linked photodynamic sensitization of a Bodipy based photosensitizer (PS) to the concentrations of sodium ions and the acidity was essentially an AND logic gate, but the system required organic solvents and organic acid to function in the desired manner. While it was considered to be noteworthy, for that approach to have practical potential, AND logic gate based enhanced selectivity should be related to cancer related biological parameters, which can generate significant changes in the photophysical character of the sensitizer in aqueous solutions.

In this work, we took advantage of two characteristics of the tumour microenvironment, lower pH, and higher glutathione concentrations [231]. Difference in pH of cancer tissue and healthy tissue is easily accessible parameter to use in therapeutic activation. A number of pH-responsive polymeric materials,

photosensitizers, nanocarriers were studied to control drug release or activation [128]. However, extracellular pH of tumor cells drops to a value not below 6.0 [232]. Thus, it is challenging to find a smart therapeutic system responsive to pH within the narrow near neutral range and essentially become active at around pH 6.0-6.5 and stay inactive above pH 7.0. Apart from some [233], [234], most related works in literature depend on activation at pH below 5.5 which actually requires nonselective lysosomal activation [235]. In this work, properties of the PS is optimized for pH activatability by making rational chemical modification on the pH responsive moiety with electron donating or withdrawing groups to adjust the pK_a to the desired near-neutral value and to get enough spectral shift in acidic aqueous solutions such that protonated PSs are exclusively excited species under the conditions of interest. Thus, the overall design (Figure **87**) involves a pH responsive unit, linked to a quencher, which could be cleaved at elevated GSH concentrations.

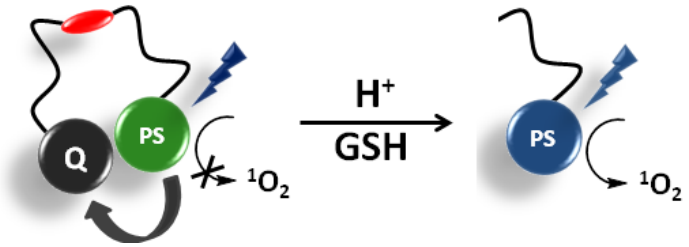

Figure 87. Schematic representation of PS activation by acid and GSH. Protonation causes a spectral shift at near neutral pH to enhance PS excitation by light of specific wavelength, whereas GSH liberates PS from quencher module by reductive cleavage of the disulfide linker.

Previously, GSH has been used as a PS activator mostly through the cleavage of disulfide bond [236]–[239] or through reactions with dinitrophenyloxy-tethered moiety [240], [241]. We used redox mediated cleavage of disulfide bond with GSH as an additional mode of activation of the photosensitizer, and attached an electronic energy acceptor module to PS, *via* disulfide bridge to quench the $^1O_2$ production, thus construct an AND molecular logic gate on the PS activation with the other input being acid (Figure **87**).

4.3. Results and Discussion

In this work, for both PS and quencher modules, Bodipy derivatives are chosen, since fine tuning the spectral properties and analyte responsiveness of these Bodipy dyes are straightforward as a result of their versatile chemistry [86], [87], [96], [148], [169], [174], [207], [242]–[244].

A spectral shift at the wavelength of excitation upon protonation would be ideal for the photosensitizer to be reversibly activated only in the acidic conditions, as we have previously demonstrated [40]. In order to optimize the pK_a values, a series of water soluble PSs have been synthesized. The structures of the compounds are given in figure **88**, the complete chemical structures can be found in the ESI.

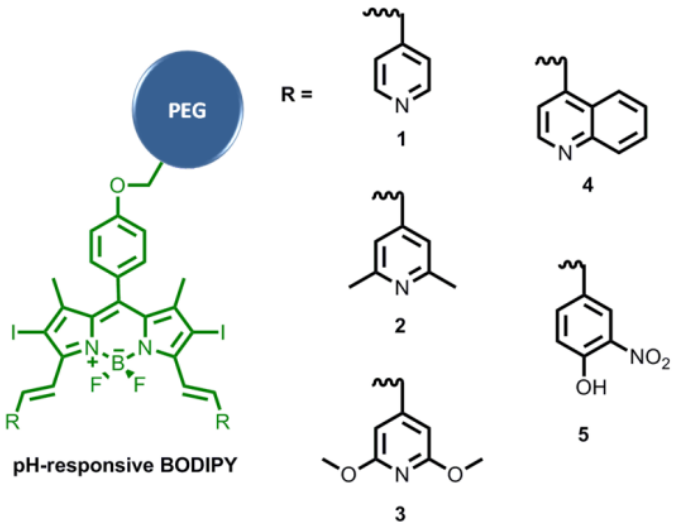

Figure 88. Structures of distyryl-BODIPYs bearing different pH-sensitive groups with polyethylene glycol (PEG) solubilising module depicted in blue.

In order to impart GSH responsiveness, a near-IR absorbing energy acceptor Bodipy dye with an appropriate spectral character for EET is attached to the PS through bioreducible disulfide linker (Figure **89**, black module). To provide relatively milder reaction conditions, the quenching module and the PS are attached to one another through disulfide bridge using copper catalysed Huisgen 1,3-dipolar cycloaddition.

The Bodipy dye which was employed as an energy sink, was prepared by the Sonogashira coupling at 2,6-positions followed by Knoevenagel condensation.

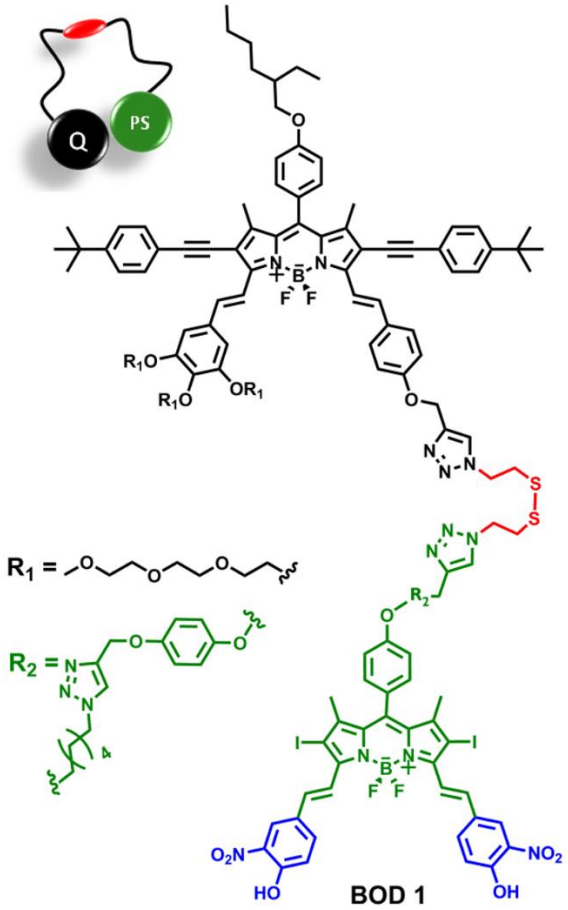

Figure 89. Chemical structure of AND logic construct of photosensitizer BOD 1 with GSH (red) and pH (blue) responsive moieties.

Water soluble distyryl-BODIPY was synthesized through condensation with appropriate aldehydes (e.g., with 4-pyridinecarboxaldehyde for compound **1**). The pK_a value for **1** was determined to be 3.42 with a protonation-induced bathochromic shift from 594 nm to 615 nm (Table **1**, Figure **90**). In addition to an insufficient spectral shift, compound **1** is not basic enough to be protonated in target biological media.

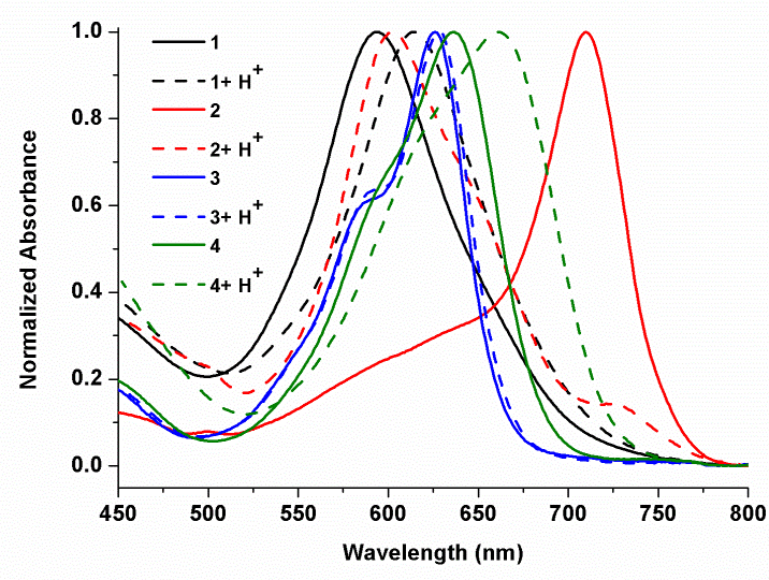

Figure 90. Normalized electronic absorption spectra of compounds **1** (black), **2** (red), **3** (blue) and **4** (green) in their neutral (solid) and protonated (dash) forms. Measurements are done in water for compounds **1** and **2** whereas 40% THF in water was used for others.

Compound	λ_1[nm]	λ_2[nm]	pKa[b]
1	615	594	3.42
2	601	723	4.21
3	626	628	-[b]
4	660	636	2.62
5	649	731	6.62
PS[c]	649	730	6.92

Table 1. Summary of protonation dependent absorbance change of compounds 1-5 and BOD1 and their experimental pKa values.[a]

(Table 1: [a] λ_1 corresponds to maximum absorbance wavelength of compounds in neutral solutions whereas λ_2 corresponds to the value of deprotonated compounds. Values are measured in water for compounds **1**, **2**, **5** and **BOD 1** and in 40% THF in water for compounds **3** and **4**. [b] pKa cannot be determined due to decomposition at high pH. [c] Micellar form of the PS part of **BOD 1** is used to determine the pKa value of **PS** in water.)

Since the desired pH-responsive behaviour cannot be reached with pyridine or quinolone derivatives we turned our attention to phenolic groups. In literature, monostyryl-Bodipy with a 3-chloro-4-hydroxyphenyl substituent was reported to have a pK_a of 7.6 [245]. As a final attempt, with the same strategy to adjust pK_a through changing inductive/resonance effects, another variation of this phenolic substituent with a stronger electron withdrawing group was targeted with an expectation of decreased the pK_a. Compound **5, BOD 1** and **PS** with a nitro group in place of chloro is synthesized with these considerations (Figure **90**).

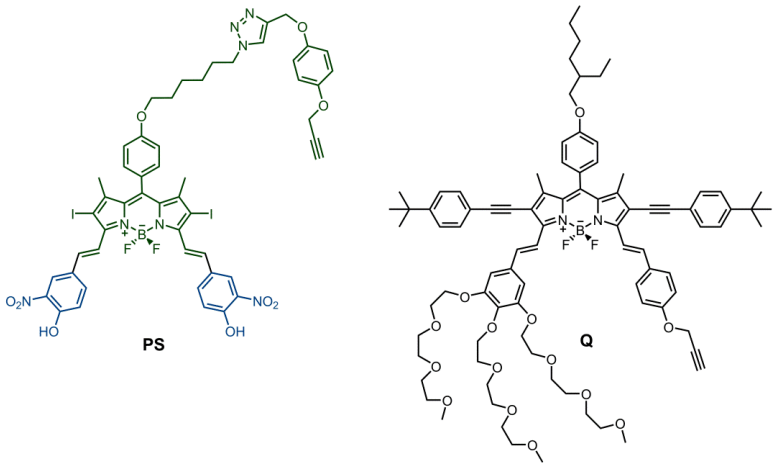

Figure 91. Chemical Structures of **PS** and Quencher (**Q**) modules.

PS is the non-water soluble module of the photosensitizer part of **BOD 1**, exact chemical structure of which is given in figure **91** (green-blue module in figure **88**). The pH response of **PS** is investigated within a micelle in aqueous solutions, since this compound and the final AND logic gate construct is not soluble in water. Fortunately, in accordance with our expectations, the compound was determined to have a pK_a of 6.92 in Cremophor EL micelles, with a very large spectral change (+81 nm) in absorbance from 649 nm to 730 nm as a result of deprotonation (Figure **92** and **93**). The spectral data clearly shows that, at the wavelength of light used for PDT measurements (625 nm, indicated with blue dashed line in Figure **93**), deprotonated compounds have substantially decreased absorbance at the selected wavelength of excitation (625 nm), which ensures selective activation of PDT agent only in acidic solutions.

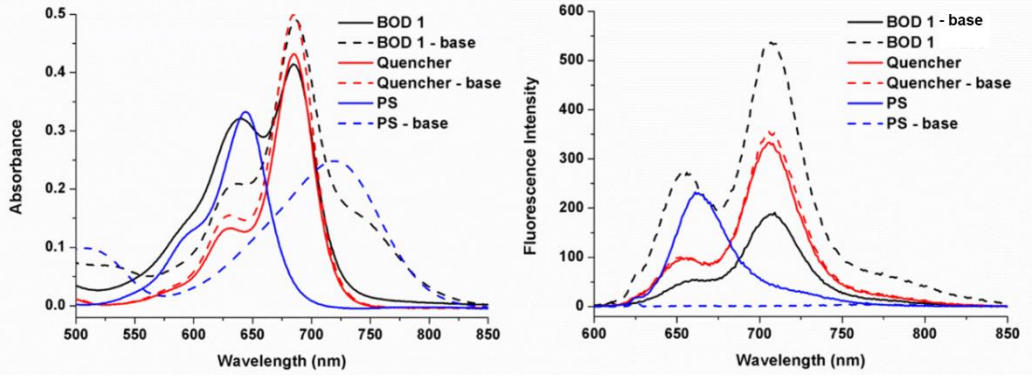

Figure 92. Electronic absorption (top) and emission (bottom) spectra of 7.50 μM BOD 1 (black), Quencher module (red) and PS module (blue) in THF. Dashed spectra are recorded after addition of base (piperidine) and fluorescence spectra are recorded by excitation at 625 nm.

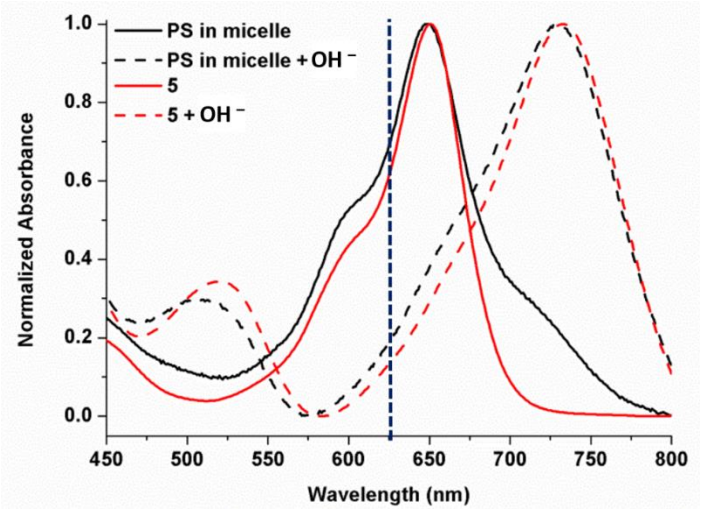

Figure 93. Normalized electronic absorption spectra of neutral (solid) and deprotonated (dash) forms of compounds **5** (red), and micellar form of **PS** module of **BOD 1** (black) in 40% THF/water and water respectively. Wavelength of excitation (625 nm) used for PDT measurements is indicated with blue dashed line.

In order to investigate if the pH response is preserved in non-micellar system, a water soluble version (compound **5**) is made and titrated in 40% THF in water. The pK_a was determined to be 6.62 (Table **1**). 0.30 unit difference may result from the fact that, relatively more hydrophobic microenvironment within the micelle may alter the deprotonation due to the fact that the charged species cannot solvated easily in micelle microenvironment. The absorption spectrum of deprotonated compound is essentially

the same as it is in micelles, except the minor broadening of the peaks. Absorption spectra of these two compounds are given in Figure **92**, **93**, **94** and Table **2**. With the promising pK_a value obtained, pH dependent component of the molecular AND logic gate is built with distyryl-BODIPYs generated through Knoevenagel condensation reaction with 4-hydroxy-3-nitrobenzaldehyde (Figure **89**).

Compound	$\lambda_{1,abs}$[nm]	$\lambda_{2,emm}$[nm]	ε ($M^{-1}cm^{-1}$)	ϕ_Φ
PS	645 720[b]	667 -	40000 30000 [b]	0.13 -
Quencher	685 685[b]	707 -	57000 63000[b]	0.76 -
BOD 1	640, 685 687[b]	654, 707 707[b]	42000[c], 56000[d] 70000[b]	0.24 0.15

Table 2. Photophysical characterization of BOD 1, PS and Quencher.[a]

(Table 2: [a] Values are determined in THF. [b]piperidine is used as a base additive. [c]calculated for absorption at 640 nm. [d]calculated for absorption at 685 nm.)

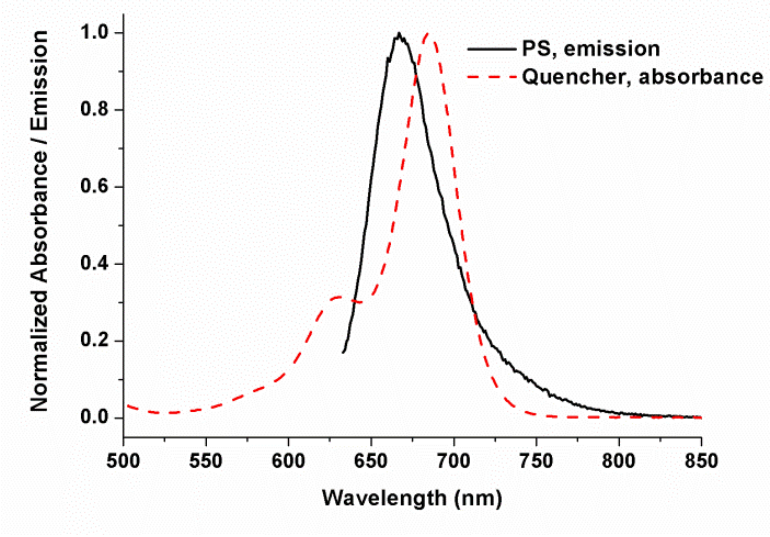

Figure 94. Comparison of normalized emission of PS module (black, solid) and absorption of Quencher module (red, dash) in THF depicting an excellent overlap for electronic energy transfer.

The electronic absorption spectrum of micellar **BOD 1** in water is given in figure **95-a**. Two peaks corresponding to two chromophore modules converge to give an essentially single peak at higher wavelength upon deprotonation, since **PS** shows a bathochromic shift under the conditions applied, whereas quencher module remains the same. For equal concentrations of compounds **PS** and **BOD 1**, emission spectra shows a decrease in the emission of photosensitizer part of **BOD 1** compared to free photosensitizer, **PS** which is an indication of energy transfer (Figure **95-b)**. Since the deprotonated form of free PS is non-emissive, the same spectral analysis cannot be performed for this form. The cleavage of the disulfide bond is analyzed by incubating the micellar **BOD 1** for 12 hour at room temperature with 2.5 equivalents of GSH and comparing it with the GSH-free **BOD 1** both *via* spectroscopic analysis and High Resolution Mass Spectra (HRMS). As shown in Figures **96**, thiol form, GSH-conjugate of free photosensitizer and both reduced and disulfide forms of quencher are detected by HRMS after 12 h incubation.

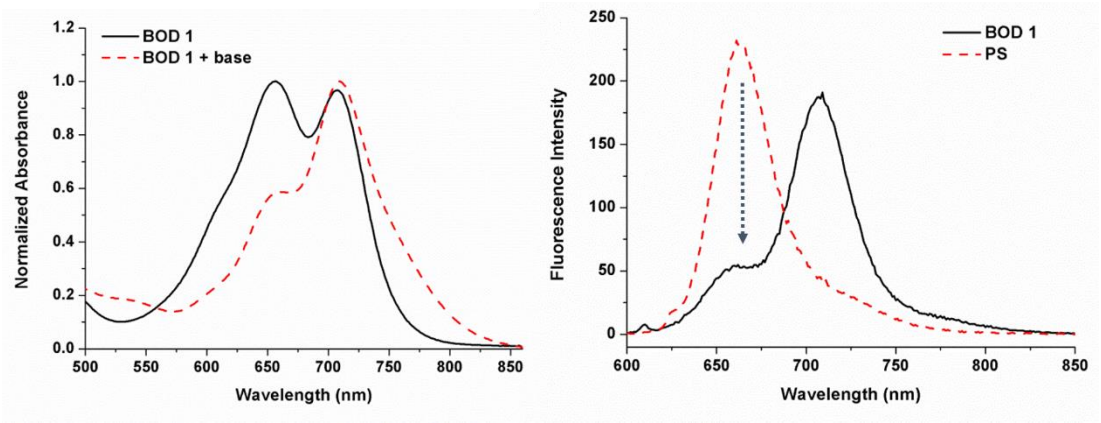

Figure 95. Electronic absorption spectra of neutral (black) and deprotonated (red) forms of micellar **BOD 1** in water (a), and comparison of fluorescence spectra of equally absorbing micellar **PS** (red, dash) and **BOD 1** (black, solid) in water (b, excited at 625 nm).

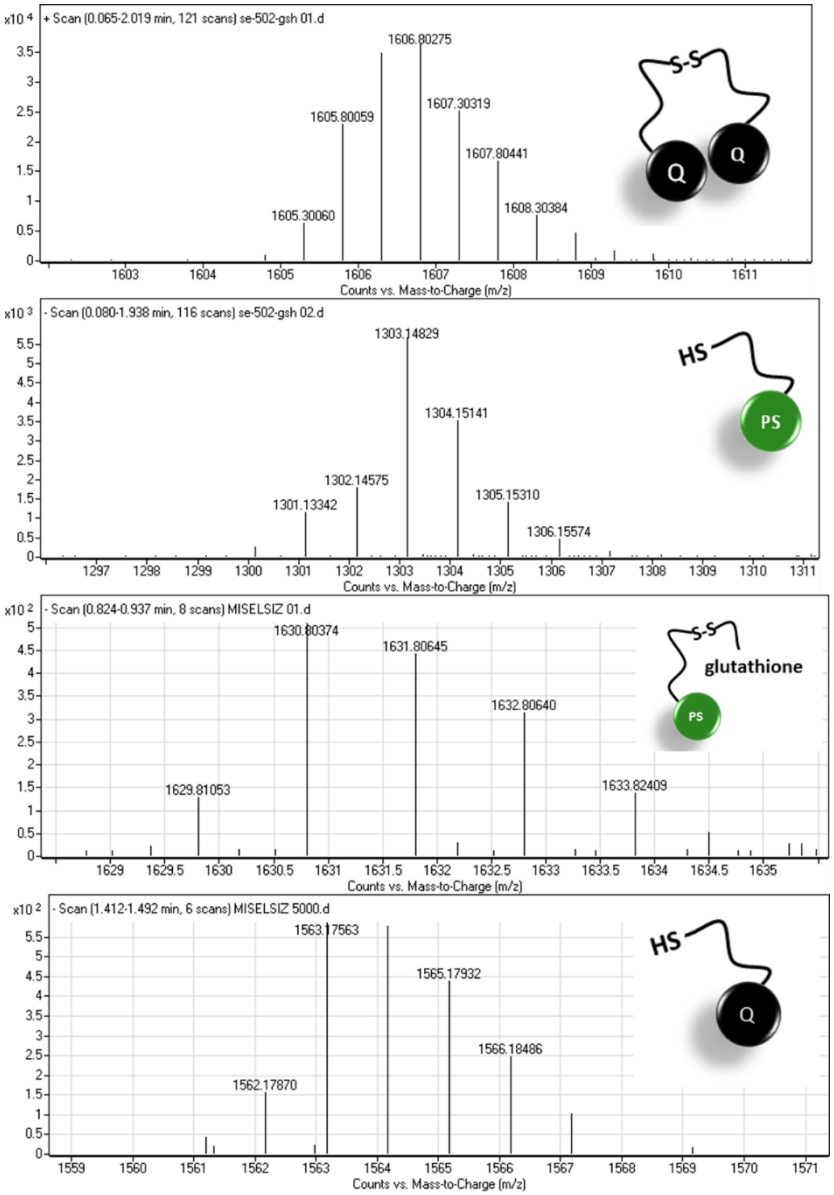

Figure 96. The cleavage of quencher from the photosensitizer in **BOD 1** after incubation with GSH for 12 h as analyzed by HRMS, (Δ = 8.8 ppm for Q-Q disulphide quencher, Δ = 4.65 ppm for thiol photosensitizer). PS-GSH adduct $(M+Na-2H)^-$ and thiol quencher $(M-F)^-$ were detected in micelle free samples.

After resolving the reduction of the disulfide linker by GSH through HRMS analysis, spectral examination was also performed to demonstrate excitation energy transfer (EET). Since the EET efficiency is expected to decrease upon release of the energy donor part, the emission of this part is predicted to increase. An increase in emission

of the PS part is clearly observed in fluorescence spectra after GSH treatment (Figure **97**) which indicates that the EET is less effective in the free form.

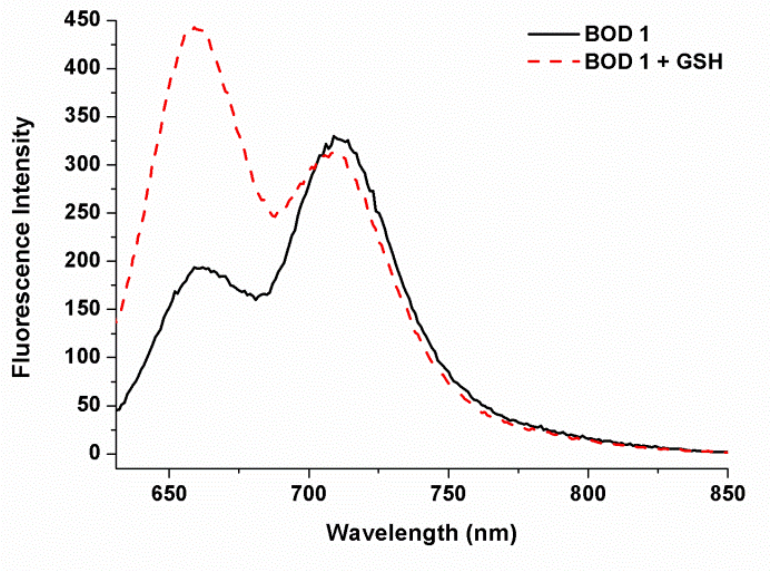

Figure 97. Emission spectra of micellar **BOD 1** at the time of addition of 2.5 equivalents of GSH (black, solid) and after 12 h incubation with glutathione (red, dash) in water. The spectrum is taken by excitation at 625 nm.

$^1O_2$ generation experiments were performed with water soluble $^1O_2$ trap and decrease in the absorption at 378 nm was followed as a measure of $^1O_2$ production rate. First, to show that the trap molecule does not decompose in the absence of photosensitizer, control experiments under dark and 625 nm irradiation, were performed in similar conditions using **PS**-free solutions. The trap is stable under experimental conditions (Figure **98**). On the other hand, the photosensitizer free from quencher shows a greater extent of $^1O_2$ generation in the presence of slightly acidic media, Figure **99**. Although **BOD 1** produces $^1O_2$ to some extent in the absence of GSH, still this is less efficient compared to free PS. The results are depicted as relative initial $^1O_2$ generation rate in Figure **100** as determined by percent decrease of trap absorption at 378 nm for each experimental condition. The threshold value of $^1O_2$ generation efficiency for AND logic gate was set as 0.30 and 0.55 for initial 5 min irradiation and 1 h irradiation respectively. Thus, the PS produces $^1O_2$, only in the presence of both inputs acid and GSH.

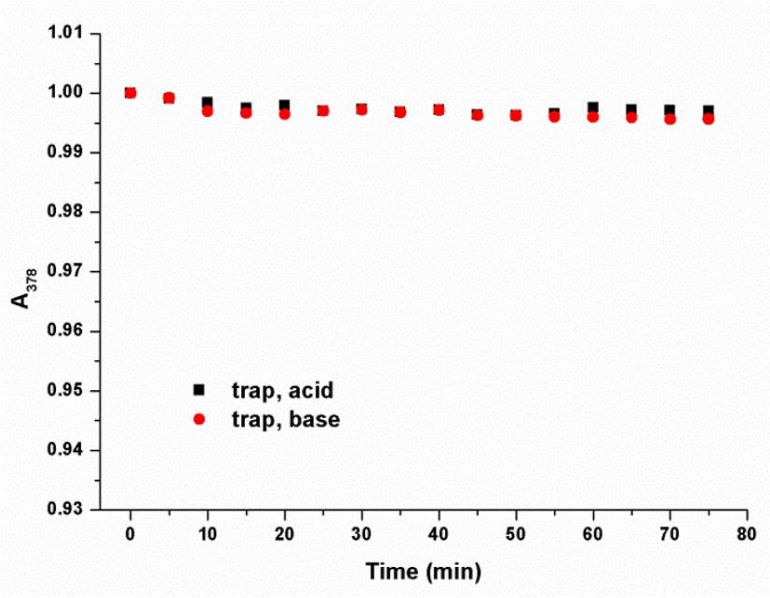

Figure 98. Control experiment with the solution containing the trap molecule only in acidic (black) and basic (red) acqueous conditions.

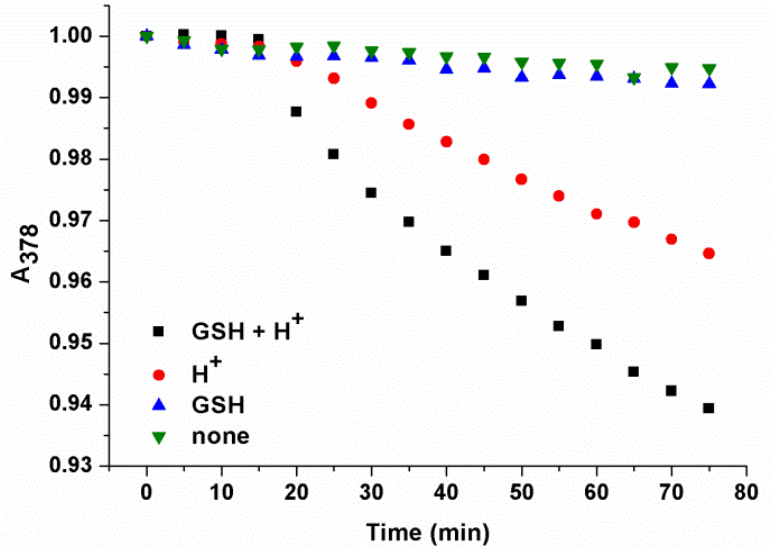

Figure 99. Comparison of $^1O_2$ generation of micellar forms of molecular AND logic construct (7.50 μM) in the presence of different combinations of inputs as followed by the decrease in $^1O_2$ trap absorbance at 378 nm in water. For the first 15 min, all the samples were kept in dark, followed by irradiation with a 625 nm LED. Acidic solutions are adjusted to pH 6.00.

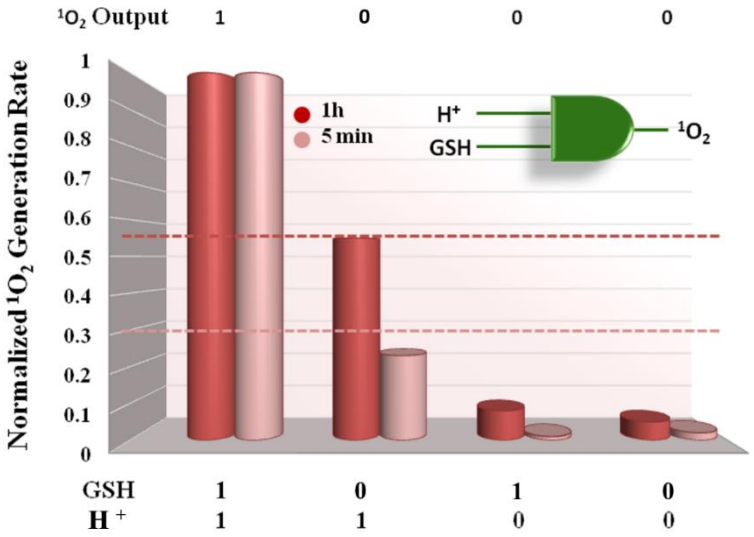

Figure 100. Comparison of initial $^1O_2$ generation rate of **BOD 1** as measured by the percent decrease in absorbance of trap molecule within 5 min (pink) or 1 h (bordeaux) of 625 nm light irradiation.

4.4. Conclusion

In this work, a viable alternative for enhanced selectivity for photodynamic action was provided. The designed PS is responsive to acidity comparable found in the tumor regions and higher GSH. Acid induced change in the absorption of the PS allows an increase of extinction coefficient at the wavelength of excitation and thus prepares it for activation. However, an energy acceptor conjugated to the PS via a reducible disulfide bond still quenches the excited state through energy transfer. Singlet oxygen generation activity of the PS was thus, shown to be significantly enhanced only when both cancer related inputs are available at above threshold values. Such AND logic constructs based on cancer related parameters as inputs, should be expected to yield more selective therapeutic agents.

4.5. Experimental Details

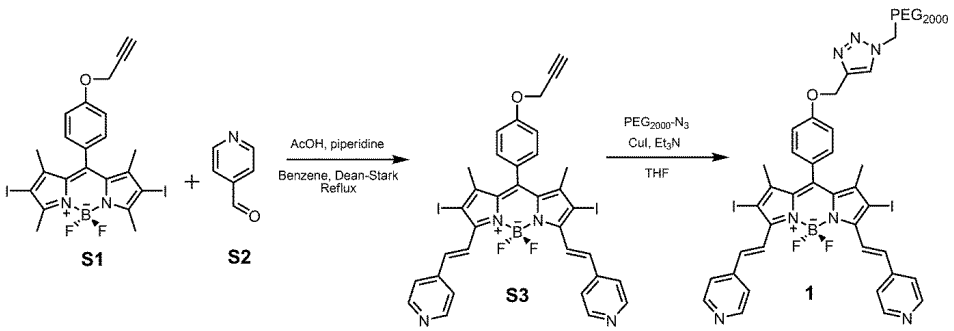

Synthesis of Compound S3

Compound **S1** [173] (120 mg, 0.19 mmol) and 4-pyridinecarboxaldehyde (51 mg, 0.48 mmol) were dissolved in benzene (40 mL). Piperidine (0.4 mL) and acetic acid (0.4 mL) were added. The reaction mixture was refluxed using Dean Stark apparatus until all aldehyde was consumed. After the reaction was completed, it was treated with water and extracted with $CHCl_3$. Organic layer was collected and dried with Na_2SO_4 then the solvent was evaporated under reduced pressure. The product was purified by silica gel column chromatography ($CHCl_3$/MeOH 95:5). Fractions containing compound **S3** were collected then the solvent was removed under reduced pressure to give dark blue (75 mg, 0.09 mmol, 49%).

^{1}H NMR (400 MHz, $CDCl_3$) δ_H 8.69 (d, 2H, J = 6.0 Hz), 8.08 (d, 2H, J = 16.7 Hz), 7.84 (d, 2H, J = 16.7 Hz), 7.50 (d, 4H, J = 6.0 Hz), 7.22 (d, 2H, J = 8.4 Hz), 7.18 (d, 2H, J = 8.4 Hz), 4.81 (d, 2H, J = 2.4 Hz), 2.60 (t, 1H, J = 2.4 Hz), 1.50 (s, 6H) ppm.

^{13}C NMR (100 MHz, $CDCl_3$) δ_C 158.8, 150.3, 149.9, 147.1, 143.7, 141.4, 136.6, 133.9, 129.3, 127.5, 122.8, 121.5, 116.2, 83.7, 77.7, 76.2, 56.1, 17.8 ppm.

HRMS (TOF-ESI): m/z calcd for $C_{34}H_{25}BF_2I_2N_4O$: 809.0252 $[M+H]^+$; found: 809.0290 $[M+H]^+$, Δ = 4.70 ppm.

Synthesis of Compound 1

Compound **S3** (50 mg, 62 μmol) and azide functionalized polyethylene glycol monomethylether (2000MW, 124 mg, 62 μmol) were dissolved in tetrahydrofuran (2 mL). Triethylamine (430 μL) and CuI (24 mg, 0.13 mmol) were added. The reaction mixture was stirred for 12 h at room temperature. After the reaction was completed, it was washed with water. The organic layer was collected and dried over Na_2SO_4, followed by evaporation of the solvent in vacuo. The product was purified by silica gel column chromatography ($CHCl_3$/MeOH 95:5). Corresponding fractions collected then the solvent was removed to give dark blue solid (100 mg, 34 μmol, 54%).

^{1}H NMR (400 MHz, $CDCl_3$) δ_H 8.62 (4H), 8.04 (d, 2H, J = 16.7 Hz), 7.80 (d, 2H, J = 16.8 Hz), 7.51 (d, 2H, J = 5.5 Hz), 7.19 (m, 4H), 5.25 (s, 2H), 4.58 (t, 2H, J = 5.1 Hz), 3.90-3.30 (PEG), 1.50 (s, 6H) ppm.

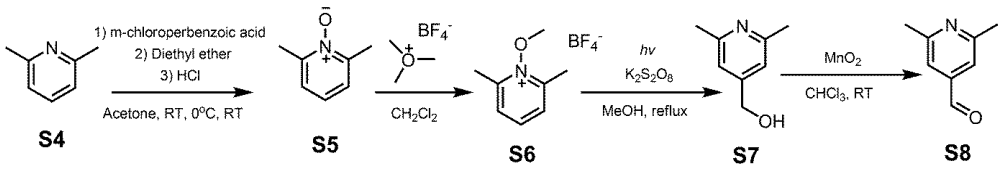

Synthesis of Compound S5 [246]

2,6-lutidine (5.0 g, 47 mmol) was dissolved in acetone (60 mL). m-chloroperbenzoic acid (13 g, 75 mmol) was dissolved in acetone (60 mL) and was added to previous mixture dropwise during the course of 10 minutes. The reaction mixture was stirred for 90 min. at room temperature. Then, it was cooled using an ice bath for 30 min. Following this, ice cold diethyl ether (20 mL) was added and HCl gas was bubbled through the reaction for 10 min. The solid produced as a result of bubbling was filtered, washed two times with ether. Then, salt was dissolved in water (20 mL); pH was adjusted to be above 10 using $NaHCO_3$. Finally, the solution was extracted with $CHCl_3$, solvent was evaporated to obtain liquid colorless compound **S5** (4.9 g, 40 mmol, 85%).

^{1}H NMR (400 MHz, $CDCl_3$) δ_H 7.18 (d, 2H, J = 7.2 Hz), 7.00 (t, 1H, J = 7.6 Hz), 2.45 (s, 6H) ppm.

^{13}C NMR (100 MHz, $CDCl_3$) δ_C 148.7, 124.4, 123.8, 18.1 ppm.

Synthesis of Compound S6 [246]

Compound **S5** (6 g, 32 mmol) was dissolved in DCM (100 mL). Equal amount of trimethyloxonium tetrafluoroborate (7.05 g, 32 mmol) was added and the reaction mixture was stirred for 5 h at rt. Solvent was was vacuum evaporated to yield a white solid (quantitative, used without further purification).

^{1}H NMR (400 MHz, D_2O) δ_H 8.18 (t, 1H, J = 7.9 Hz), 7.75 (d, 2H, J = 7.9 Hz), 4.22 (s, 3H), 2.81 (s, 6H) ppm.

^{13}C NMR (100 MHz, D_2O) δ_C 153.6, 143.8, 128.0, 66.6, 16.7 ppm.

Synthesis of Compound S7 [246]

Compound **S6** (5.19 g, 23.1 mmol) was dissolved in MeOH (65 mL). Potassium peroxodisulfate (1.53 g, 5.65 mmol) was dissolved in H_2O (6 mL) and was added to previous reaction mixture. The solution was refluxed for 30 min while it was irradiated with light. Following this, more of potassium peroxydisulfate (3.06 g, 11.3 mmol) was added and the reaction was refluxed for additional 30 min. The excess $K_2S_2O_8$ was filtered off and the solvent was vacuum evaporated to yield brown oil. The product was further purified by column chromatography using $CHCl_3$:MeOH (9:1) to give yellow oil (0.86 g, 6.3 mmol, 27%).

^{1}H NMR (400 MHz, $CDCl_3$) δ_H 7.48 (s, 2H), 4.91 (s, 1H), 2.60 (s, 6H) ppm.

^{13}C NMR (100 MHz, $CDCl_3$) δ_C 161.6, 152.5, 121.1, 61.5, 18.5 ppm.

Synthesis of Compound S8 [247]

Compound **S7** (864 mg, 6.30 mmol) was dissolved in $CHCl_3$ (2.5 mL) and methanol (1 mL). The solution was heated to 35^{o}C to dissolve the compound. Then, 1.1

equivalents of MnO_2 (0.6 g, 7 mmol) was added at rt. After stirring 2 h at rt, additional amount of MnO_2 (0.5 g, 6 mmol) was added. After 2 h, the solid precipitates were removed by filtering over celite. The solvent was removed by vacuum evaporation. Then the product was purified further by precipitation of the impurities in $CHCl_3$ to get white solid (101 mg, 0.75 mmol, 12%).

^{1}H NMR (400 MHz, $CDCl_3$) δ_H 9.93 (s, 1H), 7.30 (s, 2H), 2.53 (s, 6H) ppm.

^{13}C NMR (100 MHz, $CDCl_3$) δ_C 192.1, 159.5, 124.1, 119.0, 24.3 ppm.

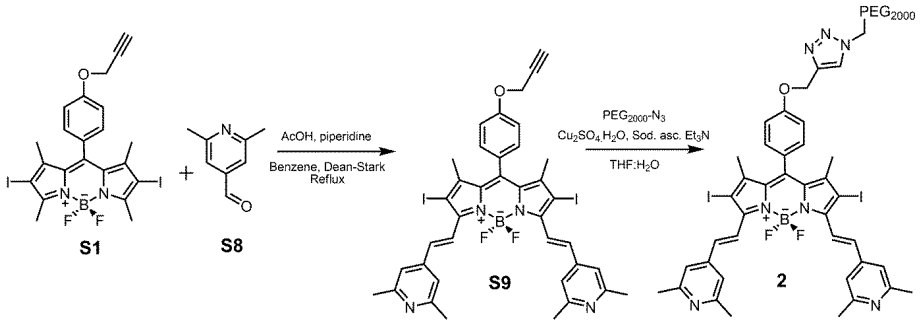

Synthesis of Compound S9

Compound **S1** (93 mg, 0.15 mmol) and 2,6-dimethyl-4-pyridinecarboxaldehyde (**S8**, 60 mg, 0.44 mmol) were dissolved in benzene (15 mL). Piperidine (0.4 mL) and acetic acid (0.4 mL) were added. The reaction mixture was refluxed using Dean Stark apparatus until all aldehyde was consumed. After the reaction was completed, it was treated with water and extracted with $CHCl_3$. Organic layer was collected and dried with Na_2SO_4 then the solvent was removed. The product was purified by silica gel column chromatography ($CHCl_3$/MeOH 95:5). Fractions containing compound **S9** were collected, then the solvent was evaporated in vacuo to yield dark blue solid (61 mg, 0.07 mmol, 47%).

^{1}H NMR (400 MHz, $CDCl_3$) δ_H 8.00 (d, 2H, J = 16.7 Hz), 7.78 (d, 2H, J = 16.7 Hz), 7.21 (d, 2H, J = 8.8 Hz), 7.18 (s, 1H), 7.18 (d 2H, J = 8.9 Hz), 4.81 (d, 2H, J = 2.4 Hz), 2.6 (s, 12H), 2.5 (1H), 1.52 (s, 6H) ppm.

^{13}C NMR (100 MHz, $CDCl_3$) δ_C 158.3, 150.1, 147.0, 144.4, 141.1, 137.2, 133.8, 129.3, 127.5, 122.3, 118.8, 118.4, 116.2, 105.9, 77.8, 76.2, 56.1, 24.1, 17.7 ppm.

HRMS (TOF-ESI): m/z calcd for $C_{38}H_{34}BF_2I_2N_4O^+$: 865.0878 $[M+H]^+$, found: 865.07406 $[M+H]^+$, Δ = 1.59 ppm.

Synthesis of Compound 2

Compound **S9** (42 mg, 49 μmol) and azide functionalized polyethylene glycol monomethylether (2000MW, 84 mg, 62 μmol) was dissolved in tetrahydrofuran (2 mL) and water (0.1 mL). Triethylamine (50 μL) was added and the reaction was stirred for 5 min. Then, $CuSO_4 \cdot 5H_2O$ (4 mg, 29 μmol) and sodium ascorbate (6 mg, 29 μmol) were added. The reaction mixture was stirred for 12 h at room temperature. After the reaction was completed then it was treated with water and extracted with $CHCl_3$. The organic layer was collected and dried over Na_2SO_4, followed by evaporation of the solvent in vacuo. The product was purified by silica gel column chromatography ($CHCl_3$/MeOH 92:8). Corresponding fractions were combined and the solvent was removed to give dark blue solid (18 mg, 6 μmol, 12%).

^{1}H NMR (400 MHz, $CDCl_3$) δ_H 8.00 (d, 2H, J = 16.7 Hz), 7.96 (s, 1H), 7.81 (d, 2H, J = 16.8 Hz), 7.25-7.15 (m, 8H), 5.29 (s, 2H), 4.62 (t, 2H, J = 4.7 Hz), 3.90-3.40 (PEG) 2.60 (s, 12H), 1.52 (s, 6H) ppm.

HRMS (TOF-ESI): Distribution around 2800 with separation of 44 corresponding to etylene glycole unit.

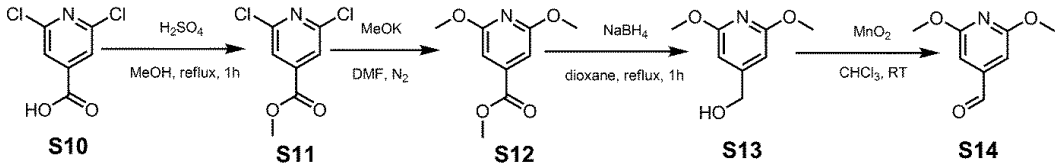

Synthesis of Compound S11 [248]

2,6-dichloronicotinic acid (500 mg, 2.6 mmol) was dissolved in MeOH (5.2 mL). 78 μl concentrated H_2SO_4 was added. The reaction mixture was refluxed for 1 h. Then,

the reaction was cooled to rt and was quenched with $NaHCO_3$. The mixture was then treated with water and extracted with $CHCl_3$. The organic layer was collected and dried over Na_2SO_4, followed by evaporation of the solvent. The product was purified by silica gel column chromatography ($CHCl_3$) to give white solid (0.49 g 2.4 mmol, 92%).

^{1}H NMR (400 MHz, $CDCl_3$) δ_H 7.84 (s, 2H), 4.01 (s, 3H) ppm.

^{13}C NMR (100 MHz, $CDCl_3$) δ_C 163.2, 151.5, 142.4, 122.6, 53.3 ppm.

Synthesis of Compound S12

Compound **S11** (250 mg, 1.21 mmol) was dissolved in anhydrous DMF (10 mL). Ar was purged in the solution for 15 min. Potassium methoxide (864 μL, 255 mg, 3.64 mmol) was added to the reaction mixture and it was refluxed for 12 h. Then, the reaction mixture was neutralized with HCl solution. It was treated with water and extracted with $CHCl_3$. The organic layer was collected and dried over Na_2SO_4, followed by evaporation of the solvent in vacuo. The product was purified by silica gel column chromatography ($CHCl_3$:Hexanes 3:2). Corresponding fractions were collected then the solvent was removed to obtain white solid (100 mg, 0.51 mmol, 42%).

^{1}H NMR (400 MHz, $CDCl_3$) δ_H 6.87 (s, 2H), 3.96 (s, 6H), 3.92 (s, 3H) ppm.

^{13}C NMR (100 MHz, $CDCl_3$) δ_C 165.6, 163.8, 142.7, 101.2, 53.9, 52.5 ppm.

Synthesis of Compound S13

Compound **S12** (800 mg, 4.06 mmol) and 2 equivalents of $NaBH_4$ (309 mg, 8.12 mmol) were dissolved in dioxane (10 mL). It was refluxed for 1 h. Then, the reaction was cooled to rt and quenched with ice cold water. It was extracted with CH_2Cl_2. The organic layer was collected and dried over Na_2SO_4, followed by evaporation of the solvent was removed under reduced pressure to yield white solid (686 mg, 4.03 mmol, quantitative).

^{1}H NMR (400 MHz, $CDCl_3$) δ_H 6.30 (s, 2H), 4.62 (s, 2H), 3.91 (s, 6H), 1.93 (b, 1H) ppm.

^{13}C NMR (100 MHz, $CDCl_3$) δ_C 163.5, 155.6, 98.3, 63.8, 53.6 ppm.

Synthesis of Compound S14

Compound **S13** (172 mg, 1.02 mmol) was dissolved in $CHCl_3$ (6 mL). 1.1 equivalents of MnO_2 (98 mg, 1.1 mmol) was added, and the reaction mixture was stirred at rt for 12 h. After completion of the reaction as followed by TLC, the reaction mixture was filtered over celite to get rid of MnO_2 by products. Solvent was evaporated in vacuo to get compound **S14** that is yellow solid (118 mg, 0.70 mmol, 68%).

^{1}H NMR (400 MHz, $CDCl_3$) δ_H 9.94 (s, 1H), 6.73 (s, 2H), 4.00 (s, 6H) ppm.

^{13}C NMR (100 MHz, $CDCl_3$) δ_C 191.2, 164.3, 147.5, 100.7, 54.0 ppm.

HRMS (TOF-ESI): m/z calcd for $C_8H_{10}NO_3^+$: 168.0655 $[M+H]^+$, found:168.06143 $[M+H]^+$, Δ = 2.42 ppm.

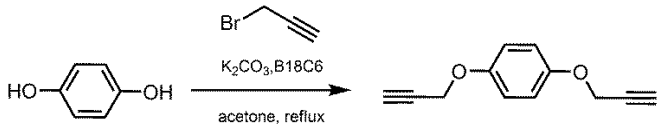

S15 **S16**

Synthesis of Compound 16

Hydroquinone (2.0 g, 18 mmol) was dissolved in acetone (30 mL). 5 equivalents of K_2CO_3 (12.6 g, 91.2 mmol) were added and the reaction mixture was refluxed for 30 min. Then, 3 equivalents of propargyl bromide (4.13 mL, 6.48 g, 54.6 mmol) was added dropwise. The reaction mixture was refluxed for additional 12 h. Then, it was cooled to rt. Following the extraction with $CHCl_3$, the organic layer was collected and dried over Na_2SO_4, followed by evaporation of the solvent under reduced pressure. Crude product was crystallized in hexanes to yield compound **S16** that is white solid (3.96 g, 18.2 mmol, quantitative).

^{1}H NMR (400 MHz, $CDCl_3$) δ_H 6.94 (s, 2H), 4.67 (d, 4H, J = 2.4 Hz), 2.53 (t, 2H, J = 2.4 Hz) ppm.

^{13}C NMR (100 MHz, $CDCl_3$) δ_C 152.4, 116.0, 78.8, 75.4, 56.5 ppm.

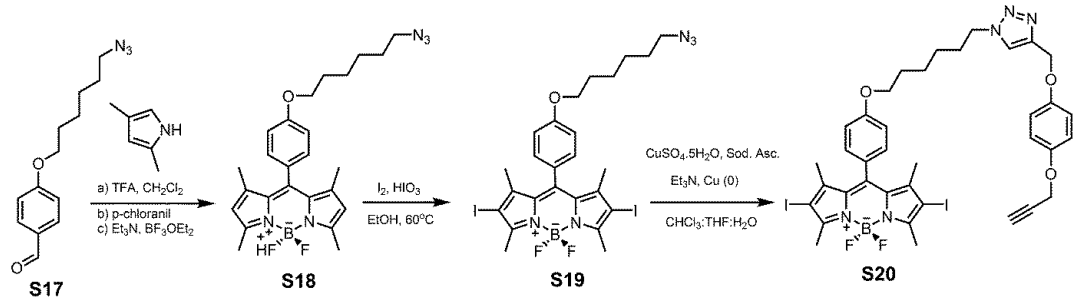

Synthesis of Compound S18

CH_2Cl_2 (300 mL) was purged with Ar for 30 min. 2,4-dimethyl pyrrole (0.96 mL, 0.88 g, 9.4 mmol) and compound **S17** (1.10 g, 4.45 mmol) were added. After the addition of 3 drops of trifluoroacetic acid, the reaction mixture was stirred at room temperature for 12 h. Then, p-Chloranil (1.09 g, 4.45 mmol) was added and the reaction mixture was stirred for additional 45 min. Then Et_3N (5 mL) and $BF_3{\cdot}OEt_2$ (5 mL) were added sequentially. After stirring at room temperature for additional 30 min, it was washed with water. Organic layer was dried with Na_2SO_4 and the solvent was evaporated under reduced pressure. The product was purified by silica gel column chromatography ($CHCl_3$). Corresponding fractions were collected then the solvent was removed to give red solid (400 mg, 0.86 mmol, 19%).

^{1}H NMR (400 MHz, $CDCl_3$) δ_H 7.20 (d, 2H, J = 8.6 Hz), 7.01 (d, 2H, J = 8.6 Hz), 6.00 (s, 2H), 4.05 (t, 2H, J = 6.4 Hz), 3.31 (t, 2H, J = 6.8 Hz), 2.58 (s, 6H), 1.86 (m, 2H), 1.70 (m, 2H), 1.55 (m, 4H), 1.45 (s, 6H) ppm.

^{13}C NMR (100 MHz, $CDCl_3$) δ_C 159.6, 155.2, 143.2, 141.9, 131.9, 129.2, 126.9, 121.1, 115.1, 67.9, 51.4, 29.1, 28.8, 26.6, 25.7, 14.6, 14.5 ppm.

Synthesis of Compound S19

Compound **S18** (270 mg, 0.581 mmol) and I_2 (368 mg, 1.45 mmol) were dissolved in ethanol (100 mL). Iodic acid, HIO_3 (44.1 μL, 204 mg, 1.16 mmol) was dissolved in a few drops of water and added into previous solution. The reaction mixture was stirred at 60°C for a few hours until all reactant was consumed. Then, saturated sodium thiosulfate solution was added (50 mL) and it was stirred at room temperature for additional 30 min. Then, it was treated with water and extracted with $CHCl_3$. Organic layer was dried with Na_2SO_4 and the solvent was evaporated under reduced pressure to give dark red solid (415 mg, 0.579 mmol, quantitative).

^{1}H NMR (400 MHz, $CDCl_3$) δ_H 7.22 (d, 2H, J = 8.7 Hz), 7.02 (d, 2H, J = 8.7 Hz), 4.04 (t, 2H, J = 6.4 Hz), 3.30 (t, 2H, J = 6.8 Hz), 2.63 (s, 6H), 1.85 (m, 2H), 1.70 (m, 2H), 1.55 (m, 4H), 1.45 (s, 6H) ppm.

^{13}C NMR (100 MHz, $CDCl_3$) δ_C 160.1, 156.6, 145.5, 141.6, 131.8, 129.1, 126.6, 115.5, 85.8, 68.0, 51.4, 29.1, 28.8, 26.6, 25.7, 17.2, 16.0 ppm.

HRMS (TOF-ESI): m/z calcd for $C_{25}H_{27}BF_2I_2N_5O^-$ 716.03716 $[M-H]^-$, found: 716.06297 $[M-H]^-$, Δ = 36.0 ppm.

Synthesis of Compound S20

Compound **S16** (519 mg, 2.80 mmol) and compound **S19** (200 mg, 0.280 mmol) were dissolved in $CHCl_3$ (3 mL) and THF (3 mL). After the addition of triethylamine (200 μl), the reaction was stirred for additional 5 min. Then, saturated solutions of $CuSO_4 \cdot 5H_2O$ (200 μL) and sodium ascorbate (200 μl) were added. Catalytic amount of Cu (0) was added. The reaction mixture was stirred for 12 h at room temperature. After the reaction was completed, it was extracted with $CHCl_3$ and organic layer was evaporated under reduced pressure. It was purified by silica gel column chromatography ($CHCl_3$) to yield dark red solid (241 mg, 0.27 mmol, 96%).

^{1}H NMR (400 MHz, $CDCl_3$) δ_H 7.60 (s, 1H), 7.21 (d, 2H, J = 8.1 Hz), 7.02 (d, 2H, J = 8.1 Hz), 6.93 (s, 4H), 5.16 (s, 2H), 4.62 (d, 2H, J = 1.52 Hz), 4.48 (t, 2H, J = 7.1

Hz), 4.01 (t, 2H, *J* = 6.3 Hz), 2.63 (s, 6H), 2.02 (t, 1H, *J* = 1.4 Hz), 1.96 (m, 2H), 1.82 (m, 2H), 1.55 (m, 2H), 1.44 (s, 6H), 1.43 (m, 2H) ppm.

^{13}C NMR (100 MHz, $CDCl_3$) δ_C 160.0, 156.5, 153.1, 152.1, 145.4, 144.4, 141.7, 131.7, 129.1, 126.6, 122.5, 116.1, 115.8, 115.4, 78.8, 75.4, 67.9, 62.7, 56.5, 50.3, 30.2, 29.0, 26.3, 25.6, 17.2, 16.0 ppm.

HRMS (TOF-ESI): m/z calcd for $C_{37}H_{38}BF_2I_2N_5NaO_3^+$: 926.1017 $[M+Na]^+$, found: 926.08227 $[M+Na]^+$, Δ = 20.98 ppm.

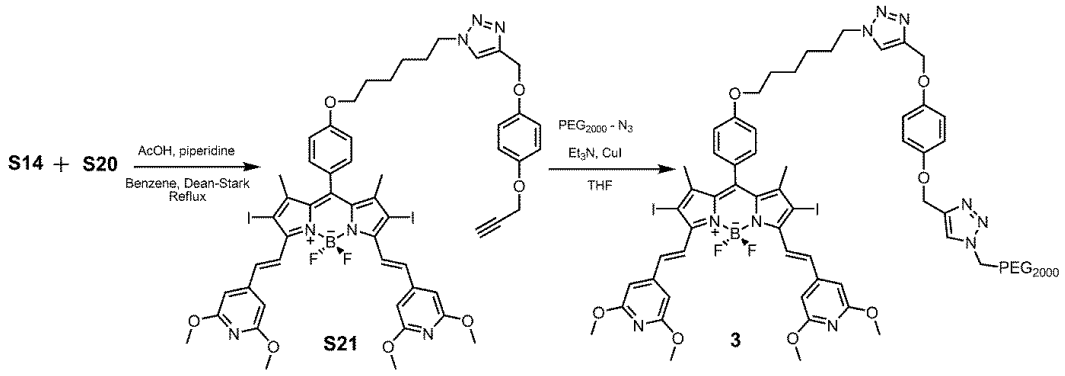

Synthesis of Compound S21

Compound **S20** (125 mg, 0.140 mmol) and 2,6-dimethoxy-4-pyridinecarboxaldehyde (**S14**, 92 mg, 0.56 mmol) were dissolved in benzene (30 mL). Piperidine (0.3 mL) and acetic acid (0.3 mL) were added. The reaction mixture was refluxed using Dean Stark apparatus until all aldehyde was consumed. After the reaction was completed, it was treated with water and extracted with $CHCl_3$. The organic layer was dried over anhydrous Na_2SO_4 and concentrated. The product was purified by silica gel column chromatography ($CHCl_3$). Corresponding fractions were collected and the solvent was removed to give dark red solid (75 mg, 62 μmol, 44%).

^{1}H NMR (400 MHz, $CDCl_3$) δ_H 7.94 (d, 2H, *J* = 16.7 Hz), 7.72 (d, 2H, *J* = 16.6 Hz), 7.59 (s, 1H), 7.16 (d, 2H, *J* = 8.6 Hz), 7.04 (d, 2H, *J* = 8.6 Hz), 6.93 (s, 4H), 6.57 (s, 4H), 5.20 (s, 2H), 4.65 (d, 2H, *J* = 2.4 Hz), 4.41 (t, 2H, t, *J* = 7.1 Hz), 4.04 (t, 2H, *J* =

6.3 Hz), 3.98 (s, 12H), 2.52 (t, 1H, J = 2.4 Hz), 2.01 (m, 2H), 1.85 (m, 2H), 1.62 (s, 6H), 1.48 (m, 4H) ppm.

^{13}C NMR (100 MHz, $CDCl_3$) δ_C 163.8, 160.2, 153.1, 152.2, 150.0, 149.0, 146.7, 144.5, 137.2, 133.8, 129.3, 128.3, 126.6, 122.4, 122.3, 116.1, 115.8, 115.5, 99.3, 78.8, 75.4, 67.9, 62.8, 56.5, 53.7, 50.3, 30.2, 29.0, 26.3, 25.6, 17.8 ppm.

HRMS (TOF-ESI): m/z calcd for $C_{53}H_{52}BF_2I_2N_7NaO_7^+$: 1224.1971 $[M+Na]^+$, found: 1224.1762 $[M+Na]^+$, Δ = 17.07 ppm.

Synthesis of Compound 3

Compound **S21** (17 mg, 14 μmol) and azide functionalized polyethylene glycol monomethylether (2000MW, 31 mg, 16 μmol) were dissolved in $CHCl_3$ (1 mL) and THF (1 mL). Triethylamine (50 μl) was added and the reaction was stirred for 5 min. Then, saturated solutions of $CuSO_4 \cdot 5H_2O$ (150 μl) and sodium ascorbate (150 μl) were added. Catalytic amount of Cu (0) was added. The reaction mixture was stirred for 12 h at room temperature. After the reaction was completed, the crude product was applied to silica gel column chromatography ($CHCl_3$/MeOH 90:10). Fractions containing compound **3** were collected then the solvent was removed under reduced pressure (26 mg, 8 μmol, 58%).

^{1}H NMR (400 MHz, $CDCl_3$) δ_H 7.96 (d, 2H, J = 16.7 Hz), 7.83 (s, 1H), 7.73 (d, 2H, J = 16.6 Hz), 7.62 (s, 1H), 7.17 (d, 2H, J = 8.8 Hz), 7.05 (d, 2H, J = 8.3 Hz), 6.93 (s, 4H), 6.54 (s, 4H), 5.19 (s, 2H), 5.17 (s, 2H), 4.58 (t, 2H, J = 5.0 Hz), 4.41 (t, 2H, t, J = 7.6 Hz), 4.10-3.30 (PEG), 2.01 (m, 2H), 1.85 (m, 2H), 1.62 (s, 6H), 1.48 (m, 4H) ppm.

HRMS (TOF-ESI): Distribution around 3000 with separation of 44 corresponding to etylene glycole unit.

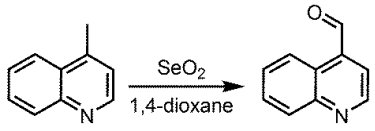

Synthesis of Compound S23 [249]

4-methylquinoline (1.3 mL, 1.4 g, 9.8 mmol) was dissolved in 1,4-dioxane (12 mL). Selenium dioxide (1.12 g, 10.1 mmol) was added to the reaction mixture and it was refluxed for 8 h. Then, solvent was evaporated in vacuo and the crude product was applied to silica gel column chromatography (EtOAc). Corresponding fractions were combined and the solvent was removed to get yellow solid (0.95 g, 6.1 mmol, 60%).

^{1}H NMR (400 MHz, $CDCl_3$) δ_H 10.50 (s, 1H), 9.19 (d, 1H, J = 4.2 Hz), 9.00 (dt, 1H, J_1 = 0.6 Hz, J_2 = 7.0 Hz), 8.21 (dt, 1H, J_1 = 0.4 Hz, J_2 = 7.2 Hz), 7.70-7.85 (m, 3H) ppm.

^{13}C NMR (100 MHz, $CDCl_3$) δ_C 192.8, 150.4, 149.3, 136.7, 130.2, 130.0, 129.4, 125.8, 124.4, 123.8 ppm.

HRMS (TOF-ESI): m/z calcd for $C_{10}H_8NO^+$: 158.0600 $[M+Na]^+$, found: 158.05593 $[M+Na]^+$, Δ = 25.75 ppm.

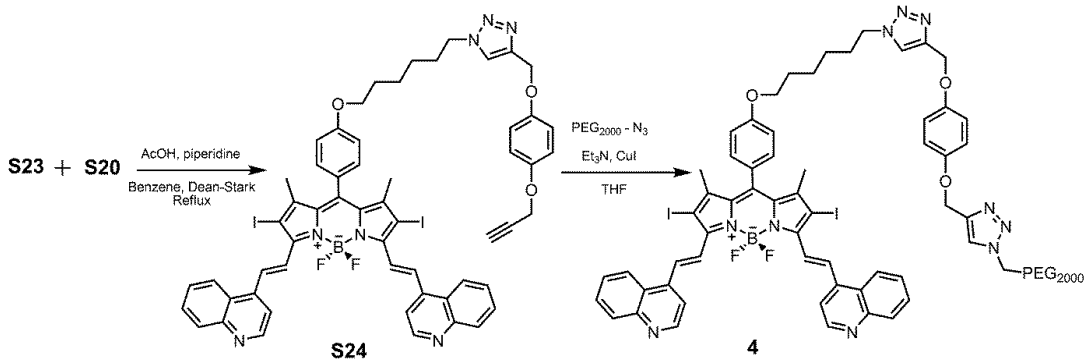

Synthesis of Compound S24

Compound **S20** (91 mg, 0.10 mmol) and quinoline-4-carboxaldehyde, compound **S23** (40 mg, 0.25 mmol) were dissolved in benzene (25 mL). Piperidine (0.3 mL) and acetic

acid (0.3 mL) were added. The reaction mixture was refluxed using Dean Stark apparatus until all aldehyde was consumed. After the reaction was completed, it was treated with water and extracted with $CHCl_3$. Organic layer was dried over anhydrous Na_2SO_4 and the solvent was removed. The product was purified by silica gel column chromatography (EtOAc) to obtain dark blue solid (99 mg, 84 μmol, 84%).

^{1}H NMR (400 MHz, $CDCl_3$) δ_H 9.01 (d, 2H, *J* = 4.6 Hz), 8.96 (d, 2H, *J* = 16.6 Hz), 8.32 (d, 2H, *J* = 8.4 Hz), 8.18 (d, 2H, *J* = 8.4 Hz), 7.94 (d, 2H, *J* = 16.5 Hz), 7.81 (d, 2H, *J* = 4.6 Hz), 7.77 (t, 2H, 7.5 Hz), 7.62 (t, 2H, *J* = 7.8 Hz), 7.22 (d, 2H, *J* = 8.4 Hz), 7.09 (d, 2H, *J* = 8.4 Hz), 6.95 (s, 4H), 5.20 (s, 2H), 4.64 (d, 2H, *J* = 2.0 Hz), 4.43 (t, 2H, *J* = 7.1 Hz), 4.05 (t, 2H, *J* = 6.2 Hz), 2.52 (t, 1H, *J* = 1. 8 Hz), 2.02 (m, 2H), 1.88 (m, 2H), 1.60 (m, 8H) ppm.

^{13}C NMR (100 MHz, $CDCl_3$) δ_C 163.8, 160.2, 153.1, 152.2, 150.0, 149.0, 146.7, 144.5, 137.2, 133.8, 129.3, 128.3, 126.6, 122.4, 122.3, 116.1, 115.8, 115.5, 99.3, 78.8, 75.4, 67.9, 62.8, 56.5, 53.7, 50.3, 30.2, 29.0, 26.3, 25.6, 17.8 ppm.

HRMS (TOF-ESI): m/z calcd for $C_{57}H_{48}BF_2I_2N_7NaO_3^+$: 1204.1861 $[M+Na]^+$, found: 1204.1620 $[M+Na]^+$, Δ = 20.01 ppm.

Synthesis of Compound 4

Compound **S24** (20 mg, 17 μmol) and azide functionalized polyethylene glycol monomethylether (2000MW, 37 mg, 19 μmol) were dissolved in $CHCl_3$ (2 mL) and THF (2 mL). Triethylamine (150 μl) was added and the reaction was stirred for 5 min. Then, saturated solutions of $CuSO_4 \cdot 5H_2O$ (250 μl) and sodium ascorbate (250 μl) were added. Catalytic amount of Cu (0) was added. The reaction mixture was stirred for 12 h at room temperature. After the reaction was completed, the crude product was applied to octadecyl functionalized silica gel column chromatography ($CHCl_3$). The mobile phase was changed to CH_2Cl_2/MeOH (80:20) after the starting compound was eluted from the column. Corresponding fractions were combined then the solvent was removed to yield dark blue solid (40 mg, 13 μmol, 76%).

^{1}H NMR (400 MHz, $CDCl_3$) δ_H 9.02-8.9 (m, 4H), 8.31 (d, 2H, *J* = 8.2 Hz), 8.17 (d, 2H, *J* = 8.2 Hz), 7.93 (d, 2H, *J* = 16.8 Hz), 7.85-7.70 (m, 5H), 7.60 (s, 1H), 7.60 (d, 2H; *J* = 8.2 Hz), 7.20 (d, 2H, *J* = 8.2 Hz), 7.09 (d, 2H, *J* = 8.4 Hz), 6.92 (s, 4H), 5.16 (s, 2H), 5.13 (s, 2H), 4.54 (t, 2H, *J* = 4.8 Hz), 4.40 (t, 2H, *J* = 6.9 Hz), 3.90-3.30 (PEG), 2.00 (m, 2H), 1.85 (m, 2H), 1.40 (m, 4H), 1.30 (s, 6H) ppm.

HRMS (TOF-ESI): Distribution around 3000 with separation of 44 corresponding to etylene glycole unit.

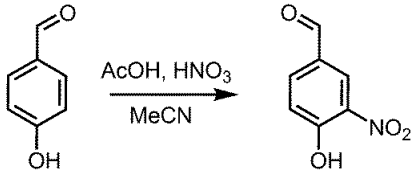

S25 **S26**

Synthesis of Compound S26 [250]

4-hydroxybenzaldehyde (1.22 g, 10 mmol) was dissolved in 20 mL acetonitrile. Acetic acid (10 mL) and nitric acid (0.75 mL) were added and the reaction was refluxed for 3 h. Then, it was cooled to room temperature. The reaction mixture was treated with water then extracted with EtOAc. Organic layer was collected and dried with Na_2SO_4 and the solvent was evaporated to get brown solid (1.52 g, 9.1 mmol, 91%).

^{1}H NMR (400 MHz, $CDCl_3$) δ_H 11.05 (s, 1H), 9.98 (s, 1H), 8.68 (s, 1H), 8.17 (d, 1H, *J* = 8.6 Hz), 7.34 (d, 1H, *J* = 8.7 Hz) ppm.

^{13}C NMR (100 MHz, $CDCl_3$) δ_C 188.7, 159.3, 136.4, 128.6, 126.2, 121.3, 115.7 ppm.

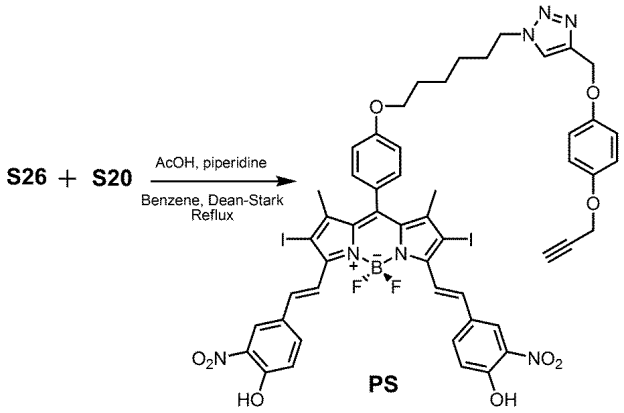

Synthesis of Compound PS

Compound **S20** (200 mg, 0.22 mmol) and 4-hydroxy-3-nitrobenzaldehyde, compound **S26** (110 mg, 0.66 mmol) were dissolved in benzene (20 mL). Piperidine (0.3 mL) and acetic acid (0.3 mL) were added. The reaction mixture was refluxed using Dean Stark apparatus. After the reaction was completed, it was extracted with CH_2Cl_2. Organic layer was collected and dried with Na_2SO_4 then the solvent was evaporated. The compound was purified by silica gel column chromatography (EtOAc) to yield dark blue solid (0.18 g, 0.15 mmol, 68%).

^{1}H NMR (400 MHz, $CDCl_3$) δ_H 8.79 (s, 2H), 8.19 (d, 2H, J = 16.8 Hz), 7.97 (d, 2H, J = 8.8 Hz), 7.60 (s, 1H), 7.60 (d, 2H, J = 16.6 Hz), 7.23 (d, 2H, J = 8.8 Hz), 7.19 (d, 2H, J = 7.4 Hz), 7.05 (d, 2H, J = 8.2 Hz), 6.93 (s, 4H), 5.20 (s, 2H), 4.64 (s, 2H), 4.41 (t, 2H, J = 7.12 Hz), 4.05 (t, 2H, J = 5.8 Hz), 2.52 (s, 1H), 1.85 (m, 2H), 1.60-1.40 (m, 12H) ppm.

^{13}C NMR cannot be recorded due to poor solubility.

HRMS (TOF-ESI): m/z calcd for $C_{51}H_{43}BF_2I_2N_7O_{9-}$ 1200.1278 $[M-H]^-$, found: 1200.13078 $[M-H]^-$, Δ = 2.48 ppm.

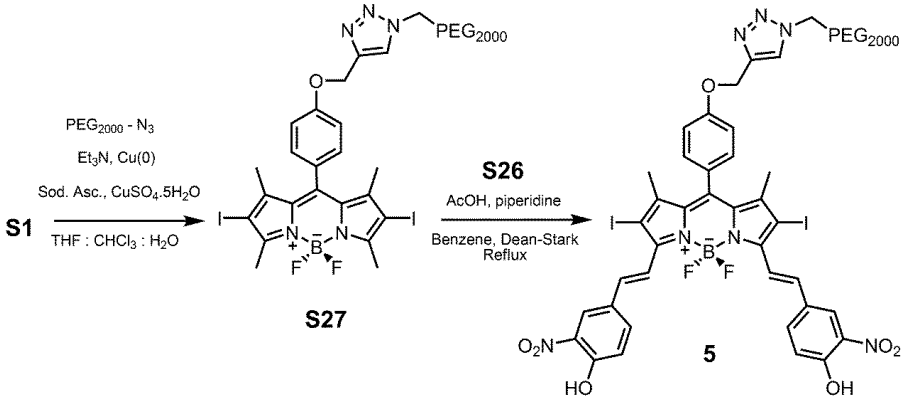

Synthesis of Compound S27

Compound **S1** (127 mg, 0.2 mmol) and azide functionalized polyethylene glycol monomethylether (2000MW, 800 mg, 0.4 mmol) were dissolved in tetrahydrofuran (2 mL). Triethylamine (1.4 mL) and CuI (77 mg, 0.4 mmol) were added. The reaction mixture was stirred for 12 h at room temperature. After the reaction was completed, the crude product was purified by silica gel column chromatography ($CHCl_3$/MeOH 93:7) to get red oil (300 mg, 0.11 mmol, 55%).

^{1}H NMR (400 MHz, $CDCl_3$) δ_H 7.93 (s, 1H), 7.12 (b, 4H), 5.24 (s, 2H), 4.58 (t, J = 4.8 Hz), 3.90-3.40 (PEG), 3.35 (s, 3H), 2.60 (s, 6H), 1.40 (s, 6H) ppm.

HRMS (TOF-ESI): Distribution around 2500 with separation of 44 corresponding to etylene glycole unit.

Synthesis of Compound 5

Compound **S27** (120 mg, 45 μmol) and compound **S26** (23 mg, 135 μmol) were dissolved in benzene (25 mL). Piperidine (0.2 mL) and acetic acid (0.2 mL) were added. The reaction mixture was refluxed using Dean Stark apparatus until all aldehyde was consumed. After the reaction was completed, the crude product was purified by silica gel column chromatography (CH_2Cl_2/MeOH 85:15). Corresponding fractions were combined then the solvent was evaporated to give dark blue solid (90 mg, 30 μmol, 66%).

^{1}H NMR ($CDCl_3$, 400 MHz, δ ppm) 8.24 (s, 2H), 8.06 (d, 2H, *J* = 16.7 Hz), 7.93 (m, 4H), 7.56 (d, 2H, *J* = 16.7 Hz), 7.20 (m, 6H), 5.28 (s, 2H), 4.60 (t, 2H, *J* = 4.4 Hz), 3.90-3.40 (PEG), 3.35 (s, 3H), 1.50 (s, 6H) ppm.

^{13}C NMR (100 MHz, $CDCl_3$) δ_C 159.6, 155.8, 149.8, 146.7, 143.2, 140.4, 136.2, 135.3, 133.7, 129.5, 127.2, 124.5, 124.4, 120.7, 119.3, 115.9, 94.3, 83.6, 72.0, 70.6, 69.6, 62.2, 59.0, 50.7, 50.4, 17.7 ppm.

HRMS (TOF-ESI): Distribution around 2800 with separation of 44 corresponding to etylene glycole unit.

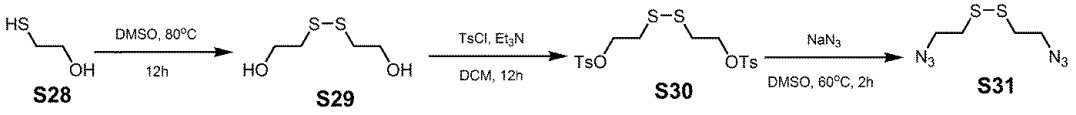

Synthesis of Compound S29 [251]

Mercaptoethanol (5.0 g, 64 mmol) was dissolved in DMSO (20 mL). The reaction mixture was stirred at 80°C for 12 h. Then, it was cooled to room temperature. The reaction mixture was treated with water and extracted with EtOAc. Organic layer was collected and dried with Na_2SO_4. The product was purified by silica gel column chromatography (Hexanes/EtOAc 3:1) to obtain light yellow oil (4.5 g, 29 mmol, 86%).

^{1}H NMR (400 MHz, $CDCl_3$) δ_H 3.90 (t, 4H, *J* = 5.8 Hz), 7.30 (t, 4H, *J* = 5.9 Hz) ppm.

^{13}C NMR (100 MHz, $CDCl_3$) δ_C 60.4, 41.3 ppm.

Synthesis of Compound S30

2-hydroxyethyldisulfide, compound S**29** (1.0 g, 6.5 mmol) was dissolved in 20 mL CH_2Cl_2 and 2 mL Et_3N. In a dropper, p-toluene sulfonyl chloride (1.4 g, 13 mmol) was dissolved in CH_2Cl_2 10 mL and was added to the previous solution dropwise while the reaction mixture was being cooled with ice bath. It was stirred for 12 h. After the washing with water, organic layer was collected and dried with Na_2SO_4. The product

was purified by silica gel column chromatography ($CHCl_3$). Fractions containing compound **S30** were collected then the solvent was removed to yield white solid (3.0 g, 6.5 mmol, quantitative).

^{1}H NMR (400 MHz, $CDCl_3$) δ_H 7.83 (d, 4H, J = 8.0 Hz), 7.38 (d, 4H, J = 7.9 Hz), 4.21 (t, 4H, J = 6.6 Hz), 2.85 (t, 4H, J = 6.5 Hz), 2.48 (s, 6H) ppm.

^{13}C NMR (100 MHz, $CDCl_3$) δ_C 145.2, 130.0, 128.0, 67.5, 36.9, 21.7 ppm.

HRMS (TOF-ESI): m/z calcd for $C_{18}H_{22}NaO_6S_4^+$ 485.0191 $[M+Na]^+$, found: 485.0104 $[M+Na]^+$, Δ = 17.94 ppm.

Synthesis of Compound S31

Compound S**30** (1.2 g, 2.6 mmol) was dissolved in DMSO (10 mL) and sodium azide (12 mmol, 780 mg) was added to the reaction mixture. It was stirred 2 h at 60 ^{o}C. After cooling to rt, the mixture was extracted with EtOAc. The solvent was evaporated under reduced pressure to give yellow oil (0.5 g, 2.5 mmol, 95%).

^{1}H NMR (400 MHz, $CDCl_3$) δ_H 3.63 (t, 4H, J = 6.8 Hz), 2.89 (t, 4H, J = 6.8 Hz) ppm.

^{13}C NMR (100 MHz, $CDCl_3$) δ_C 49.9, 37.6 ppm.

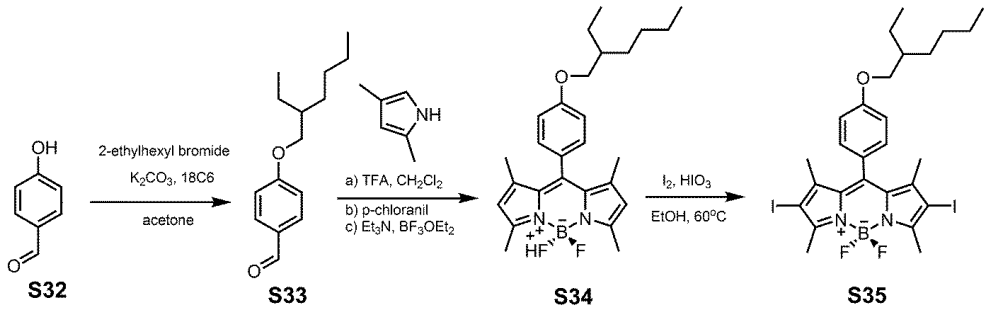

Synthesis of Compound S33

4-hydroxybenzaldehyde (4 g, 33 mmol), 2-ethylhexyl bromide (6.7 mL, 36 mmol) and catalytic amount of benzo-18-crown-6 were dissolved in CH_3CN (60 mL). K_2CO_3 (14 g, 98 mmol) was added and the reaction mixture was refluxed for 12 h. The solvent

was evaporated under reduced pressure. The crude product was treated with water and extracted with CH_2Cl_2. Organic layer was collected and the solvent was evaporated under reduced pressure to get yellowish oil (7.7 g, 33 mmol, quantitative).

^{1}H NMR (400 MHz, $CDCl_3$) δ_H 9.88 (s, 1H), 7.83 (d, 2H, J = 8.2 Hz), 7.01 (d, 2H, J = 8.3 Hz), 3.94 (d, 2H, J = 5.6 Hz), 1.77 (m, 1H), 1.45 (m, 4H), 1.32 (m, 4H), 0.93 (m, 6H) ppm.

^{13}C NMR (100 MHz, $CDCl_3$) δ_C 190.7, 164.5, 131.9, 129.7, 114.8, 70.9, 39.3, 30.4, 29.0, 23.8, 23.0, 14.0, 11.1 ppm.

HRMS (TOF-ESI): m/z calcd for $C_{15}H_{23}O_2^+$ 235.16926 $[M+H]^+$, found: 235.17327 $[M+H]^+$, Δ = 17.1 ppm.

Synthesis of Compound S34

CH_2Cl_2 (300 mL) was purged with Ar for 30 min. 2,4-dimethyl pyrrole (2.3 mL, 2.1 g, 22.5 mmol) and compound **S33** (2.4 g, 10.2 mmol) were added. After the addition of 3 drops of trifluoroacetic acid, the reaction mixture was stirred at room temperature for 12 h. Then, p-Chloranil (2.5 g, 10.2 mmol) was added and the reaction mixture was stirred for additional 45 min. Then Et_3N (5 mL) and $BF_3{\cdot}OEt_2$ (5 mL) were added sequentially. After stirring at room temperature for 1 h, it was washed with water. The product was purified by silica gel column chromatography ($CHCl_3$) then (EtOAc/Hexanes 20:80) to yield red solid (0.81 g, 1.8 mmol, 18%).

^{1}H NMR (400 MHz, $CDCl_3$) δ_H 7.17 (d, 2H, J = 8.8 Hz), 7.01 (d, 2H, J = 8.8 Hz), 5.99 (s, 2H), 3.92 (d, 2H, J = 5.9 Hz), 2.55 (s, 6H), 1.79 (m, 1H), 1.60-1.40 (m, 4H), 1.60-1.40 (s, 6H), 1.37 (m, 4H), 0.96 (m, 6H) ppm.

^{13}C NMR (100 MHz, $CDCl_3$) δ_C 160.0, 155.2, 143.2, 142.1, 131.9, 129.1, 126.8, 121.1, 114.8, 70.9, 39.4, 30.6, 29.1, 23.9, 23.0, 14.6, 14.1, 11.2 ppm.

Synthesis of Compound S35

Compound S**34** (330 mg, 0.73 mmol) and I_2 (389 mg, 1.53 mmol) were dissolved in EtOH (200 mL). Iodic acid, HIO_3 (256 mg, 1.46 mmol) was dissolved in a few drops of water and added into previous solution. The reaction mixture was stirred at 60°C for 1 h until all reactant was consumed. Then, saturated sodium thiosulfate solution (50 mL) was added and it was stirred at room temperature for additional 30 min. The mixture was treated with water then extracted with $CHCl_3$. Organic layer was collected and dried with Na_2SO_4 and the solvent was removed to obtain brown solid (514 mg, 0.73 mmol quantitative).

^{1}H NMR (400 MHz, $CDCl_3$) δ_H 7.12 (d, 2H, J = 8.7 Hz), 7.03 (d, 2H, J = 8.7 Hz), 3.92 (d, 2H, J = 5.9 Hz), 2.64 (s, 6H), 1.79 (m, 1H), 1.60-1.40 (s, 4H), 1.60-1.40 (m, 4H), 1.36 (m, 4H), 0.96 (m, 6H) ppm.

^{13}C NMR (100 MHz, $CDCl_3$) δ_C 160.2, 156.7, 145.8, 142.1, 132.1, 129.8, 126.8, 115.8, 85.9, 71.2, 39.6, 31.0, 24.3, 17.6, 16.3, 14.3, 11.7 ppm.

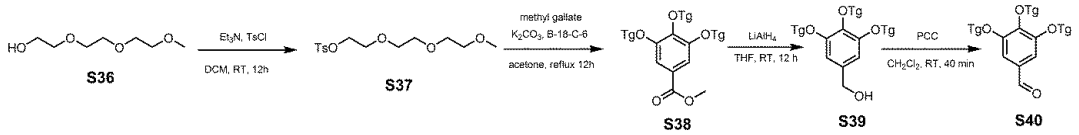

Synthesis of Compound S37

Triethyleneglycol monomethyl ether (10 g, 61 mmol) was dissolved in the mixture of DCM (100 mL) and Et_3N (13 mL). In a dropper, p-toluene sulfonyl chloride (12 g, 63 mmol) was dissolved in CH_2Cl_2 (20 mL) and was added to the previous solution dropwise while the reaction mixture was being cooled with ice bath. It was stirred for 12 h. After the washing with water, organic layer was collected and dried with Na_2SO_4. The solvent was evaporated in vacuo to give yellow oil (17 g, 55 mmol, 90%).

^{1}H NMR (400 MHz, $CDCl_3$) δ_H 7.78 (d, 2H; J = 8.2 Hz), 7.32 (d, 2H, J = 8.0 Hz) 4.15 (t, 2H; J = 4.8 Hz), 3.67 (m, 4H), 3.60 (m, 4H), 3.51 (m, 2H). 3.34 (s, 3H), 2.42 (s, 3H) ppm.

^{13}C NMR (100 MHz, $CDCl_3$) δ_C 144.8, 133.0, 129.8, 127.9, 71.9, 70.7, 70.5, 70.5, 69.3, 68.6, 59.0, 21.6 ppm.

HRMS (TOF-ESI): m/z calcd for $C_{14}H_{22}NaO_6S^+$ 341.1029 $[M+Na]^+$, found: 341.10639 $[M+Na]^+$, Δ = 10.23 ppm.

Synthesis of Compound S38

Methyl-3,4,5-trihydroxybenzoate (2.8 g, 15 mmol), compound **S37** (15 g, 47 mmol) and catalytic amount of benzo-18-crown-6 were dissolved acetone (60 mL). K_2CO_3 (8.3 g, 60 mmol) were added then the reaction mixture was refluxed for 18 h. The solvent was removed under reduced pressure and the crude product was treated with water and extracted with EtOAc. Organic layer was dried with Na_2SO_4. The product was purified by silica gel column chromatography (EtOAc). Corresponding fractions were collected and the solvent was removed to yield colorless liquid (6.0 g, 9.6 mmol, 64%).

^{1}H NMR (400 MHz, $CDCl_3$) δ_H 7.30 (s, 2H), 4.22 (m, 6H), 3.88 (m, 7H), 3.80 (m, 2H), 3.74 (m, 6H). 3.65 (m, 12H), 3.56 (m, 6H), 3.38 (s, 9H) ppm.

^{13}C NMR (100 MHz, $CDCl_3$) δ_C 166.5, 152.3, 142.6, 124.9, 109.0, 72.4, 71.9, 70.8, 70.7, 70.6, 70.5, 69.6, 68.8, 52.1 ppm.

Synthesis of Compound S39

Compound **S38** (3.0 g, 4.8 mmol) was dissolved in freshly distilled THF (20 mL) while the flask was being cooled within ice bath. To this solution, $LiAlH_4$ (347 mg, 9.60 mmol) was added portion wise. Then the reaction mixture was stirred 12 h at room temperature. The excess $LiAlH_4$ was carefully quenched with cold water then the reaction mixture was treated with water and extracted with EtOAc. The product was

purified by silica gel column chromatography (EtOAc). Fractions containing compound **S39** were collected then the solvent was evaporated in vacuo to give colorless liquid (2.5 g, 4.2 mmol, 88%).

^{1}H NMR (400 MHz, $CDCl_3$) δ_H 6.63 (s, 2H), 4.58 (s, 2H), 4.15 (m, 6H), 3.84 (t, 4H, J = 5.3 Hz), 3.79 (t, 2H, J = 5.4 Hz), 3.73 (m, 6H). 3.65 (m, 12H), 3.54 (m, 6H), 3.38 (s, 9H) ppm.

^{13}C NMR (100 MHz, $CDCl_3$) δ_C 152.7, 137.8, 136.7, 106.6, 72.3, 71.9, 70.8, 70.7, 70.5, 69.8, 68.9, 65.2, 59.0 ppm.

Synthesis of Compound S40

Compound **S39** (2.4 g, 4.0 mmol) was dissolved in CH_2Cl_2 (25 mL). Pyridinium chlorochromate (2.2 g, 10 mmol) was added to the reaction mixture and it was stirred for 40 min at rt. Then, it was directly applied to silica column chromatography (EtOAc/MeOH 95/5) to yield colorless oil (2.4 g, 4.0 mmol, quantitative).

^{1}H NMR (400 MHz, $CDCl_3$) δ_H 9.82 (s, 1H), 7.14 (s, 2H), 4.21 (m, 6H), 3.89 (m, 4H), 3.82 (m, 2H), 3.80-3.50 (m, 24H), 3.38 (s, 9H) ppm.

^{13}C NMR (100 MHz, $CDCl_3$) δ_C 191.0, 153.0, 144.1, 131.6, 109.0, 72.5, 71.9, 70.8, 70.7, 70.6, 70.5, 69.6, 68.9, 59.0 ppm.

HRMS (TOF-ESI): m/z calcd for $C_{28}H_{48}NaO_{13}^{+}$ 615.2987 $[M+Na]^+$, found: 615.28633 $[M+Na]^+$, Δ = 20.10 ppm.

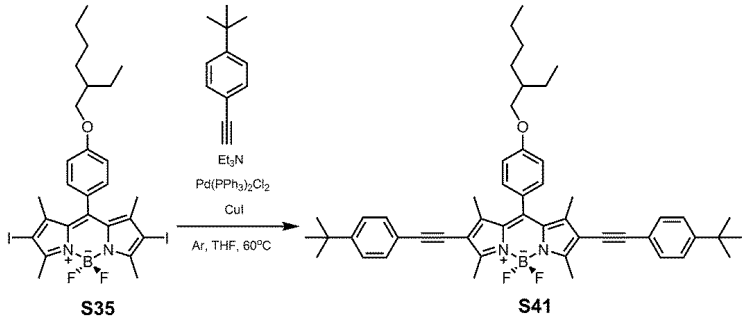

Synthesis of Compound S41

Compound **S35** (100 mg, 0.14 mmol) was dissolved in THF (30 mL) and triethylamine (5 mL). Argon was purged for 30 min. Then, 15% mole equivalent of $Pd(PPh_3)_4$ (24 mg, 21 μmol) was added. 4-(Tert-butyl)phenylacetylene (88 μL, 0.49 mmol) was added via syringe and the reaction mixture was stirred 12 h at 60°C. After it was cooled to rt, the mixture was treated with water then extracted with CH_2Cl_2. Organic layer was dried with Na_2SO_4 and the solvent was removed under reduced pressure. The product was purified by silica gel column chromatography (EtOAc/Hexanes 10:90). Fractions containing compound **S41** were collected then the solvent was evaporated to obtain dark blue solid (92 mg, 0.12 mmol, 86%).

^{1}H NMR (400 MHz, $CDCl_3$) δ_H 7.43 (d, 4H, J = 8.2 Hz), 7.37 (d, 4H, J = 8.5 Hz), 7.18 (d, 2H, J = 8.5 Hz), 7.06 (d, 2H, J = 8.6 Hz), 3.95 (d, 2H, J = 5.8 Hz), 2.73 (s, 6H), 1.80 (m, 1H), 1.60-1.30 (m, 28H), 0.96 (m, 6H) ppm.

^{13}C NMR (100 MHz, $CDCl_3$) δ_C 160.3, 158.1, 151.4, 143.9, 142.7, 131.7, 131.1, 129.1, 126.2, 125.4, 120.4, 116.2, 115.4, 96.5, 81.0, 70.9, 39.4, 34.8, 31.2, 30.6, 29.2, 23.9, 23.1, 14.1, 13.7, 13.6, 11.2 ppm.

HRMS (TOF-ESI): m/z calcd for $C_{51}H_{60}BF_2N_2O^+$ 765.4761 $[M+H]^+$, found: 765.4540 $[M+H]^+$, Δ = 28.87 ppm.

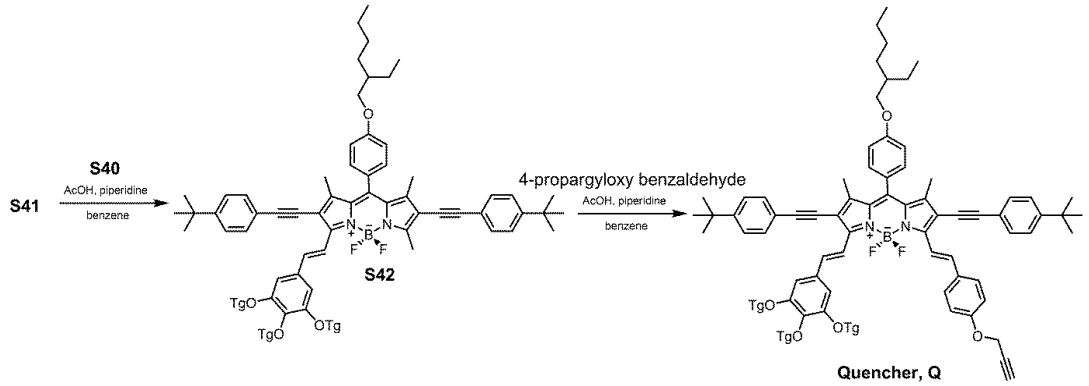

Synthesis of Compound S42

Compound **S41** (150 mg, 0.20 mmol) and compound **S40** (100 mg, 0.17 mmol) were dissolved in benzene (45 mL). Piperidine (0.3 mL) and acetic acid (0.3 mL) were added. The reaction mixture was refluxed using Dean Stark apparatus until all aldehyde was consumed. After the reaction was completed, it was extracted with CH_2Cl_2. The product was purified by silica gel column chromatography (EtOAc/MeOH 85:15). Corresponding fractions were collected and the solvent was evaporated under reduced pressure to get dark blue solid (55 mg, 41 μmol, 21%).

^{1}H NMR (400 MHz, $CDCl_3$) δ_H 8.34 (d, 1H, J = 16.2 Hz), 7.62 (d, 1H, J = 16. 2 Hz), 7.50-7.30 (m, 8H), 7.21 (d, 2H, J = 8.6 Hz), 7.06 (d, 2H, J = 8.6 Hz), 6.87 (s, 2H), 4.25 (m, 6H), 3.95 (d, 2H, J = 4.6 Hz), 3.90 (t, 4H, J = 5.4 Hz), 3.85 (t, 2H, J = 4.4 Hz), 3.80-3.50 (m, 24H), 3.38 (s, 9H), 2.77 (s, 3H), 1.8 (m, 1H), 1.65 (s, 3H), 1.63 (s, 3H), 1.60-1.40 (m, 6H), 1.40-1.20 (m, 20H), 0.95 (m, 6H) ppm.

^{13}C NMR (100 MHz, $CDCl_3$) δ_C 160.3, 152.9, 151.7, 151.5, 141.4, 140.0, 138.8, 132.5, 131.1, 130.8, 129.3, 126.4, 125.5, 125.4, 120.5, 120.4, 115.4, 107.5, 98.1, 96.7, 83.3, 81.0, 72.5, 72.0, 71.9, 71.0, 70.9, 70.7, 70.6, 69.8, 69.0, 59.0, 39.4, 34.8, 31.2, 30.6, 29.2, 23.9, 23.0, 14.1, 13.7, 13.4, 11.2 ppm.

HRMS (TOF-ESI): m/z calcd for $C_{79}H_{105}BF_2N_2NaO_{13}^+$ 1361.7570 $[M+Na]^+$, found: 1361.7296 $[M+Na]^+$, Δ = 20.12 ppm.

Synthesis of Quencher Module, Q

Compound **S42** (45 mg, 30 μmol) and 4-propargyloxy benzaldehyde (9.1 mg, 56 μmol) were dissolved in benzene (25 mL). Piperidine (0.2 mL) and acetic acid (0.2 mL) were added. The reaction mixture was refluxed using Dean Stark apparatus. After the reaction was completed then it was treated with water and extracted with CH_2Cl_2. Organic layer was collected and dried with Na_2SO_4 and the solvent removed under reduced pressure. The product was purified by silica gel column chromatography (EtOAc/MeOH 90/10) to yield dark blue solid (40 mg, 27 μmol, 90%).

^{1}H NMR (400 MHz, $CDCl_3$) δ_H 8.49 (d, 1H, J = 16.2 Hz), 8.34 (d, 1H, J = 16.2 Hz), 7.74 (d, 1H, J = 16.6 Hz), 7.65 (s 1H), 7.65 (d, 2H), 7.65 (d, 2H), 7.50-7.30 (m, 8H), 7.21 (d, 2H, J = 8.1 Hz), 7.10-7.00 (m, 4H), 6.90 (s, 2H), 4.77 (2H), 4.25 (m, 6H), 4.00- 3.50 (m, 32H), 3.40 (s, 3H), 3.37 (s, 6H), 2.60 (1H), 1.80-1.20 (m, 23H), 0.98 (m, 6H) ppm.

^{13}C NMR (100 MHz, $CDCl_3$) δ_C 160.3, 158.6, 152.9, 151.7, 145.3, 140.2, 139.7, 138.8, 132.7, 130.8, 130.7, 129.6, 129.2, 126.6, 125.6, 125.5, 120.6, 120.5, 115.3, 107.9, 98.4, 98.2, 83.4, 83.1, 77.4, 77.1, 76.7, 75.9, 72.5, 72.0, 71.9, 69.9, 69.2, 59.0, 59.0, 59.0, 55.9, 39.4, 34.8, 31.2, 30.6, 29.2, 23.9, 23.1, 14.1, 11.2 ppm.

HRMS (TOF-ESI): m/z calcd for $C_{89}H_{111}BF_2N_2NaO_{14}^+$ 1503.7989 $[M+Na]^+$, found: 1503.7684 $[M+Na]^+$, Δ = 20.28 ppm.

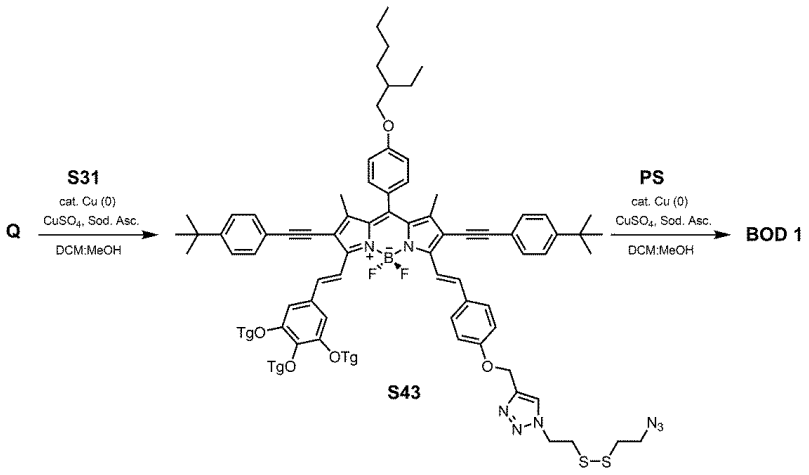

Synthesis of Compound S43

Compound **Q** (45 mg, 30 μmol) and compound **S31** (62 mg, 300 μmol) were dissolved in CH_2Cl_2 (6 mL) and MeOH (3 mL). Saturated solutions of $CuSO_4 \cdot 5H_2O$ (100 μL) and sodium ascorbate (100 μL) were added. Catalytic amount of Cu (0) was added. The reaction mixture was stirred for 12 h at room temperature. After the reaction was completed, the mixture was extracted with CH_2Cl_2. Organic layer was collected and dried with Na_2SO_4 and the solvent evaporated under reduced pressure. The product was purified by silica gel column chromatography (EtOAc/MeOH 85:15). Corresponding fractions were combined then the solvent was removed under reduced pressure to obtain dark blue solid (30 mg, 18 μmol, 60%).

^{1}H NMR (400 MHz, $CDCl_3$) δ_H 8.48 (d, 1H, J = 16.3 Hz), 8.34 (d, 1H, J = 16.3 Hz), 7.75-7.60 (m, 6H), 7.50-7.30 (m, 8H), 7.21 (d, 2H, J = 8.3 Hz), 7.08 (d, 2H, J = 3.5 Hz), 7.05 (d, 2H, J = 3.4 Hz), 6.91 (s, 2H), 5.31 (s, 2H), 4.73 (t, 2H, J = 6.6 Hz), 4.25 (m, 6H), 4.00- 3.50 (m, 32H), 3.40 (s, 3H), 3.37 (s, 6H), 3.22 (t, 2H, J = 6.6 Hz), 2.89 (m, 4H), 1.80-1.20 (m, 23H), 0.98 (m, 6H) ppm.

^{13}C NMR (100 MHz, $CDCl_3$) δ_C 160.3, 159.3, 153.0, 151.8, 145.3, 144.4, 140.1, 139.6, 138.9, 133.4, 132.7, 132.2, 131.9, 130.8, 130.4, 129.6, 128.6, 126.7, 125.5, 123.6, 120.6, 118.4, 117.1, 116.1, 115.3, 114.0, 107.9, 107.2, 98.4, 98.2, 83.3, 72.5, 71.9, 70.9, 70.8, 70.7, 70.5, 70.4, 69.8, 69.2, 68.9, 62.1, 59.0, 49.9, 48.9, 39.5, 37.7, 34.9, 31.3, 30.6, 29.2, 23.9, 23.1, 14.1, 13.5 ppm.

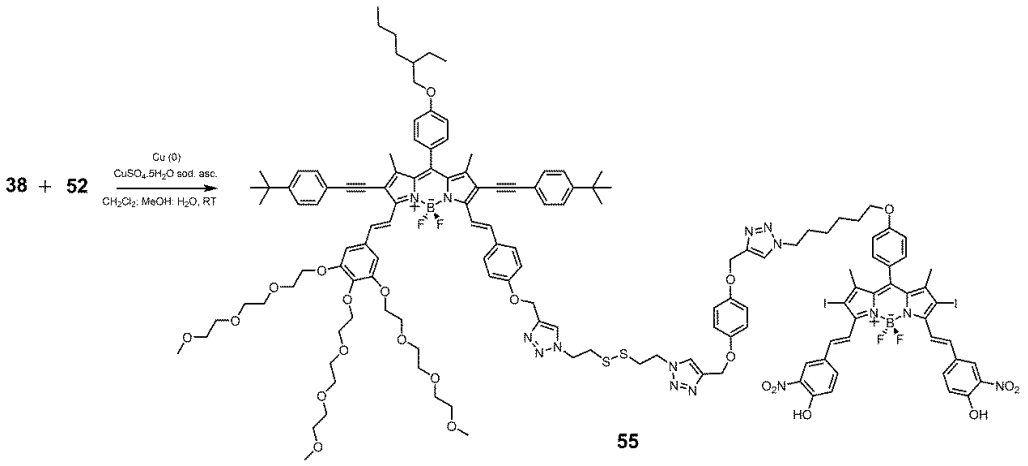

Synthesis of BOD 1

Compound **S43** (40 mg, 24 μmol) and compound **PS** (45 mg, 37 μmol) were dissolved in DCM (6 mL) and MeOH (3 mL). Saturated solutions of $CuSO_4 \cdot 5H_2O$ (100 μl) and sodium ascorbate (100 μl) were added. Catalytic amount of Cu (0) was added. The reaction mixture was stirred for 12 h at room temperature. Then the reaction mixture was treated with water and extracted with CH_2Cl_2. Organic layer was collected and dried with Na_2SO_4. The product was purified by silica gel column chromatography (EtOAc/MeOH 85:15) to get dark blue solid (35 mg, 12 μmol, 50%).

^{1}H NMR (400 MHz, $CDCl_3$) δ_H 8.48 (d, 1H, J = 15.9 Hz), 8.32 (d, 1H, J = 15.8 Hz), 8.29 (s, 2H), 8.09 (d, J = 16.5 Hz, 2H), 7.95 (d, J = 8.0 Hz, 2H), 7.8-7.5 (m, 10H), 7.50-7.30 (m, 10H), 7.25-7.10 (m, 6H), 7.10-7.0 (m, 5H), 6.90 (m, 6H), 5.30 (s, 2H), 5.15 (s, 4H), 4.65 (s, 4H), 4.40 (m, 2H), 4.2 (m, 6H), 4.10-3.50 (m, 36H), 3.30 (s, 3H), 3.30 (s, 6H), 3.15 (m, 4H), 2.05 (m, 18H), 1.8 (m, 4H), 1.60-1.0 (m, 21H), 0.95 (m, 6H) ppm.

^{13}C NMR (100 MHz, $CDCl_3$) δ_C 167.8, 160.3, 160.2, 159.2, 158.6, 155.6, 152.8, 151.7, 149.8, 146.6, 138.8, 136.2, 135.4, 133.7, 132.7, 130.8, 130.3, 129.6, 129.5, 129.4, 129.3, 126.6, 125.6, 125.5, 124.4, 123.7, 120.7, 120.4, 119.4, 115.9, 115.8, 115.5, 115.3, 107.8, 72.4, 71.9, 70.9, 70.8, 70.6, 70.5, 69.8, 69.1, 59.0, 58.9, 48.9, 40.6, 39.4, 31.2, 30.6, 30.2, 29.2, 26.3, 25.6, 23.9, 23.0, 17.8, 14.1, 13.5, 11.2 ppm.

HRMS (TOF-ESI): m/z calcd for $C_{144}H_{162}B_2F_4I_2N_{15}O_{23}S_2^-$ 2884.9 $[M-H]^-$, found: 2884.9 [M-H].

4.5.1. Additional Information

pKa Determination. Aqueous solutions of each compound are prepared and titrated with aliquots of acid (HCl) and base (NaOH) solutions. Each time, pH of the solution is measured with the aid of a pH meter and the spectra are recorded.Since there are two different absorbing species, one protonated/deprotonated and one neutral, two different peak absorbance wavelengths are observed. Plotting pH versus the ratio of

absorbance at these two wavelengths and subsequent non-linear curve fit in Origin software gives the experimental pKa values in water. For some compounds 3, 4 and PS 40% THF was used to increase solubility. Since PS is the true module of the target compound (**BOD 1**) and is not soluble in water, the pKa measurements are performed after the formation of micelle.

Micelle Preparation. Micelles of PS module are prepared with Cremophor EL using the procedure in literature [252]. 50 mg Cremophor EL and **PS** (6 mg, 5 μmol) or **BOD 1** (14 mg, 5 μmol) are dissolved in 330 mL freshly distilled tetrahydrofuran. The solution is sonicated for 30 min, while the sonication water bath is kept below 35ºC. Then, THF is evaporated under reduced pressure and the remaining compounds are dissolved in water (5 mL). The suspension is filtered through 0.45 μm PTFE filter. For each measurement micelles are prepared freshly. Concentrations of solutions of the compounds in micelles are predicted using their extinction coefficients in THF. GSH (2.5 equivalent) is added to the solution of **BOD 1** before the preparation of the micelle and the sample is incubated at room temperature for 12 h at room temperature, before HRMS and spectroscopic analysis are performed.

$^1O_2$ Generation Experiments. $^1O_2$ dependent degradation of water soluble trap, 2,2'-(anthracene-9,10-diylbis(methylene) dimalonic acid is used to measure photodynamic activity since the absorption of this compound decreases upon reaction indicating the generation of $^1O_2$ [253]. Since the water solubility of the anthracene-based trap is poor in water, samples are sonicated for 15 min to obtain clear solutions. Measurements are performed using 625 nm LED and samples are irradiated with the light source from a 5 cm distance. All samples are aerated for 5 min prior to experiments. After incubation under dark for 15 min, light is irradiated for 60 min and UV-Vis spectra are recorded at each 5 min intervals. Relative singlet oxygen efficiency is calculated by the percent decrease in trap absorbance at 378 nm within 60 min light irradiation period.

CHAPTER 5

5. BODIPY Assisted Dopamine Recognition

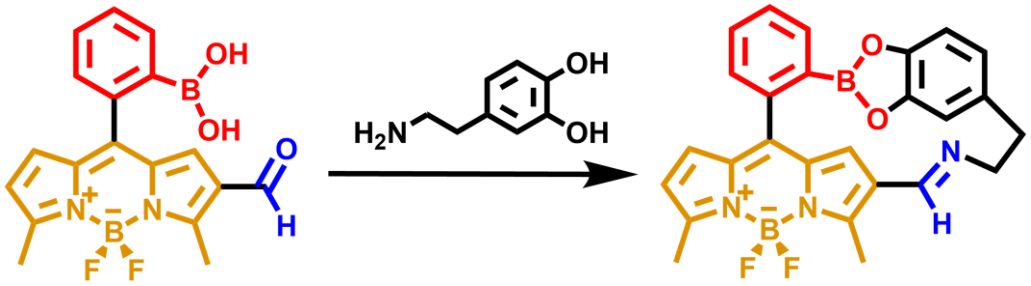

5.1. Objective

Dopamine (DA), which is the a member of catecholamine family participates in number of central nerve diseases such as Parkinson's disease and schizophrenia. Therefore, sensing and monitoring of DA is significant field. In this study, we designed water-soluble fluorescent chemosensor to sense DA. Bodipy based fluorophore was functionalized with amine and diol moieties.

5.2. Introduction

Catecholamines, including dopamines, neroephirines and epinephrines (adrenaline) participated in numerous important biological processes. Catecholamines are principal neurotransmitters that deal with many differences in central nervous system [254]. By this way, they increase heart rate, blood pressure, muscle strength and mental alertness and they prepare the body for the "fight-or-flight" response. Also they play critical role in some of the diseases and disorders such as hyperactivity disorder, Parkinson's disease, schizophrenia, hypertension and addiction [255].

Boronic acids have high affinity to diol group including compounds [256], [257]. Because of that reason boronic acid containing molecules were designed and synthesized for sensing of carbohydrates and some other biological compounds. 2-anthrylboronic acid was the first example to fluorescent chemosensor for diol containing compounds in 1992 [258].

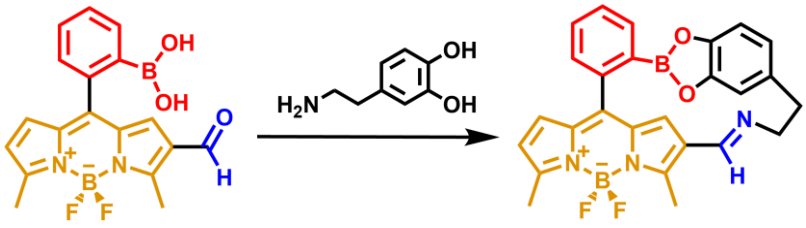

Figure 101. Mechanism of dopamine sensing with target molecule.

In this study, our target molecule is the sensor for catecholamines. There is boronic acid group to sense diol groups and it has also amine moiety. Binding of dopamine

prevents the movement of phenylboronic acid group at meso position of Bodipy and that increases emission of Bodipy core.

5.3. Results and Discussion

In fluorescent dyes, steric constrain increases quantum yields. Without steric hindrance, phenyl group has free rotation so quantum yield is very low. In the existence of methyl groups at 1 and 7 positions of Bodipy core, phenyl group cannot rotate because of the methyl groups and by this way increasing in quantum efficiency is observed (Figure **102**). There is a non-radiative energy loss from the excited states because of the rotational molecular motions and methyl groups at 1 and 7 positions prevent the non-radiative energy loss due to free rotation.

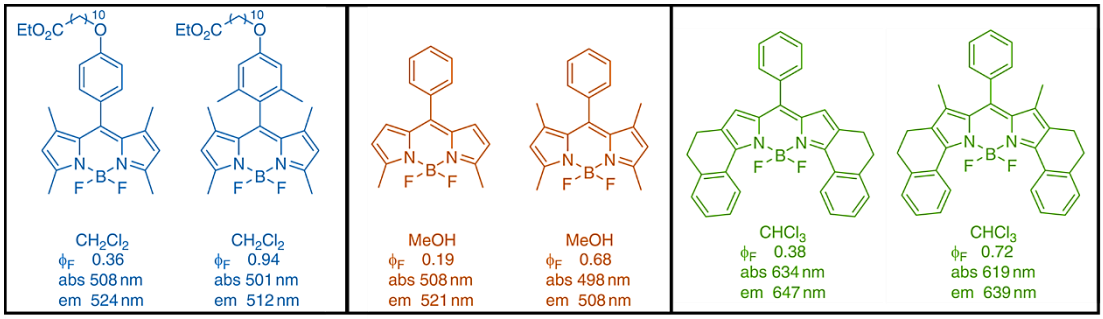

Figure 102. Structure-quantum yield relationship in Bodipy derivatives [259].

In our design, Bodipy dye was used as fluorophore and it was functionalized with boronic acid for diol sensing. There was also formyl group attached to Bodipy core for amine sensing. Dopamine molecule has diol and amine groups and it binds to both boronic acid and formyl groups of compound **3** at the same time. Binding of dopamine prevents the free rotation, therefore quantum yields will increase.

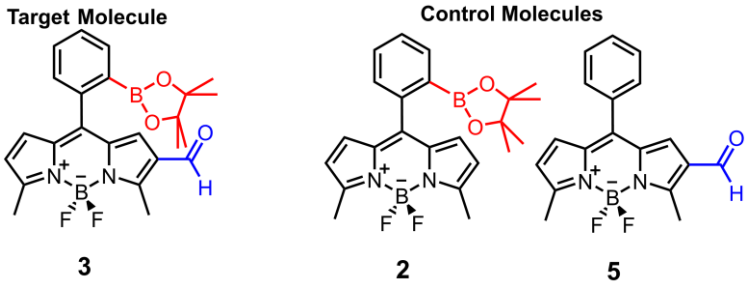

Figure 103. Structure of target and control molecules.

In synthesis part, three different Bodipy derivatives was aimed (Figure **103**). At the beginning, diol group of 2-formylphenylboronic acid was protected with pinacol for solubility in organic solvents and to prevent decomposition of compound **2**. Then the protected aldehyde was placed at meso position of Bodipy core by reaction with 2-methylpyrrole. Then, formylation of Bodipy core was achieved with Vilsmeier-Haack reaction. Synthesis of compound **4** and **5** was accomplished with the procedure which is similar synthesis of compound **3**.

Target molecule was used without deprotection in the fluorescence measurements because it was expected that the hydrolysis completes in aqueous media [260], [261].

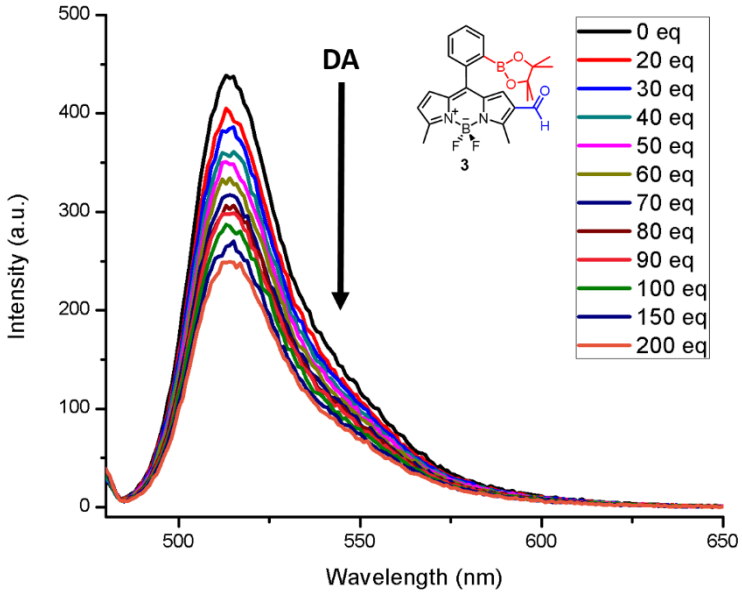

Figure 104. Fluorescence spectra of the compound **3** (1 μM) upon increasing dopamine concentrations (0-200 equiv) in 1x PBS buffer solution (pH=7.4, λ_{ex} = 480 nm at 25°C).

It was supposed that compound **3** doesn't have emission because of the free rotation then it will start to give emission with binding of dopamine (Figure **101**). However, we carried the measurements and results were different from expected. According to the fluorescence spectra, adding of dopamine decreased the emission of compound **3** (Figure **104**). It can be explained that $B(OR)_2$ group is large and very close to the Bodipy core, so there is no free rotation because of the steric hindrance. The binding may cause photoinduced electron transfer (PET) and decreasing in the emission was observed.

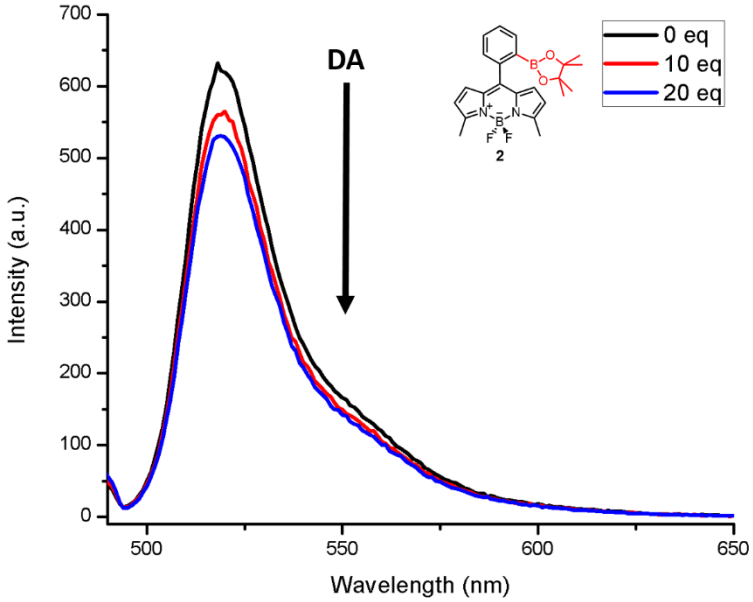

Figure 105. Fluorescence spectra of the compound **2** (1 μM) upon increasing dopamine concentrations (0-20 equiv) in 1x PBS buffer solution (pH=7.4, λ_{ex} = 480 nm at 25ºC).

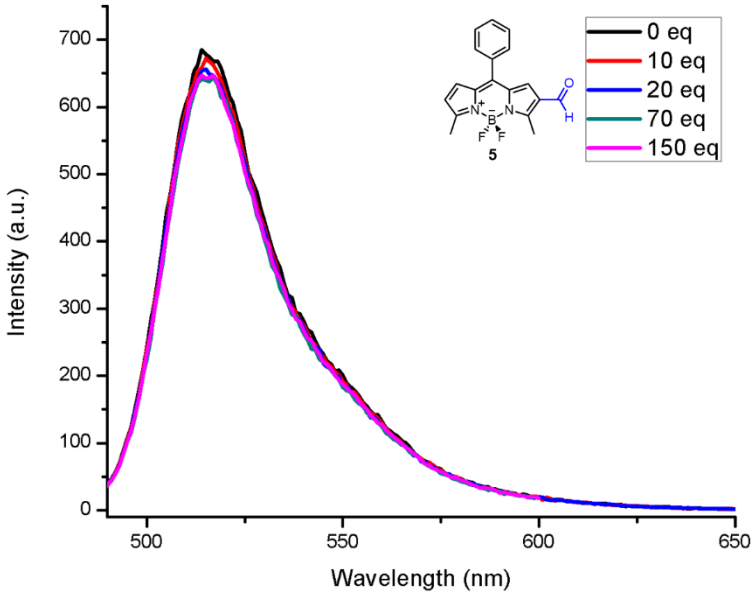

Figure 106. Fluorescence spectra of the compound **5** (1 μM) upon increasing dopamine concentrations (0-150 equiv) in 1x PBS buffer solution (pH=7.4, λ_{ex} = 470 nm at 25ºC).

Emission spectrums of target molecule and control molecules shows that it did not work as planned. Control molecules were designed to understand working principle of diol and amine moieties. In the emission spectrums of compound **2**, adding dopamine decreases emission intensity (Figure **105**) and that is similar to fluorescence spectra of compound **3**. There is no change in the spectrum of compound **5** that means there is no binding to amine moiety.

5.4. Conclusion

In conclusion, we designed a chemosensor for dopamine (DA) sensing. The idea behind this study was that preventing the free rotation of phenyl group at meso position of Bodipy core results in enhancement in quantum yield. However, the fluorescence spectra was dissimilar to desired one. The study didn't achieve the expected results.

5.5. Experimental Details

Synthetic Pathway:

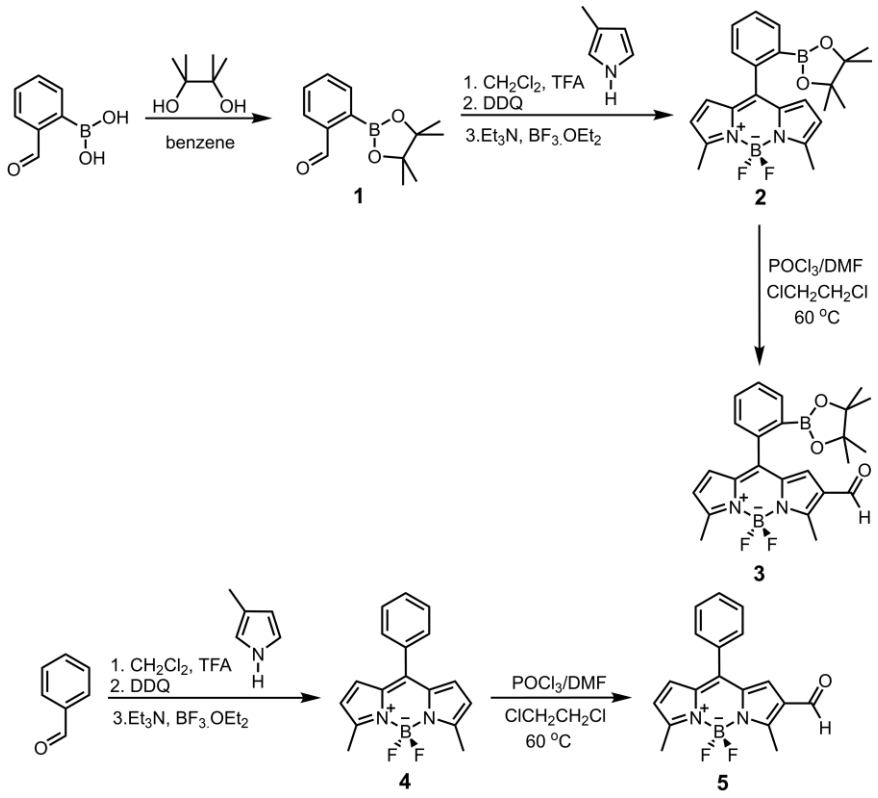

Synthesis of Compound 1

2-formylphenylboronic acid (1.0 g, 6.6 mmol) was dissolved in benzene (25 mL) and pinacol (1.1 eq, 0. 86 g, 7.3 mmol) was added to solution. A Dean-Stark trap was filled with benzene and attached to flask. The reaction mixture was refluxed for 5 h and the water that formed in reaction was hold by trap. The mixture was cooled to room temperature then it was filtered through $MgSO_4$ pad. The pure product which is thick and yellow oil was obtained (1.50 g, 6.5 mmol, 95%).

^{1}H NMR (400 MHz, $CDCl_3$) δ_H 10.56 (s, 1H), 7.96 (d, J = 7.9 Hz, 1H), 7.88 (d, J = 7.1 Hz, 1H), 7.65 – 7.49 (m, 2H), 1.41 (s, 12H) ppm.

^{13}C NMR (100 MHz, $CDCl_3$) δ_C 213.0, 194.6, 141.3, 135.5, 133.0, 130.7, 127.9, 24.7 ppm.

Synthesis of Compound 2

Compound 1 (1.08 g, 4.65 mmol) was dissolved in DCM (200 mL) and the solution was bubbled with Argon for 15 min. Then 2-methylpyrrole (2.2 eq, 0.76 mL, 0.69 g, 10.2 mmol) and a few drops of TFA were added and the solution was stirred overnight at rt. p-chloranil (0.57 g, 2.3 mmol) was added to the reaction mixture and stirring continued for 45 min. Finally, Et_3N (3 mL) and $BF_3{\cdot}OEt_2$ (3 mL) were added to the reaction sequentially. After stirring 1 h, the reaction mixture washed with water (3x150 mL) and the organic phase dried with Na_2SO_4. The solvent was evaporated under vacuum then the residue was purified with silica gel column chromatography (DCM:Hex 2:1) to yield reddish solid (0.59 g, 1.4 mmol, 30%).

^{1}H NMR (400 MHz, $CDCl_3$) δ_H 7.81 (s, 1H), 7.49 (dd, J = 5.5, 2.9 Hz, 2H), 7.41 (d, J = 3.8 Hz, 1H), 6.55 (d, J = 3.8 Hz, 2H), 6.22 (d, J = 4.0 Hz, 2H), 2.66 (s, 6H), 1.08 (s, 12H) ppm.

^{13}C NMR (100 MHz, $CDCl_3$) δ_C 156.9, 139.0, 134.2, 130.1, 130.0, 129.8, 129.6, 128.6, 128.3, 118.9, 118.9, 84.0, 24.4, 14.8 ppm.

HRMS (TOF-ESI): m/z calcd for $C_{23}H_{26}B_2F_2N_2O_2^+$: 420.22156 $[M]^+$, Found: 420.22221 $[M]^+$, Δ=1.55 ppm.

Synthesis of Compound 3

DMF (12 mL) and $POCl_3$ (12 mL) were stirred in ice bath for 5 min under Ar gas. After warming to room temperature, the mixture was stirred for another 30 min. Compound 2 (477 mg, 1.1 mmol) dissolved in dichloroethane (40 mL) was added and the reaction mixture was stirred for additional 2 h at 50 ^{o}C. The reaction mixture poured in to ice cold $NaHCO_3$ solution (150 mL). After stirring 30 min, the solution was washed with water (3x100 mL). The organic layers was dried with Na_2SO_4 and the solvent was removed under vacuum. The crude product was purified with silica gel column chromatography (DCM: Hex 2:1) to get reddish solid (483 mg, 1.1 mmol, 95%).

^{1}H NMR (400 MHz, $CDCl_3$) δ_H 9.87 (s, 1H), 7.94 – 7.80 (m, 1H), 7.68 – 7.50 (m, 2H), 7.46 – 7.37 (m, 1H), 6.91 (s, 1H), 6.78 (d, *J* = 4.3 Hz, 1H), 6.42 (d, *J* = 4.4 Hz, 1H), 2.90 (s, 3H), 2.73 (s, 3H), 1.06 (s, 12H) ppm.

^{13}C NMR (100 MHz, $CDCl_3$) δ_C 185.5, 163.4, 155.8, 146.4, 138.2, 137.7, 134.8, 134.4, 133.4, 130.1, 129.4, 129.2, 128.7, 128.4, 122.6, 84.0, 24.4, 15.3, 13.2 ppm.

HRMS (TOF-ESI): m/z calcd for $C_{24}H_{27}B_2F_2N_2O_3^+$: 449.22430 $[M+H]^+$, Found: 449.22024 $[M+H]^+$, Δ=9.04 ppm.

Synthesis of Compound 4

Benzaldehyde (0.57 mL, 0.60 g, 5.7 mmol) was dissolved in DCM (200 mL) and the solution was bubbled with Ar for 15 min. Then 2-methylpyrrole (2.2 eq, 0.93 mL, 0.85 g, 12.5 mmol) and a few drops of TFA were added and the solution was stirred overnight at rt. p-chloranil (0.71 g, 2.8 mmol) was added to the reaction mixture and stirring continued for 45 min. Finally, Et_3N (3 mL) and $BF_3{\cdot}OEt_2$ (3 mL) were added to the reaction sequentially. After stirring 1 h, the reaction mixture washed with water (3x150 mL) and the organic phase dried with Na_2SO_4. The solvent was evaporated under vacuum then the residue was purified with silica gel column chromatography (DCM) to yield red solid (0.59 g, 2.0 mmol, 35%).

^{1}H NMR (400 MHz, $CDCl_3$) δ_H 7.64 – 7.38 (m, 5H), 6.74 (d, *J* = 4.1 Hz, 1H), 6.32 (d, *J* = 4.1 Hz, 1H), 2.71 (s, 6H) ppm.

^{13}C NMR (100 MHz, $CDCl_3$) δ_C 157.6, 142.6, 134.6, 134.1, 130.4, 130.4, 129.9, 128.2, 119.4, 14.90 ppm.

HRMS (TOF-ESI): m/z calcd for $C_{17}H_{16}BF_2N_2^+$: 296.14054 $[M+H]^+$, Found: 296.13707 $[M+H]^+$, Δ=11.73 ppm.

Synthesis of Compound 5

DMF (12 mL) and $POCl_3$ (12 mL) were stirred in ice bath for 5 min under Ar gas. After warming to room temperature, the mixture was stirred for another 30 min. Compound 4 (355 mg, 1.2 mmol) dissolved in dichloroethane (40 mL) was added and the reaction mixture was stirred for additional 2 h at 50 ^{o}C. The reaction mixture poured in to ice cold $NaHCO_3$ solution (150 mL). After stirring 30 min, the solution was washed with water (3x100 mL). The organic layers was dried with Na_2SO_4 and the solvent was removed under vacuum. The crude product was purified with silica gel column chromatography (DCM: Hex 1:1) to get red solid (365 mg, 1.1 mmol, 94%).

^{1}H NMR (400 MHz, $CDCl_3$) δ_H 9.92 (s, 1H), 7.70 – 7.46 (m, 5H), 7.13 (s, 1H), 6.97 (d, J = 4.3 Hz, 1H), 6.49 (d, J = 4.4 Hz, 1H), 2.91 (s, 3H), 2.75 (s, 3H) ppm.

^{13}C NMR (100 MHz, $CDCl_3$) δ_C 185.3, 164.1, 156.5, 144.4, 136.7, 133.9, 133.2, 132.9, 130.6, 130.3, 129.1, 128.8, 128.5, 123.1, 15.5, 13.2 ppm.

HRMS (TOF-ESI): m/z calcd for $C_{18}H_{16}BF_2N_2O^+$: 324.13546 $[M+H]^+$, Found: 324.13522 $[M+H]^+$, Δ=0.73 ppm.

EPILOGUE

In this thesis, we have achieved hopeful results in the field of BODIPY chemistry, molecular logic gates, cage compounds and as well as photodynamic therapy concepts. Four different studies were carried out in these application areas. Since BODIPY dyes have adorable properties, they were preferred fluorescent fluorophore in our projects in the design of photosensitizers and chemosensors.

In the Chapter 2, we have reported cascaded molecular logic gate that metal ions and light were used as signals. Molecular logic gate is promising area which can be alternative to silicon based logic gates because they are too small that may solution to miniaturization problem. Our cascaded molecular logic gate consist of three modules which are an INH and two AND gates. In first part is INH module and the output is Zn (II) ion while the inputs are 360 nm light and lack of EDTA. Then AND module is used whose inputs are Zn (II) and 560 nm light. The output in this gate is through space energy transfer. The last one is AND gate which has 560 nm light and Hg (II) as inputs and finally we get the response that 660 nm light. By this way cascaded molecular logic gate was introduced whose structure is INH-AND-AND. In this study, the inspiring point is that combination of cage compounds and molecular logic gates in one pot.

A novel design of cage compounds was described in Chapter 3. Cage compounds are up-and-coming field of chemistry and they can be used in the biological applications. Especially releasing metal ions is a very crucial area in terms of mimicking the biological process. For example, releasing zinc ion which is very important in human body because of the critical roles such as second intercellular messenger and significance in some disorders like Alzheimer's disease, epilepsy, Parkinson's disease. However, cage compounds have a drawback in the uncaging process. Almost all of cage compounds work in UV region that inappropriate for biological applications because it can gives rise to DNA damage. Another problem about UV light is that its penetration to tissues is limited. Our novel design which consists of BODIPY based photosensitizers and dithioethenyl bond provide uncaging in Near-IR region. The brief

working mechanism is that photosensitizer generate singlet oxygen irradiation with Near-IR light. Then singlet oxygen break dithioethenyl bond that causes lower metal ion affinity and that results releasing of metal ion. Our cage compounds is tunable that working wavelength can be arranged to intended value In this way, disadvantages of UV light which are DNA damage and penetration problems can be solved.

Chapter 4 is about pH and glutathione (GSH) responsive BODIPY based photosensitizers (PS). We designed AND logic gate which is formed pH responsive photosensitizer and quencher that attached with disulfide bond. In this logic gate, inputs are proton ion and GSH. In presence of proton and GSH, our photosensitizer started to produce singlet oxygen. The idea behind this molecular logic gate is that tumour microenvironment is more acidic and glutathione amount is more than normal cells, so our photosensitizer starts to work only in cancer cells. PS is quenched by excitation energy transfer (EET) in the condition that PS and quencher BODIPY is connected with disulfide bond. In the existence of glutathione, disulfide bond is reduced that means cleaved. Then, free photosensitizer can begin to generate singlet oxygen.

In the Chapter 5, we proposed a fluorescence chemosensor to sense dopamine, which participates in some crucial functions of brain such as memory, learning, attention etc. The phenomena, which we used in this study is that rigid structure increases the fluorescence quantum yield of fluorophores. Therefore, binding of dopamine to both diol and amine moieties will result in increment of fluorescence intensity. However, we didn’t reach the desired aim.

To conclude, there are three reported studies in the areas of molecular logic gates, cage compounds and singlet oxygen generation. In spite of all the promising results at these projects, they are still based on proof-of-principle mostly. So, we will head for applications of molecular logic gates and mimicking the nature in the fields from treatment of illnesses to nanotechnology.

BIBLIOGRAPHY

[1] D. J. Cram, "The design of molecular hosts, guests, and their complexes," *J. Incl. Phenom.*, vol. 6, no. 4, pp. 397–413, 1988.

[2] J. M. Lehn, "Cryptates: inclusion complexes of macropolycyclic receptor molecules," *Pure Appl. Chem.*, vol. 50, no. 9–10, pp. 871–892, 1978.

[3] H. E. Fischer, "Sitzung vom 29. October 1894," *Berichte der Dtsch. Chem. Gesellschaft*, vol. 27, no. 3, pp. 2871–2871, 1894.

[4] A. Werner, "Beitrag zur Konstitution anorganischer Verbindungen," *Zeitschrift für Anorg. Chemie*, vol. 3, no. 1, pp. 267–330, 1893.

[5] K. L. Wolf, H. Frahm, and H. Harms, "The State of Arrangement of Melecules in Liquids," *Z. Phys. Chem.*, vol. 36, pp. 237–287, 1937.

[6] J. D. Watson and F. H. C. Crick, "Molecular structure of nucleic acids," *J. Am. Med. Assoc.*, vol. 296, no. 15, pp. 1966–1967, 1993.

[7] C. J. Pedersen, "Cyclic Polyethers and Their Complexes with Metal Slats," *J. Am. Chem. Soc.*, vol. 89, no. 26, pp. 7017–7036, 1967.

[8] J. W. Steed and J. L. Atwood, *Supramolecular Chemistry*. Wiley-VCH Verlag GmbH & Co. KGaA, 2009.

[9] D. Philp and J. F. Stoddart, "Self-Assembly in Natural and Unnatural Systems," *Angew. Chemie - Int. Ed.*, vol. 35, no. 11, pp. 1154–1196, 1996.

[10] P. D. Beer, F. Szemes, V. Balzani, C. M. Sala, M. G. B. Drew, S. W. Dent, and M. Maestri, "Anion selective recognition and sensing by novel macrocyclic transition metal receptor systems. 1H NMR, electrochemical, and photophysical investigations," *J. Am. Chem. Soc.*, vol. 119, no. 49, pp. 11864–11875, 1997.

[11] B. L. Feringa, "The art of building small: From molecular switches to molecular motors," *J. Org. Chem.*, vol. 72, no. 18, pp. 6635–6652, 2007.

[12] D. T. McQuade, A. H. Hegedus, and T. M. Swager, "Signal amplification of a 'turn-on' sensor: Harvesting the light captured by a conjugated polymer," *J. Am. Chem. Soc.*, vol. 122, no. 49, pp. 12389–12390, 2000.

[13] S. C. Lo and P. L. Burn, "Development of dendrimers: Macromolecules for use in organic light-emitting diodes and solar cells," *Chem. Rev.*, vol. 107, no. 4, pp. 1097–1116, 2007.

[14] A. Credi, "Molecules that make decisions," *Angew. Chemie - Int. Ed.*, vol. 46, no. 29, pp. 5472–5475, 2007.

[15] V. Bernard, *Molecular fluorescence: principles and applications*, vol. 8. Wiley-VCH Verlag GmbH & Co. KGaA, 2001.

[16] A. Jabło'nski, "Efficiency of Anti-Stokes Fluorescence in Dyes," *Nature*, vol. 131, no. 3319, pp. 839–840, 1933.

[17] G. G. Stokes, "On the Change of Refrangibility of Light," *Philos. Trans. R. Soc. London*, vol. 143, pp. 463–562, 1852.

[18] M. Kasha, "Characterization of electronic transitions in complex molecules," *Discuss. Faraday Soc.*, vol. 9, pp. 14, 1950.

[19] T. Klikauer, *Reflections on phishing for phools: The economics of manipulation and deception*, vol. 14, no. 1, 2016.

[20] L. Song, E. J. Hennink, I. T. Young, and H. J. Tanke, "Photobleaching kinetics of fluorescein in quantitative fluorescence microscopy," *Biophys. J.*, vol. 68, no. 6, pp. 2588–2600, 1995.

[21] M. J. Geisow, "Fluorescein conjugates as indicators of subcellular pH. A critical evaluation," *Exp. Cell Res.*, vol. 150, no. 1, pp. 29–35, 1984.

[22] Y. Egawa, R. Hayashida, T. Seki, and J. ichi Anzai, "Fluorometric determination of heparin based on self-quenching of fluorescein-labeled protamine," *Talanta*, vol. 76, no. 4, pp. 736–741, 2008.

[23] F. Chemosensors, M. Recognition, A. C. S. S. Series, and A. C. Society, *Fluorescent Chemosensors for Ion and Molecule Recognition*, vol. 22, no. 4. American Chemical Society, 1994.

[24] Y. L. Ji, K. K. Sung, H. J. Jong, and S. K. Jong, "Bifunctional fluorescent calix[4]arene chemosensor for both a cation and an anion," *J. Org. Chem.*, vol. 70, no. 4, pp. 1463–1466, 2005.

[25] Z. Xu, J. Yoon, and D. R. Spring, "Fluorescent chemosensors for Zn(2+).," *Chem. Soc. Rev.*, vol. 39, no. 6, pp. 1996–2006, 2010.

[26] K. Rurack and U. Resch-Genger, "Rigidization, preorientation and electronic decoupling the 'magic triangle' for the design of highly efficient fluorescent sensors and switches.," *Chem. Soc. Rev.*, vol. 31, no. 2, pp. 116–127, 2002.

[27] A. P. De Silva, H. Q. N. Gunaratne, and C. P. McCoy, "A molecular photoionic AND gate based on fluorescent signalling," *Nature*, vol. 364, no. 6432, pp. 42–44, 1993.

[28] C. N. Baki and E. U. Akkaya, "Boradiazaindacene-appended calix[4]arene: Fluorescence sensing of pH near neutrality," *J. Org. Chem.*, vol. 66, no. 4, pp. 1512–1513, 2001.

[29] L. Fabbrizzi and A. Poggi, “Sensors and switches from supramolecular chemistry,” *Chem. Soc. Rev.*, vol. 24, no. 3, pp. 197, 1995.

[30] a P. de Silva, T. S. Moody, and G. D. Wright, “Fluorescent PET (photoinduced electron transfer) sensors as potent analytical tools.,” *Analyst*, vol. 134, no. 12, pp. 2385–2393, 2009.

[31] a. P. de Silva and S. a. de Silva, “Fluorescent signalling crown ethers; 'switching on' of fluorescence by alkali metal ion recognition and binding in situ ,” *J. Chem. Soc. Chem. Commun.*, no. 23, pp. 1709, 1986.

[32] A. P. de Silva, H. Q. Nimal Gunaratne, and K. R. A. Samankumara Sandanayake, “A new benzo-annelated cryptand and a derivative with alkali cation-sensitive fluorescence,” *Tetrahedron Lett.*, vol. 31, no. 36, pp. 5193–5196, 1990.

[33] L. Fabbrizzi, M. Licchelli, P. Pallavicini, A. Perotti, and D. Sacchi, “A fluorescence sensor for transition metal ions based on anthracene,” *Angew. Chemie*, vol. 106, no. 19, pp. 2051–3, 1994.

[34] B. Turfan and E. U. Akkaya, “Modulation of boradiazaindacene emission by cation-mediated oxidative PET,” *Org. Lett.*, vol. 4, no. 17, pp. 2857–2859, 2002.

[35] A. W. C. J. P. Desvergne, “Chemosensors of Ion and Molecule Recognition,” pp. 245, 1997.

[36] B. Valeur, “Design principles of fluorescent molecular sensors for cation recognition,” *Coord. Chem. Rev.*, vol. 205, no. 1, pp. 3–40, 2000.

[37] H. G. Loehr and F. Voegtle, “Chromo- and fluoroionophores. A new class of dye reagents,” *Acc. Chem. Res.*, vol. 18, no. 3, pp. 65–72, 1985.

[38] N. Mateeva, V. Enchev, L. Antonov, T. Deligeorgiev, and M. Mitewa, “Spectroscopic study of the complexation of an aza-15-crown-5 containing chromofluoroionophore with Ba2+ and Ca2+ cations,” *J. Incl. Phenom. Mol. Recognit. Chem.*, vol. 20, no. 4, pp. 323–333, 1994.

[39] M. M. Martin, P. Plaza, Y. H. Meyer, L. Bégin, J. Bourson, and B. Valeur, “A new concept of photogeneration of cations: Evidence for photoejection of Ca2+ and Li+ from complexes with a crown-ether-linked merocyanine by picosecond spectroscopy,” *J. Fluoresc.*, vol. 4, no. 4, pp. 271–273, 1994.

[40] E. Deniz, G. C. Isbasar, Ö. A. Bozdemir, L. T. Yildirim, A. Siemiarczuk, and E. U. Akkaya, “Bidirectional switching of near IR emitting boradiazaindacene fluorophores,” *Org. Lett.*, vol. 10, no. 16, pp. 3401–3403, 2008.

[41] V. Balzani, A. Credi, and M. Venturi, “Light-Harvesting Antennae,” in

Molecular Devices and Machines– A Journey into the Nano World, Wiley-VCH Verlag GmbH & Co. KGaA, 2004, pp. 96–131.

[42] S. E. Webber, "Photon-Harvesting Polymers," *Chem. Rev.*, vol. 90, no. 8, pp. 1469–1482, 1990.

[43] M. Devices, A. Credi, and M. Venturi, "Photoinduced Charge Separation and Solar Energy Conversion," in *Molecular Devices and Machines – A Journey into the Nano World*, Wiley-VCH Verlag GmbH & Co. KGaA, 2003, pp. 132–173.

[44] N. J. Turro, *Modern molecular photochemistry*. Mill Valley, Cal.: University Science Books, 1991.

[45] D. L. Dexter, "a Theory of Sensitized Luminescence in Solids," *J. Chem. Phys.*, vol. 21, no. 5, pp. 836–850, 1953.

[46] C. W. Wan, A. Burghart, J. Chen, F. Bergstrom, L. B. A. Johansson, M. F. Wolford, T. G. Kim, M. R. Topp, R. M. Hochstrasser, and K. Burgess, "Anthracene - BODIPY cassettes: Syntheses and energy transfer," *Chem. - A Eur. J.*, vol. 9, no. 18, pp. 4430–4441, 2003.

[47] A. Harriman, L. J. Mallon, K. J. Elliot, A. Haefele, G. Ulrich, and R. Ziessel, "Length dependence for intramolecular energy transfer in three- and four-color donor-spacer-acceptor arrays," *J. Am. Chem. Soc.*, vol. 131, no. 37, pp. 13375–13386, 2009.

[48] T. Förster, "Energiewanderung und Fluoreszenz," *Naturwissenschaften*, vol. 33, no. 6, pp. 166–175, 1946.

[49] T. Förster, "10th Spiers Memorial Lecture. Transfer mechanisms of electronic excitation," *Discuss. Faraday Soc.*, vol. 27, no. 10, pp. 7, 1959.

[50] V. K. Praveen, C. Ranjith, E. Bandini, A. Ajayaghosh, and N. Armaroli, "Oligo(phenylenevinylene) hybrids and self-assemblies: versatile materials for excitation energy transfer.," *Chem. Soc. Rev.*, vol. 43, no. 12, pp. 4222–4242, 2014.

[51] M. D. Yilmaz, O. A. Bozdemir, and E. U. Akkaya, "Light harvesting and efficient energy transfer in a boron-dipyrrin (BODIPY) functionalized perylenediimide derivative," *Org. Lett.*, vol. 8, no. 13, pp. 2871–2873, 2006.

[52] Z. Xiaolin, X. Yi, and Q. Xuhong, "Highly efficient energy transfer in the light harvesting system composed of three kinds of boron-dipyrromethene derivatives," *Org. Lett.*, vol. 10, no. 1, pp. 29–32, 2008.

[53] R. J. P. Williams, "Role of transition metal ions in biological processes," *R. Inst. Chem. Rev.*, vol. 1, no. 1, pp. 13, 1968.

[54] T. Anastassopoulou, J.; Theophanides, “The Role of Metal Ions in Biological Systems and Medicine,” in *NATO ASI Ser., Ser. C*, vol. 459, D. P. Kessissoglou, Ed. Dordrecht: Springer Netherlands, 1995, pp. 209–218.

[55] C. Andreini, I. Bertini, G. Cavallaro, G. L. Holliday, and J. M. Thornton, “Metal ions in biological catalysis: From enzyme databases to general principles,” *J. Biol. Inorg. Chem.*, vol. 13, no. 8, pp. 1205–1218, 2008.

[56] D. A. Doyle, J. Morais Cabral, R. A. Pfuetzner, A. Kuo, J. M. Gulbis, S. L. Cohen, B. T. Chait, and R. MacKinnon, “The structure of the potassium channel: Molecular basis of K^+ conduction and selectivity.,” *Science (80-.).*, vol. 280, no. 5360, pp. 69–77, 1998.

[57] I. S. Kim, K. H. Kang, P. Johnson-Green, and E. J. Lee, “Investigation of heavy metal accumulation in Polygonum thunbergii for phytoextraction,” *Environ. Pollut.*, vol. 126, no. 2, pp. 235–243, 2003.

[58] K. Yamada, Y. Nomura, D. Citterio, N. Iwasawa, and K. Suzuki, “Highly sodium-selective fluoroionophore based on conformational restriction of oligoethyleneglycol-bridged biaryl boron-dipyrromethene,” *J. Am. Chem. Soc.*, vol. 127, no. 19, pp. 6956–6957, 2005.

[59] J. Du, J. Fan, X. Peng, H. Li, J. Wang, and S. Sun, “Highly selective and anions controlled fluorescent sensor for Hg(2+) in aqueous environment.,” *J. Fluoresc.*, vol. 18, no. 5, pp. 919–924, 2008.

[60] E. M. Nolan and S. J. Lippard, “A ‘Turn-on’ Fluorescent Sensor for the Selective Detection of Mercuric Ion in Aqueous Media,” *J. Am. Chem. Soc.*, vol. 125, no. 47, pp. 14270–14271, 2003.

[61] A. Coskun and E. U. Akkaya, “Signal ratio amplification via modulation of resonance energy transfer: Proof of principle in an emission ratiometric Hg(II) sensor,” *J. Am. Chem. Soc.*, vol. 128, no. 45, pp. 14474–14475, 2006.

[62] S. C. Burdette, G. K. Walkup, B. Spingler, R. Y. Tsien, and S. J. Lippard, “Fluorescent sensors for Zn2+ based on a fluorescein platform: Synthesis, properties and intracellular distribution,” *J. Am. Chem. Soc.*, vol. 123, no. 32, pp. 7831–7841, 2001.

[63] P. Carol, S. Sreejith, and A. Ajayaghosh, “Ratiometric and near-infrared molecular probes for the detection and imaging of zinc ions,” *Chem. - An Asian J.*, vol. 2, no. 3, pp. 338–348, 2007.

[64] T. K. Sen and D. Gomez, “Adsorption of zinc (Zn2+) from aqueous solution on natural bentonite,” *Desalination*, vol. 267, no. 2–3, pp. 286–294, 2011.

[65] C. C. Woodroofe and S. J. Lippard, “A novel two-fluorophore approach to ratiometric sensing of Zn2+,” *J. Am. Chem. Soc.*, vol. 125, no. 38, pp. 11458–

11459, 2003.

[66] M. Taki, J. L. Wolford, and T. V. O'Halloran, "Emission Ratiometric Imaging of Intracellular Zinc: Design of a Benzoxazole Fluorescent Sensor and Its Application in Two-Photon Microscopy," *J. Am. Chem. Soc.*, vol. 126, no. 3, pp. 712–713, 2004.

[67] S. Zhang, C. N. Ong, and H. M. Shen, "Critical roles of intracellular thiols and calcium in parthenolide-induced apoptosis in human colorectal cancer cells," *Cancer Lett.*, vol. 208, no. 2, pp. 143–153, 2004.

[68] A. Pastore, F. Piemonte, M. Locatelli, A. L. Russo, L. M. Gaeta, G. Tozzi, and G. Federici, "Determination of blood total, reduced, and oxidized glutathione in pediatric subjects," *Clin. Chem.*, vol. 47, no. 8, pp. 1467–1469, 2001.

[69] G. Vendemiale, I. Grattagliano, and E. Altomare, "An update on the role of free radicals and antioxidant defense in human disease," *Int. J. Clin. Lab. Res.*, vol. 29, no. 2, pp. 49–55, 1999.

[70] D. M. Townsend, K. D. Tew, and H. Tapiero, "The importance of glutathione in human disease," *Biomed. Pharmacother.*, vol. 57, no. 3, pp. 145–155, 2003.

[71] C. Cecchi, S. Latorraca, S. Sorbi, T. Iantomasi, F. Favilli, M. T. Vincenzini, and G. Liguri, "Gluthatione level is altered in lymphoblasts from patients with familial Alzheimer's disease," *Neurosci. Lett.*, vol. 275, no. 2, pp. 152–154, 1999.

[72] X. Chen, Y. Zhou, X. Peng, and J. Yoon, "Fluorescent and colorimetric probes for detection of thiols.," *Chem. Soc. Rev.*, vol. 39, no. 6, pp. 2120–35, 2010.

[73] M. E. Jun, B. Roy, and K. H. Ahn, "'Turn-on' fluorescent sensing with 'reactive' probes.," *Chem. Commun.*, vol. 47, no. 27, pp. 7583–7601, 2011.

[74] L. Y. Niu, Y. S. Guan, Y. Z. Chen, L. Z. Wu, C. H. Tung, and Q. Z. Yang, "BODIPY-based ratiometric fluorescent sensor for highly selective detection of glutathione over cysteine and homocysteine," *J. Am. Chem. Soc.*, vol. 134, no. 46, pp. 18928–18931, 2012.

[75] T.-K. Kim, D.-N. Lee, and H.-J. Kim, "Highly selective fluorescent sensor for homocysteine and cysteine," *Tetrahedron Lett.*, vol. 49, no. 33, pp. 4879–4881, 2008.

[76] W. Lin, L. Yuan, Z. Cao, Y. Feng, and L. Long, "A sensitive and selective fluorescent thiol probe in water based on the conjugate 1,4-addition of thiols to alpha,beta-unsaturated ketones," *Chem. - A Eur. J.*, vol. 15, no. 20, pp. 5096–5103, 2009.

[77] H. Maeda, H. Matsuno, M. Ushida, K. Katayama, K. Saeki, and N. Itoh, "2,4-

Dinitrobenzenesulfonyl fluoresceins as fluorescent alternatives to Ellman's reagent in thiol-quantification enzyme assays," *Angew. Chemie - Int. Ed.*, vol. 44, no. 19, pp. 2922–2925, 2005.

[78] O. Rusin, N. N. St. Luce, R. A. Agbaria, J. O. Escobedo, S. Jiang, I. M. Warner, F. B. Dawan, K. Lian, and R. M. Strongin, "Visual Detection of Cysteine and Homocysteine," *J. Am. Chem. Soc.*, vol. 126, no. 2, pp. 438–439, 2004.

[79] H. S. Jung, J. H. Han, Y. Habata, C. Kang, and J. S. Kim, "An iminocoumarin-Cu(II) ensemble-based chemodosimeter toward thiols.," *Chem. Commun.*, vol. 47, no. 18, pp. 5142–4, 2011.

[80] X. Cao, W. Lin, and Q. Yu, "A ratiometric fluorescent probe for thiols based on a tetrakis(4- hydroxyphenyl)porphyrin-coumarin scaffold," *J. Org. Chem.*, vol. 76, no. 18, pp. 7423–7430, 2011.

[81] J. Yang, H. Chen, I. R. Vlahov, J.-X. Cheng, and P. S. Low, "Evaluation of disulfide reduction during receptor-mediated endocytosis by using FRET imaging.," *Proc. Natl. Acad. Sci. U. S. A.*, vol. 103, no. 37, pp. 13872–13877, 2006.

[82] A. Treibs and F.-H. Kreuzer, "Difluorboryl-Komplexe von Di- und Tripyrrylmethenen," *Justus Liebigs Ann. Chem.*, vol. 718, no. 1, pp. 208–223, 1968.

[83] F. J. Monsma, C. Barton, H. C. Kang, D. L. Brassard, R. P. Haugland, and D. R. Sibley, "Characterization of novel fluorescent ligands with high affinity for D1 and D2 dopaminergic receptors.," *J. Neurochem.*, vol. 52, no. 5, pp. 1641–1644, 1989.

[84] R. P. Haugland, H. C. Kang, "Chemically Reactive Dipyrrometheneboron Difluoride Dyes," Patent No.4,774,339, 1988.

[85] H. Kim, A. Burghart, M. B. Welch, J. Reibenspies, and K. Burgess, "Synthesis and spectroscopic properties of a new 4-bora-3a,4a-diaza-s-indacene (BODIPY®) dye," *Chem. Commun.*, vol. 718, no. 18, pp. 1889–1890, 1999.

[86] A. Loudet and K. Burgess, "BODIPY dyes and their derivatives: Syntheses and spectroscopic properties," *Chem. Rev.*, vol. 107, no. 11, pp. 4891–4932, 2007.

[87] G. Ulrich, R. Ziessel, and A. Harriman, "The chemistry of fluorescent bodipy dyes: Versatility unsurpassed," *Angew. Chemie - Int. Ed.*, vol. 47, no. 7, pp. 1184–1201, 2008.

[88] J. H. Boyer, A. M. Haag, G. Sathyamoorthi, and T. G. Pavlopoulos, "Pyrromethene-BF2 Complexes as Laser Dyes: 2," *Heteroat. Chem.*, vol. 4, no. 1, pp. 39–49, 1993.

[89] T. Yogo, Y. Urano, Y. Ishitsuka, F. Maniwa, and T. Nagano, “Highly efficient and photostable photosensitizer based on BODIPY chromophore,” *J. Am. Chem. Soc.*, vol. 127, no. 35, pp. 12162–12163, 2005.

[90] W. Qin, M. Baruah, M. Van Der Auweraer, F. C. De Schryver, and N. Boens, “Photophysical properties of borondipyrromethene analogues in solution,” *J. Phys. Chem. A*, vol. 109, no. 33, pp. 7371–7384, 2005.

[91] C. Goze, G. Ulrich, and R. Ziessel, “Unusual fluorescent monomeric and dimeric dialkynyl dipyrromethene-borane complexes,” *Org. Lett.*, vol. 8, no. 20, pp. 4445–4448, 2006.

[92] K. Rurack, M. Kollmannsberger, and J. Daub, “A highly efficient sensor molecule emitting in the near infrared (NIR): 3,5-distyryl-8-(p-dimethylaminophenyl)difluoroboradiaza-s-indacene,” *New J. Chem.*, vol. 25, no. 2, pp. 289–292, 2001.

[93] E. Knoevenagel, “Condensation von Malonsäure mit aromatischen Aldehyden durch Ammoniak und Amine,” *Berichte der Dtsch. Chem. Gesellschaft*, vol. 31, no. 3, pp. 2596–2619, 1898.

[94] E. W. Dean and D. D. Stark, “A Convenient Method for the Determination of Water in Petroleum and Other Organic Emulsions.,” *Ind. Eng. Chem.*, vol. 12, no. 5, pp. 486–490, 1920.

[95] Y. H. Yu, A. B. Descalzo, Z. Shen, H. Röhr, Q. Liu, Y. W. Wang, M. Spieles, Y. Z. Li, K. Rurack, and X. Z. You, “Mono- and di(dimethylamino)styryl-substituted borondipyrromethene and borondiindomethene dyes with intense near-infrared fluorescence,” *Chem. - An Asian J.*, vol. 1, no. 1–2, pp. 176–187, 2006.

[96] O. Buyukcakir, O. A. Bozdemir, S. Kolemen, S. Erbas, and E. U. Akkaya, “Tetrastyryl-bodipy dyes: Convenient synthesis and characterization of elusive near IR fluorophores,” *Org. Lett.*, vol. 11, no. 20, pp. 4644–4647, 2009.

[97] T. Bura, P. Retailleau, G. Ulrich, and R. Ziessel, “Highly substituted bodipy dyes with spectroscopic features sensitive to the environment,” *J. Org. Chem.*, vol. 76, no. 4, pp. 1109–1117, 2011.

[98] M. Kollmannsberger, T. Gareis, S. Heini, J. Breu, and J. Daub, “Electrogenerated Chemiluminescence and Proton-Dependent Switching of Fluorescence: Functionalized Difluoroboradiaza-s-indacenes,” *Angew. Chemie - Int. Ed.*, vol. 36, no. 12, pp. 1333–1335, 1997.

[99] H. Koutaka, J. Kosuge, N. Fukasaku, T. Hirano, K. Kikuchi, Y. Urano, H. Kojima, and T. Nagano, “A novel fluorescent probe for zinc ion based on boron dipyrromethene (BODIPY) chromophore.,” *Chem. Pharm. Bull. (Tokyo).*, vol. 52, no. 6, pp. 700–703, 2004.

[100] X. Peng, J. Du, J. Fan, J. Wang, Y. Wu, J. Zhao, S. Sun, and T. Xu, "A selective fluorescent sensor for imaging Cd2+ in living cells," *J. Am. Chem. Soc.*, vol. 129, no. 6, pp. 1500–1501, 2007.

[101] C. Goze, G. Ulrich, L. Charbonniere, M. Cesario, T. Prange, and R. Ziessel, "Cation sensors based on terpyridine-functionalized boradiazaindacene," *Chem. - A Eur. J.*, vol. 9, no. 16, pp. 3748–3755, 2003.

[102] S. Atilgan, Z. Ekmekci, a L. Dogan, D. Guc, and E. U. Akkaya, "Water soluble distyryl-boradiazaindacenes as efficient photosensitizers for photodynamic therapy," *Chem. Commun.*, no. 42, pp. 4398–4400, 2006.

[103] L. Li, J. Han, B. Nguyen, and K. Burgess, "Syntheses and spectral properties of functionalized, water-soluble BODIPY derivatives," *J. Org. Chem.*, vol. 73, no. 5, pp. 1963–1970, 2008.

[104] C. Thivierge, R. Bandichhor, and K. Burgess, "Spectral dispersion and water solubilization of BODIPY dyes via palladium-catalyzed C-H functionalization," *Org. Lett.*, vol. 9, no. 11, pp. 2135–2138, 2007.

[105] S. Erten-Ela, M. D. Yilmaz, B. Icli, Y. Dede, S. Icli, and E. U. Akkaya, "A panchromatic boradiazaindacene (BODIPY) sensitizer for dye-sensitized solar cells," *Org. Lett.*, vol. 10, no. 15, pp. 3299–3302, 2008.

[106] T. J. Dougherty, C. J. Gomer, B. W. Henderson, G. Jori, D. Kessel, M. Korbelik, J. Moan, and Q. Peng, "Photodynamic Therapy," *JNCI J. Natl. Cancer Inst.*, vol. 90, no. 12, pp. 889–905, 1998.

[107] D. E. J. G. Dolmans, D. Fukumura, and R. K. Jain, "Photodynamic therapy for cancer," *Nat. Rev. Cancer*, vol. 3, no. 5, pp. 380–387, 2003.

[108] A. Juzeniene, Q. Peng, and J. Moan, "Milestones in the development of photodynamic therapy and fluorescence diagnosis.," *Photochem. Photobiol. Sci.*, vol. 6, no. 12, pp. 1234–1245, 2007.

[109] S. Pervaiz and M. Olivo, "Art And Science Of Photodynamic Therapy Frontiers," *Clin. Exp. Pharmacol. Physiol.*, vol. 33, no. 5–6, pp. 551–556, 2006.

[110] Á. Juarranz, P. Jaén, F. Sanz-Rodríguez, J. Cuevas, and S. González, "Photodynamic therapy of cancer. Basic principles and applications," *Clin. Transl. Oncol.*, vol. 10, no. 3, pp. 148–154, 2008.

[111] C. Brlickner, "Tetrahedron report number 447 Porphyrin-based Photosensitizers for Use in Photodynamic Therapy," *Tetrahedron*, vol. 54, no. 17, pp. 4151--4202, 1998.

[112] T. Dai, B. B. Fuchs, J. J. Coleman, R. A. Prates, C. Astrakas, T. G. St. Denis, M. S. Ribeiro, E. Mylonakis, M. R. Hamblin, and G. P. Tegos, "Concepts and

principles of photodynamic therapy as an alternative antifungal discovery platform," *Front. Microbiol.*, vol. 3, pp. 120, 2012.

[113] M. R. Detty, S. L. Gibson, and S. J. Wagner, "Current clinical and preclinical photosensitizers for use in photodynamic therapy," *J. Med. Chem.*, vol. 47, no. 16, pp. 3897–3915, 2004.

[114] J. Killoran, L. Allen, J. F. Gallagher, W. M. Gallagher, and D. F. O′Shea, "Synthesis of BF_2 chelates of tetraarylazadipyrromethenes and evidence for their photodynamic therapeutic behaviour," *Chem. Commun.*, vol. 24, no. 17, pp. 1862–1863, 2002.

[115] S. Ozlem and E. U. Akkaya, "Thinking outside the silicon box: Molecular and logic as an additional layer of selectivity in singlet oxygen generation for photodynamic therapy," *J. Am. Chem. Soc.*, vol. 131, no. 1, pp. 48–49, 2009.

[116] W. F. Cheong, S. A. Prahl, and A. J. Welch, "A review of the optical properties of biological tissues," *IEEE J. Quantum Electron.*, vol. 26, pp. 2166–2185, 1990.

[117] C. Wilson, W. Patrick, M. Lowe, and C. Wilson, "in Vivo and Post Mortem Measurements of the Attenuation Spectra of Light in Mammalian," *Photochem. Photobiol.*, vol. 42, no. 2, pp. 153–162, 1985.

[118] A. A. Frimer, "The reaction of singlet oxygen with olefins: the question of mechanism," *Chem. Rev.*, vol. 79, no. 5, pp. 359–387, 1979.

[119] A. Rotaru and A. Mokhir, "Nucleic acid binders activated by light of selectable wavelength," *Angew. Chemie - Int. Ed.*, vol. 46, no. 32, pp. 6180–6183, 2007.

[120] S. D. P. Baugh, Z. Yang, D. K. Leung, D. M. Wilson, and R. Breslow, "Cyclodextrin dimers as cleavable carriers of photodynamic sensitizers," *J. Am. Chem. Soc.*, vol. 123, no. 50, pp. 12488–12494, 2001.

[121] P. Klán, T. Šolomek, C. G. Bochet, A. Blanc, R. Givens, M. Rubina, V. Popik, A. Kostikov, and J. Wirz, "Photoremovable protecting groups in chemistry and biology: Reaction mechanisms and efficacy," *Chem. Rev.*, vol. 113, no. 1, pp. 119–191, 2013.

[122] H. Yu, J. Li, D. Wu, Z. Qiu, and Y. Zhang, "Chemistry and biological applications of photo-labile organic molecules.," *Chem. Soc. Rev.*, vol. 39, no. 2, pp. 464–473, 2010.

[123] J. H. Kaplan and A. P. Somlyo, "Flash photolysis of caged compounds: New tools for cellular physiology," *Trends Neurosci.*, vol. 12, no. 2, pp. 54–59, 1989.

[124] G. Zhang and M. Mastalerz, "Organic cage compounds--from shape-persistency to function.," *Chem. Soc. Rev.*, vol. 43, no. 6, pp. 1934, 2014.

[125] A. P. Pelliccioli and J. Wirz, “Photoremovable protecting groups: reaction mechanisms and applications,” *Photochem. Photobiol. Sci.*, vol. 1, no. 7, pp. 441–458, 2002.

[126] N. Hoffmann, “Photochemical reactions as key steps in organic synthesis,” *Chem. Rev.*, vol. 108, no. 3, pp. 1052–1103, 2008.

[127] G. P. Hess, R. W. Lewis, and Y. Chen, “Caged neurotransmitters and other caged compounds: Design and application,” *Cold Spring Harb. Protoc.*, vol. 2014, no. 10, pp. 1027–1039, 2014.

[128] J. F. Lovell, T. W. B. Liu, J. Chen, and G. Zheng, “Activatable photosensitizers for imaging and therapy,” *Chem. Rev.*, vol. 110, no. 5, pp. 2839–2857, 2010.

[129] J. H. Kaplan, B. Forbush, and J. F. Hoffman, “Rapid photolytic release of adenosine 5’-triphosphate from a protected analog - utilization by Na-K pump of human red blood-cell ghosts.,” *Biochemistry*, vol. 17, no. 10, pp. 1929–1935, 1978.

[130] G. C. R. Ellis-Davies, “Caged compounds: photorelease technology for control of cellular chemistry and physiology.,” *Nat. Methods*, vol. 4, no. 8, pp. 619–28, 2007.

[131] G. Y. Wiederschain, “The Molecular Probes handbook. A guide to fluorescent probes and labeling technologies,” *Biochem.*, vol. 76, no. 11, pp. 1276–1276, 2011.

[132] S. Yamasaki, K. Sakata-Sogawa, A. Hasegawa, T. Suzuki, K. Kabu, E. Sato, T. Kurosaki, S. Yamashita, M. Tokunaga, K. Nishida, and T. Hirano, “Zinc is a novel intracellular second messenger,” *J. Cell Biol.*, vol. 177, no. 4, pp. 637–645, 2007.

[133] H. M. D. Bandara, D. P. Kennedy, E. Akin, C. D. Incarvito, and S. C. Burdette, “Photoinduced release of Zn2+ with ZinCleav-1: A nitrobenzyl-based caged complex,” *Inorg. Chem.*, vol. 48, no. 17, pp. 8445–8455, 2009.

[134] S. Frings, B. Wiesner, V. Hagen, S. Helm, D. Lorenz, and U. B. Kaupp, “Synthesis , photochemistry and application of (7-methoxycoumarin-nanosecond time region,” *J. Photochem. Photobiol. B.*, vol. 53, no. 1–3, pp. 91–102, 1999.

[135] K. Szaciłowski, W. Macyk, A. Drzewiecka-Matuszek, M. Brindell, and G. Stochel, “Bioinorganic photochemistry: Frontiers and mechanisms,” *Chem. Rev.*, vol. 105, no. 6, pp. 2647–2694, 2005.

[136] J. E. T. Corrie, T. Furuta, R. S. Givens, A. L. Yousef, and M. Goeldner, “Photoremovable Protecting Groups Used for the Caging of Biomolecules,” in *Dynamic Studies in Biology: Phototriggers, Photoswitches and Caged*

Biomolecules, Wiley-VCH Verlag GmbH & Co. KGaA, 2005, pp. 1–94.

[137] J. C. Sheehan, R. M. Wilson, and A. W. Oxford, "The Photolysis of Methoxy-Substituted Benzoin Esters. A Photosensitive Protecting Group for Carboxylic Acids," *J. Am. Chem. Soc.*, vol. 93, no. 26, pp. 7222–7228, 1971.

[138] G. Boole, *The Mathematical Analysis of Logic*. Cambridge: Cambridge University Press, 1847.

[139] G. Boole, "Proposed question in the theory of probabilities," *Cambridge Dublin Math. J.*, vol. 6, no. 186, pp. 29–32, 1851.

[140] J. Millman and A. Grabel, *Microelectronics*. New York, NY, USA: McGraw-Hill, Inc., 1987.

[141] N. Hush, "Molecular electronics: Cool computing," *Nat. Mater.*, vol. 2, no. 3, pp. 134, 2003.

[142] A. Moore, J. Allman, and R. M. Goodman, "A Real-Time Neural System for Color Constancy," *IEEE Transactions on Neural Networks*, vol. 2, no. 2. pp. 237–247, 1991.

[143] A. Prasanna de Silva, H. Q. Nimal Gunaratne, and C. P. McCoy, "Molecular photoionic AND logic gates with bright fluorescence and 'off-on' digital action," *J. Am. Chem. Soc.*, vol. 119, no. 33, pp. 7891–7892, 1997.

[144] P. A. De Silva and N. D. McClenaghan, "Simultaneously multiply-configurable or superposed molecular logic systems composed of ICT (internal charge transfer) chromophores and fluorophores integrated with one- or two-ion receptors," *Chem. - A Eur. J.*, vol. 8, no. 21, pp. 4935–4945, 2002.

[145] A. Prasanna De Silva and N. D. McClenaghan, "Proof-of-principle of molecular-scale arithmetic [2]," *J. Am. Chem. Soc.*, vol. 122, no. 16, pp. 3965–3966, 2000.

[146] D. Margulies, G. Melman, and A. Shanzer, "Fluorescein as a model molecular calculator with reset capability," *Nat. Mater.*, vol. 4, no. 10, pp. 768–771, 2005.

[147] J. Andréasson and U. Pischel, "Smart molecules at work--mimicking advanced logic operations.," *Chem. Soc. Rev.*, vol. 39, no. 1, pp. 174–188, 2010.

[148] O. A. Bozdemir, R. Guliyev, O. Buyukcakir, S. Selcuk, S. Kolemen, G. Gulseren, T. Nalbantoglu, H. Boyaci, and E. U. Akkaya, "Selective manipulation of ICT and PET processes in styryl-bodipy derivatives: Applications in molecular logic and fluorescence sensing of metal ions," *J. Am. Chem. Soc.*, vol. 132, no. 23, pp. 8029–8036, 2010.

[149] a P. de Silva and S. Uchiyama, "Molecular logic and computing.," *Nat.*

Nanotechnol., vol. 2, no. 7, pp. 399–410, 2007.

[150] N. Kaur, N. Singh, D. Cairns, and J. F. Callan, "A multifunctional tripodal fluorescent probe: 'off-on' detection of sodium as well as two-input and molecular logic behavior," *Org. Lett.*, vol. 11, no. 11, pp. 2229–2232, 2009.

[151] H. Komatsu, S. Matsumoto, S. ichi Tamaru, K. Kaneko, M. Ikeda, and I. Hamachi, "Supramolecular hydrogel exhibiting four basic logic gate functions to fine-tune substance release," *J. Am. Chem. Soc.*, vol. 131, no. 15, pp. 5580–5585, 2009.

[152] T. Gupta and M. E. Van Der Boom, "Redox-active monolayers as a versatile platform for integrating boolean logic gates," *Angew. Chemie - Int. Ed.*, vol. 47, no. 29, pp. 5322–5326, 2008.

[153] K. Szaciłowski, "Digital information processing in molecular systems," *Chem. Rev.*, vol. 108, no. 9, pp. 3481–3548, 2008.

[154] U. Pischel, "Chemical approaches to molecular logic elements for addition and subtraction," *Angew. Chemie - Int. Ed.*, vol. 46, no. 22, pp. 4026–4040, 2007.

[155] D. Margulies, G. Melman, and A. Shanzer, "A molecular full-adder and full-subtractor, an additional step toward a moleculator," *J. Am. Chem. Soc.*, vol. 128, no. 14, pp. 4865–4871, 2006.

[156] S. Kou, N. L. Han, D. Van Noort, K. M. K. Swamy, H. K. So, H. S. Jung, K. M. Lee, S. W. Nam, J. Yoon, and S. Park, "Fluorescent molecular logic gates using microfluidic devices," *Angew. Chemie - Int. Ed.*, vol. 47, no. 5, pp. 872–876, 2008.

[157] G. De Ruiter and M. E. Van Der Boom, "Surface-confined assemblies and polymers for molecular logic," *Acc. Chem. Res.*, vol. 44, no. 8, pp. 563–573, 2011.

[158] G. De Ruiter, E. Tartakovsky, N. Oded, and M. E. Van Der Boom, "Sequential logic operations with surface-confined polypyridyl complexes displaying molecular random access memory features," *Angew. Chemie - Int. Ed.*, vol. 49, no. 1, pp. 169–172, 2010.

[159] U. Pischel and J. Andréasson, "A simplicity-guided approach toward molecular set–reset memories," *New J. Chem.*, vol. 34, no. 12, pp. 2701, 2010.

[160] G. De Ruiter, L. Motiei, J. Choudhury, N. Oded, and M. E. Van Der Boom, "Electrically addressable multistate volatile memory with flip-flop and flip-flap-flop logic circuits on a solid support," *Angew. Chemie - Int. Ed.*, vol. 49, no. 28, pp. 4780–4783, 2010.

[161] R. Baron, A. Onopriyenko, E. Katz, O. Lioubashevski, I. Willner, S. Wang, and

H. Tian, “An electrochemical/photochemical information processing system using a monolayer-functionalized electrode.,” *Chem. Commun.*, vol. 2, no. 20, pp. 2147–2149, 2006.

[162] U. Pischel, J. Andraasson, D. Gust, and V. F. Pais, “Information processing with molecules - Quo vadis?,” *ChemPhysChem*, vol. 14, no. 1, pp. 28–46, 2013.

[163] S. Erbas-Cakmak, O. A. Bozdemir, Y. Cakmak, and E. U. Akkaya, “Proof of principle for a molecular 1 : 2 demultiplexer to function as an autonomously switching theranostic device,” *Chem. Sci.*, vol. 4, no. 2, pp. 858–862, 2013.

[164] R. J. Amir, M. Popkov, R. A. Lerner, C. F. Barbas, and D. Shabat, “Prodrug activation gated by a molecular ‘OR’ logic trigger,” *Angew. Chemie - Int. Ed.*, vol. 44, no. 28, pp. 4378–4381, 2005.

[165] E. Katz, V. Bocharova, and M. Privman, “Electronic interfaces switchable by logically processed multiple biochemical and physiological signals,” *J. Mater. Chem.*, vol. 22, no. 17, pp. 8171, 2012.

[166] N. Graf and R. Krämer, “Enzymatic amplification in a bioinspired, autonomous signal cascade.,” *Chem. Commun.*, vol. 4, no. 42, pp. 4375–6, 2006.

[167] S. Silvi, E. C. Constable, C. E. Housecroft, J. E. Beves, E. L. Dunphy, M. Tomasulo, F. M. Raymo, and A. Credi, “All-optical integrated logic operations based on chemical communication between molecular switches,” *Chem. - A Eur. J.*, vol. 15, no. 1, pp. 178–185, 2009.

[168] G. C. R. Ellis-Davies, “Neurobiology with caged calcium,” *Chem. Rev.*, vol. 108, no. 5, pp. 1603–1613, 2008.

[169] R. Guliyev, S. Ozturk, Z. Kostereli, and E. U. Akkaya, “From virtual to physical: Integration of chemical logic gates,” *Angew. Chemie - Int. Ed.*, vol. 50, no. 42, pp. 9826–9831, 2011.

[170] N. Boens, V. Leen, and W. Dehaen, “Fluorescent indicators based on BODIPY,” *Chem. Soc. Rev.*, vol. 41, no. 3, pp. 1130–1172, 2012.

[171] R. Ziessel, G. Ulrich, and A. Harriman, “The chemistry of Bodipy: A new *El Dorado* for fluorescence tools,” *New J. Chem.*, vol. 31, no. 4, pp. 496–501, 2007.

[172] S. Atilgan, T. Ozdemir, and E. U. Akkaya, “Selective Hg(II) sensing with improved stokes shift by coupling the internal charge transfer process to excitation energy transfer,” *Org. Lett.*, vol. 12, no. 21, pp. 4792–4795, 2010.

[173] S. Erbas, A. Gorgulu, M. Kocakusakogullari, and E. U. Akkaya, “Non-covalent functionalized SWNTs as delivery agents for novel Bodipy-based potential PDT sensitizers.,” *Chem. Commun.*, no. 33, pp. 4956–4958, 2009.

[174] O. Altan Bozdemir, S. Erbas-Cakmak, O. O. Ekiz, A. Dana, and E. U. Akkaya, "Towards unimolecular luminescent solar concentrators: Bodipy-based dendritic energy-transfer cascade with panchromatic absorption and monochromatized emission," *Angew. Chemie - Int. Ed.*, vol. 50, no. 46, pp. 10907–10912, 2011.

[175] T. Kobayashi, T. Komatsu, M. Kamiya, C. Campos, M. Gonzalez-Gaitan, T. Terai, K. Hanaoka, T. Nagano, and Y. Urano, "Highly activatable and environment-insensitive optical highlighters for selective spatiotemporal imaging of target proteins," *J. Am. Chem. Soc.*, vol. 134, no. 27, pp. 11153–11160, 2012.

[176] T. Matsumoto, Y. Urano, T. Shoda, H. Kojima, and T. Nagano, "A thiol-reactive fluorescence probe based on donor-excited photoinduced electron transfer: Key role of ortho substitution," *Org. Lett.*, vol. 9, no. 17, pp. 3375–3377, 2007.

[177] H. Sunahara, Y. Urano, H. Kojima, and T. Nagano, "Design and synthesis of a library of BODIPY-based environmental polarity sensors utilizing photoinduced electron-transfer-controlled fluorescence ON/OFF switching," *J. Am. Chem. Soc.*, vol. 129, no. 17, pp. 5597–5604, 2007.

[178] Y. Gabe, Y. Urano, K. Kikuchi, H. Kojima, and T. Nagano, "Highly Sensitive Fluorescence Probes for Nitric Oxide Based on Boron Dipyrromethene Chromophore - Rational Design of Potentially Useful Bioimaging Fluorescence Probe," *J. Am. Chem. Soc.*, vol. 126, no. 10, pp. 3357–3367, 2004.

[179] Y. Gabe, T. Ueno, Y. Urano, H. Kojima, and T. Nagano, "Tunable design strategy for fluorescence probes based on 4-substituted BODIPY chromophore: Improvement of highly sensitive fluorescence probe for nitric oxide," *Anal. Bioanal. Chem.*, vol. 386, no. 3, pp. 621–626, 2006.

[180] K. Rurack, M. Kollmannsberger, U. Resch-Genger, and J. Daub, "A selective and sensitive fluoroionophore for Hg(II), Ag(I), and Cu(II) with virtually decoupled fluorophore and receptor units [10]," *J. Am. Chem. Soc.*, vol. 122, no. 5, pp. 968–969, 2000.

[181] M. Kollmannsberger, K. Rurack, U. Resch-Genger, and J. Daub, "Ultrafast charge transfer in amino-substituted boron dipyrromethene dyes and its inhibition by cation complexation: A new design concept for highly sensitive fluorescent probes," *J. Phys. Chem. A*, vol. 102, no. 50, pp. 10211–10220, 1998.

[182] P. M. Paduraru, R. T. W. Popoff, R. Nair, R. Gries, G. Gries, and E. Plettner, "Synthesis of substituted alkoxy benzene minilibraries, for the discovery of new insect olfaction or gustation inhibitors," *J. Comb. Chem.*, vol. 10, no. 1, pp. 123–134, 2008.

[183] T. Cardinaels, J. Ramaekers, P. Nockemann, K. Driesen, K. Van Hecke, L. Van Meervelt, S. Lei, S. De Feyter, D. Guillon, B. Donnio, and K. Binnemans, "Imidazo[4,5-f]-1,10-phenanthrolines: Versatile ligands for the design of metallomesogens," *Chem. Mater.*, vol. 20, no. 4, pp. 1278–1291, 2008.

[184] M. J. Berridge, M. D. Bootman, and P. Lipp, "Calcium--a life and death signal.," *Nature*, vol. 395, no. 6703, pp. 645–8, 1998.

[185] C. J. Frederickson, J.-Y. Koh, and A. I. Bush, "The neurobiology of zinc in health and disease.," *Nat. Rev. Neurosci.*, vol. 6, no. 6, pp. 449–62, 2005.

[186] C. F. Walker and R. E. Black, "Zinc and the Risk for Infectious Disease," *Annu. Rev. Nutr.*, vol. 24, no. 1, pp. 255–275, 2004.

[187] P. J. Fraker and L. E. King, "Reprogramming of the Immune System During Zinc Deficiency," *Annu. Rev. Nutr*, vol. 24, no. 1, pp. 277–98, 2004.

[188] G. C. R. Ellis-Davies, "Neurobiology with caged calcium," *Chem. Rev.*, vol. 108, no. 5, pp. 1603–1613, 2008.

[189] S. R. Adams, J. P. Y. Kao, G. Grynkiewicz, A. Minta, and R. Y. Tsien, "Biologically useful chelators that release Ca2+ upon illumination," *J. Am. Chem. Soc.*, vol. 110, no. 10, pp. 3212–3220, 1988.

[190] S. Adams, "Controlling Cell Chemistry with Caged Compounds," *Annu. Rev. Physiol.*, vol. 55, no. 1, pp. 755–784, 1993.

[191] H. W. Mbatia, H. M. D. Bandara, and S. C. Burdette, "CuproCleav-1, a first generation photocage for Cu+.," *Chem. Commun.*, vol. 48, no. 43, pp. 5331–3, 2012.

[192] H. M. D. Bandara, T. P. Walsh, and S. C. Burdette, "A second-generation photocage for Zn2+ inspired by TPEN: Characterization and insight into the uncaging quantum yields of ZinCleav chelators," *Chem. - A Eur. J.*, vol. 17, no. 14, pp. 3932–3941, 2011.

[193] R. Weissleder, "A clearer vision for in vivo imaging Progress continues in the development of smaller , more penetrable probes for biological imaging . Toward the phosphoproteome," *Nat. Biotechnol.*, vol. 19, no. 4, pp. 316–317, 2001.

[194] C. J. Carling, F. Nourmohammadian, J. C. Boyer, and N. R. Branda, "Remote-control photorelease of caged compounds using near-infrared light and upconverting nanoparticles," *Angew. Chemie - Int. Ed.*, vol. 49, no. 22, pp. 3782–3785, 2010.

[195] Y. H. Chien, Y. L. Chou, S. W. Wang, S. T. Hung, M. C. Liau, Y. J. Chao, C. H. Su, and C. S. Yeh, "Near-infrared light photocontrolled targeting,

bioimaging, and chemotherapy with caged upconversion nanoparticles in vitro and in vivo," *ACS Nano*, vol. 7, no. 10, pp. 8516–8528, 2013.

[196] M. K. G. Jayakumar, N. M. Idris, and Y. Zhang, "Remote activation of biomolecules in deep tissues using near-infrared-to-UV upconversion nanotransducers," *Proc. Natl. Acad. Sci.*, vol. 109, no. 22, pp. 8483–8488, 2012.

[197] C. Wang, L. Cheng, and Z. Liu, "Upconversion nanoparticles for photodynamic therapy and other cancer therapeutics," *Theranostics*, vol. 3, no. 5, pp. 317–330, 2013.

[198] G. Bort, T. Gallavardin, D. Ogden, and P. I. Dalko, "From one-photon to two-photon probes: 'caged' compounds, actuators, and photoswitches," *Angew. Chemie - Int. Ed.*, vol. 52, no. 17, pp. 4526–4537, 2013.

[199] E. B. Brown, J. B. Shear, S. R. Adams, R. Y. Tsien, and W. W. Webb, "Photolysis of caged calcium in femtoliter volumes using two-photon excitation.," *Biophys. J.*, vol. 76, no. 1 Pt 1, pp. 489–99, 1999.

[200] M. Petit, G. Bort, B. T. Doan, C. Sicard, D. Ogden, D. Scherman, C. Ferroud, and P. I. Dalko, "X-ray photolysis to release ligands from caged reagents by an intramolecular antenna sensitive to magnetic resonance imaging," *Angew. Chemie - Int. Ed.*, vol. 50, no. 41, pp. 9708–9711, 2011.

[201] K. L. Ciesienski, K. L. Haas, M. G. Dickens, Y. T. Tesema, and K. J. Franz, "A photolabile ligand for light-activated release of caged copper," *J. Am. Chem. Soc.*, vol. 130, no. 37, pp. 12246–12247, 2008.

[202] T. M. Dore, "Multiphoton Phototriggers for Exploring Cell Physiology," in *Dynamic Studies in Biology: Phototriggers, Photoswitches and Caged Biomolecules*, Wiley-VCH Verlag GmbH & Co. KGaA, 2005, pp. 435–459.

[203] A. M. L. Hossion, M. Bio, G. Nkepang, S. G. Awuah, and Y. You, "Visible light controlled release of anticancer drug through double activation of prodrug," *ACS Med. Chem. Lett.*, vol. 4, no. 1, pp. 124–127, 2013.

[204] R. S. Murthy, M. Bio, and Y. You, "Low energy light-triggered oxidative cleavage of olefins," *Tetrahedron Lett.*, vol. 50, no. 9, pp. 1041–1044, 2009.

[205] a Ruebner, Z. Yang, D. Leung, and R. Breslow, "A cyclodextrin dimer with a photocleavable linker as a possible carrier for the photosensitizer in photodynamic tumor therapy.," *Proc. Natl. Acad. Sci. U. S. A.*, vol. 96, no. 26, pp. 14692–14693, 1999.

[206] D. Arian, L. Kovbasyuk, and A. Mokhir, "1,9-dialkoxyanthracene as a 1O2-sensitive linker," *J. Am. Chem. Soc.*, vol. 133, no. 11, pp. 3972–3980, 2011.

[207] S. Erbas-Cakmak and E. U. Akkaya, "Toward singlet oxygen delivery at a

measured rate: A self-reporting photosensitizer," *Org. Lett.*, vol. 16, no. 11, pp. 2946–2949, 2014.

[208] S. Erbas-Cakmak and E. U. Akkaya, "Cascading of molecular logic gates for advanced functions: A self-reporting, activatable photosensitizer," *Angew. Chemie - Int. Ed.*, vol. 52, no. 43, pp. 11364–11368, 2013.

[209] A. I. Bush, W. H. Pettingell, G. Multhaup, M. d Paradis, J. P. Vonsattel, J. F. Gusella, K. Beyreuther, C. L. Masters, and R. E. Tanzi, "Rapid induction of Alzheimer A beta amyloid formation by zinc.," *Science (80-.).*, vol. 265, no. 5177, pp. 1464–1467, 1994.

[210] L. C. Costello and R. B. Franklin, "'Why do tumour cells glycolyse?': From glycolysis through citrate to lipogenesis," *Mol. Cell. Biochem.*, vol. 280, no. 1–2, pp. 1–8, 2005.

[211] J. H. Weiss, S. L. Sensi, and J. Y. Koh, "Zn2+: a novel ionic mediator of neural injury in brain disease," *Trends Pharmacol. Sci.*, vol. 21, no. 10, pp. 395–401, 2000.

[212] S. Ozcubukcu, E. Ozkal, C. Jimeno, and M. A. Perices, "A highly active catalyst for huisgen 1, 3-dipolar cycloadditions based on the tris(triazolyl)methanol-Cu(I) structure," *Org. Lett.*, vol. 11, no. 20, pp. 4680–4683, 2009.

[213] A. Harriman, M. A. H. Alamiry, J. P. Hagon, D. Hablot, and R. Ziessel, "Through-space electronic energy transfer across proximal molecular dyads," *Angew. Chemie*, vol. 125, no. 26, pp. 6743–6747, 2013.

[214] D. Hablot, A. Harriman, and R. Ziessel, "Using a photoacid generator to switch the direction of electronic energy transfer in a molecular triad," *Angew. Chemie - Int. Ed.*, vol. 50, no. 34, pp. 7833–7836, 2011.

[215] T. Bura, P. Retailleau, and R. Ziessel, "Efficient synthesis of panchromatic dyes for energy concentration," *Angew. Chemie - Int. Ed.*, vol. 49, no. 37, pp. 6659–6663, 2010.

[216] R. Ziessel, M. A. H. Alamiry, K. J. Elliott, and A. Harriman, "Exploring the limits of förster theory for energy transfer at a separation of 20 A," *Angew. Chemie - Int. Ed.*, vol. 48, no. 15, pp. 2772–2776, 2009.

[217] E. T. Ecik, A. Atilgan, R. Guliyev, T. B. Uyar, A. Gumus, and E. U. Akkaya, "Modular logic gates: cascading independent logic gates via metal ion signals.," *Dalt. Trans.*, vol. 43, no. 1, pp. 67–70, 2014.

[218] T. Shimizu, S. Komatsuzaki, and K. Hirabayashi, "Synthesis, structure, and complexation behavior of 14- and 28-membered partially unsaturated thiacrown ethers," *Heteroat. Chem.*, vol. 22, no. 3–4, pp. 287–293, 2011.

[219] N. Adarsh, R. R. Avirah, and D. Ramaiah, “Tuning photosensitized singlet oxygen generation efficiency of novel Aza-BODIPY dyes,” *Org. Lett.*, vol. 12, no. 24, pp. 5720–5723, 2010.

[220] M. Mirenda, C. A. Strassert, L. E. Dicelio, and E. S. Román, “Dye-polyelectrolyte layer-by-layer self-assembled materials: Molecular aggregation, structural stability, and singlet oxygen photogeneration,” *ACS Appl. Mater. Interfaces*, vol. 2, no. 6, pp. 1556–1560, 2010.

[221] J. Andréasson and U. Pischel, “Molecules with a sense of logic: a progress report.,” *Chem. Soc. Rev.*, vol. 44, no. 5, pp. 1053–69, 2015.

[222] B. Rout, P. Milko, M. A. Iron, L. Motiei, and D. Margulies, “Authorizing multiple chemical passwords by a combinatorial molecular keypad lock,” *J. Am. Chem. Soc.*, vol. 135, no. 41, pp. 15330–15333, 2013.

[223] S. Angelos, Y. W. Yang, N. M. Khashab, J. F. Stoddart, and J. I. Zink, “Dual-controlled nanoparticles exhibiting and logic,” *J. Am. Chem. Soc.*, vol. 131, no. 32, pp. 11344–11346, 2009.

[224] K.-W. Kim, Y. E. Kim, V. Bocharova, J. Halámek, C.-W. Lee, E. Katz, and M.-K. Oh, “Logic circuit upon angiogenic response controlled by enzyme-linked iron oxide microparticles--towards biocomputing in human cells.,” *Chem. Commun.*, vol. 48, no. 55, pp. 6918–20, 2012.

[225] J. Wang and E. Katz, “Digital biosensors with built-in logic for biomedical applications,” *Isr. J. Chem.*, vol. 51, no. 1, pp. 141–150, 2011.

[226] V. Bocharova, O. Zavalov, K. MacVittie, M. a. Arugula, N. V. Guz, M. E. Dokukin, J. Halámek, I. Sokolov, V. Privman, and E. Katz, “A biochemical logic approach to biomarker-activated drug release,” *J. Mater. Chem.*, vol. 22, no. 37, pp. 19709, 2012.

[227] M. Ikeda, T. Tanida, T. Yoshii, K. Kurotani, S. Onogi, K. Urayama, and I. Hamachi, “Installing logic-gate responses to a variety of biological substances in supramolecular hydrogel-enzyme hybrids.,” *Nat. Chem.*, vol. 6, no. 6, pp. 511–8, 2014.

[228] I. Takashima, R. Kawagoe, I. Hamachi, and A. Ojida, “Development of an AND logic-gate-type fluorescent probe for ratiometric imaging of autolysosome in cell autophagy,” *Chem. - A Eur. J.*, vol. 21, no. 5, pp. 2038–2044, 2015.

[229] T. Konry and D. R. Walt, “Intelligent medical diagnostics via molecular logic,” *J. Am. Chem. Soc.*, vol. 131, no. 37, pp. 13232–13233, 2009.

[230] M. N. Stojanovic, T. E. Mitchell, and D. Stefanovic, “Deoxyribozyme-based logic gates,” *J. Am. Chem. Soc.*, vol. 124, no. 14, pp. 3555–3561, 2002.

[231] R. Cairns, I. Harris, and T. Mak, “Regulation of cancer cell metabolism,” *Nat. Rev. Cancer*, vol. 11, no. 2, pp. 85–95, 2011.

[232] R. A. Gatenby and R. J. Gillies, “Why do cancers have high aerobic glycolysis?,” *Nat. Rev. Cancer*, vol. 4, no. 11, pp. 891–899, 2004.

[233] X. J. Jiang, P. C. Lo, Y. M. Tsang, S. L. Yeung, W. P. Fong, and D. K. P. Ng, “Phthalocyanine-polyamine conjugates as pH-controlled photosensitizers for photodynamic therapy,” *Chem. - A Eur. J.*, vol. 16, no. 16, pp. 4777–4783, 2010.

[234] M.-R. Ke, D. K. P. Ng, and P.-C. Lo, “A pH-responsive fluorescent probe and photosensitiser based on a self-quenched phthalocyanine dimer,” *Chem. Commun.*, vol. 48, no. 72, pp. 9065–9067, 2012.

[235] J. A. Mindell, “Lysosomal acidification mechanisms,” *Annu Rev Physiol*, vol. 74, no. 1, pp. 69–86, 2012.

[236] J. T. F. Lau, X.-J. Jiang, D. K. P. Ng, and P.-C. Lo, “A disulfide-linked conjugate of ferrocenyl chalcone and silicon(IV) phthalocyanine as an activatable photosensitiser.,” *Chem. Commun.*, vol. 49, no. 39, pp. 4274–6, 2013.

[237] L. Li, M. Nurunnabi, M. Nafiujjaman, Y. Y. Jeong, Y. Lee, and K. M. Huh, “A photosensitizer-conjugated magnetic iron oxide/gold hybrid nanoparticle as an activatable platform for photodynamic cancer therapy,” *J. Mater. Chem. B*, vol. 2, no. 19, pp. 2929, 2014.

[238] Y. Cho and Y. Choi, “Graphene oxide–photosensitizer conjugate as a redox-responsive theranostic agent,” *Chem. Commun.*, vol. 48, no. 79, pp. 9912, 2012.

[239] H. Kim, S. Mun, and Y. Choi, “Photosensitizer-conjugated polymeric nanoparticles for redox-responsive fluorescence imaging and photodynamic therapy,” *J. Mater. Chem. B*, vol. 1, no. 4, pp. 429, 2013.

[240] J. Bhaumik, R. Weissleder, and J. R. McCarthy, “Synthesis and photophysical properties of sulfonamidophenyl porphyrins as models for activatable photosensitizers,” *J. Org. Chem.*, vol. 74, no. 16, pp. 5894–5901, 2009.

[241] I. S. Turan, F. P. Cakmak, D. C. Yildirim, R. Cetin-Atalay, and E. U. Akkaya, “Near-IR absorbing BODIPY derivatives as glutathione-activated photosensitizers for selective photodynamic action,” *Chem. - A Eur. J.*, vol. 20, no. 49, pp. 16088–16092, 2014.

[242] Y. Cakmak, S. Kolemen, S. Duman, Y. Dede, Y. Dolen, B. Kilic, Z. Kostereli, L. T. Yildirim, A. L. Dogan, D. Guc, and E. U. Akkaya, “Designing excited states: Theory-guided access to efficient photosensitizers for photodynamic action,” *Angew. Chemie - Int. Ed.*, vol. 50, no. 50, pp. 11937–11941, 2011.

[243] Y. Cakmak, T. Nalbantoglu, T. Durgut, and E. U. Akkaya, "PEGylated calix[4]arene as a carrier for a Bodipy-based photosensitizer," *Tetrahedron Lett.*, vol. 55, no. 2, pp. 538–540, 2014.

[244] A. Atilgan, E. Tanriverdi Ecik, R. Guliyev, T. B. Uyar, S. Erbas-Cakmak, E. U. Akkaya, E. Tanriverdi Eçik, R. Guliyev, T. B. Uyar, S. Erbas-Cakmak, and E. U. Akkaya, "Near-IR-triggered, remote-controlled release of metal ions: A novel strategy for caged ions," *Angew. Chemie - Int. Ed.*, vol. 53, no. 40, pp. 10678–10681, 2014.

[245] W. Qin, M. Baruah, W. M. De Borggraeve, and N. Boens, "Photophysical properties of an on/off fluorescent pH indicator excitable with visible light based on a borondipyrromethene-linked phenol," *J. Photochem. Photobiol. A Chem.*, vol. 183, no. 1–2, pp. 190–197, 2006.

[246] M. A. AmrollahiBiyouki, R. A. J.Smith, J. J. Bedford, and J. P. Leader, "Hydroxymethylation and Carbamoylation of Di-And Tetramethylpyridines Using Radical Substitution (Minisci) Reactions," *Synth. Commun.*, vol. 28, no. 20, pp. 3817–3825, 1998.

[247] K. J. Arm, W. Leslie, and J. A. G. Williams, "Synthesis and pH-sensitive luminescence of bis-terpyridyl iridium(III) complexes incorporating pendent pyridyl groups," *Inorganica Chim. Acta*, vol. 359, no. 4, pp. 1222–1232, 2006.

[248] D. Zornik, R. M. Meudtner, T. Ela Malah, C. M. Thiele, and S. Hecht, "Designing structural motifs for clickamers: Exploiting the 1,2,3-triazole moiety to generate conformationally restricted molecular architectures," *Chem. - A Eur. J.*, vol. 17, no. 5, pp. 1473–1484, 2011.

[249] C. Pérez-Melero, A. B. S. Maya, B. Del Rey, R. Peláez, E. Caballero, and M. Medarde, "A new family of quinoline and quinoxaline analogues of combretastatins," *Bioorganic Med. Chem. Lett.*, vol. 14, no. 14, pp. 3771–3774, 2004.

[250] N. Morakot, B. Tomapatanaget, W. Ngeon-tae, W. Aeungmaitrepirom, and T. Tuntulani, "Synthesis and Fluorescence Sensing Properties of Calix [4] arenes Containing Fluorophores," *Supramol. Chem.*, vol. 17, no. 8, pp. 655–659, 2005.

[251] Y. Wang, R. Zhang, N. Xu, F. S. Du, Y. L. Wang, Y. X. Tan, S. P. Ji, D. H. Liang, and Z. C. Li, "Reduction-degradable linear cationic polymers as gene carriers prepared by Cu(I)-catalyzed azide-alkyne cycloaddition," *Biomacromolecules*, vol. 12, no. 1, pp. 66–74, 2011.

[252] S. O. McDonnell, M. J. Hall, L. T. Allen, A. Byrne, W. M. Gallagher, and D. F. O'Shea, "Supramolecular photonic therapeutic agents," *J. Am. Chem. Soc.*, vol. 127, no. 47, pp. 16360–16361, 2005.

[253] N. A. Kuznetsova, N. S. Gretsova, O. A. Yuzhakova, V. M. Negrimovskii, O.

L. Kaliya, and E. A. Luk'yanets, "New reagents for determination of the quantum efficiency of singlet oxygen generation in aqueous media," *Russ. J. Gen. Chem.*, vol. 71, no. 1, pp. 36–41, 2001.

[254] K. Kobayashi, "Role of catecholamine signaling in brain and nervous system functions: new insights from mouse molecular genetic study.," *J. Investig. Dermatol. Symp. Proc.*, vol. 6, no. 1, pp. 115–121, 2001.

[255] J. A. Gingrich and M. G. Caron, "Recent Advances in the Molecular Biology of Dopamine Receptors," *Annu. Rev. Neurosci.*, vol. 16, no. 1, pp. 299–321, 1993.

[256] J. M. Sugihara and C. M. C. M. Bowman, "Cyclic Benzeneboronate Esters," *J. Am. Chem. Soc.*, vol. 80, no. 10, pp. 2443–2446, 1958.

[257] J. P. Lorand and J. O. Edwards, "Polyol Complexes and Structure of the Benzeneboronate Ion," *J. Org. Chem.*, vol. 24, no. 6, pp. 769–774, 1959.

[258] J. Yoon and A. W. Czarnik, "Fluorescent chemosensors of carbohydrates. A means of chemically communicating the binding of polyols in water based on chelation-enhanced quenching," *J. Am. Chem. Soc.*, vol. 114, no. 14, pp. 5874–5875, 1992.

[259] E. Kim and S. Park, "Discovery of New Fluorescent Dyes: Targeted Synthesis or Combinatorial Approach?," in *Advanced Fluorescence Reporters in Chemistry and Biology I SE - 5*, vol. 8, A. P. Demchenko, Ed. Berlin, Heidelberg: Springer Berlin Heidelberg, 2010, pp. 149–186.

[260] J. S. Hansen, M. Ficker, J. F. Petersen, J. B. Christensen, and T. Hoeg-Jensen, "Ortho-Substituted fluorescent aryl monoboronic acid displays physiological binding of d-glucose," *Tetrahedron Lett.*, vol. 54, no. 14, pp. 1849–1852, 2013.

[261] J. S. Hansen, J. F. Petersen, T. Hoeg-Jensen, and J. B. Christensen, "Buffer and sugar concentration dependent fluorescence response of a BODIPY-based aryl monoboronic acid sensor," *Tetrahedron Lett.*, vol. 53, no. 44, pp. 5852–5855, 2012.

APPENDIX

A1. Modular Logic Gates: Cascading Independent Logic Gates via Metal Ion Signals (^{1}H, ^{13}C and Mass Spectra)

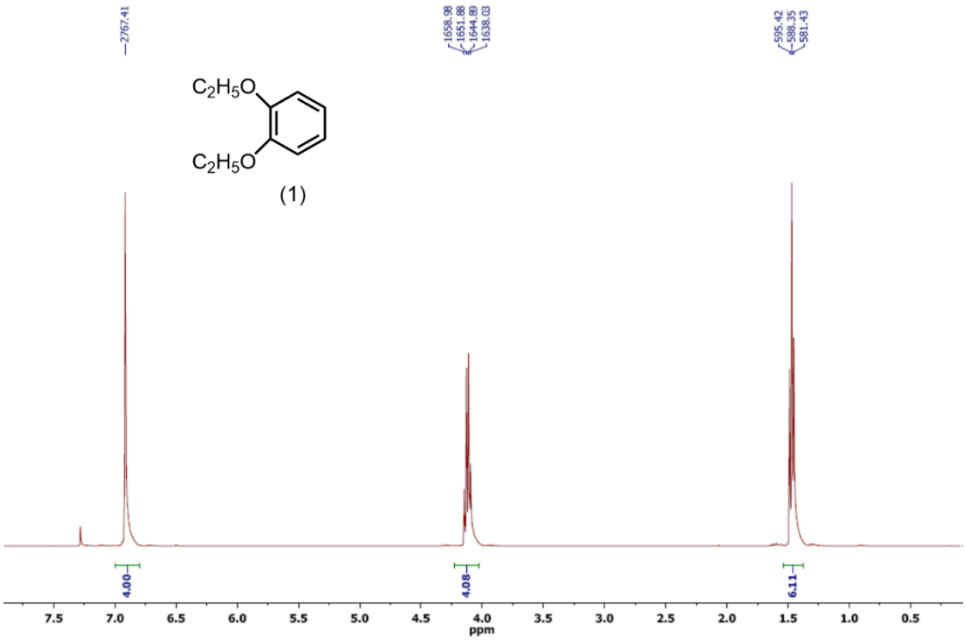

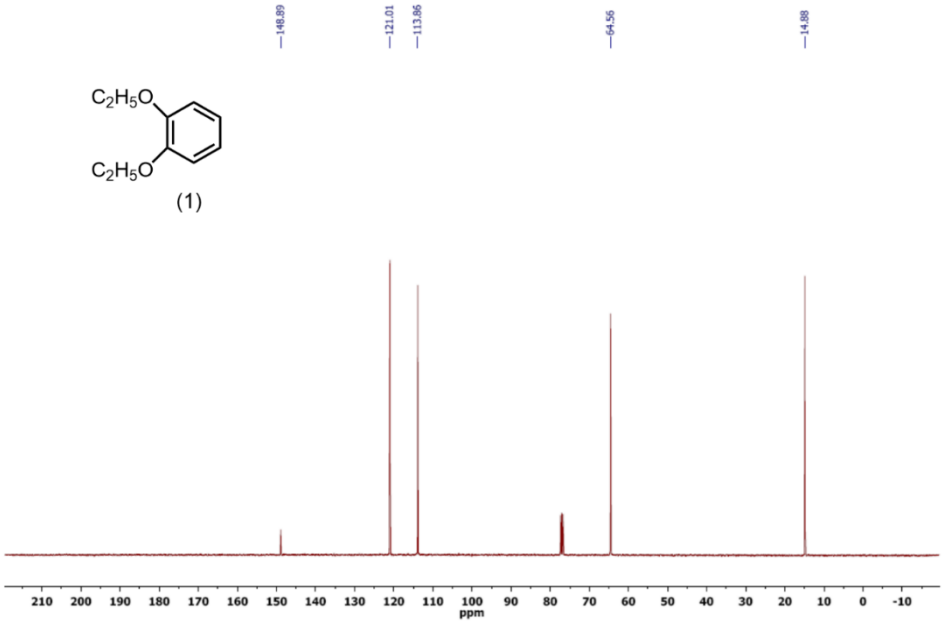

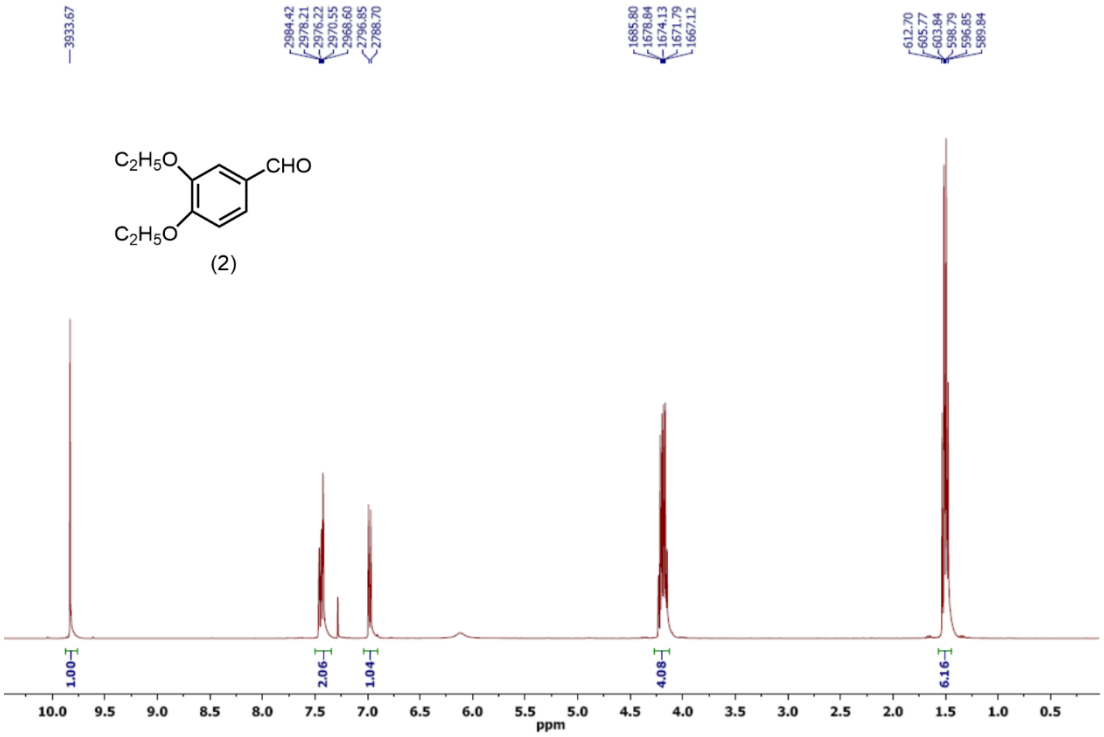
3933.67
2984.42
2978.21
2976.22
2970.55
2968.60
2796.85
2788.70
1685.80
1678.84
1674.13
1671.79
1667.12
612.70
605.77
603.84
598.79
596.85
589.84
C2H5O
CHO
C2H5O
(2)
1.00
2.06
1.04
4.08
6.16
10.0
9.5
9.0
8.5
8.0
7.5
7.0
6.5
6.0
5.5
5.0
4.5
4.0
3.5
3.0
2.5
2.0
1.5
1.0
0.5
ppm

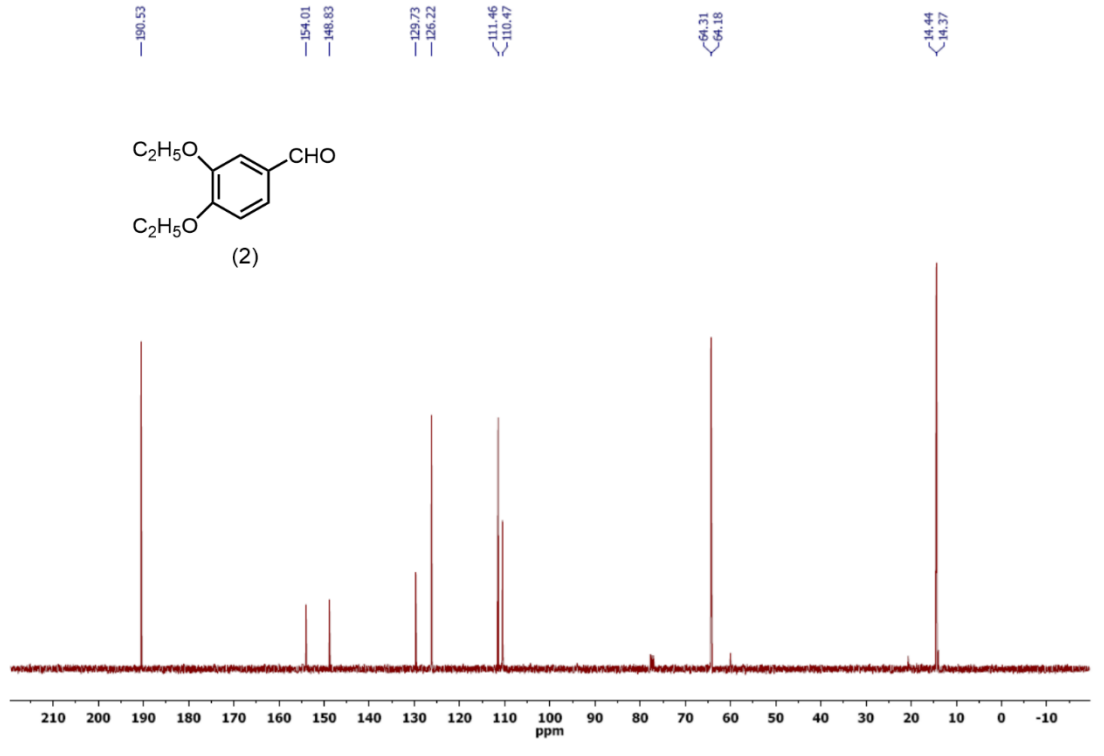
190.53
154.01
148.83
129.73
126.22
111.46
110.47
64.31
64.18
14.44
14.37
C2H5O
CHO
C2H5O
(2)
210
200
190
180
170
160
150
140
130
120
110
100
90
80
70
60
50
40
30
20
10
0
-10
ppm

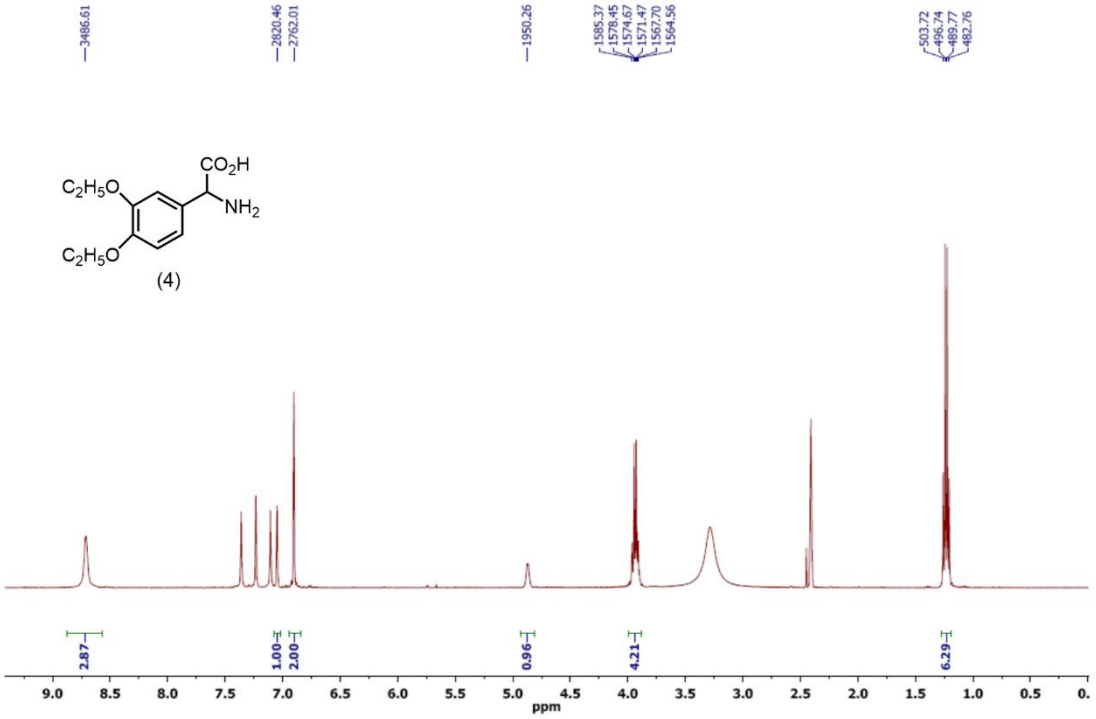
3486.61
2820.46
2762.01
1950.26
1585.37
1578.45
1574.67
1571.47
1567.70
1564.56
503.72
496.74
489.77
482.76
CO2H
C2H5O
NH2
C2H5O
(4)
2.87
1.00
2.00
0.96
4.21
6.29
ppm

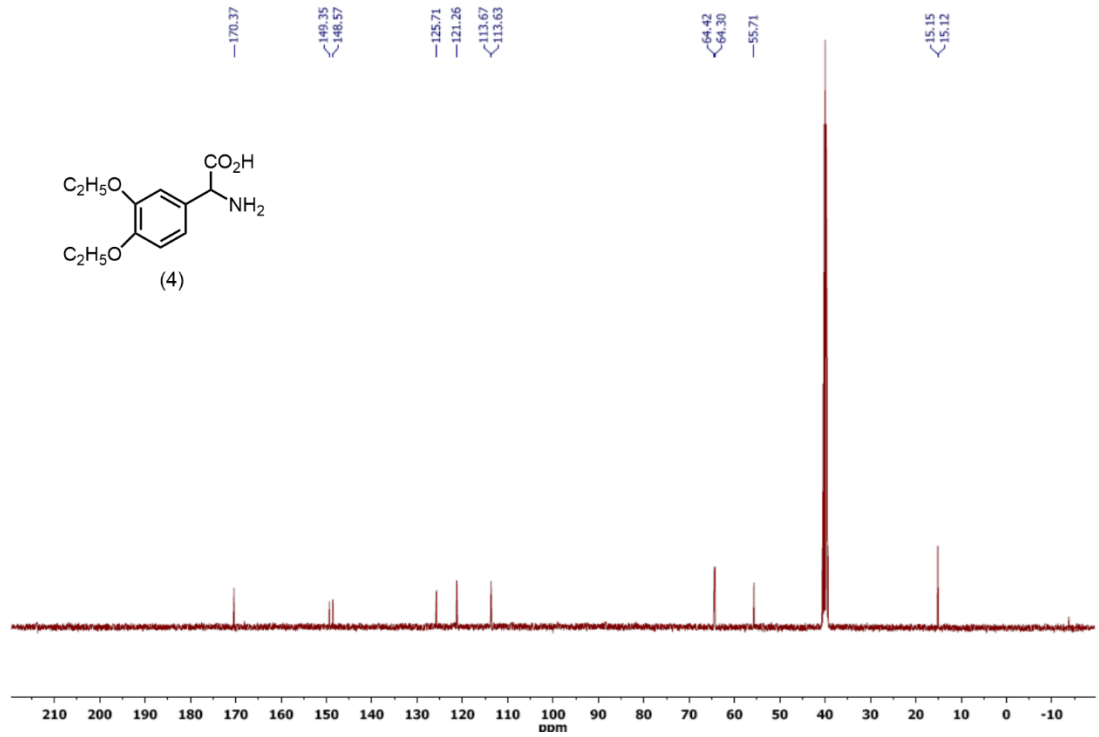
170.37
149.35
148.57
125.71
121.26
113.67
113.63
64.42
64.30
55.71
15.15
15.12
CO2H
C2H5O
NH2
C2H5O
(4)
ppm

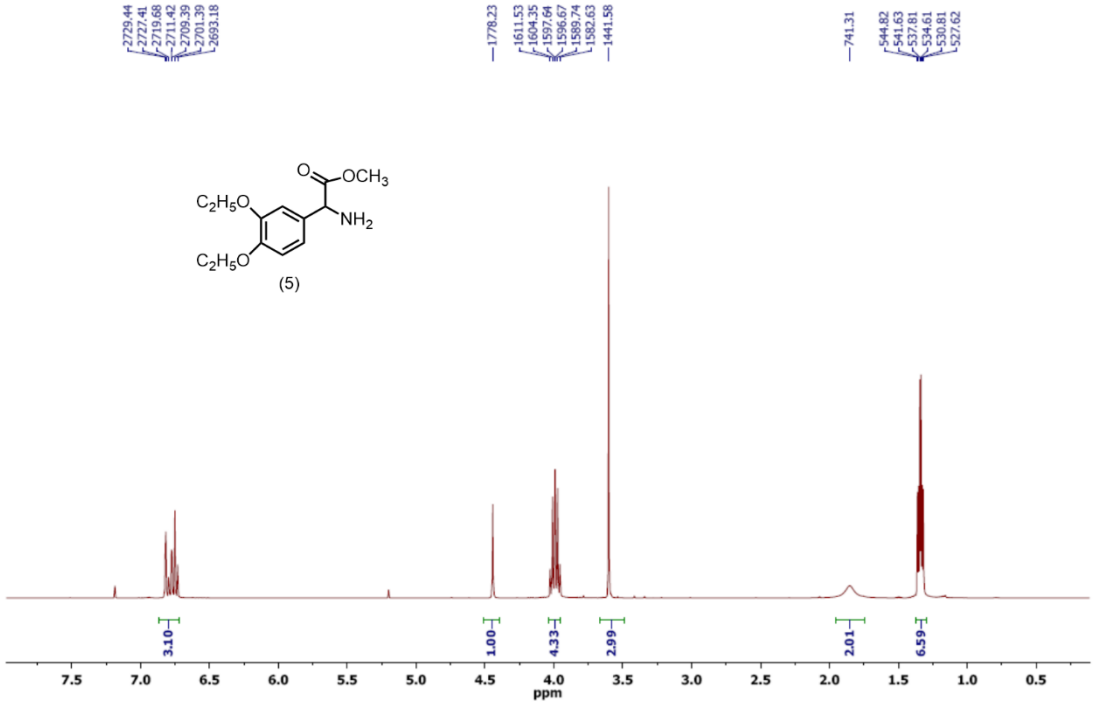
2729.44
2727.41
2719.68
2711.42
2709.39
2701.39
2693.18
1778.23
1611.53
1604.35
1597.64
1596.67
1589.74
1582.63
1441.58
741.31
544.82
541.63
537.81
534.61
530.81
527.62
O
OCH3
C2H5O
NH2
C2H5O
(5)
3.10
1.00
4.33
2.99
2.01
6.59
7.5
7.0
6.5
6.0
5.5
5.0
4.5
4.0
3.5
3.0
2.5
2.0
1.5
1.0
0.5
ppm

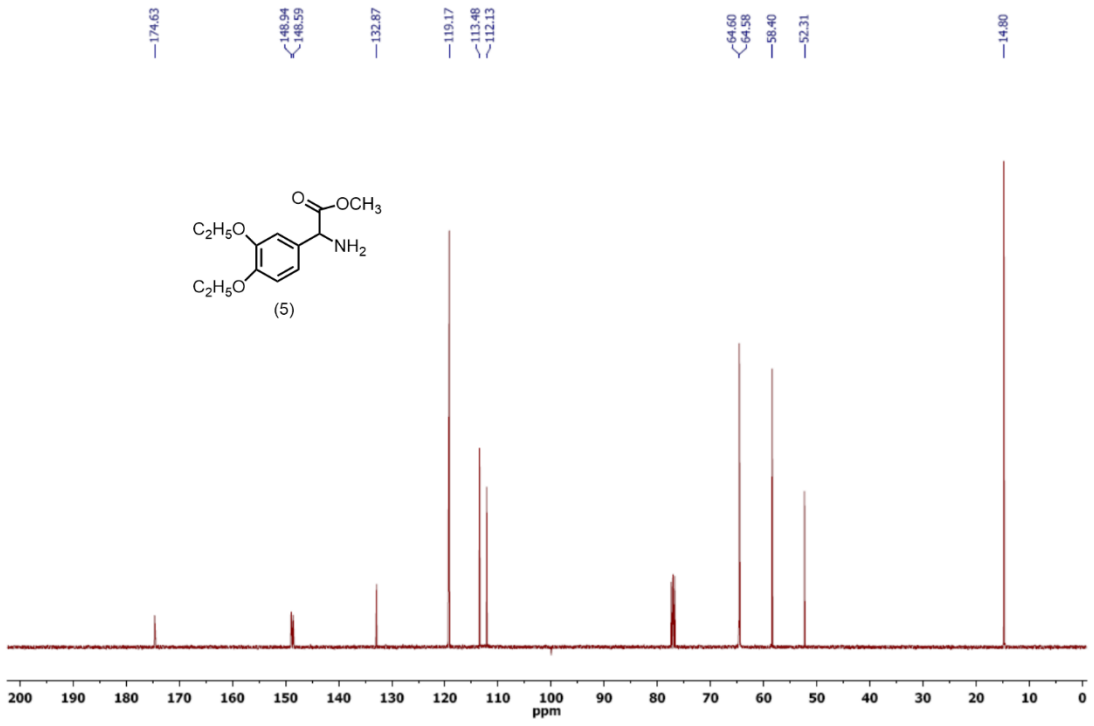
174.63
148.94
148.59
132.87
119.17
113.48
112.13
64.60
64.58
58.40
52.31
14.80
O
OCH3
C2H5O
NH2
C2H5O
(5)
200
190
180
170
160
150
140
130
120
110
100
90
80
70
60
50
40
30
20
10
0
ppm

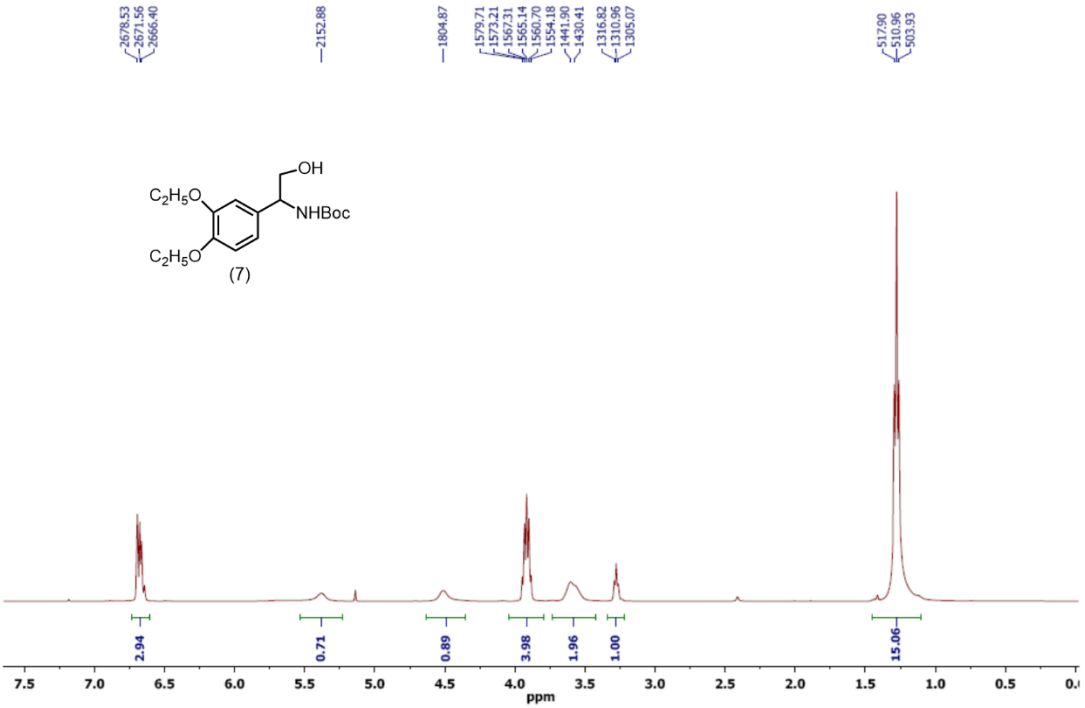
2678.53
2671.56
2666.40
2152.88
1804.87
1579.71
1573.21
1567.31
1565.14
1560.70
1554.18
1441.90
1430.41
1316.82
1310.96
1305.07
517.90
510.96
503.93
OH
NHBoc
C_2H_5O
C_2H_5O
(7)
2.94
0.71
0.89
3.98
1.96
1.00
15.06
7.5 7.0 6.5 6.0 5.5 5.0 4.5 4.0 3.5 3.0 2.5 2.0 1.5 1.0 0.5
ppm

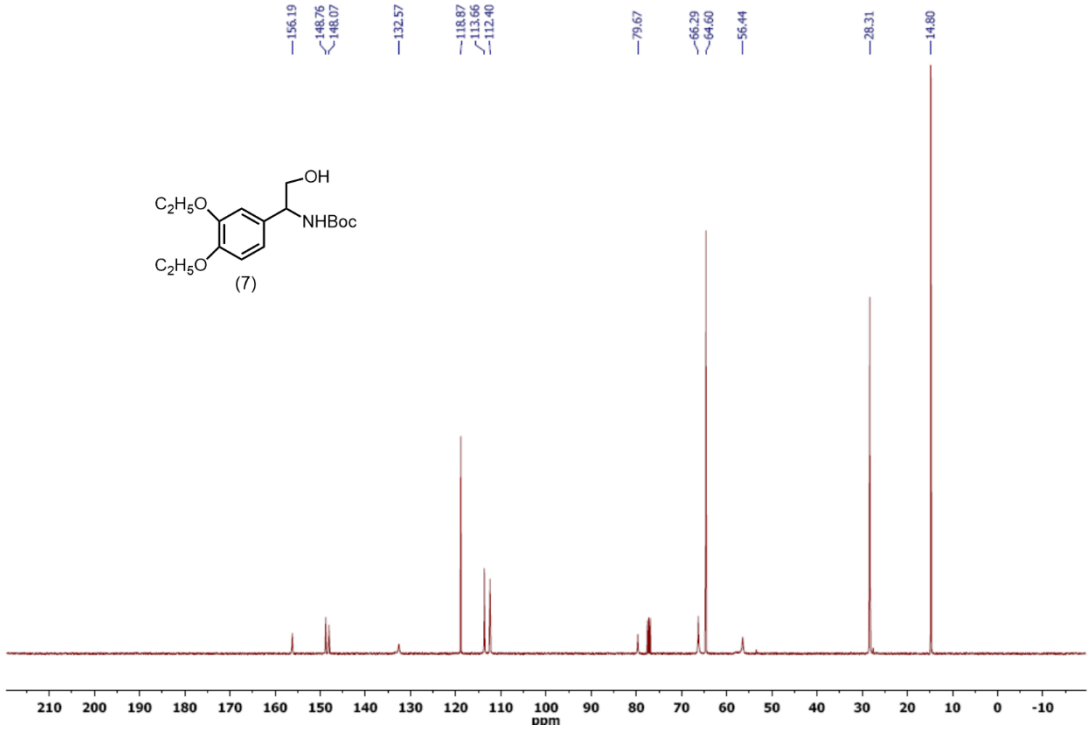
156.19
148.76
148.07
132.57
118.87
113.66
112.40
79.67
66.29
64.60
56.44
28.31
14.80
OH
NHBoc
C_2H_5O
C_2H_5O
(7)
210 200 190 180 170 160 150 140 130 120 110 100 90 80 70 60 50 40 30 20 10 0 -10
ppm

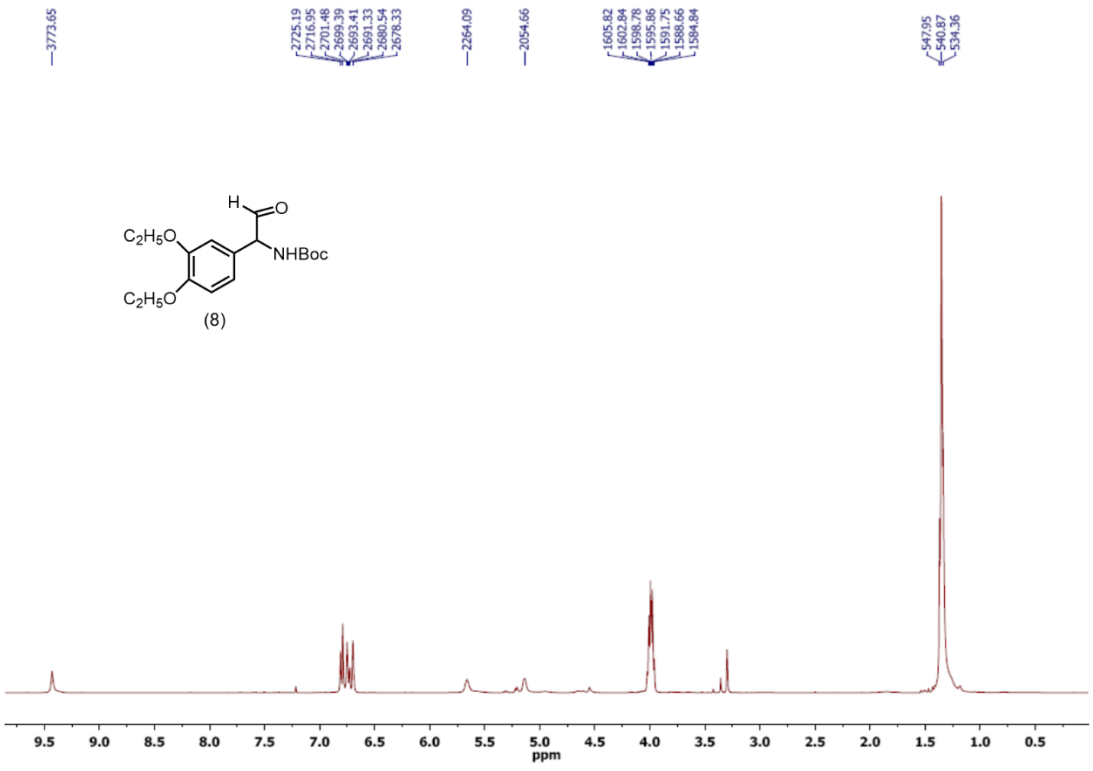
3773.65
2725.19
2716.95
2701.48
2699.39
2693.41
2691.33
2680.54
2678.33
2264.09
2054.66
1605.82
1602.84
1598.78
1595.86
1591.75
1588.66
1584.84
547.95
540.87
534.36
H
O
C2H5O
NHBoc
C2H5O
(8)
9.5 9.0 8.5 8.0 7.5 7.0 6.5 6.0 5.5 5.0 4.5 4.0 3.5 3.0 2.5 2.0 1.5 1.0 0.5
ppm

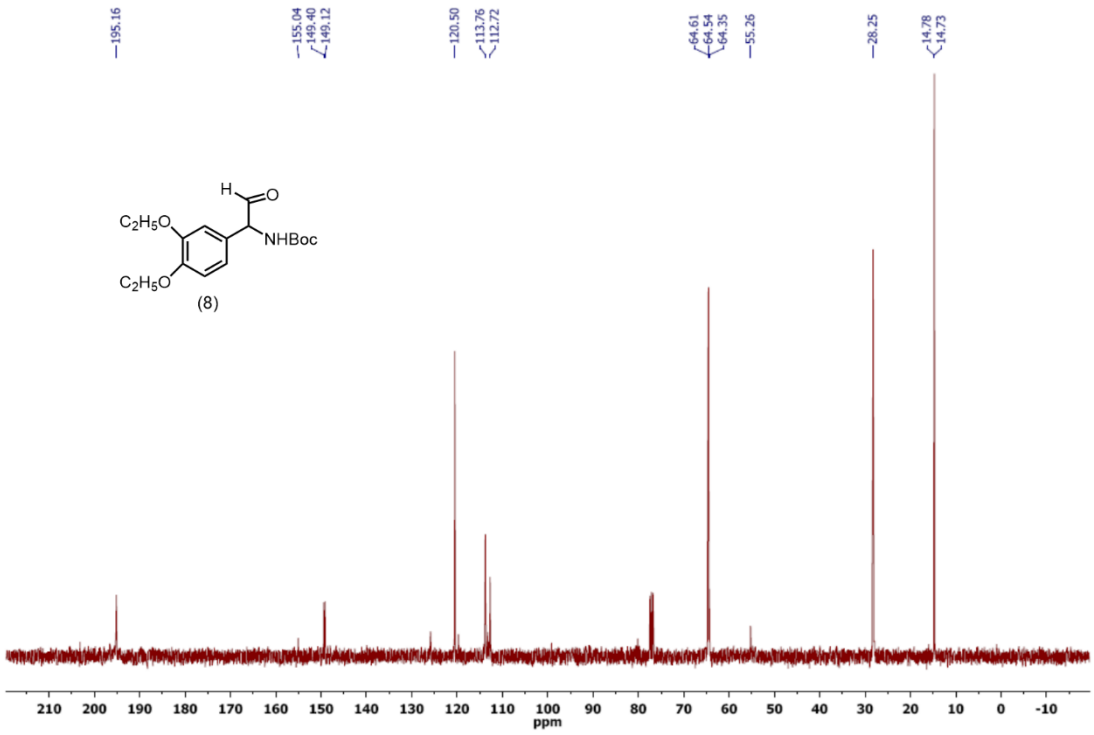
195.16
155.04
149.40
149.12
120.50
113.76
112.72
64.61
64.54
64.35
55.26
28.25
14.78
14.73
H
O
C2H5O
NHBoc
C2H5O
(8)
210 200 190 180 170 160 150 140 130 120 110 100 90 80 70 60 50 40 30 20 10 0 -10
ppm

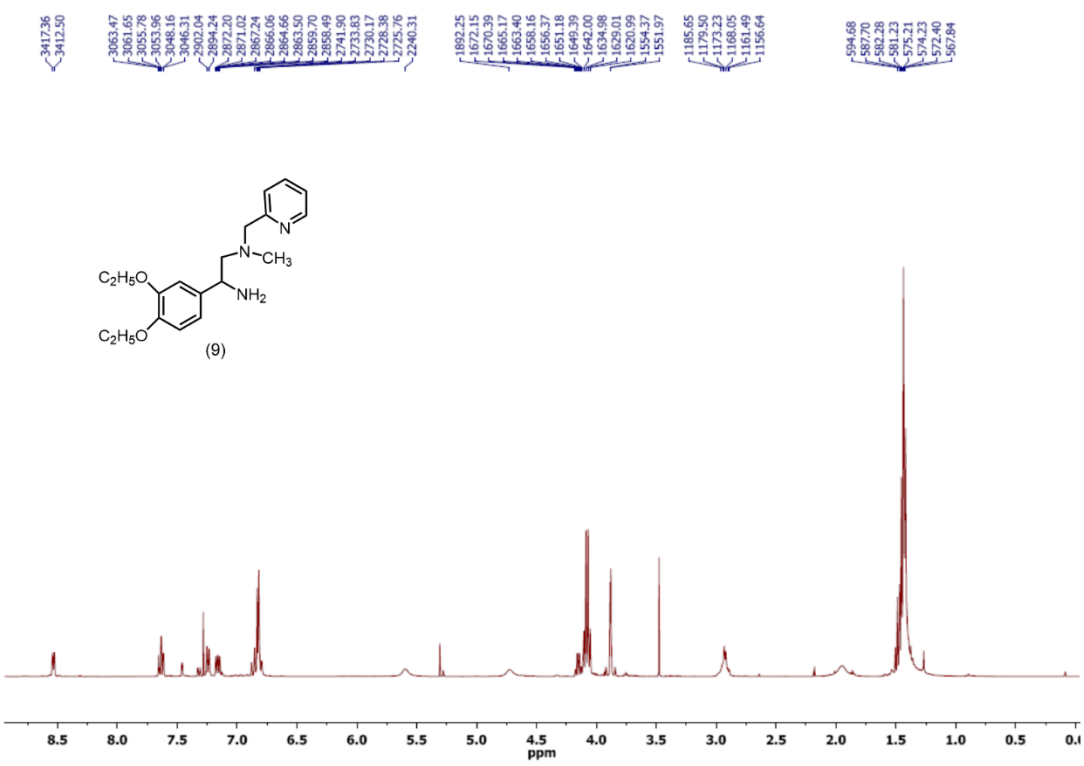
3417.36
3412.50
3063.47
3061.65
3055.78
3053.96
3048.16
3046.31
2902.04
2894.24
2872.20
2871.02
2867.24
2866.06
2864.66
2863.50
2859.70
2858.49
2741.90
2733.83
2730.17
2728.38
2725.76
2240.31
1892.25
1672.15
1670.39
1665.17
1663.40
1658.16
1656.37
1651.18
1649.39
1642.00
1634.98
1629.01
1620.99
1554.37
1551.97
1185.65
1179.50
1173.23
1168.05
1161.49
1156.64
594.68
587.70
582.28
581.23
575.21
574.23
572.40
567.84
N
N
CH3
NH2
C2H5O
C2H5O
(9)
8.5
8.0
7.5
7.0
6.5
6.0
5.5
5.0
4.5
4.0
3.5
3.0
2.5
2.0
1.5
1.0
0.5
ppm

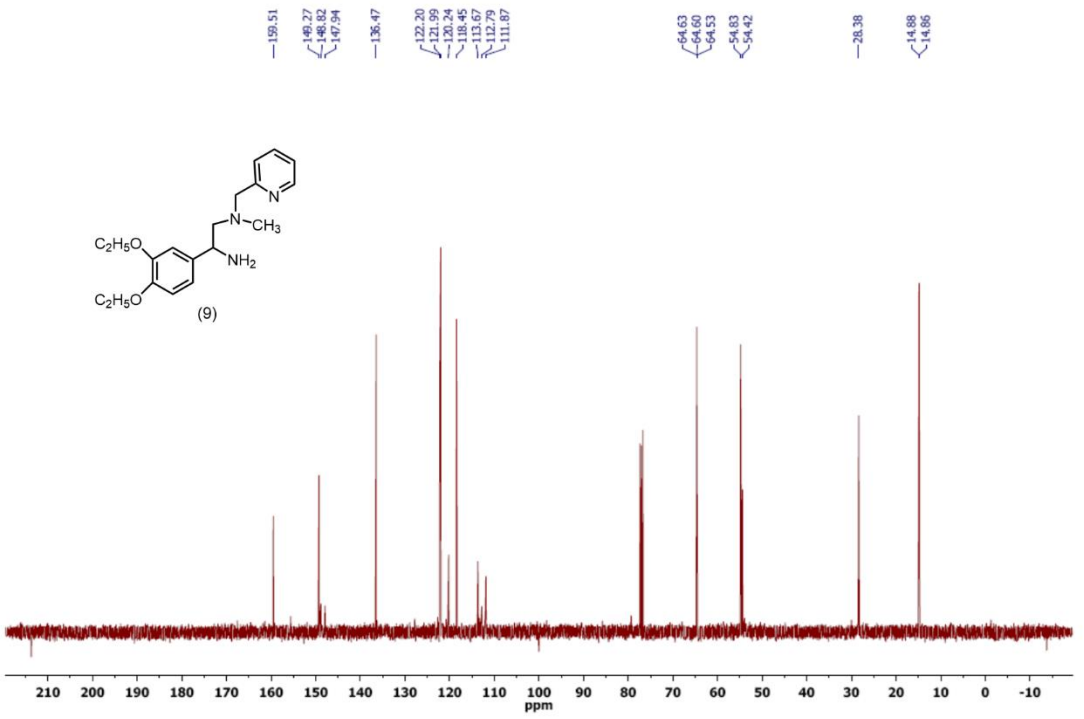
159.51
149.27
148.82
147.94
136.47
122.20
121.99
120.24
118.45
113.67
112.79
111.87
64.63
64.60
64.53
54.83
54.42
28.38
14.88
14.86
N
N
CH3
NH2
C2H5O
C2H5O
(9)
210
200
190
180
170
160
150
140
130
120
110
100
90
80
70
60
50
40
30
20
10
0
-10
ppm

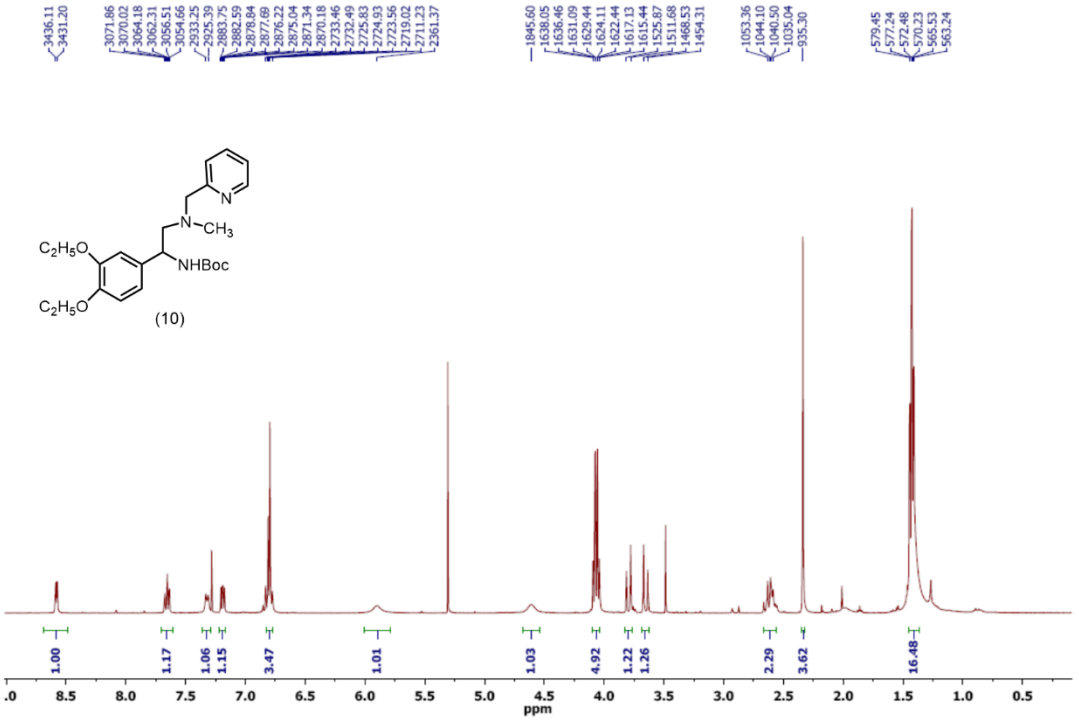
3436.11
3431.20
3071.86
3070.02
3064.18
3062.31
3056.51
3054.66
2933.25
2925.39
2883.75
2882.59
2878.84
2877.69
2876.22
2875.04
2871.34
2870.18
2733.46
2732.49
2725.83
2724.93
2723.56
2719.02
2711.23
2361.37
1945.60
1638.05
1636.46
1631.09
1629.44
1624.11
1622.44
1617.13
1615.44
1525.87
1511.68
1468.53
1454.31
1053.36
1044.10
1040.50
1035.04
935.30
579.45
577.24
572.48
570.23
565.53
563.24
N
N
CH3
C2H5O
C2H5O
NHBoc
(10)
1.00
1.17
1.06
1.15
3.47
1.01
1.03
4.92
1.22
1.26
2.29
3.62
16.48
ppm

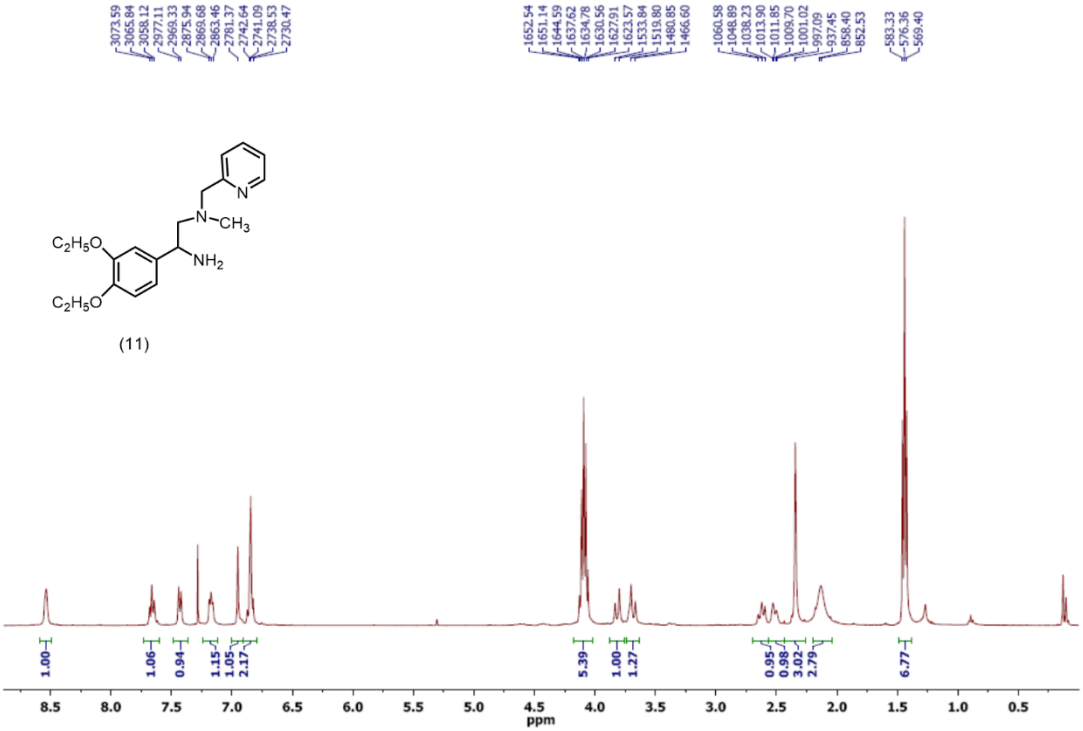
3073.59
3065.84
3058.12
2977.11
2969.33
2875.94
2869.68
2863.46
2781.37
2742.64
2741.09
2738.53
2730.47
1652.54
1651.14
1644.99
1637.62
1634.78
1630.56
1627.91
1623.57
1533.84
1519.80
1480.85
1466.60
1060.58
1048.89
1038.23
1013.90
1011.85
1009.70
1001.02
997.09
937.45
858.40
852.53
583.33
576.36
569.40
N
N
CH3
C2H5O
C2H5O
NH2
(11)
1.00
1.06
0.94
1.15
1.05
2.17
5.39
1.00
1.27
0.95
0.98
3.02
2.79
6.77
ppm

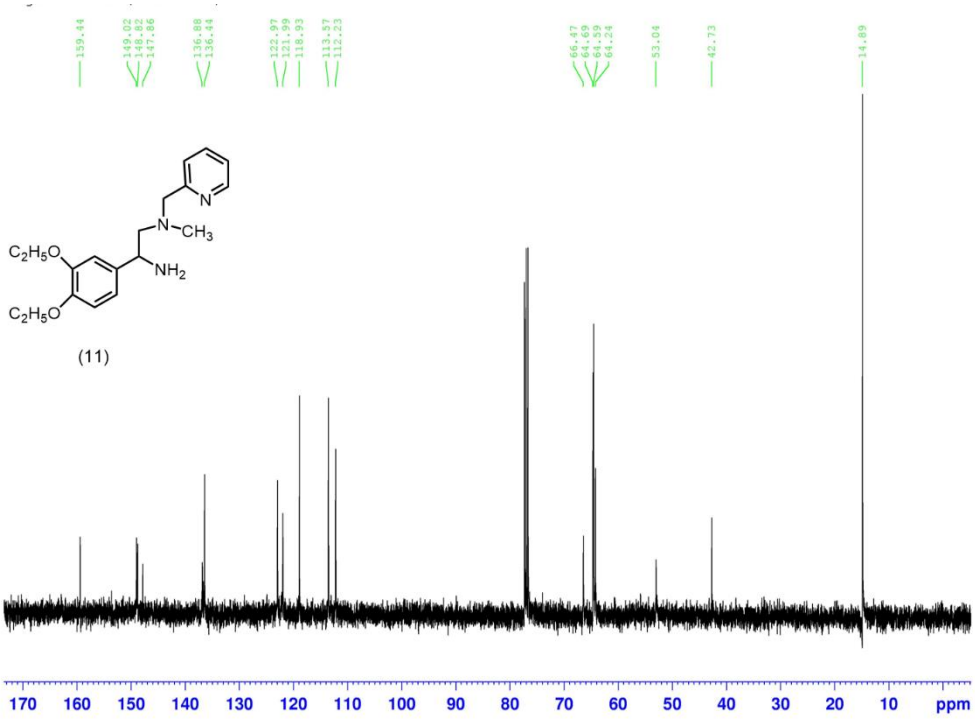
159.44
149.02
148.82
147.86
136.88
136.44
122.97
121.99
118.93
113.57
112.23
66.47
64.69
64.59
64.24
53.04
42.73
14.09
N
N
CH3
NH2
C2H5O
C2H5O
170 160 150 140 130 120 110 100 90 80 70 60 50 40 30 20 10 ppm

(11)

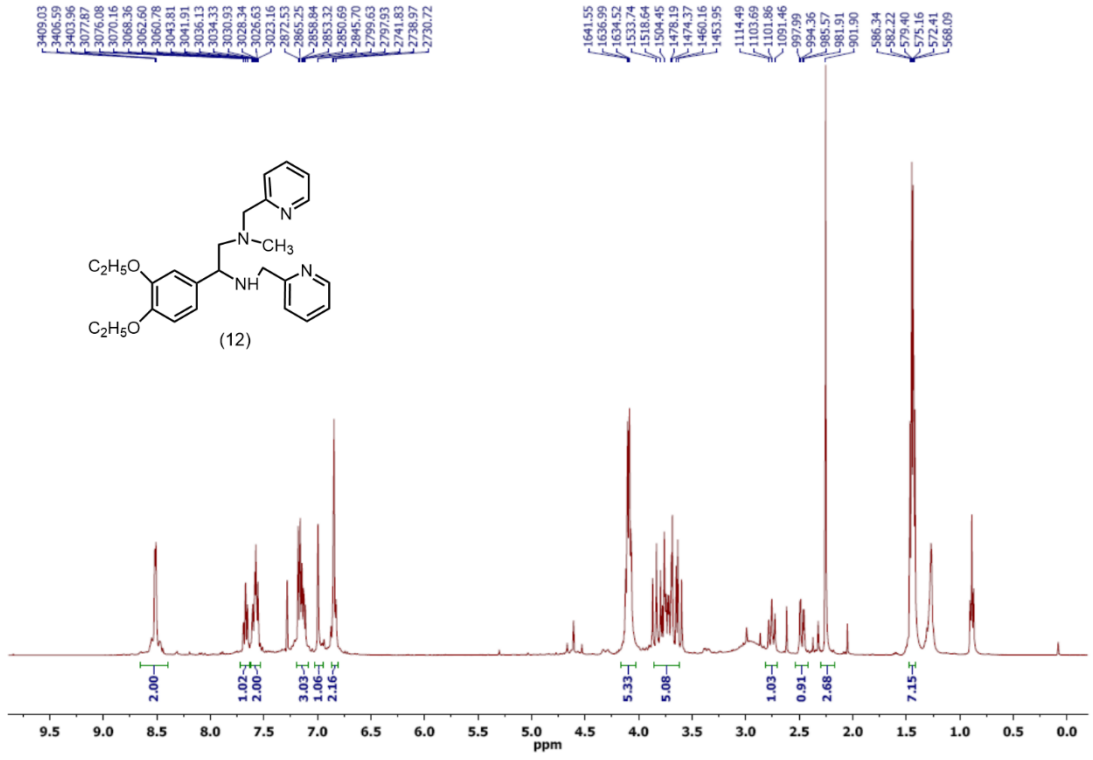
3409.03
3406.59
3403.96
3077.87
3076.08
3070.16
3068.36
3062.60
3060.78
3043.81
3041.91
3036.13
3034.33
3030.93
3028.34
3026.63
3023.16
2872.53
2865.25
2858.84
2853.32
2850.69
2845.70
2799.63
2797.93
2741.83
2738.97
2730.72
1641.55
1636.99
1634.52
1533.74
1518.64
1504.45
1478.19
1474.37
1460.16
1453.95
1114.49
1103.69
1101.86
1091.46
997.99
994.36
985.57
981.91
901.90
586.34
582.22
579.40
575.16
572.41
568.09
N
N
CH3
NH
N
C2H5O
C2H5O
2.00
1.02
2.00
3.03
1.06
2.16
5.33
5.08
1.03
0.91
2.68
7.15
9.5 9.0 8.5 8.0 7.5 7.0 6.5 6.0 5.5 5.0 4.5 4.0 3.5 3.0 2.5 2.0 1.5 1.0 0.5 0.0
ppm

(12)

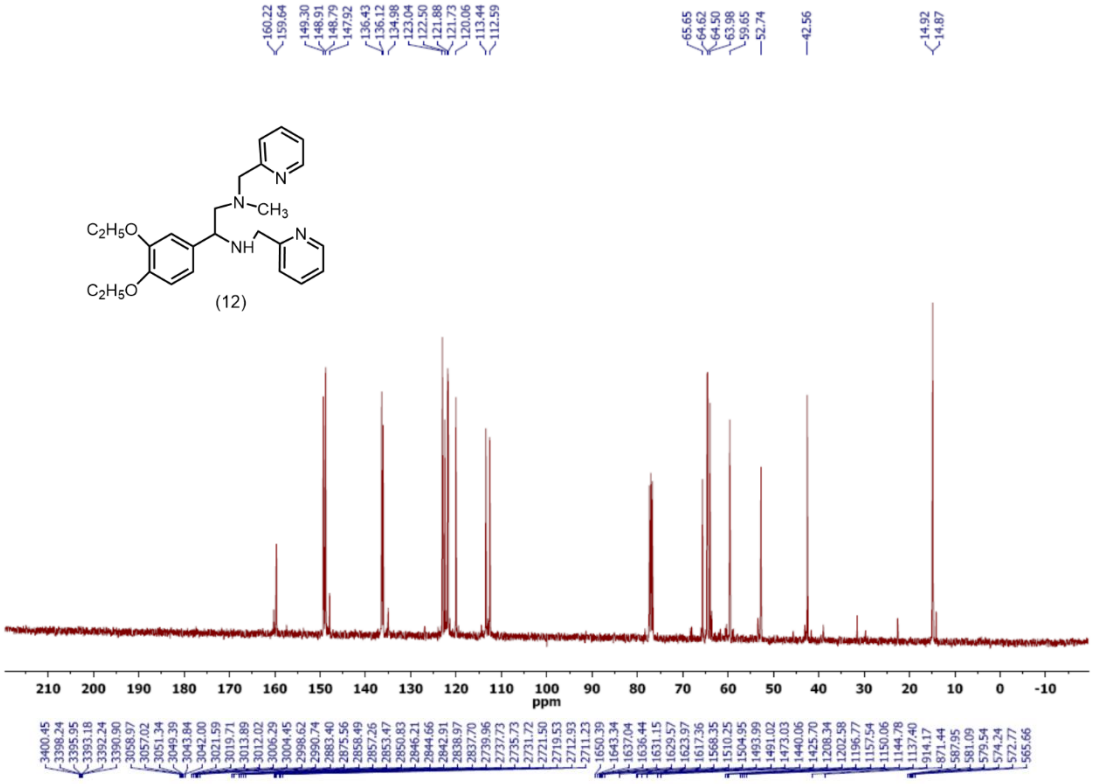
160.22
159.64
149.30
148.91
148.79
147.92
136.43
136.12
134.98
123.04
122.50
121.88
121.73
120.06
113.44
112.59
65.65
64.62
64.50
63.98
59.65
52.74
42.56
14.92
14.87
(12)
ppm
(13)
ppm

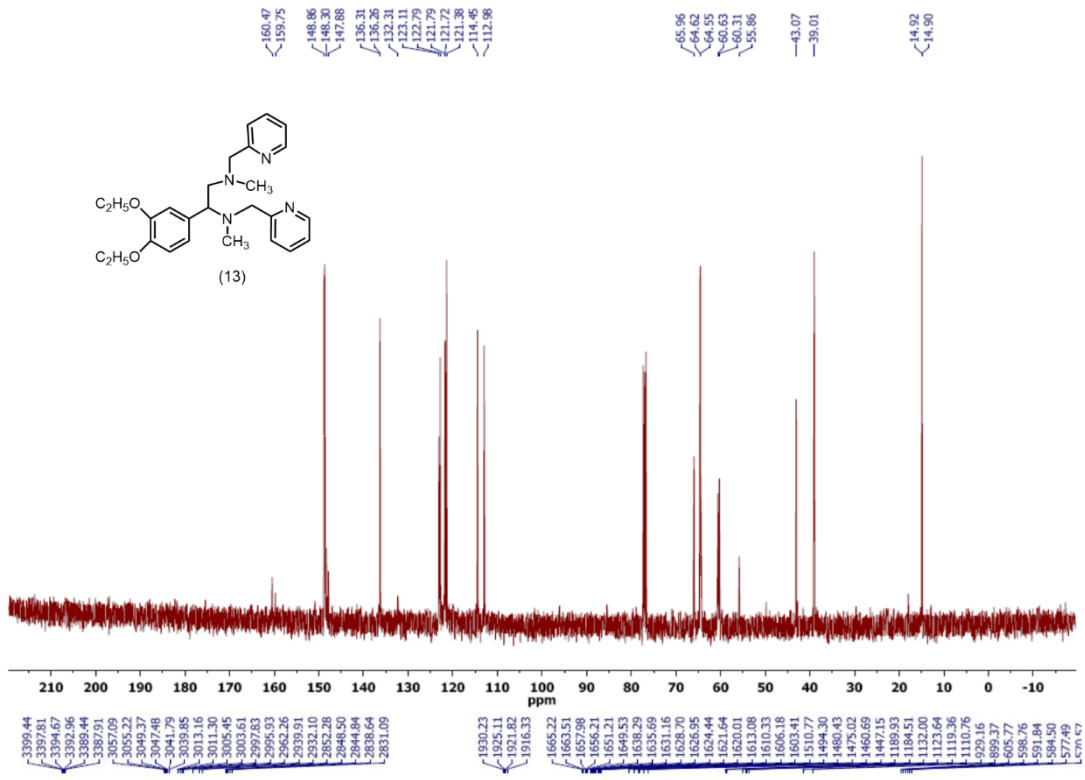
(13)
ppm

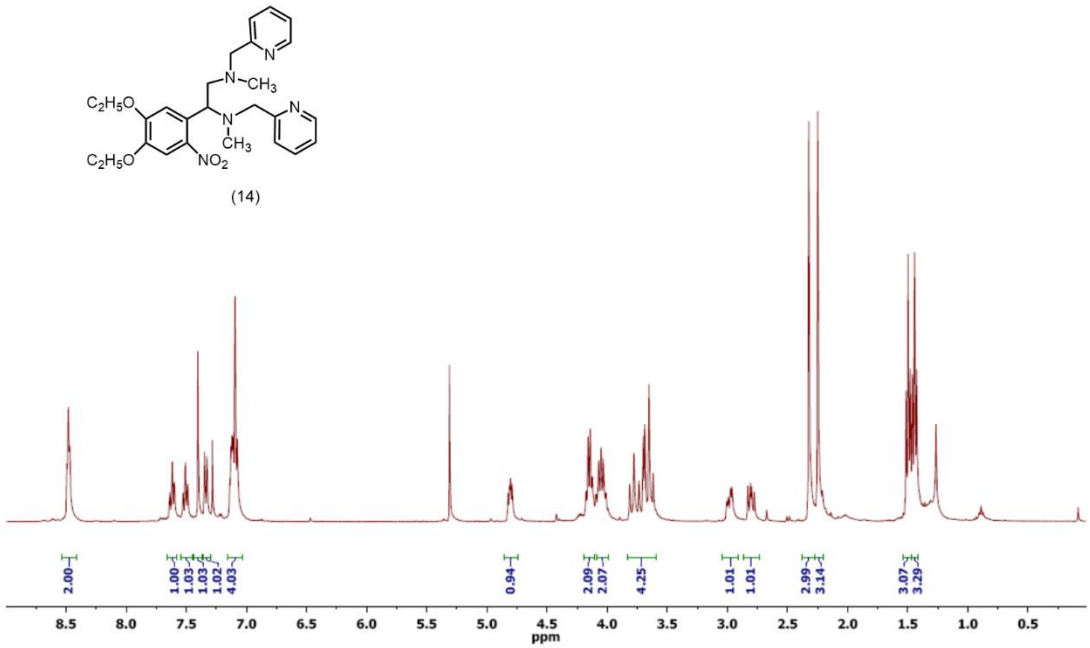
(14)
ppm

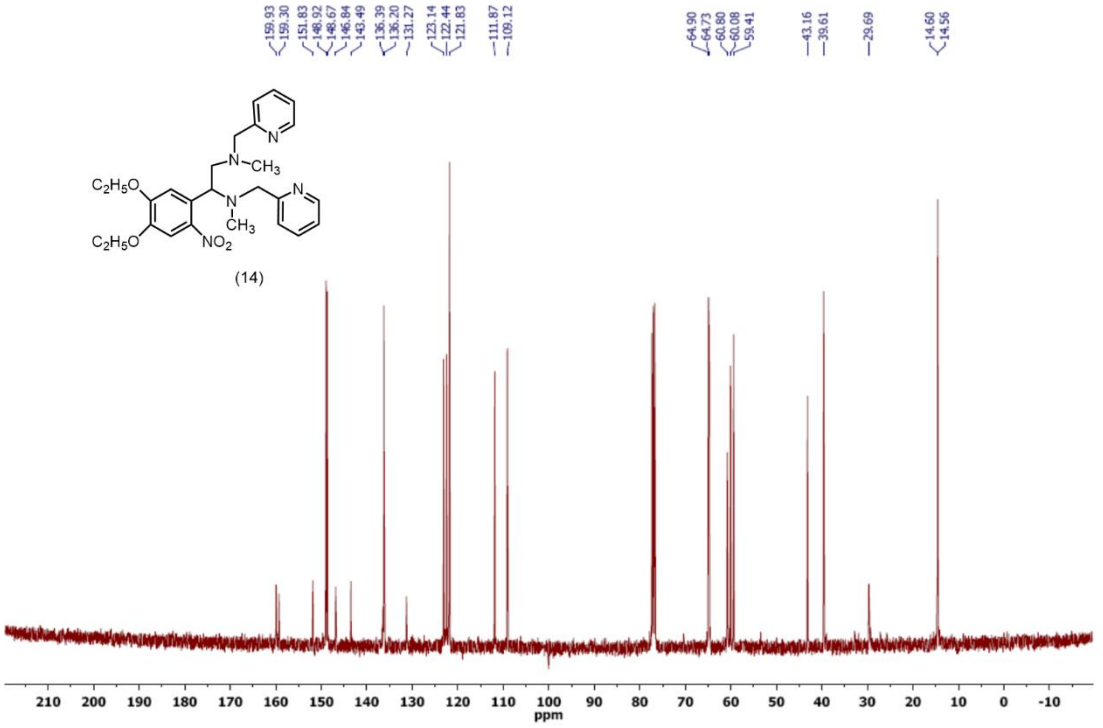
159.93
159.30
151.83
148.92
148.67
146.84
143.49
136.39
136.20
131.27
123.14
122.44
121.83
111.87
109.12
64.90
64.73
60.80
60.08
59.41
43.16
39.61
29.69
14.60
14.56
(14)
ppm

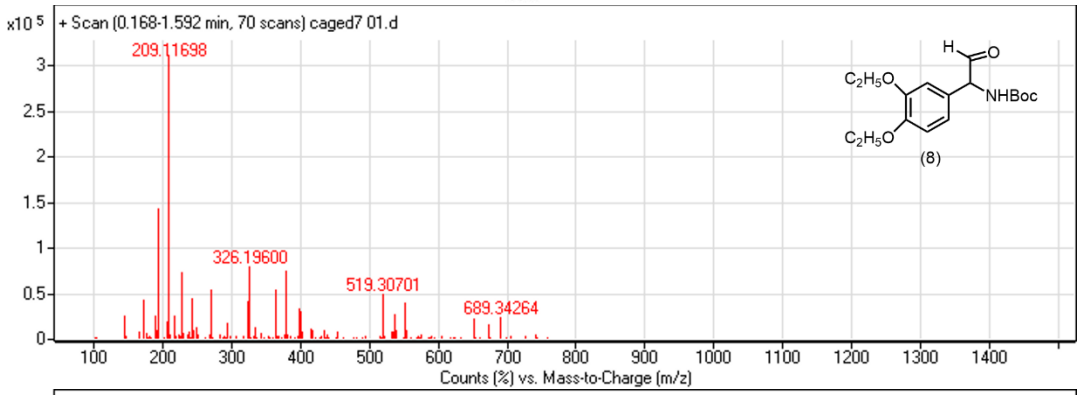
+ Scan (0.168-1.592 min, 70 scans) caged7 01.d
209.11698
326.19600
519.30701
689.34264
(8)
Counts (%) vs. Mass-to-Charge (m/z)

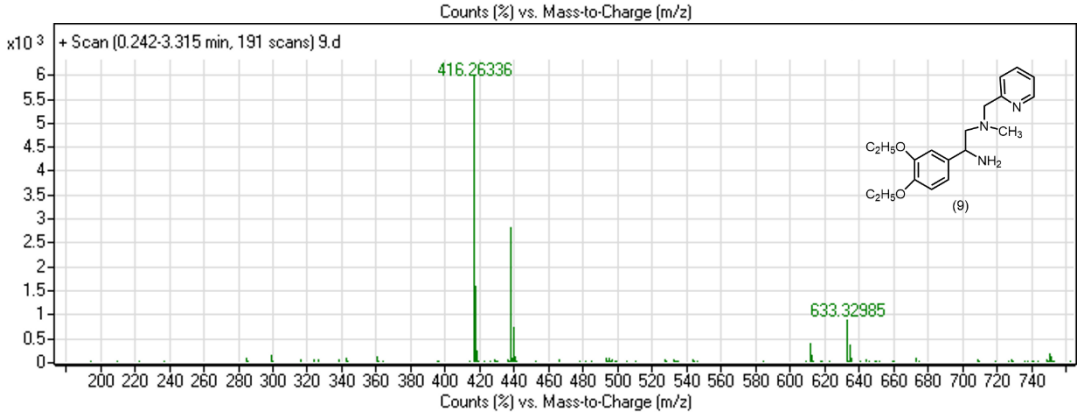
+ Scan (0.242-3.315 min, 191 scans) 9.d
416.26336
633.32985
(9)
Counts (%) vs. Mass-to-Charge (m/z)

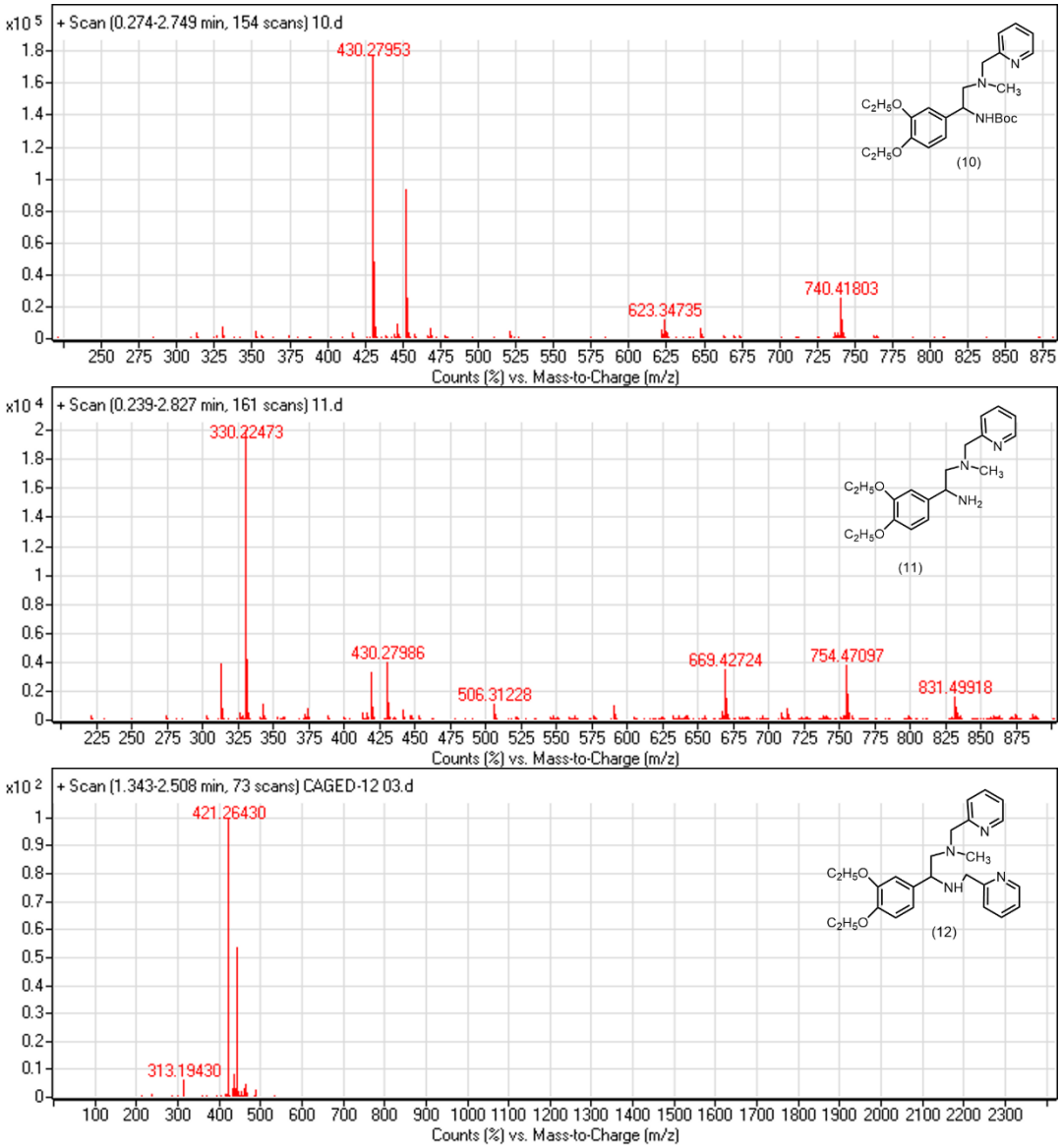
x10 5
+ Scan (0.274-2.749 min, 154 scans) 10.d
430.27953
623.34735
740.41803
(10)
Counts (%) vs. Mass-to-Charge (m/z)
x10 4
+ Scan (0.239-2.827 min, 161 scans) 11.d
330.22473
430.27986
506.31228
669.42724
754.47097
831.49918
(11)
Counts (%) vs. Mass-to-Charge (m/z)
x10 2
+ Scan (1.343-2.508 min, 73 scans) CAGED-12 03.d
421.26430
313.19430
(12)
Counts (%) vs. Mass-to-Charge (m/z)

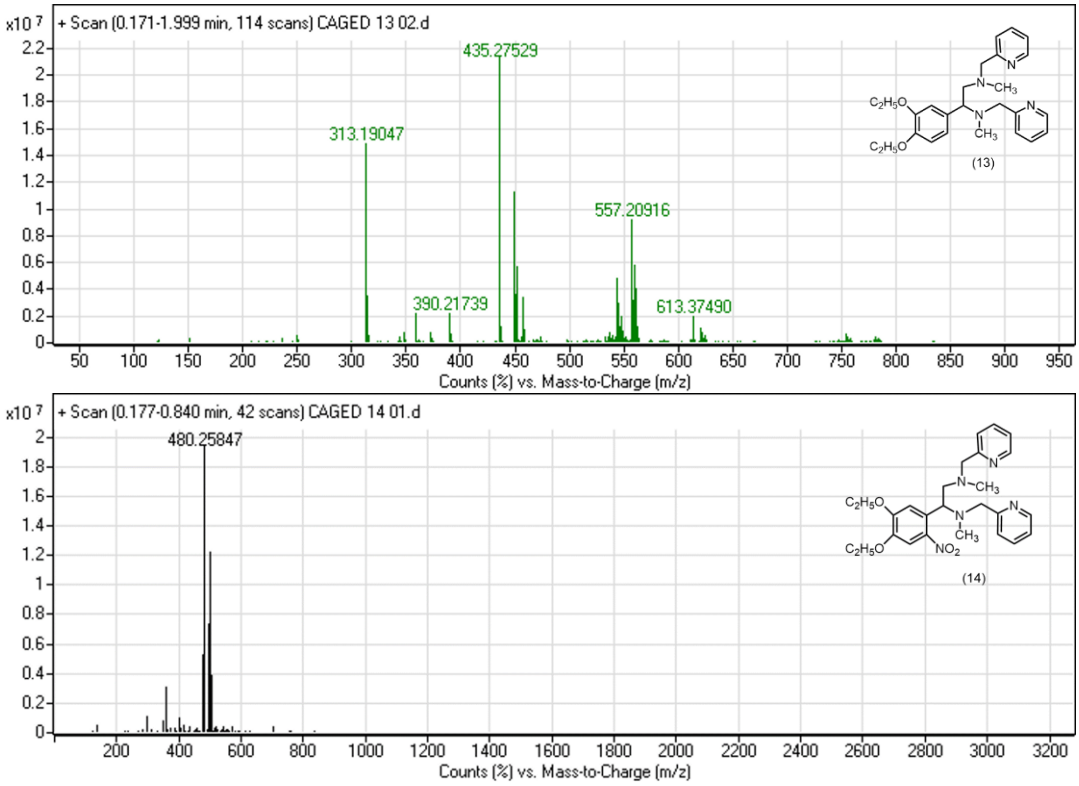
x10 7
+ Scan (0.171-1.999 min, 114 scans) CAGED 13 02.d
435.27529
313.19047
557.20916
390.21739
613.37490
(13)
Counts (%) vs. Mass-to-Charge (m/z)
x10 7
+ Scan (0.177-0.840 min, 42 scans) CAGED 14 01.d
480.25847
(14)
Counts (%) vs. Mass-to-Charge (m/z)

A2. Near IR Triggered, Remote Controlled Release of Metal Ions: A Novel Strategy for Caged Ions (^{1}H, ^{13}C and Mass Spectra)

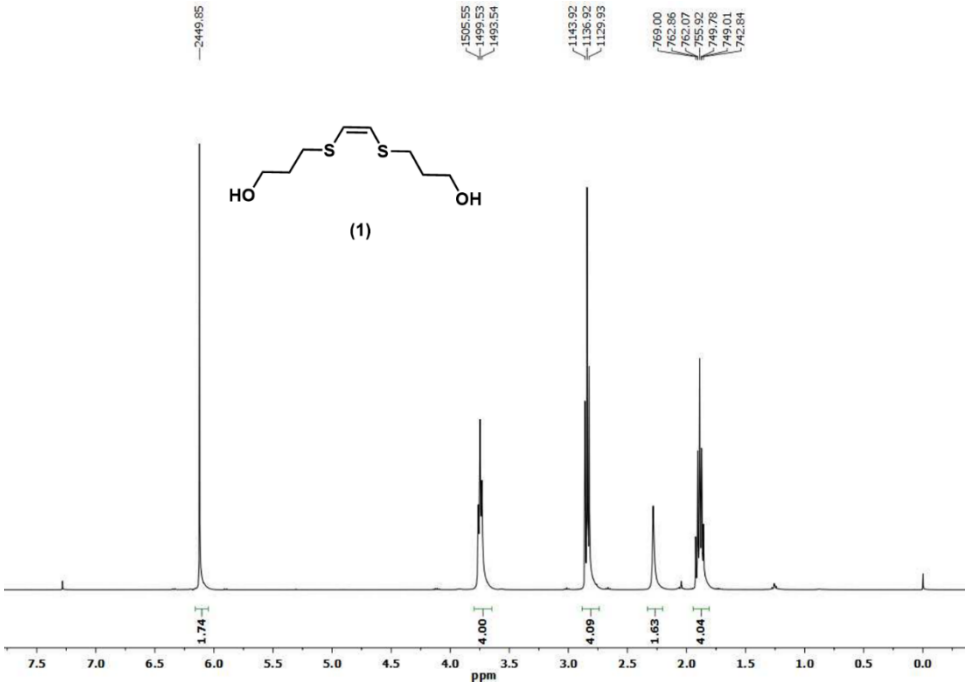

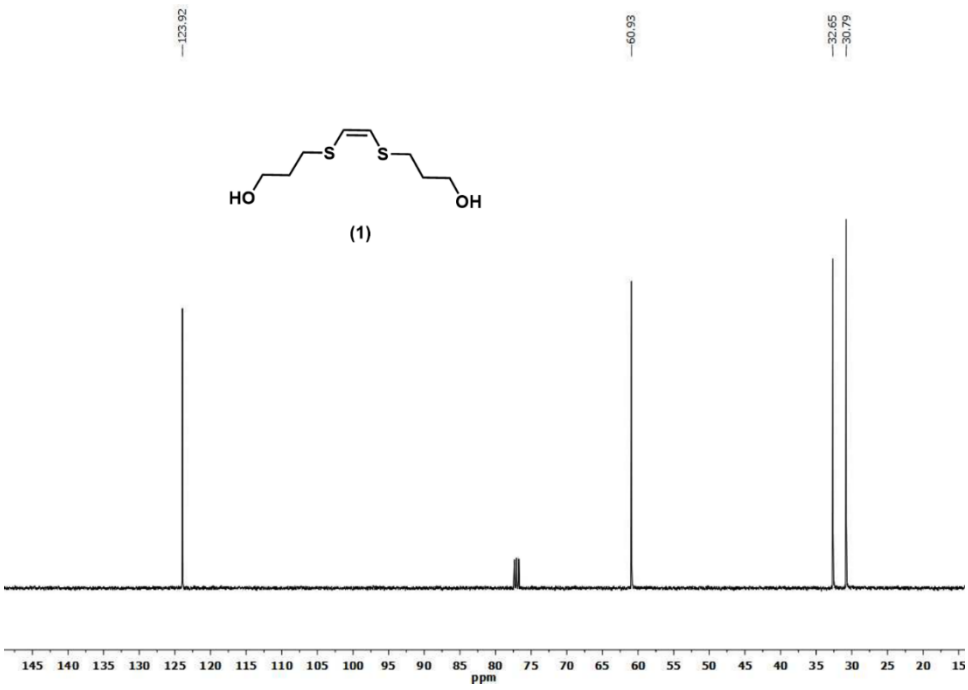

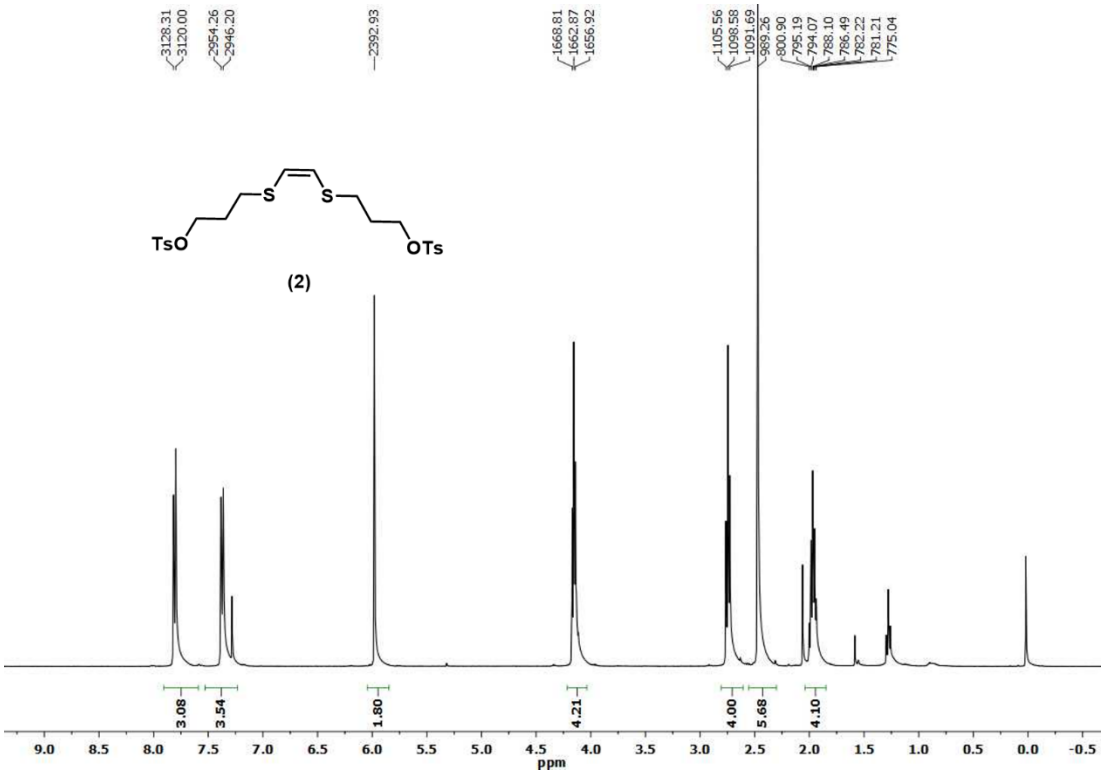
3128.31
3120.00
2954.26
2946.20
2392.93
1668.81
1662.87
1656.92
1105.56
1098.58
1091.69
989.26
800.90
795.19
794.07
788.10
786.49
782.22
781.21
775.04
TsO
OTs
(2)
3.08
3.54
1.80
4.21
4.00
5.68
4.10
ppm

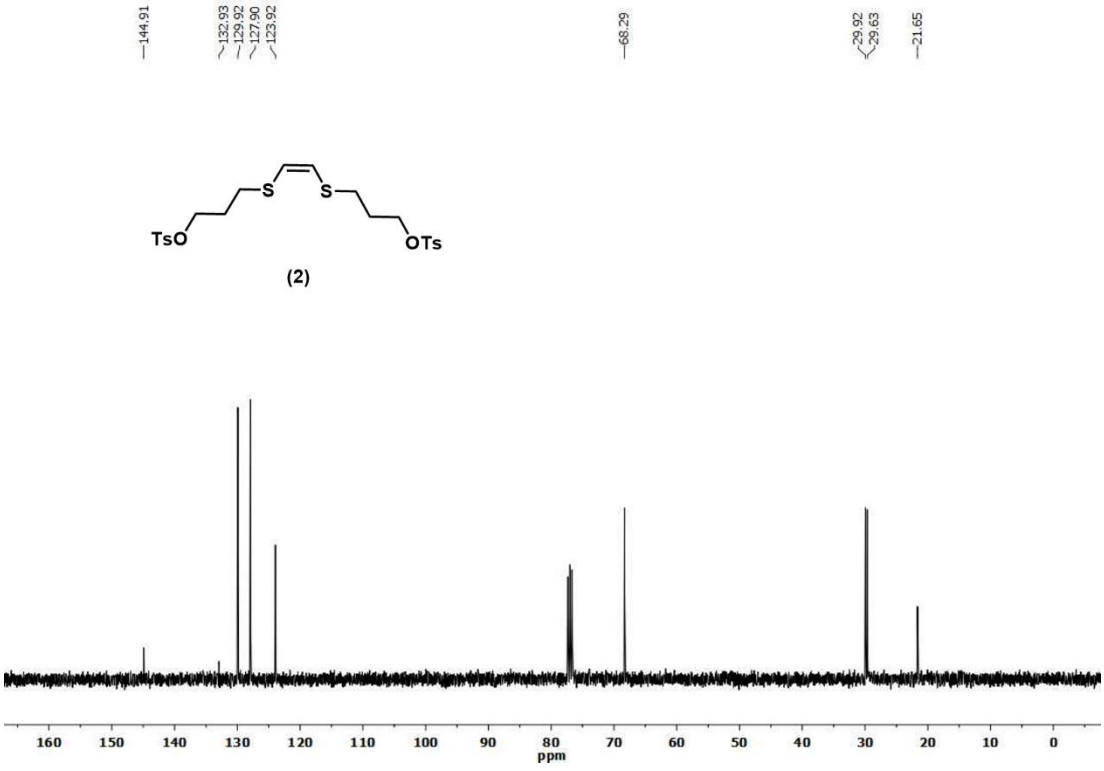
144.91
132.93
129.92
127.90
123.92
68.29
29.92
29.63
21.65
TsO
OTs
(2)
ppm

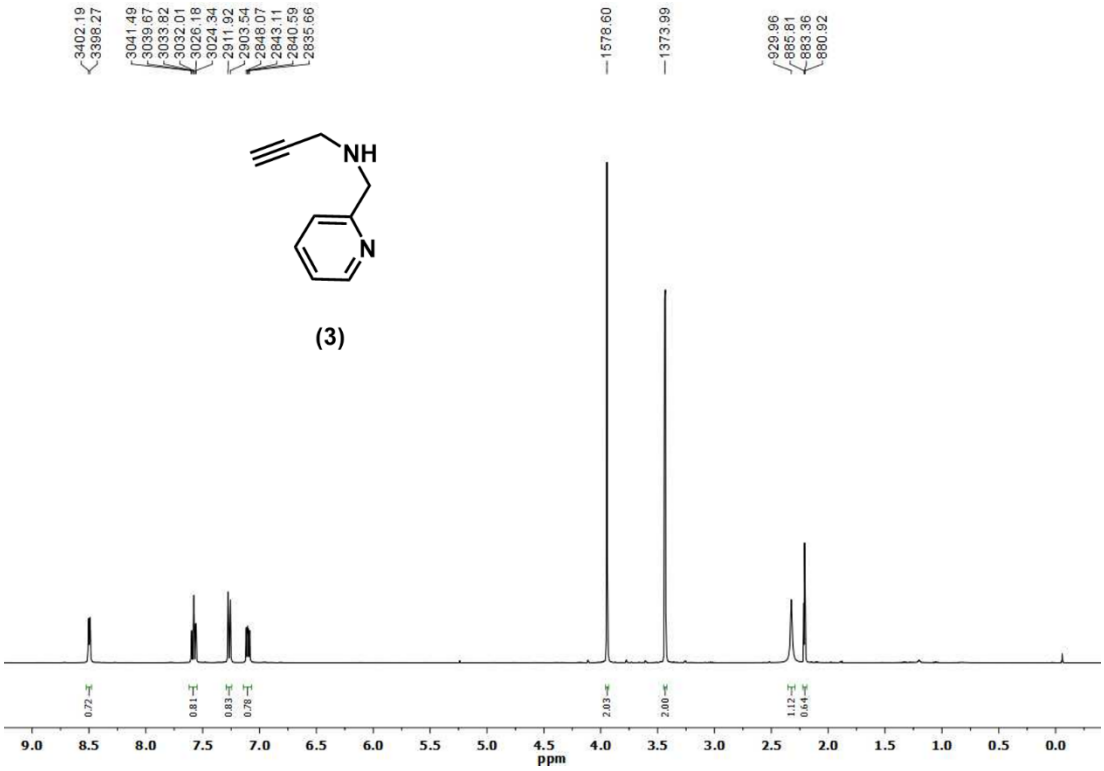
3402.19
3398.27
3041.49
3039.67
3033.82
3032.01
3026.18
3024.34
2911.92
2903.54
2848.07
2843.11
2840.59
2835.66
1578.60
1373.99
929.96
885.81
883.36
880.92
NH
N
(3)
0.73
0.81
0.83
0.78
2.03
2.00
1.12
0.64
9.0
8.5
8.0
7.5
7.0
6.5
6.0
5.5
5.0
4.5
4.0
3.5
3.0
2.5
2.0
1.5
1.0
0.5
0.0
ppm

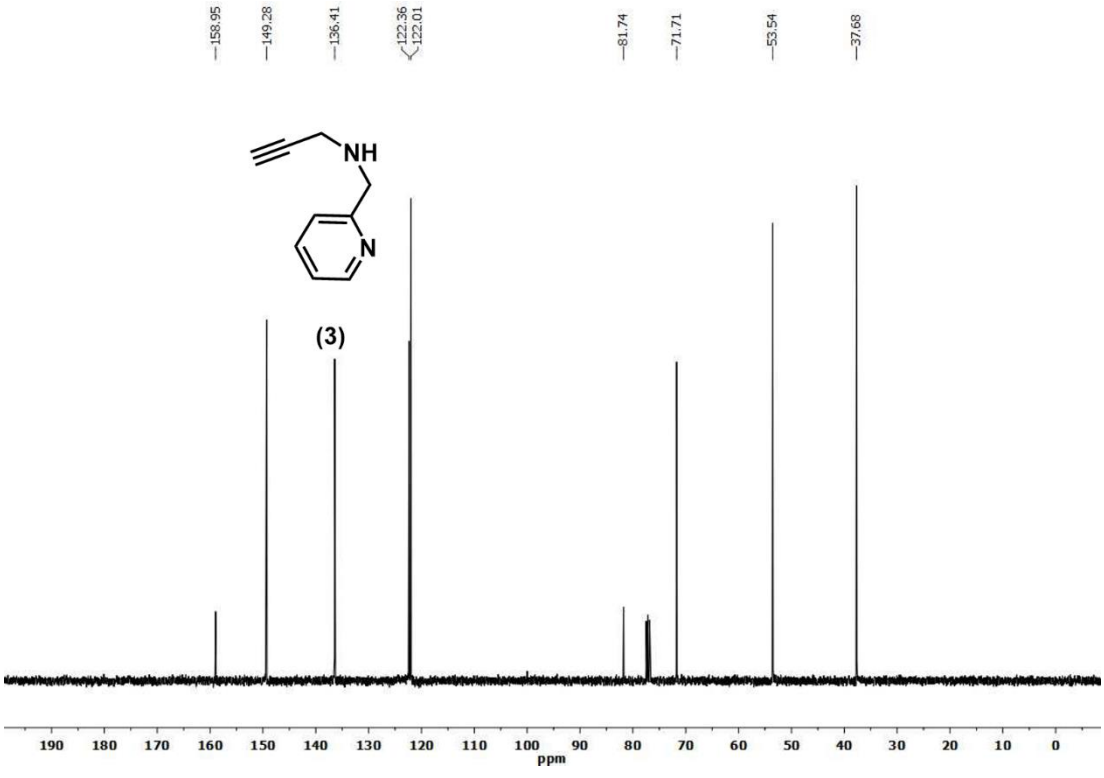
158.95
149.28
136.41
122.36
122.01
81.74
71.71
53.54
37.68
NH
N
(3)
190
180
170
160
150
140
130
120
110
100
90
80
70
60
50
40
30
20
10
0
ppm

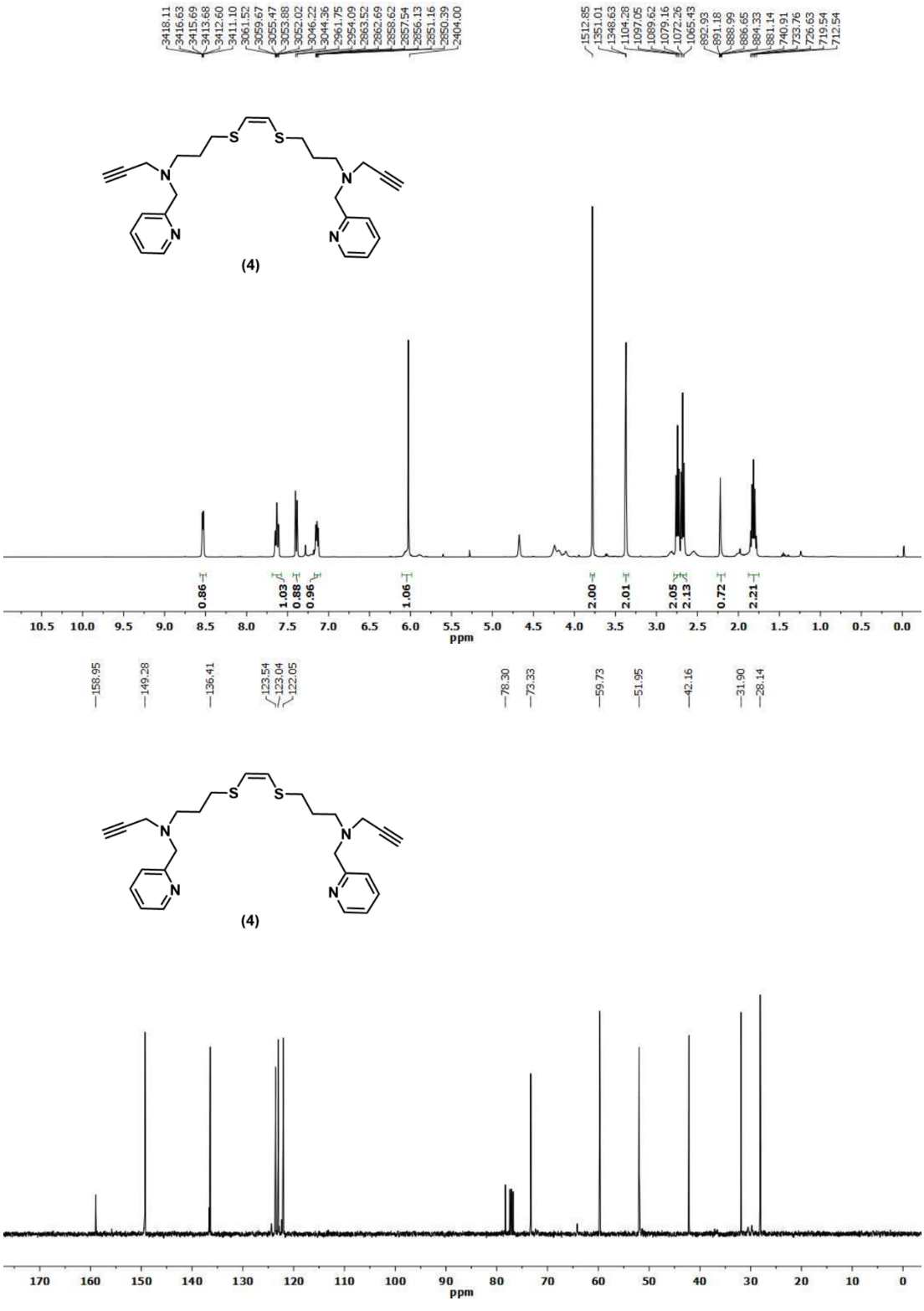
3418.11
3416.63
3415.69
3413.68
3412.60
3411.10
3061.52
3059.67
3055.47
3053.88
3052.02
3046.22
3044.36
2961.75
2954.09
2863.52
2862.69
2858.62
2857.54
2856.13
2851.16
2850.39
2404.00
1512.85
1351.01
1348.63
1104.28
1097.05
1089.62
1079.16
1072.26
1065.43
892.93
891.18
888.99
886.65
884.33
881.14
740.91
733.76
726.63
719.54
712.54
(4)
0.86
1.03
0.88
0.96
1.06
2.00
2.01
2.05
2.13
0.72
2.21
ppm
158.95
149.28
136.41
123.54
123.04
122.05
78.30
73.33
59.73
51.95
42.16
31.90
28.14
(4)
ppm

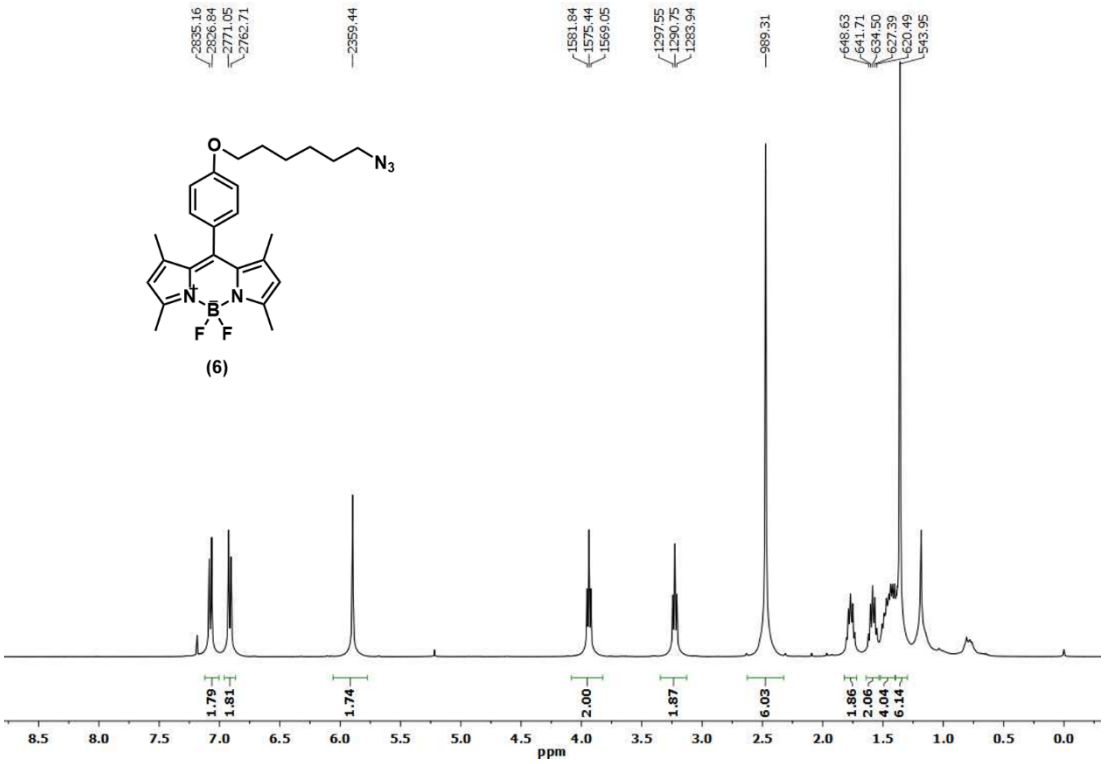
2835.16
2826.84
2771.05
2762.71
2359.44
1581.84
1575.44
1569.05
1297.55
1290.75
1283.94
989.31
648.63
641.71
634.50
627.39
620.49
543.95
O
N3
N+
B-
N
F
F
(6)
1.79
1.81
1.74
2.00
1.87
6.03
1.86
2.06
4.04
6.14
8.5
8.0
7.5
7.0
6.5
6.0
5.5
5.0
4.5
4.0
3.5
3.0
2.5
2.0
1.5
1.0
0.5
0.0
ppm

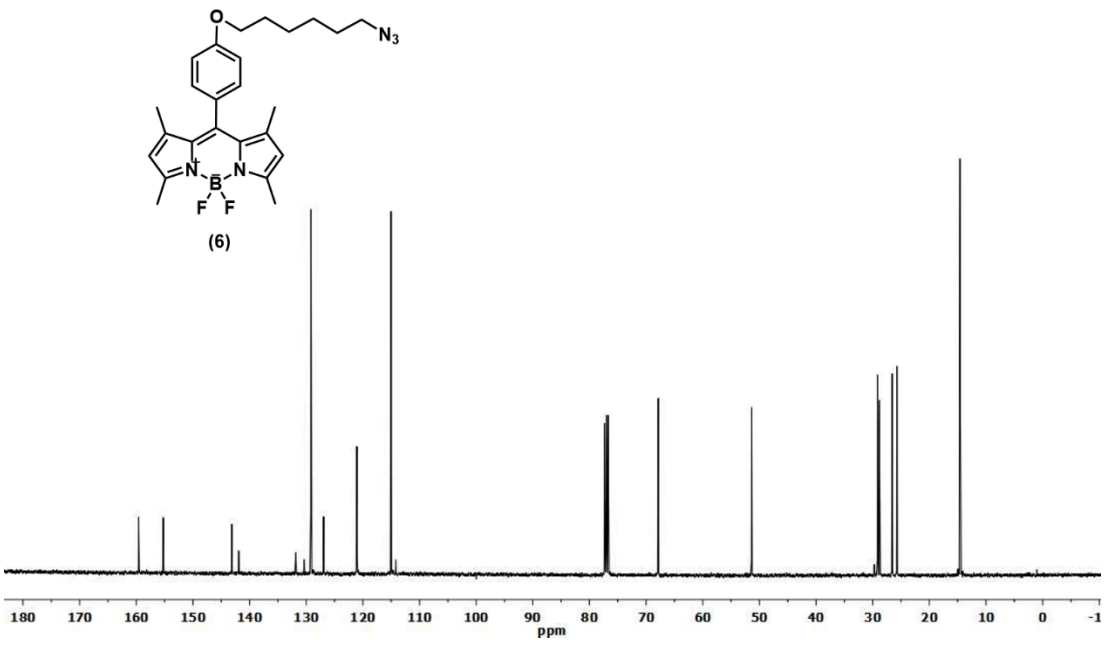
159.60
155.22
143.14
141.91
131.85
129.17
126.93
121.07
115.03
67.86
51.38
29.13
28.80
26.56
25.71
14.58
14.55
O
N3
N+
B-
N
F
F
(6)
180
170
160
150
140
130
120
110
100
90
80
70
60
50
40
30
20
10
0
-1
ppm

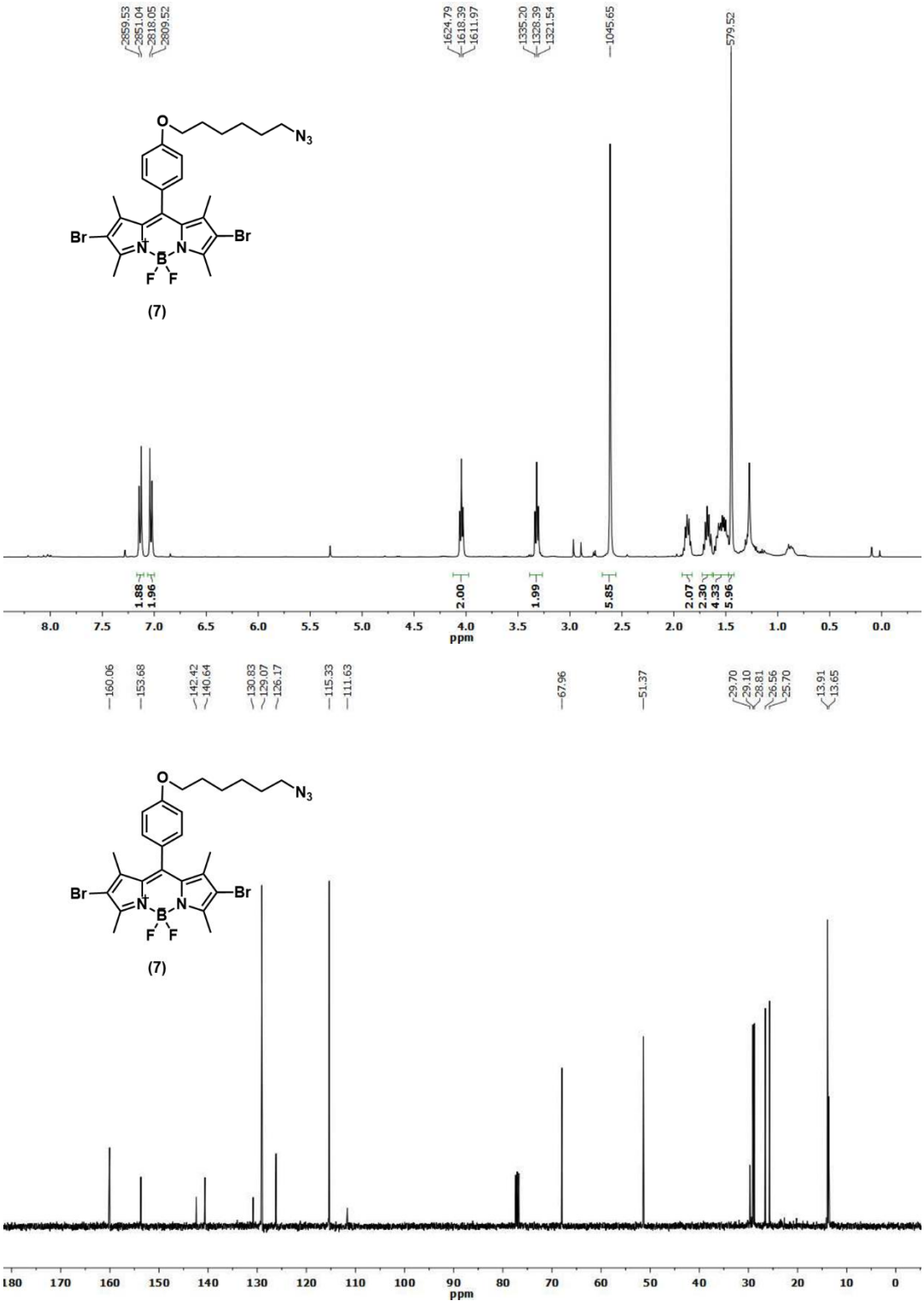
2859.53
2851.04
2818.05
2809.52
1624.79
1618.39
1611.97
1335.20
1328.39
1321.54
1045.65
579.52
O
N3
Br
Br
N+
B
N
F
F
(7)
1.88
1.96
2.00
1.99
5.85
2.07
2.30
4.33
5.96
8.0
7.5
7.0
6.5
6.0
5.5
5.0
4.5
4.0
3.5
3.0
2.5
2.0
1.5
1.0
0.5
0.0
ppm
160.06
153.68
142.42
140.64
130.83
129.07
126.17
115.33
111.63
67.96
51.37
29.70
29.10
28.81
26.56
25.70
13.91
13.65
O
N3
Br
Br
N+
B
N
F
F
(7)
180
170
160
150
140
130
120
110
100
90
80
70
60
50
40
30
20
10
0
ppm

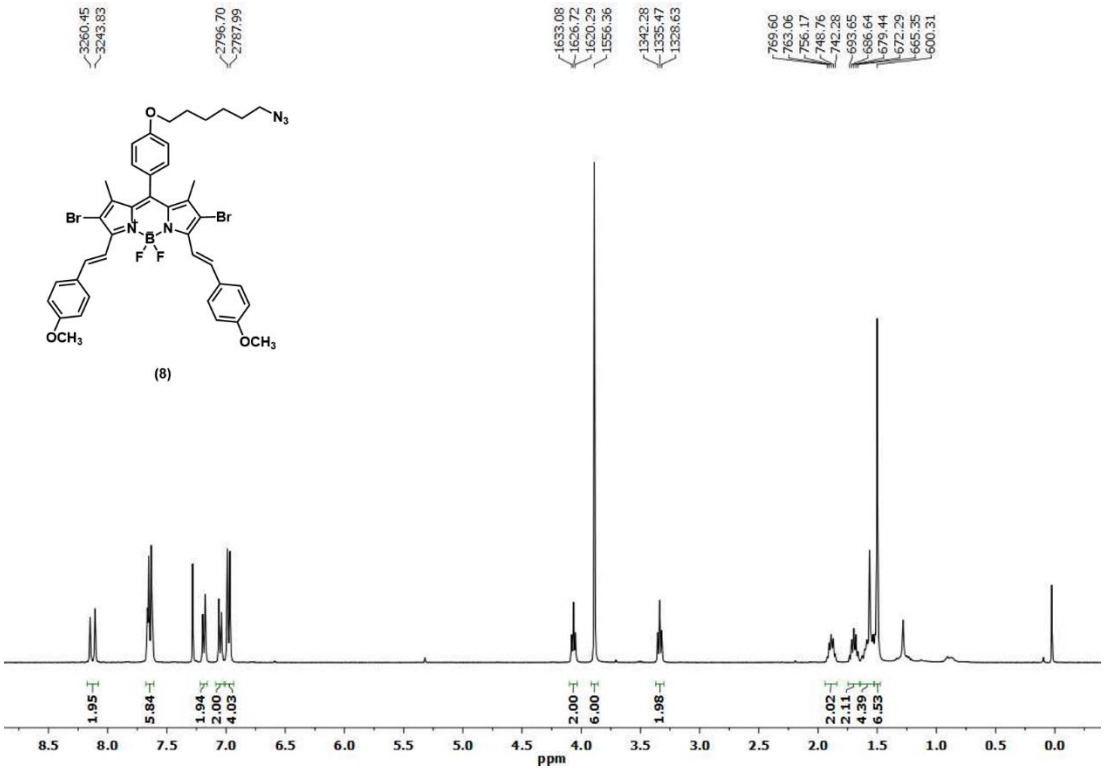
3260.45
3243.83
2796.70
2787.99
1633.08
1626.72
1620.29
1556.36
1342.28
1335.47
1328.63
769.60
763.06
756.17
748.76
742.28
693.65
686.64
679.44
672.29
665.35
600.31
Br
Br
N+
B
F F
N
O
N3
OCH3
OCH3
1.95
5.84
1.94
2.00
4.03
2.00
6.00
1.98
2.02
2.11
4.39
6.53
8.5 8.0 7.5 7.0 6.5 6.0 5.5 5.0 4.5 4.0 3.5 3.0 2.5 2.0 1.5 1.0 0.5 0.0
ppm

(8)

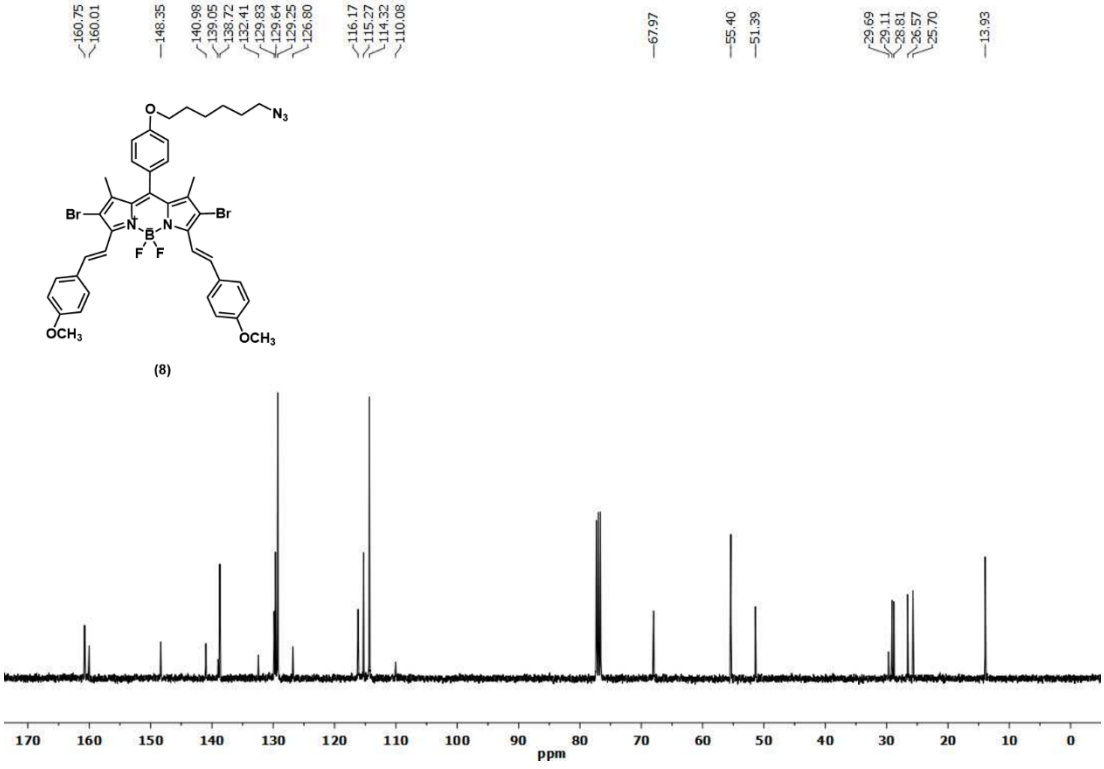
160.75
160.01
148.35
140.98
139.05
138.72
132.41
129.83
129.64
129.25
126.80
116.17
115.27
114.32
110.08
67.97
55.40
51.39
29.69
29.11
28.81
26.57
25.70
13.93
Br
Br
N+
B
F F
N
O
N3
OCH3
OCH3
170 160 150 140 130 120 110 100 90 80 70 60 50 40 30 20 10 0
ppm

(8)

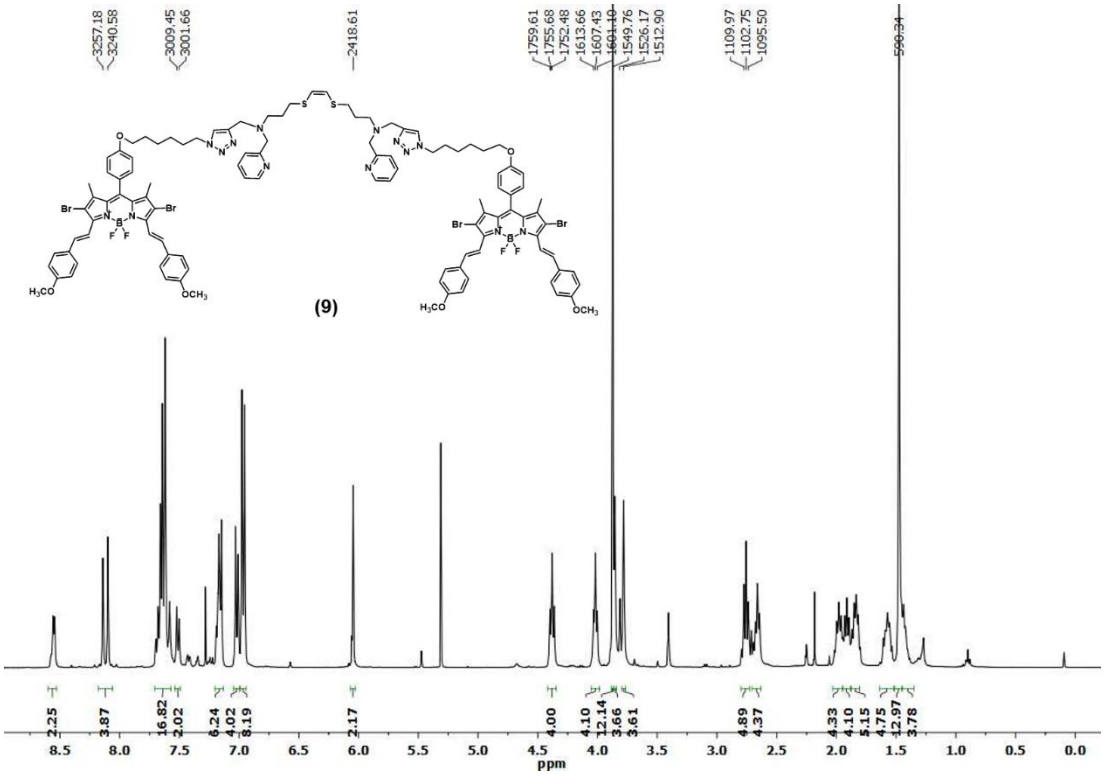
3257.18
3240.58
3009.45
3001.66
2418.61
1759.61
1755.68
1752.48
1613.66
1607.43
1604.10
1549.76
1526.17
1512.90
1109.97
1102.75
1095.50
590.34
(9)
2.25
3.87
16.82
2.02
6.24
4.02
8.19
2.17
4.00
4.10
12.14
3.66
3.61
4.89
4.37
4.33
4.10
5.15
4.75
12.97
3.78
ppm

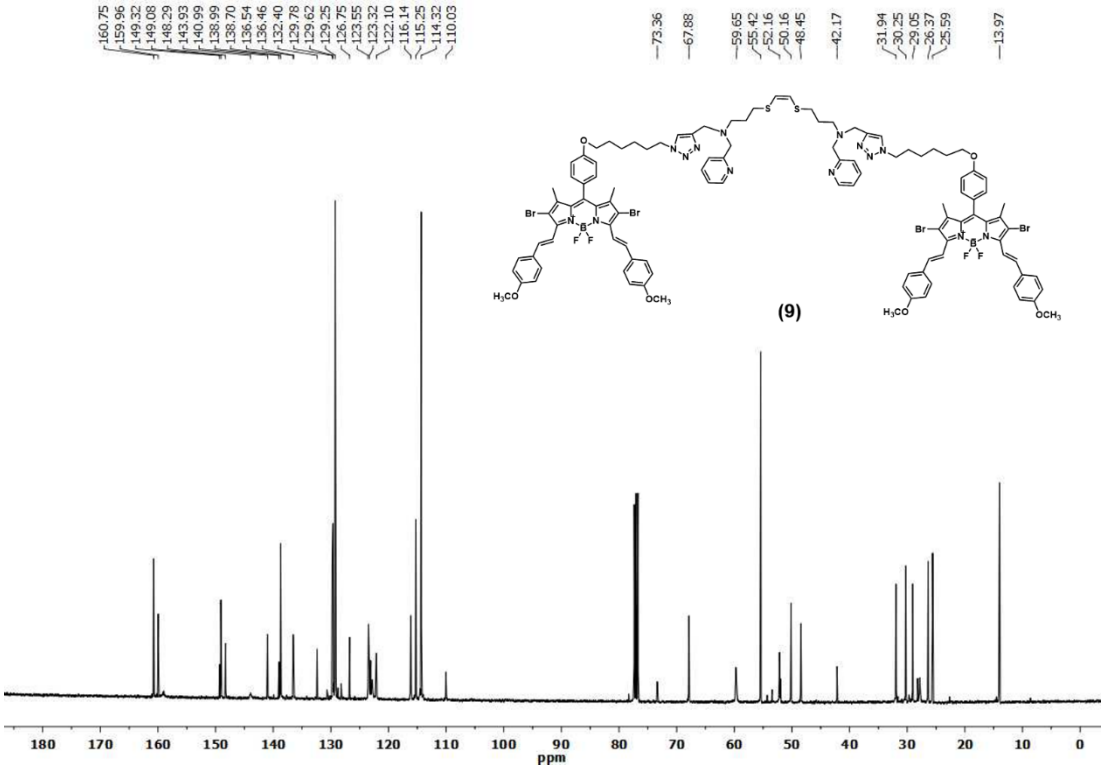
160.75
159.96
149.32
149.08
148.29
143.93
140.99
138.99
138.70
136.54
136.46
132.40
129.78
129.62
129.25
126.75
123.55
123.32
122.10
116.14
115.25
114.32
110.03
73.36
67.88
59.65
55.42
52.16
50.16
48.45
42.17
31.94
30.25
29.05
26.37
25.59
13.97
(9)
ppm

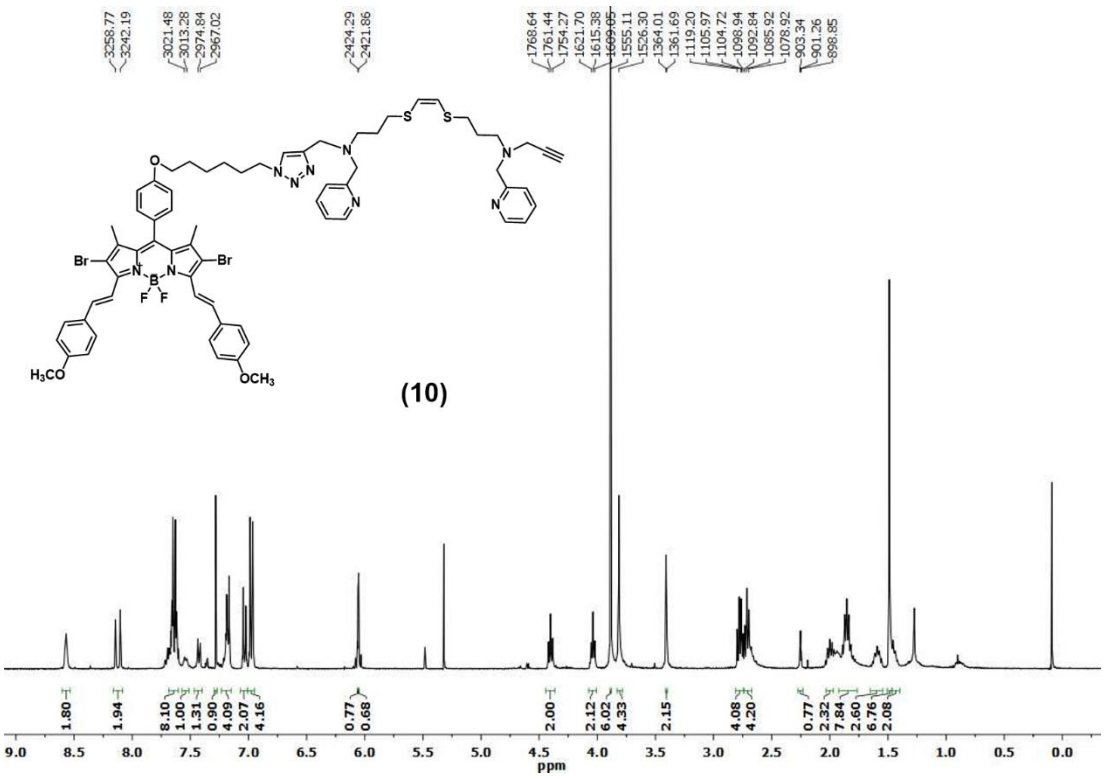
3258.77
3242.19
3021.48
3013.28
2974.84
2967.02
2424.29
2421.86
1768.64
1761.44
1754.27
1621.70
1615.38
1609.65
1555.11
1526.30
1364.01
1361.69
1119.20
1105.97
1104.72
1098.94
1092.84
1085.92
1078.92
903.34
901.26
898.85
Br
Br
F
F
H3CO
OCH3
(10)
1.80
1.94
8.10
1.00
1.31
0.90
4.09
2.07
4.16
0.77
0.68
2.00
2.12
6.02
4.33
2.15
4.08
4.20
0.77
2.32
7.84
2.60
6.76
2.08
ppm

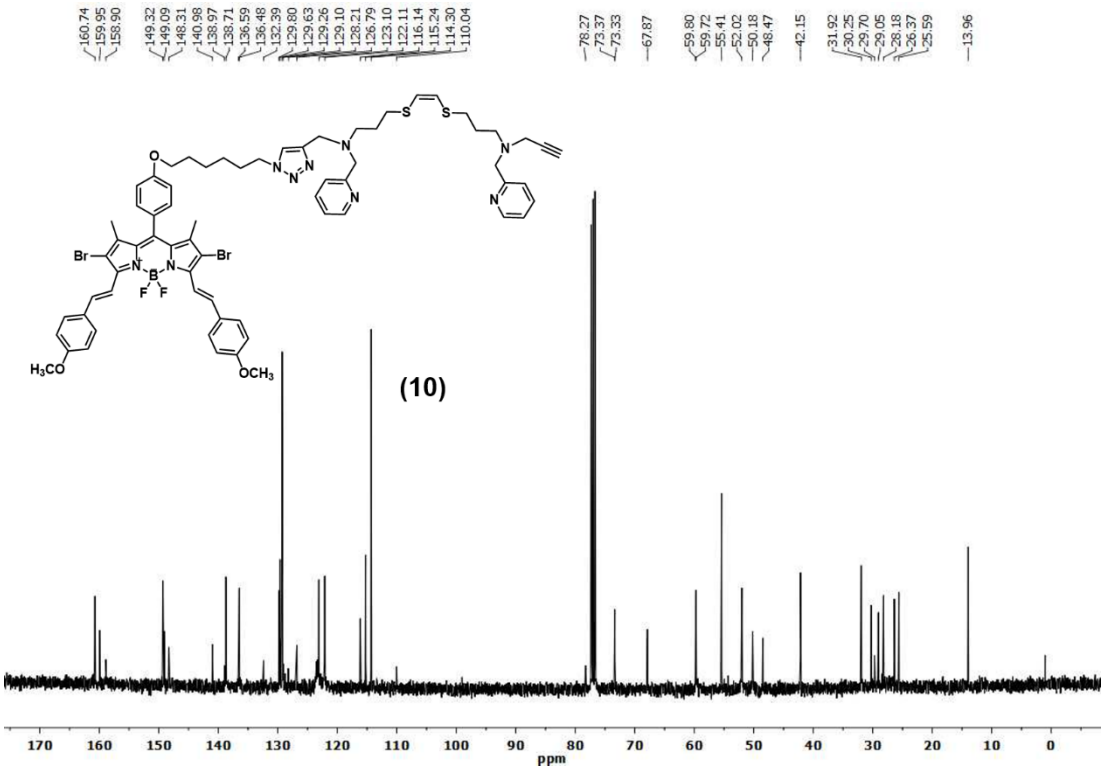
160.74
159.95
158.90
149.32
149.09
148.31
140.98
138.97
138.71
136.59
136.48
132.39
129.80
129.63
129.26
129.10
128.21
126.79
123.10
122.11
116.14
115.24
114.30
110.04
78.27
73.37
73.33
67.87
59.80
59.72
55.41
52.02
50.18
48.47
42.15
31.92
30.25
29.70
29.05
28.18
26.37
25.59
13.96
Br
Br
F
F
H3CO
OCH3
(10)
ppm

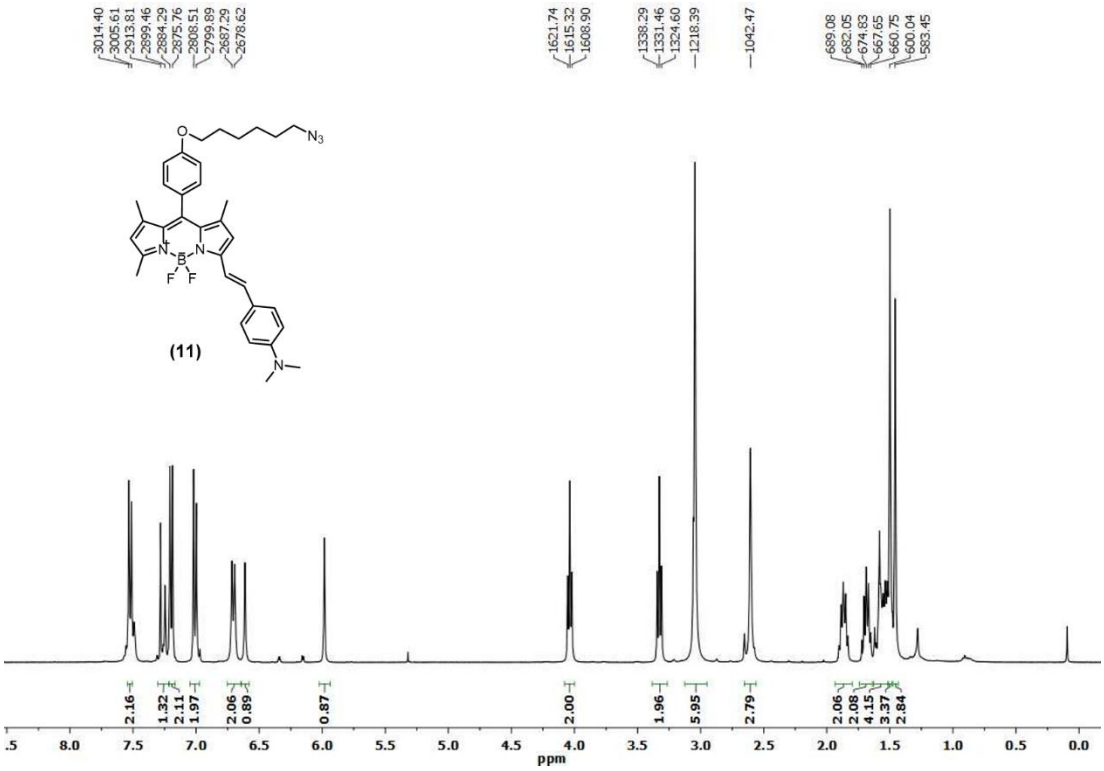
3014.40
3005.61
2913.81
2899.46
2884.29
2875.76
2808.51
2799.89
2687.29
2678.62
1621.74
1615.32
1608.90
1338.29
1331.46
1324.60
1218.39
1042.47
689.08
682.05
674.83
667.65
660.75
600.04
583.45
(11)
2.16
1.32
2.11
1.97
2.06
0.89
0.87
2.00
1.96
5.95
2.79
2.06
2.08
4.15
3.37
2.84
ppm

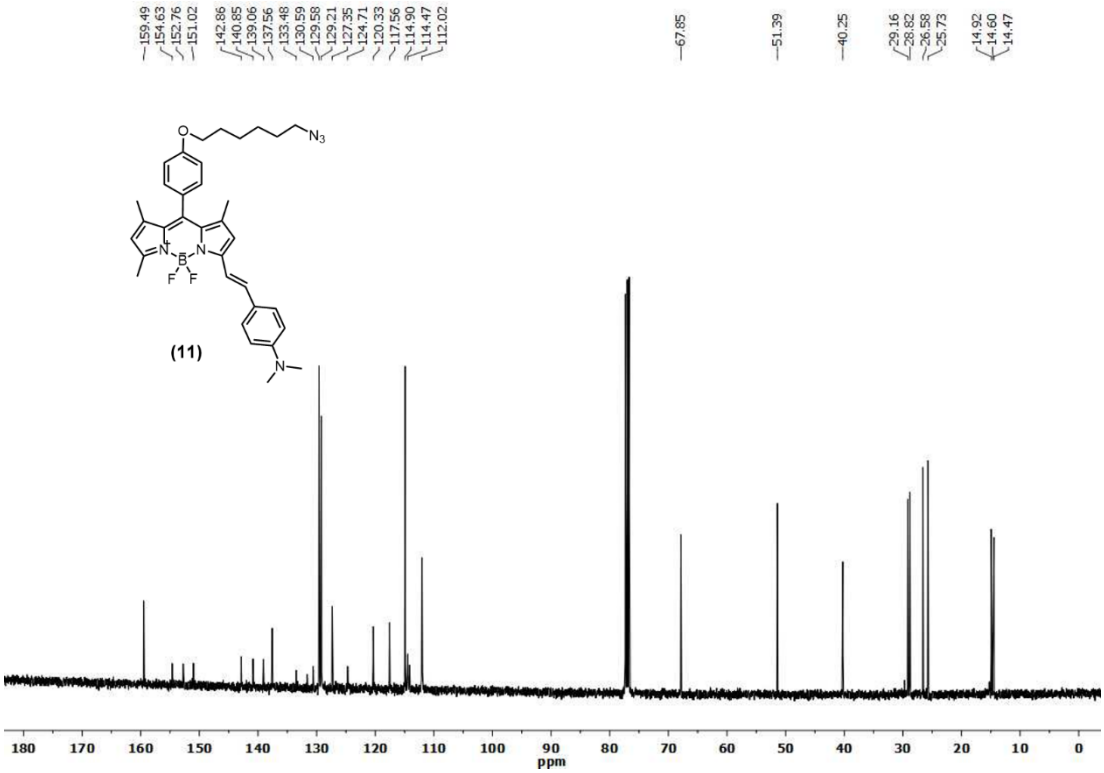
159.49
154.63
152.76
151.02
142.86
140.85
139.06
137.56
133.48
130.59
129.58
129.21
127.35
124.71
120.33
117.56
114.90
114.47
112.02
67.85
51.39
40.25
29.16
28.82
26.58
25.73
14.92
14.60
14.47
(11)
ppm

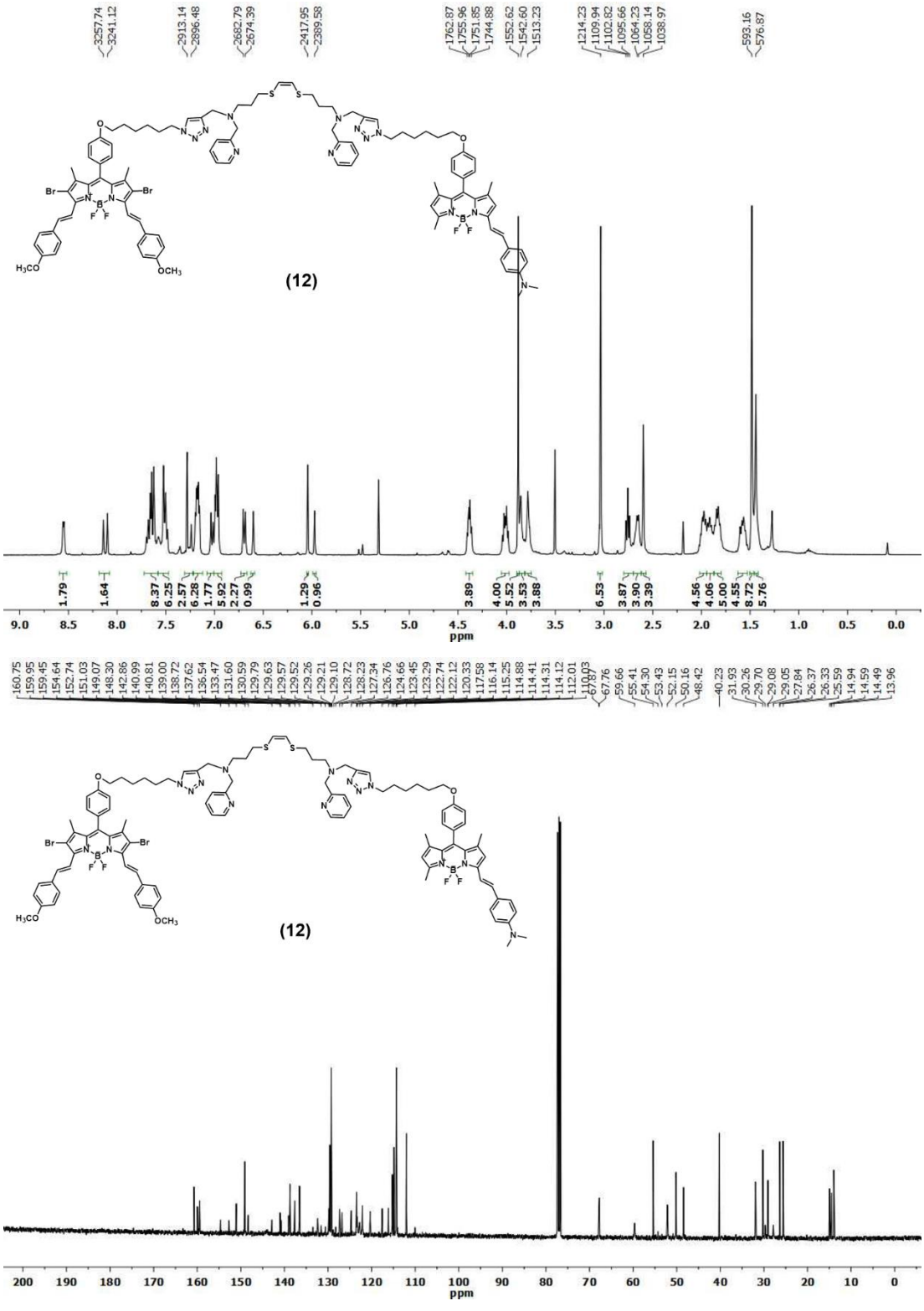
3257.74
3241.12
2913.14
2896.48
2682.79
2674.39
2417.95
2389.58
1762.87
1755.96
1751.85
1744.88
1552.62
1542.60
1513.23
1214.23
1109.94
1102.82
1095.66
1064.23
1058.14
1038.97
593.16
576.87
(12)
1.79
1.64
8.37
6.25
2.57
6.28
1.77
5.92
2.27
0.99
1.29
0.96
3.89
4.00
5.52
3.53
3.88
6.53
3.87
3.90
3.39
4.56
4.06
5.00
4.55
8.72
5.76
ppm
(12)
ppm

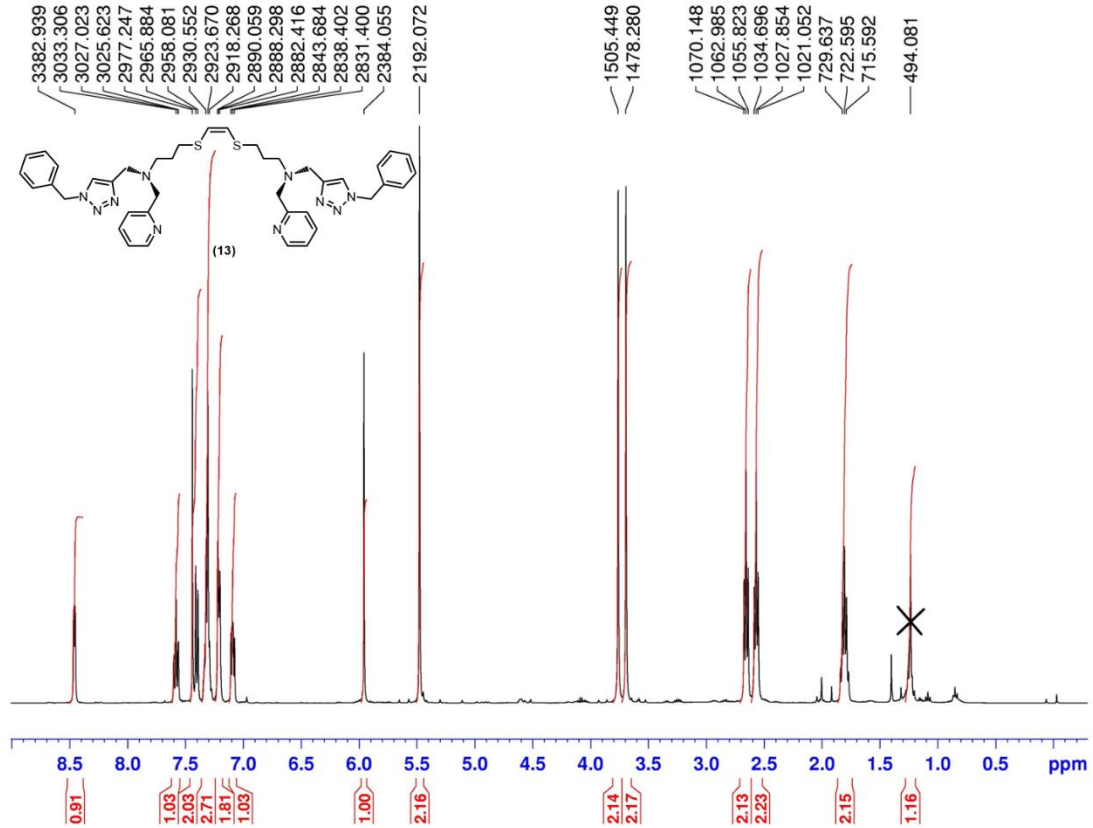
3382.939
3033.306
3027.023
3025.623
2977.247
2965.884
2958.081
2930.552
2923.670
2918.268
2890.059
2888.298
2882.416
2843.684
2838.402
2831.400
2384.055
2192.072
1505.449
1478.280
1070.148
1062.985
1055.823
1034.696
1027.854
1021.052
729.637
722.595
715.592
494.081
(13)
8.5 8.0 7.5 7.0 6.5 6.0 5.5 5.0 4.5 4.0 3.5 3.0 2.5 2.0 1.5 1.0 0.5 ppm
0.91 1.03 2.03 2.71 1.81 1.03 1.00 2.16 2.14 2.17 2.13 2.23 2.15 1.16

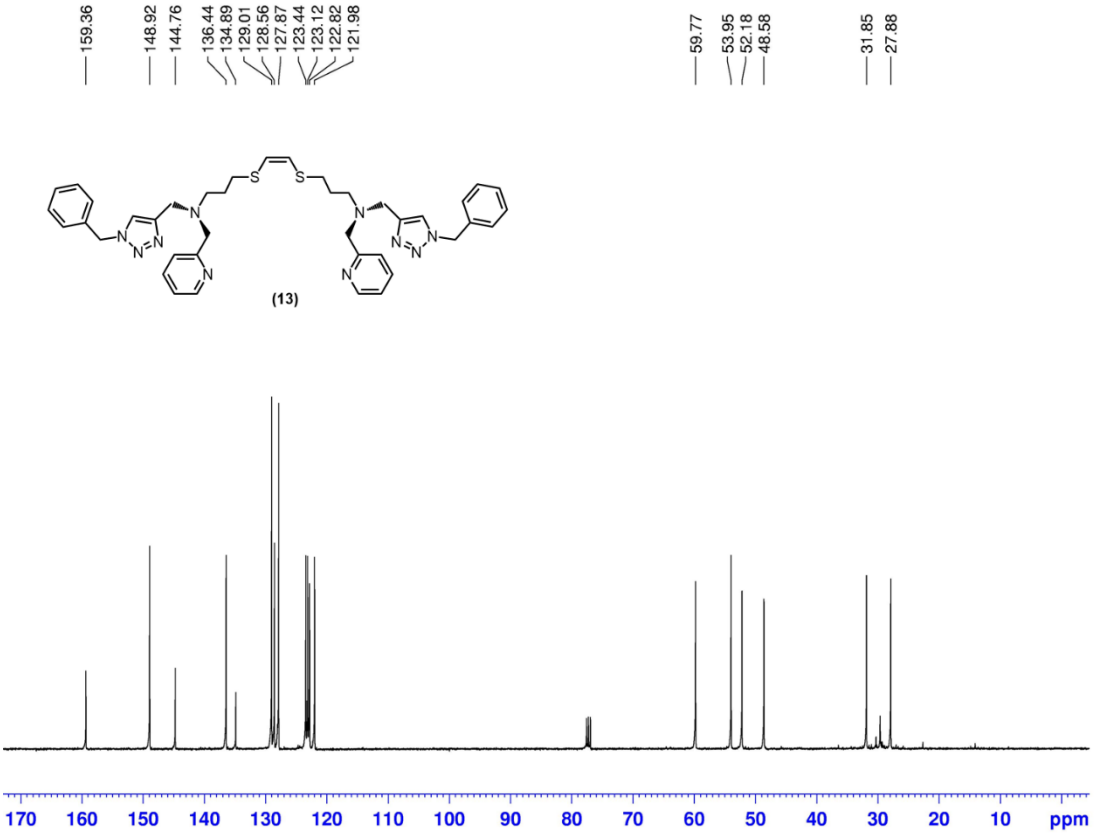
159.36
148.92
144.76
136.44
134.89
129.01
128.56
127.87
123.44
123.12
122.82
121.98
59.77
53.95
52.18
48.58
31.85
27.88
(13)
170 160 150 140 130 120 110 100 90 80 70 60 50 40 30 20 10 ppm

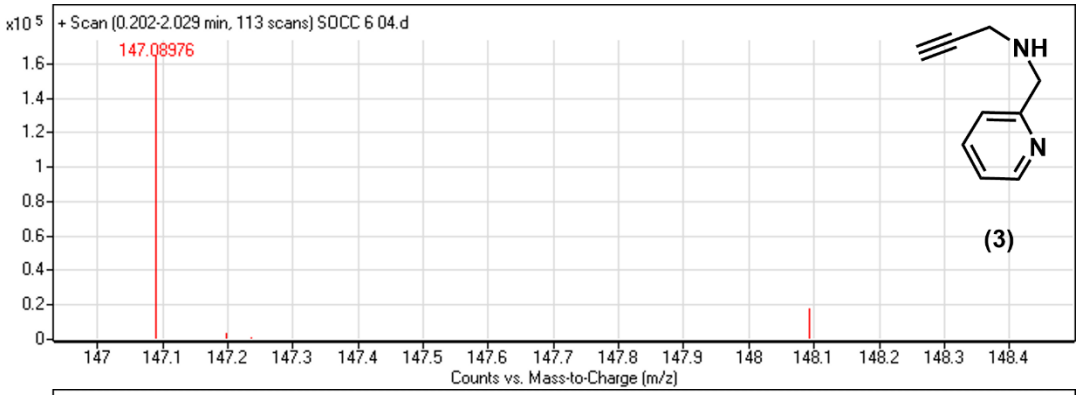
+ Scan (0.202-2.029 min, 113 scans) SOCC 6 04.d
147.08976
NH
N
(3)
Counts vs. Mass-to-Charge (m/z)

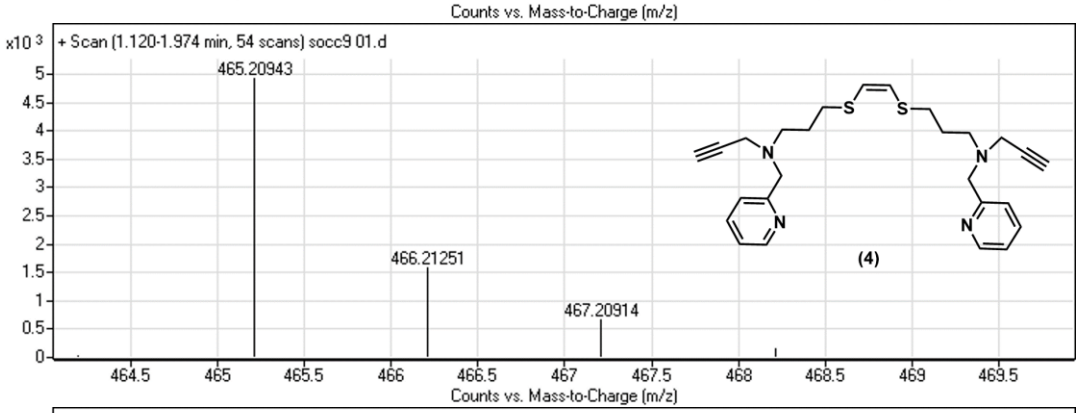
+ Scan (1.120-1.974 min, 54 scans) socc9 01.d
465.20943
466.21251
467.20914
S
S
N
N
N
(4)
Counts vs. Mass-to-Charge (m/z)

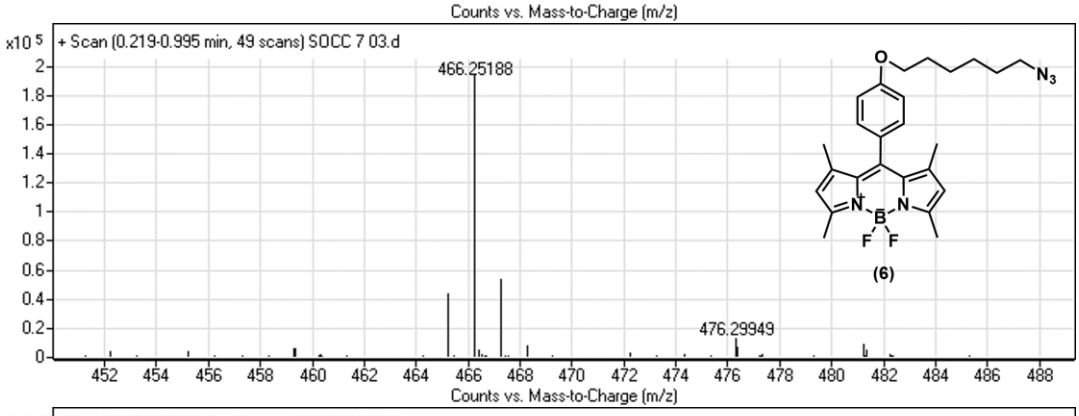
+ Scan (0.219-0.995 min, 49 scans) SOCC 7 03.d
466.25188
476.29949
O
N3
N
B
F
F
(6)
Counts vs. Mass-to-Charge (m/z)

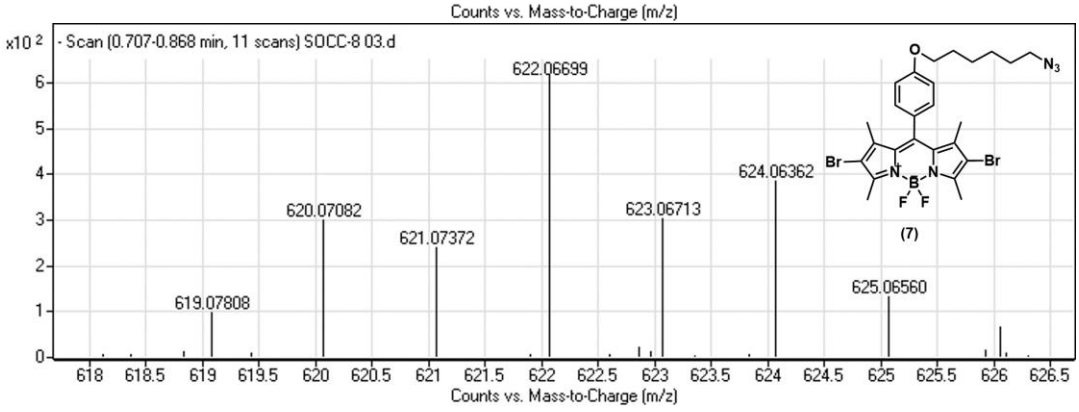
- Scan (0.707-0.868 min, 11 scans) SOCC-8 03.d
622.06699
624.06362
620.07082
623.06713
621.07372
619.07808
625.06560
O
N3
Br
Br
N
B
F
F
(7)
Counts vs. Mass-to-Charge (m/z)

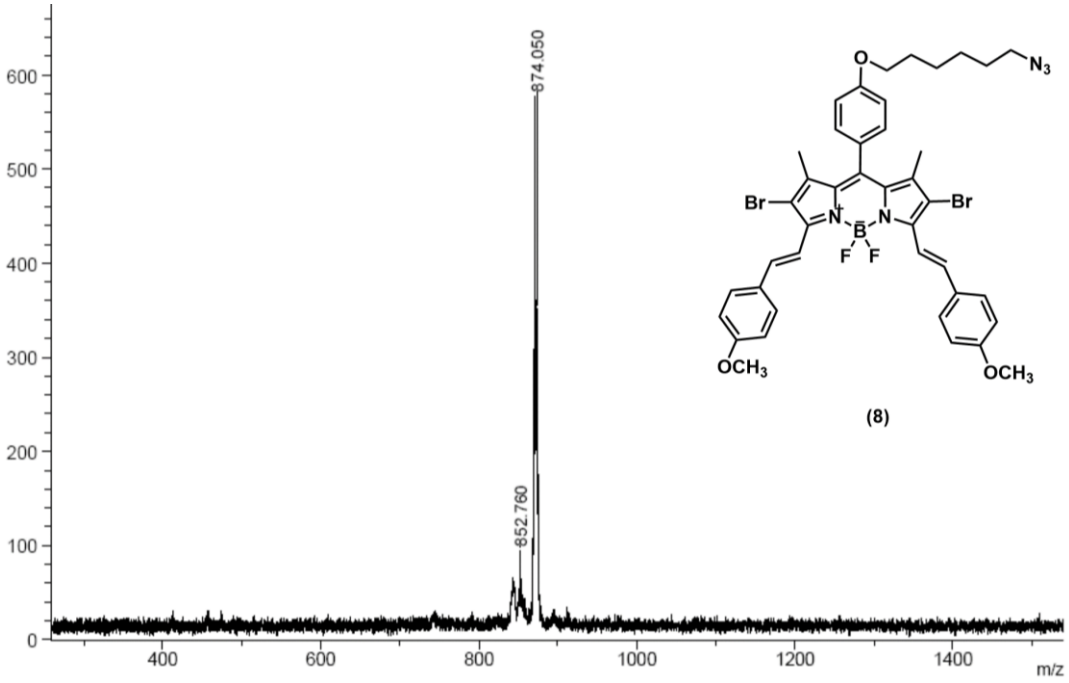
874.050
852.760
600
500
400
300
200
100
0
400
600
800
1000
1200
1400
m/z
O
N3
Br
Br
N
B
N
F
F
OCH3
OCH3

(8)

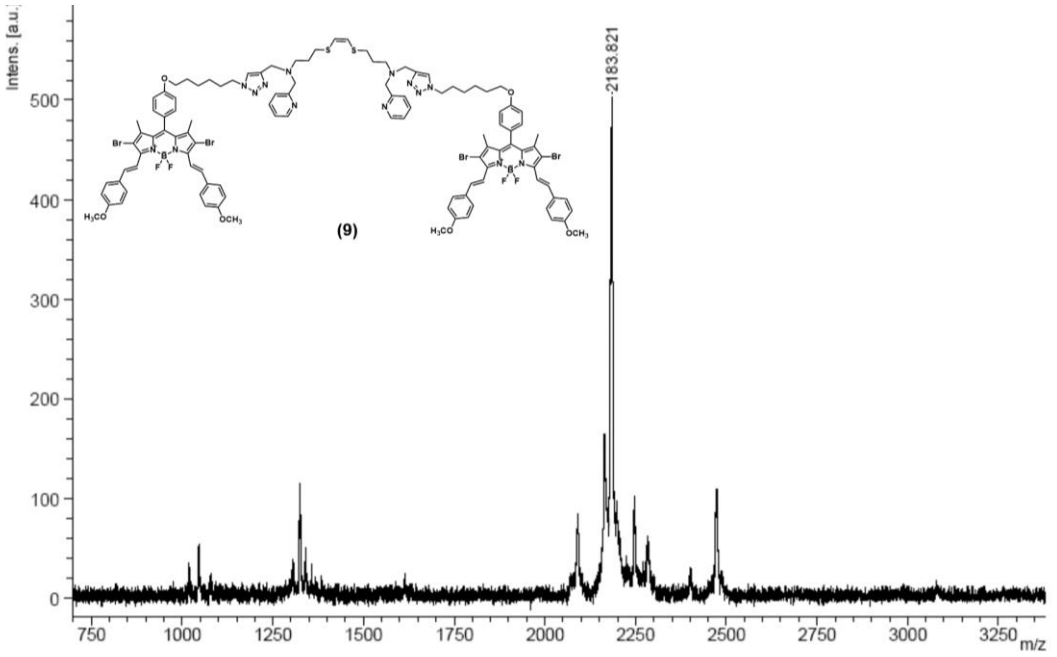
Intens. [a.u.]
2183.821
500
400
300
200
100
0
750
1000
1250
1500
1750
2000
2250
2500
2750
3000
3250
m/z

(9)

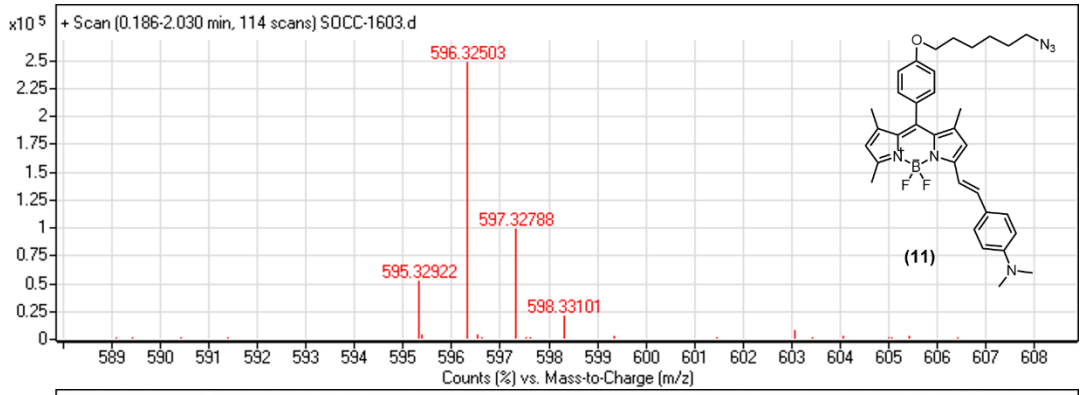
+ Scan (0.186-2.030 min, 114 scans) SOCC-1603.d
596.32503
597.32788
595.32922
598.33101
(11)
Counts (%) vs. Mass-to-Charge (m/z)

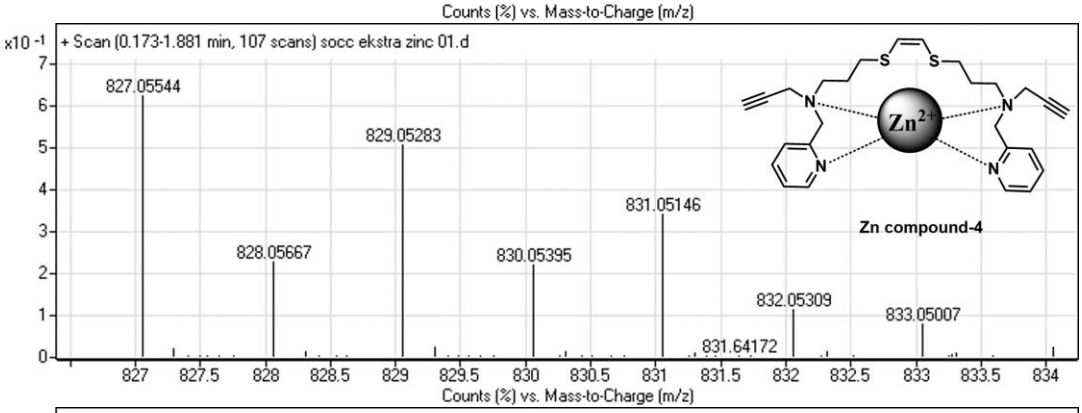
+ Scan (0.173-1.881 min, 107 scans) socc ekstra zinc 01.d
827.05544
829.05283
831.05146
828.05667
830.05395
832.05309
833.05007
831.64172
Zn compound-4
Counts (%) vs. Mass-to-Charge (m/z)

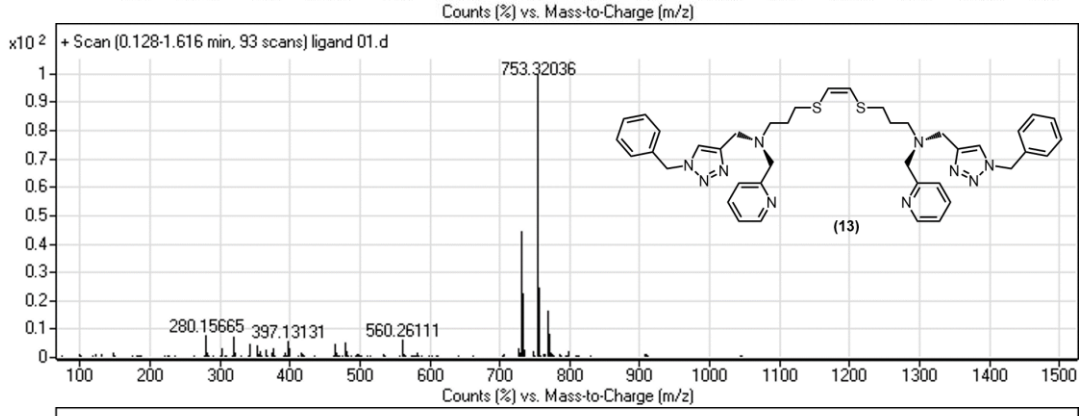
+ Scan (0.128-1.616 min, 93 scans) ligand 01.d
753.32036
280.15665
397.13131
560.26111
(13)
Counts (%) vs. Mass-to-Charge (m/z)

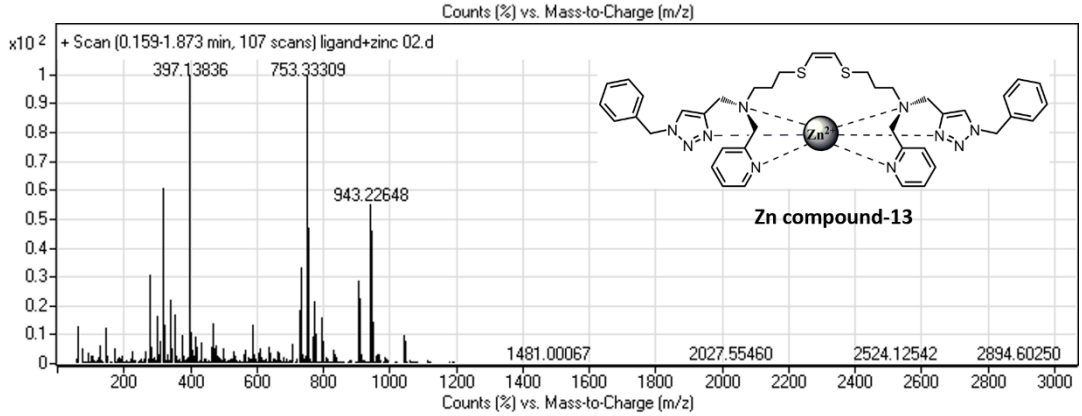
+ Scan (0.159-1.873 min, 107 scans) ligand+zinc 02.d
397.13836
753.33309
943.22648
1481.00067
2027.55460
2524.12542
2894.60250
Zn compound-13
Counts (%) vs. Mass-to-Charge (m/z)

A3. Selective Photosensitization through AND Logic Response: Optimization of pH and Glutathione Response of Activatable Photosensitizers (^{1}H, ^{13}C and Mass Spectra)

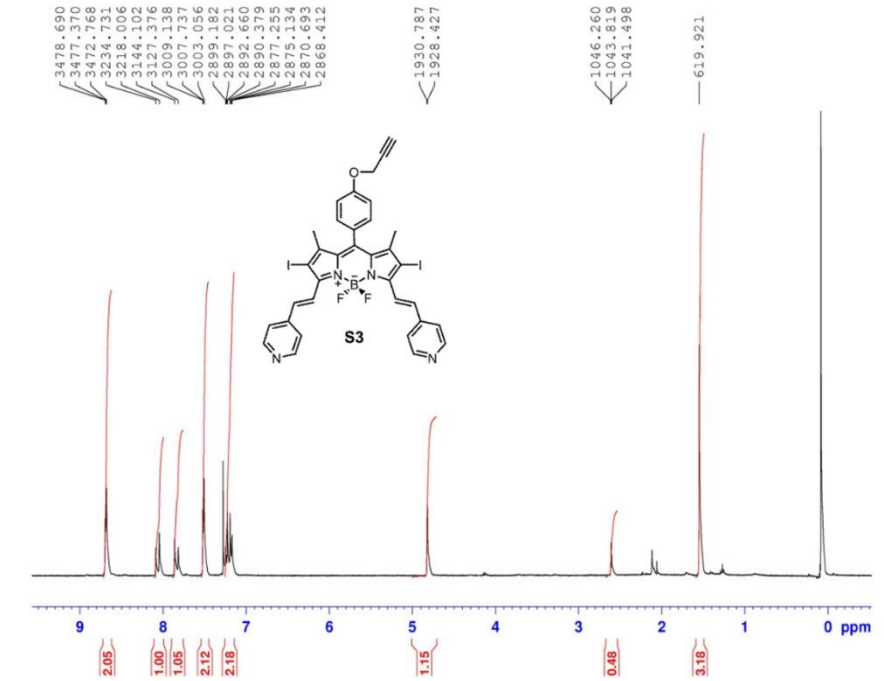

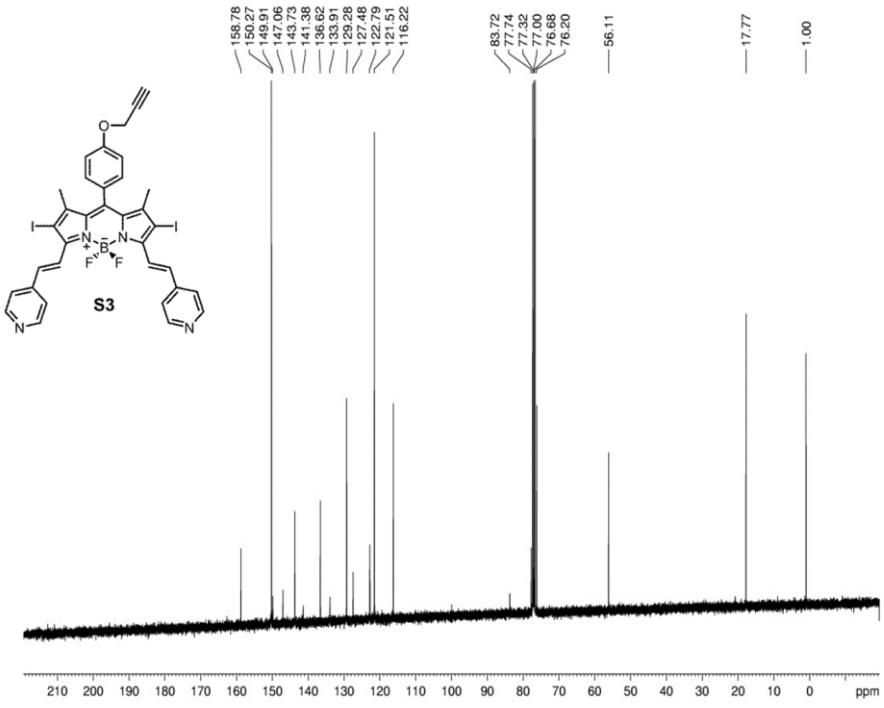

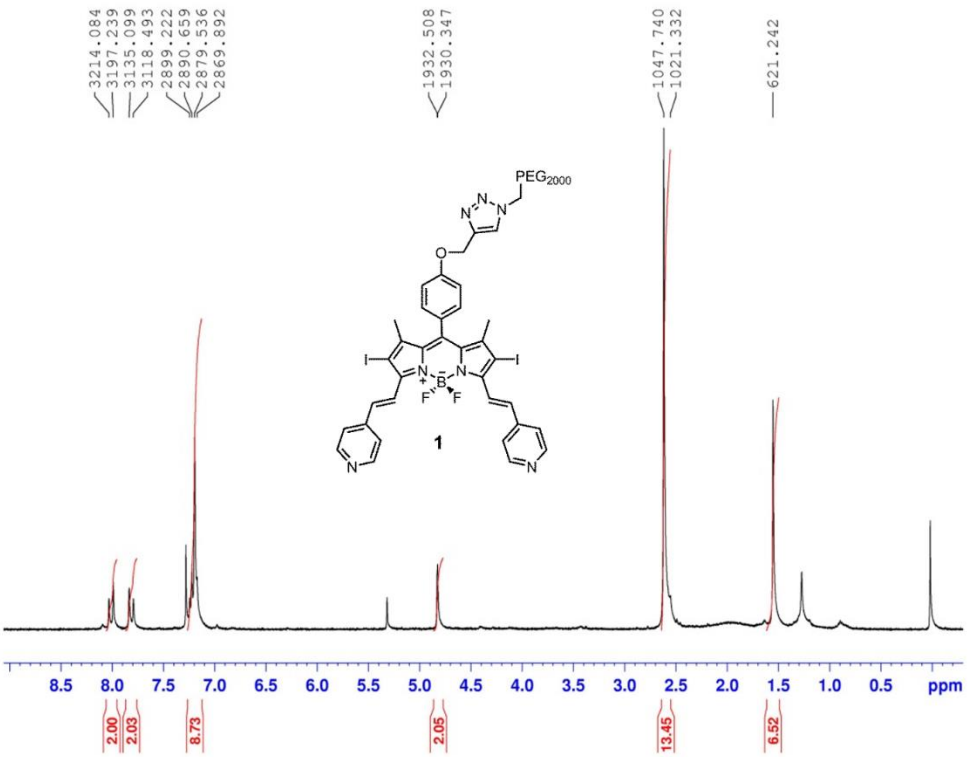
3214.084
3197.239
3135.099
3118.493
2899.222
2890.659
2879.536
2869.892
1932.508
1930.347
1047.740
1021.332
621.242
PEG2000
1
8.5 8.0 7.5 7.0 6.5 6.0 5.5 5.0 4.5 4.0 3.5 3.0 2.5 2.0 1.5 1.0 0.5 ppm
2.00
2.03
8.73
2.05
13.45
6.52

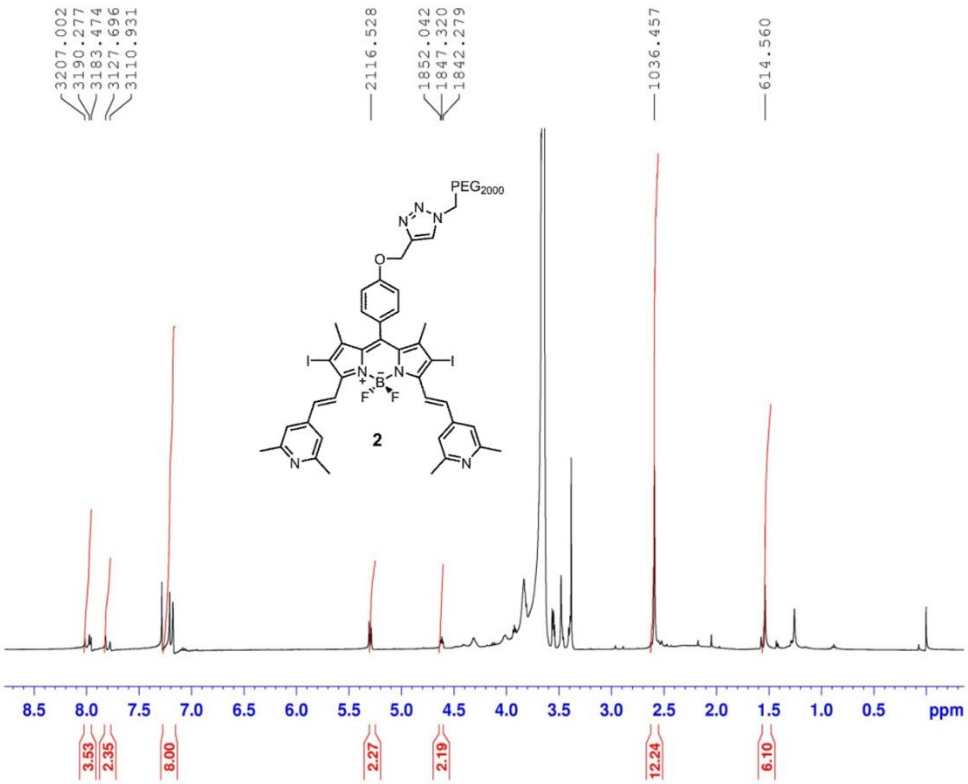
3207.002
3190.277
3183.474
3127.696
3110.931
2116.528
1852.042
1847.320
1842.279
1036.457
614.560
PEG2000
2
8.5 8.0 7.5 7.0 6.5 6.0 5.5 5.0 4.5 4.0 3.5 3.0 2.5 2.0 1.5 1.0 0.5 ppm
3.53
2.35
8.00
2.27
2.19
12.24
6.10

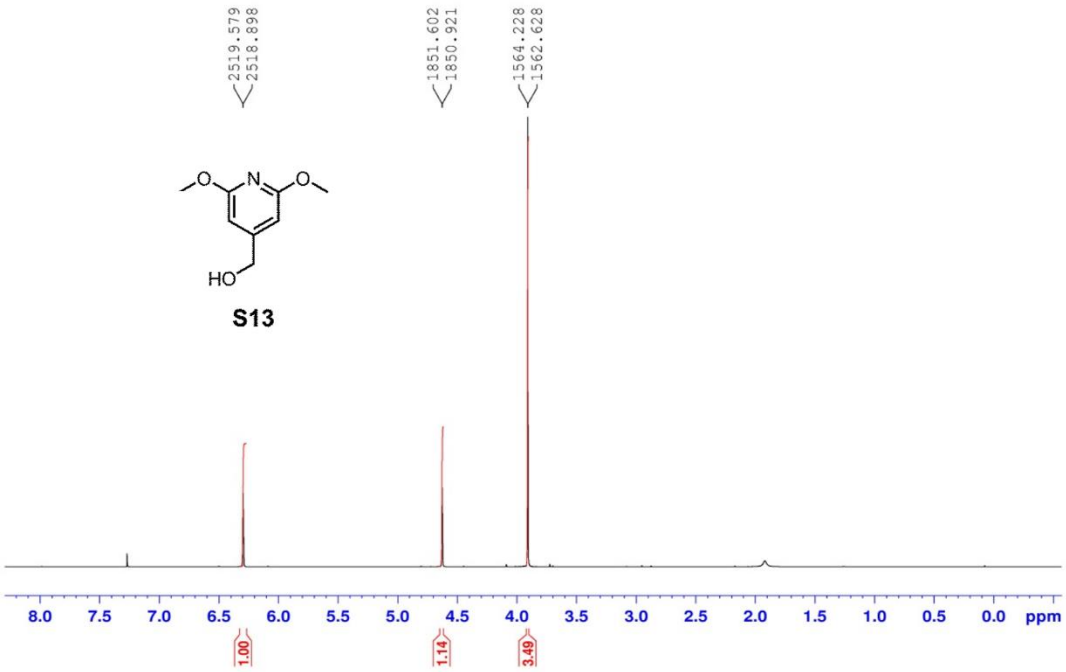
2519.579
2518.898
1851.602
1850.921
1564.228
1562.628
O
N
O
HO
8.0 7.5 7.0 6.5 6.0 5.5 5.0 4.5 4.0 3.5 3.0 2.5 2.0 1.5 1.0 0.5 0.0 ppm
1.00
1.14
3.49

S13

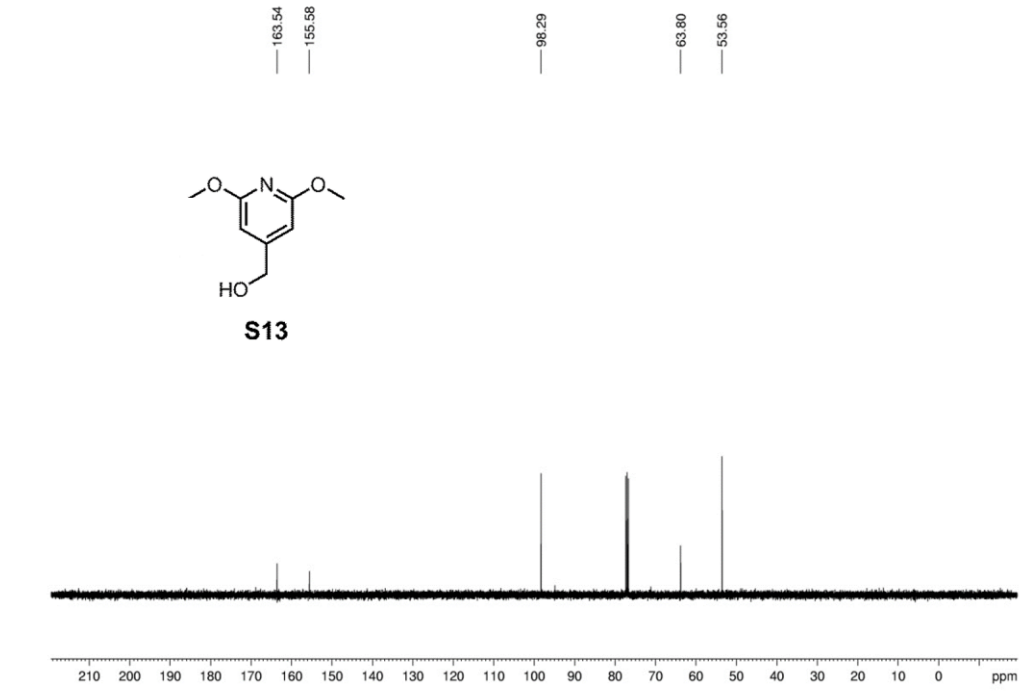
163.54
155.58
98.29
63.80
53.56
O
N
O
HO
210 200 190 180 170 160 150 140 130 120 110 100 90 80 70 60 50 40 30 20 10 0 ppm

S13

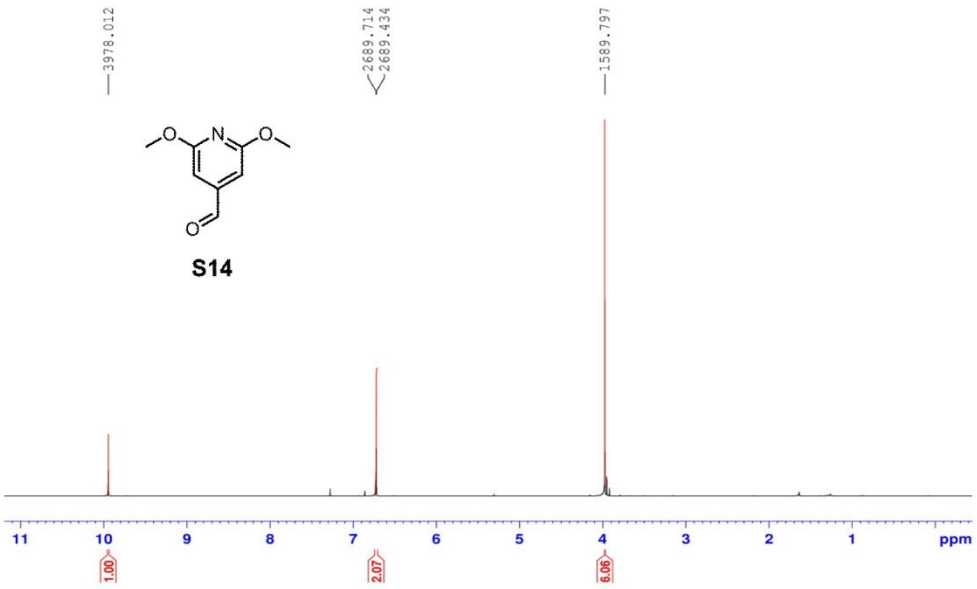
3978.012
2689.714
2689.434
1589.797
S14
11
10
9
8
7
6
5
4
3
2
1
ppm
1.00
2.07
6.06

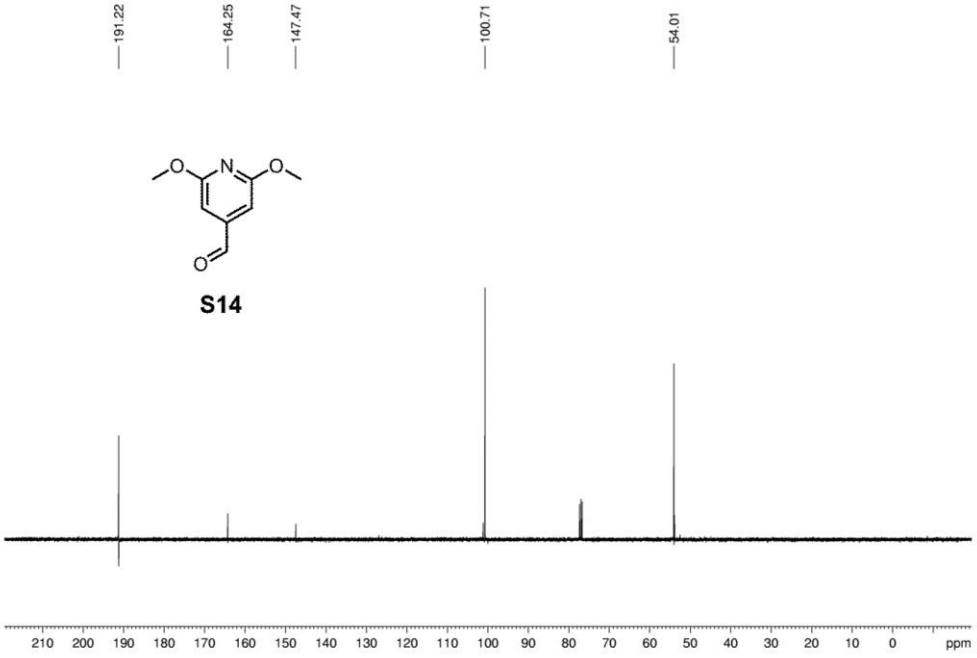
191.22
164.25
147.47
100.71
54.01
S14
210
200
190
180
170
160
150
140
130
120
110
100
90
80
70
60
50
40
30
20
10
0
ppm

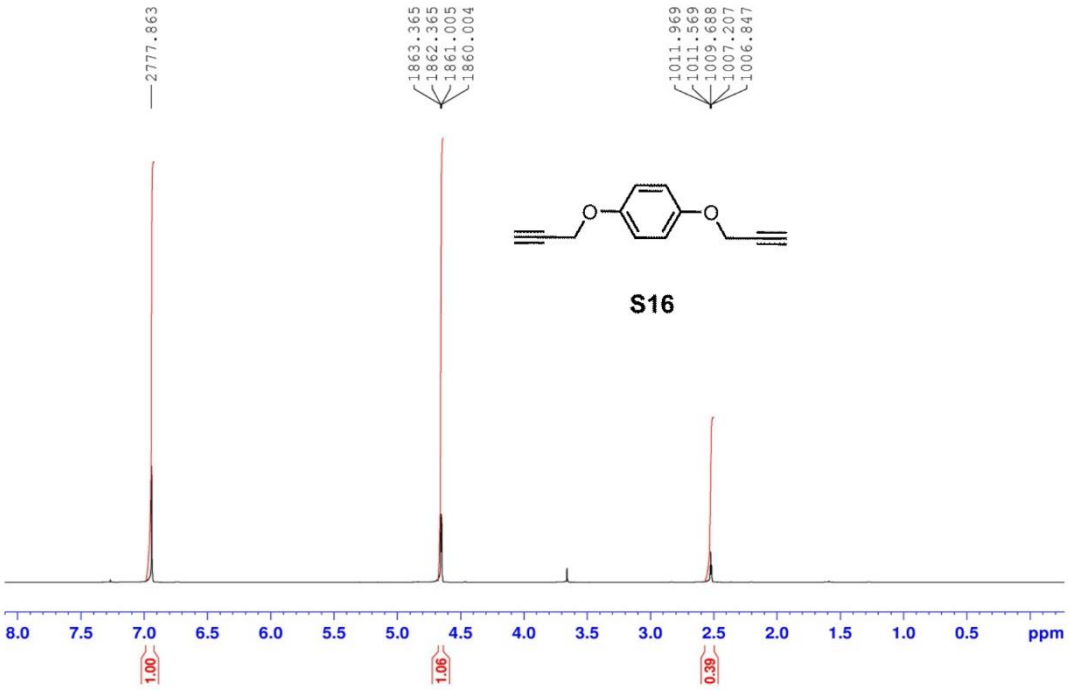
2777.863
1863.365
1862.365
1861.005
1860.004
1011.969
1011.569
1009.688
1007.207
1006.847
S16
8.0
7.5
7.0
6.5
6.0
5.5
5.0
4.5
4.0
3.5
3.0
2.5
2.0
1.5
1.0
0.5
ppm
1.00
1.06
0.39

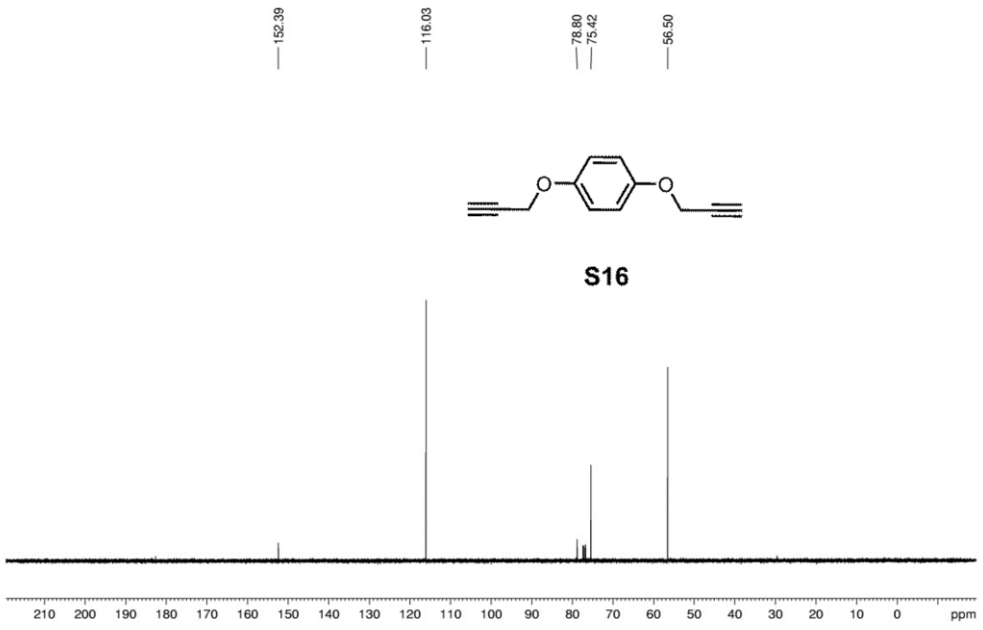
152.39
116.03
78.80
75.42
56.50
S16
210
200
190
180
170
160
150
140
130
120
110
100
90
80
70
60
50
40
30
20
10
0
ppm

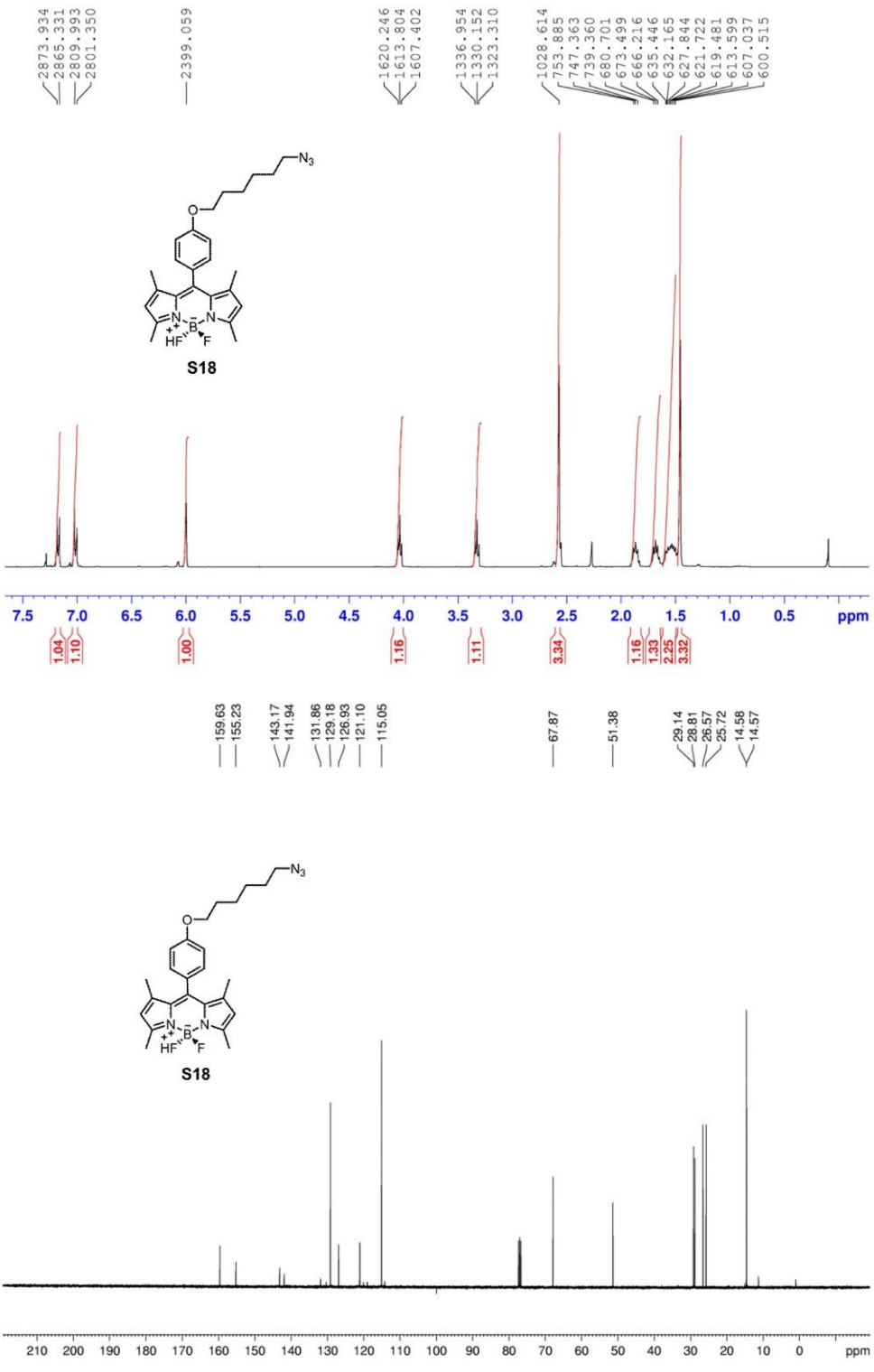
2873.934
2865.331
2809.993
2801.350
2399.059
1620.246
1613.804
1607.402
1336.954
1330.152
1323.310
1028.614
753.885
747.363
739.360
680.701
673.499
666.216
635.446
632.165
627.844
621.722
619.481
613.599
607.037
600.515
N3
O
N
B
HF
F
S18
7.5 7.0 6.5 6.0 5.5 5.0 4.5 4.0 3.5 3.0 2.5 2.0 1.5 1.0 0.5 ppm
1.04 1.10 1.00 1.16 1.11 3.34 1.16 1.33 2.25 3.32
159.63
155.23
143.17
141.94
131.86
129.18
126.93
121.10
115.05
67.87
51.38
29.14
28.81
26.57
25.72
14.58
14.57
N3
O
N
B
HF
F
S18
210 200 190 180 170 160 150 140 130 120 110 100 90 80 70 60 50 40 30 20 10 0 ppm

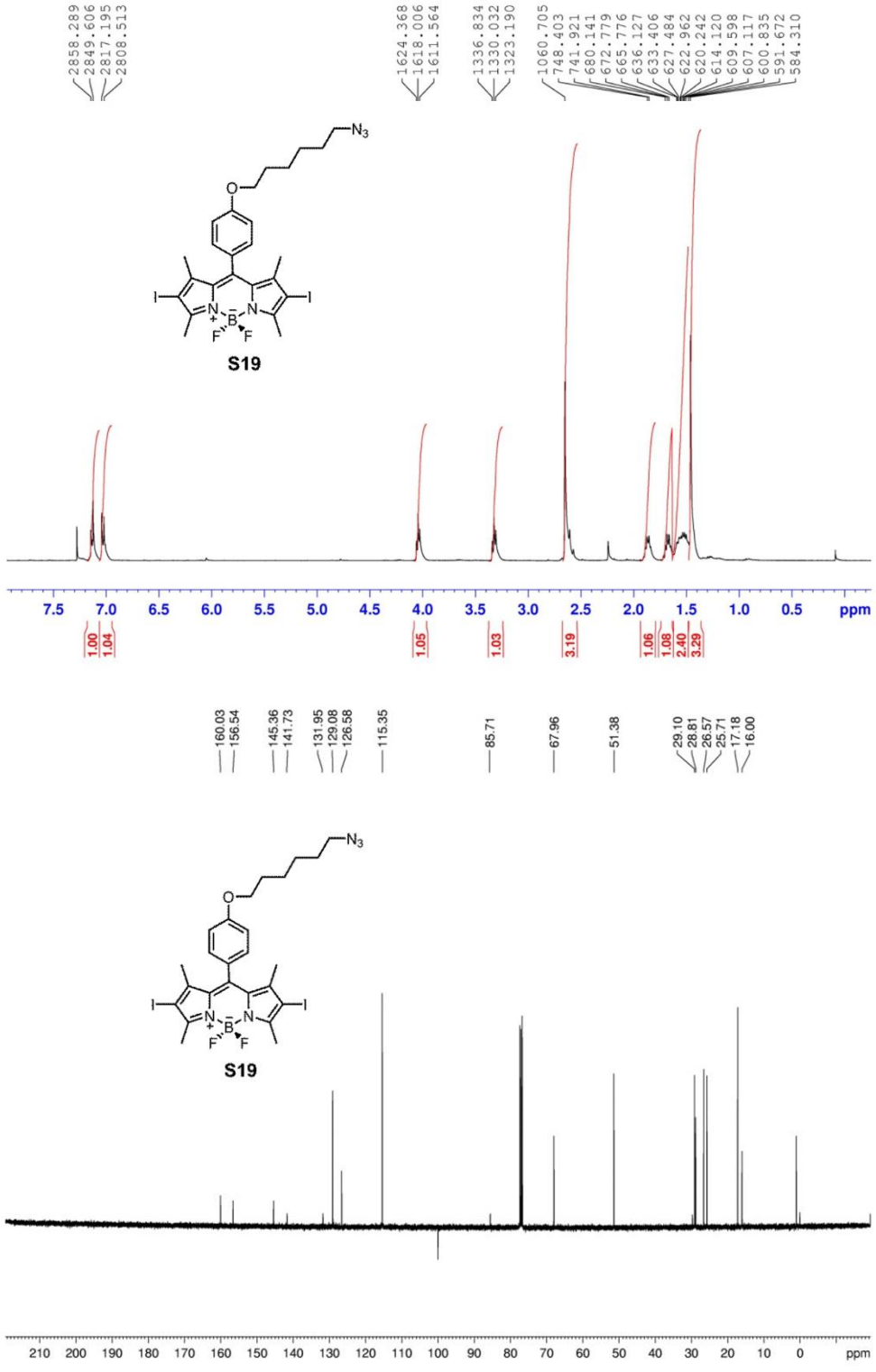
2858.289
2849.606
2817.195
2808.513
1624.368
1618.006
1611.564
1336.834
1330.032
1323.190
1060.705
748.403
741.921
680.141
672.779
665.776
636.127
633.406
627.484
622.962
620.242
614.120
609.598
607.117
600.835
591.672
584.310
N3
O
I
I
N
B
N
F
F
S19
7.5
7.0
6.5
6.0
5.5
5.0
4.5
4.0
3.5
3.0
2.5
2.0
1.5
1.0
0.5
ppm
1.00
1.04
1.05
1.03
3.19
1.06
1.08
2.40
3.29
160.03
156.54
145.36
141.73
131.95
129.08
126.58
115.35
85.71
67.96
51.38
29.10
28.81
26.57
25.71
17.18
16.00
N3
O
I
I
N
B
N
F
F
S19
210
200
190
180
170
160
150
140
130
120
110
100
90
80
70
60
50
40
30
20
10
0
ppm

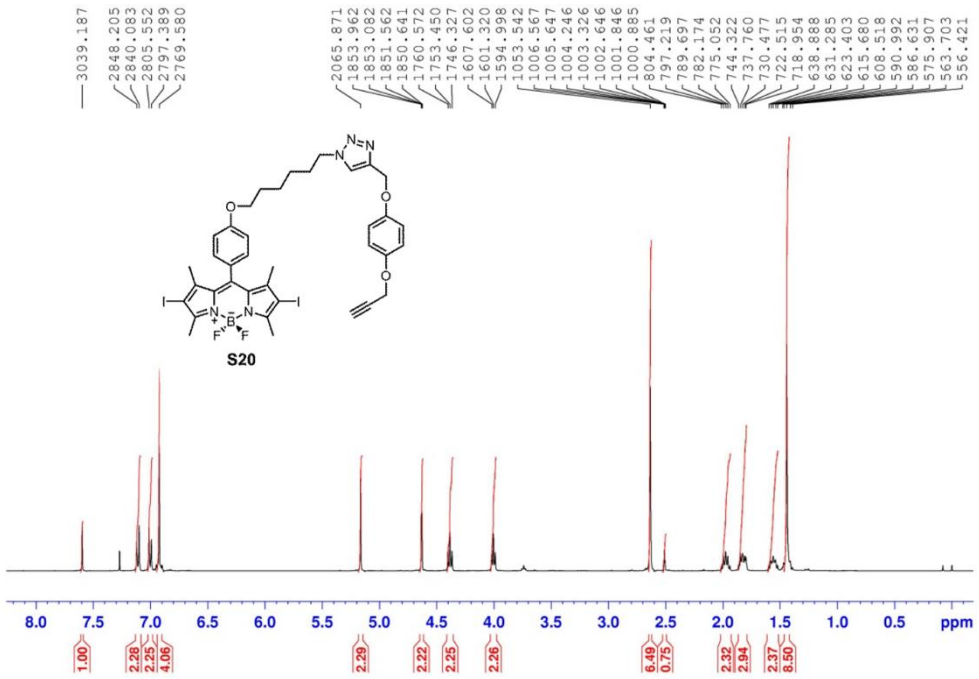
3039.187
2848.205
2840.083
2805.552
2797.389
2769.580
2065.871
1853.962
1853.082
1851.562
1850.641
1760.572
1753.450
1746.327
1607.602
1601.320
1594.998
1053.542
1006.567
1005.647
1004.246
1003.326
1002.646
1001.846
1000.885
804.461
797.219
789.697
782.174
775.052
744.322
737.760
730.477
722.515
718.954
638.888
631.285
623.403
615.680
608.518
590.992
586.631
575.907
563.703
556.421
S20
8.0
7.5
7.0
6.5
6.0
5.5
5.0
4.5
4.0
3.5
3.0
2.5
2.0
1.5
1.0
0.5
ppm
1.00
2.28
2.25
4.06
2.29
2.22
2.25
2.26
6.49
0.75
2.32
2.94
2.37
8.50

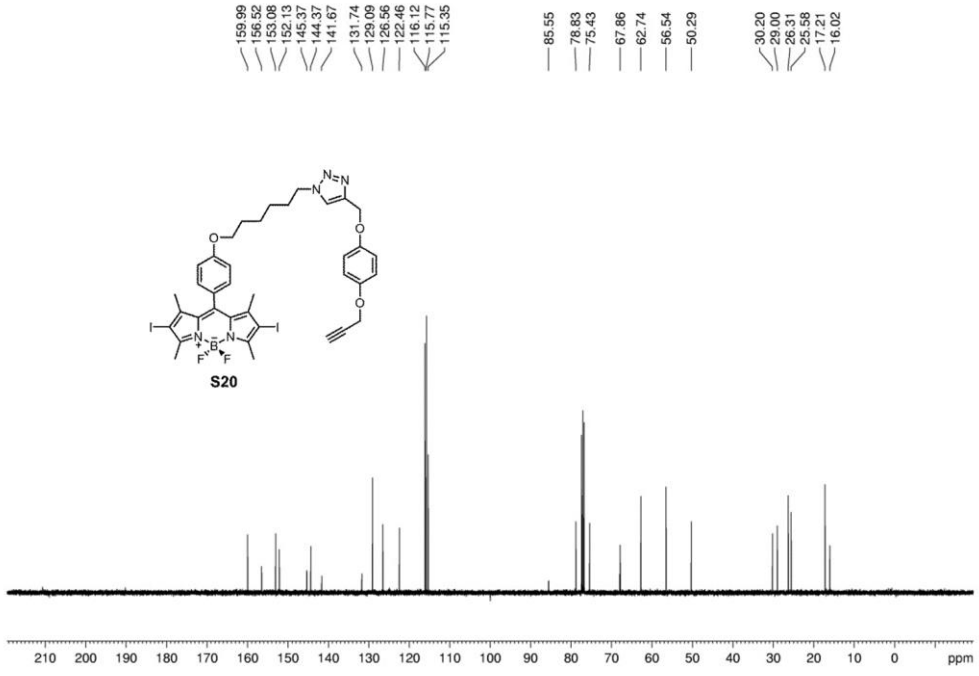
159.99
156.52
153.08
152.13
145.37
144.37
141.67
131.74
129.09
126.56
122.46
116.12
115.77
115.35
85.55
78.83
75.43
67.86
62.74
56.54
50.29
30.20
29.00
26.31
25.58
17.21
16.02
S20
210
200
190
180
170
160
150
140
130
120
110
100
90
80
70
60
50
40
30
20
10
0
ppm

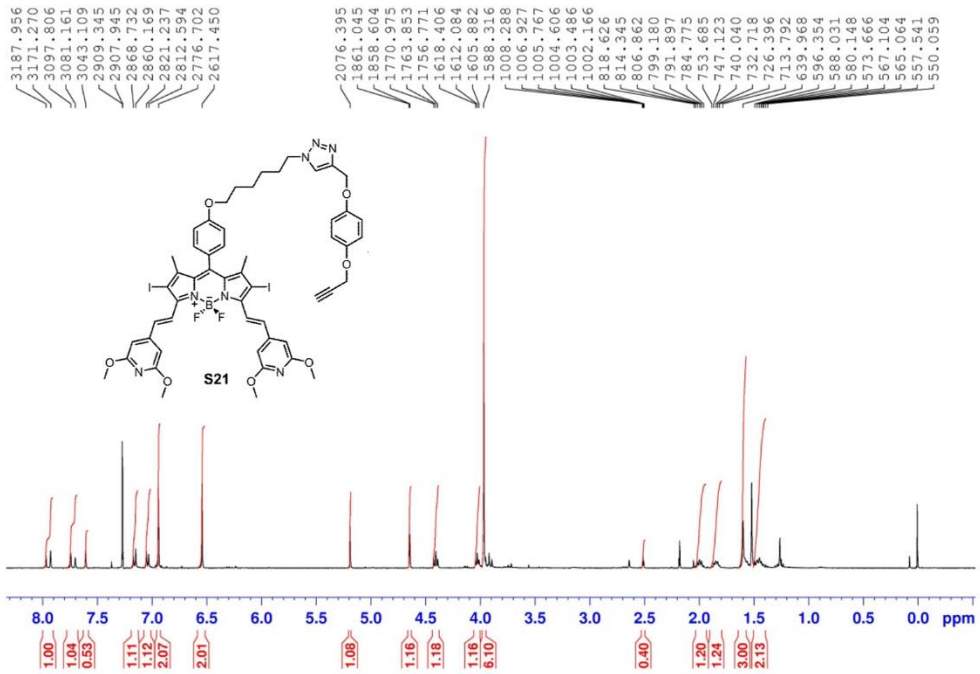
3187.956
3171.270
3097.806
3081.161
3043.109
2909.345
2907.945
2868.732
2860.169
2821.237
2812.594
2776.702
2617.450
2076.395
1861.045
1858.604
1770.975
1763.853
1756.771
1618.406
1612.084
1605.882
1588.316
1008.288
1006.927
1005.767
1004.606
1003.486
1002.166
818.626
814.345
806.862
799.180
791.897
784.775
753.685
747.123
740.040
732.718
726.396
713.792
639.968
596.354
588.031
580.148
573.666
567.104
565.064
557.541
550.059
S21
8.0
7.5
7.0
6.5
6.0
5.5
5.0
4.5
4.0
3.5
3.0
2.5
2.0
1.5
1.0
0.5
0.0
ppm
1.00
1.04
0.53
1.11
1.12
2.07
2.01
1.08
1.16
1.18
1.16
6.10
0.40
1.20
1.24
3.00
2.13

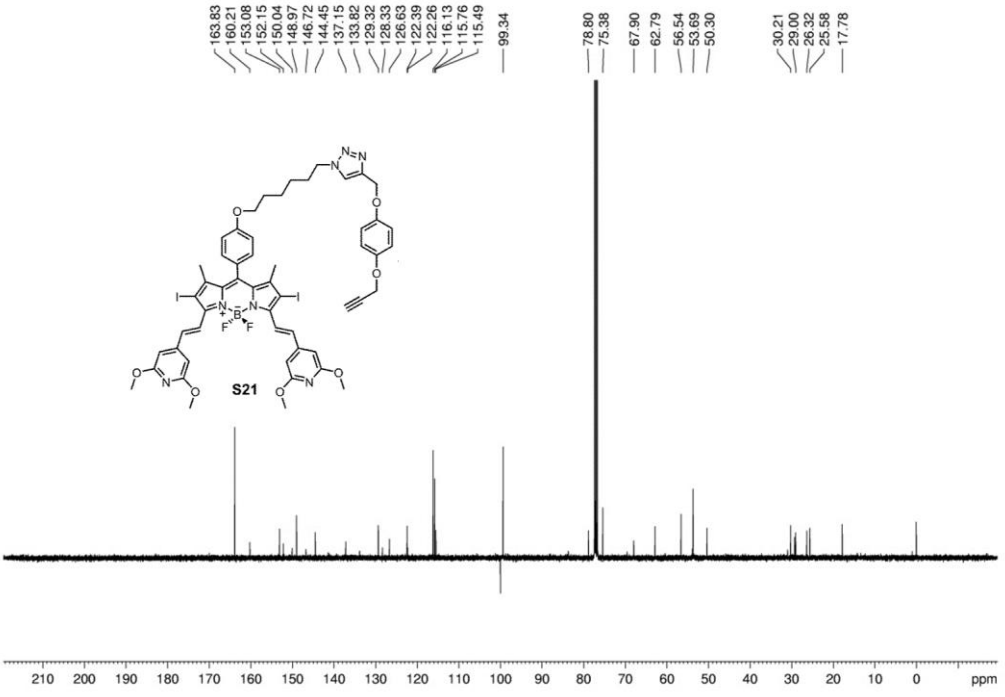
163.83
160.21
153.08
152.15
150.04
148.97
146.72
144.45
137.15
133.82
129.32
128.33
126.63
122.39
122.26
116.13
115.76
115.49
99.34
78.80
75.38
67.90
62.79
56.54
53.69
50.30
30.21
29.00
26.32
25.58
17.78
S21
210
200
190
180
170
160
150
140
130
120
110
100
90
80
70
60
50
40
30
20
10
0
ppm

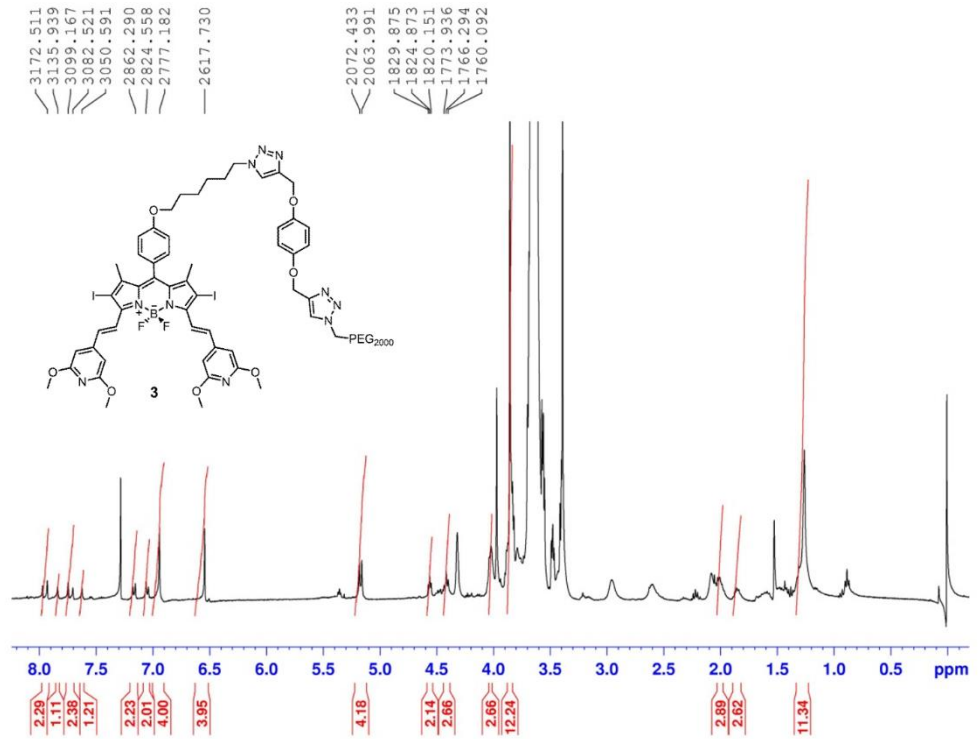
3172.511
3135.939
3099.167
3082.521
3050.591
2862.290
2824.558
2777.182
2617.730
2072.433
2063.991
1829.875
1824.873
1820.151
1773.936
1766.294
1760.092
PEG2000
3
8.0
7.5
7.0
6.5
6.0
5.5
5.0
4.5
4.0
3.5
3.0
2.5
2.0
1.5
1.0
0.5
ppm
2.29
1.11
2.38
1.21
2.23
2.01
4.00
3.95
4.18
2.14
2.66
2.66
12.24
2.89
2.62
11.34

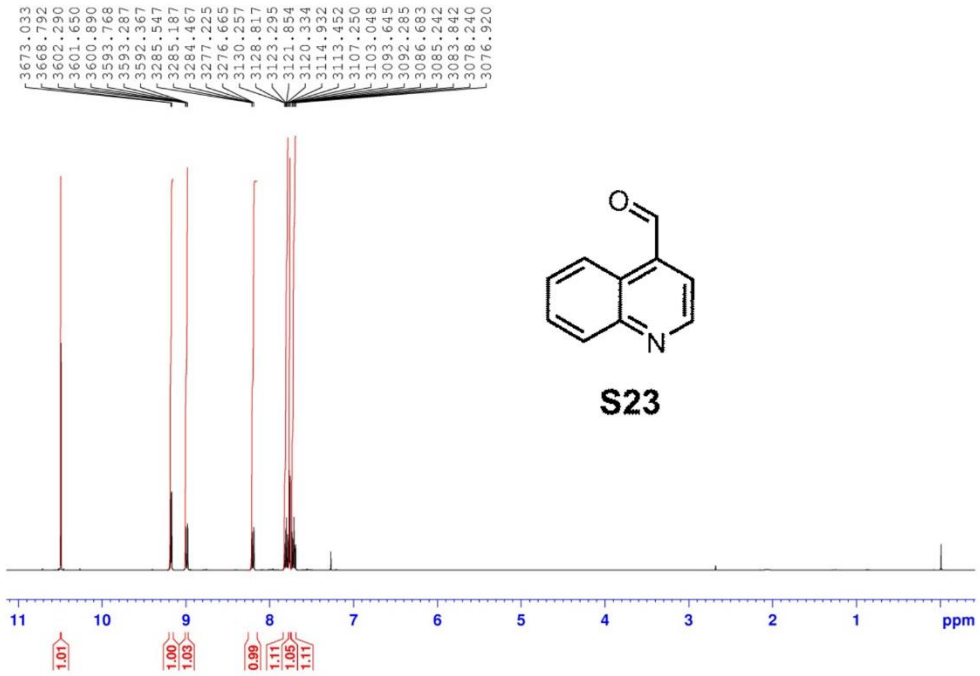
3673.033
3668.792
3602.290
3601.650
3600.890
3593.768
3593.287
3592.367
3285.547
3285.187
3284.467
3277.225
3276.665
3130.257
3128.817
3123.295
3121.854
3120.334
3114.932
3113.452
3107.250
3103.048
3093.645
3092.285
3086.683
3085.242
3083.842
3078.240
3076.920
O
N
11
10
9
8
7
6
5
4
3
2
1
ppm
1.01
1.00
1.03
0.99
1.11
1.05
1.11

S23

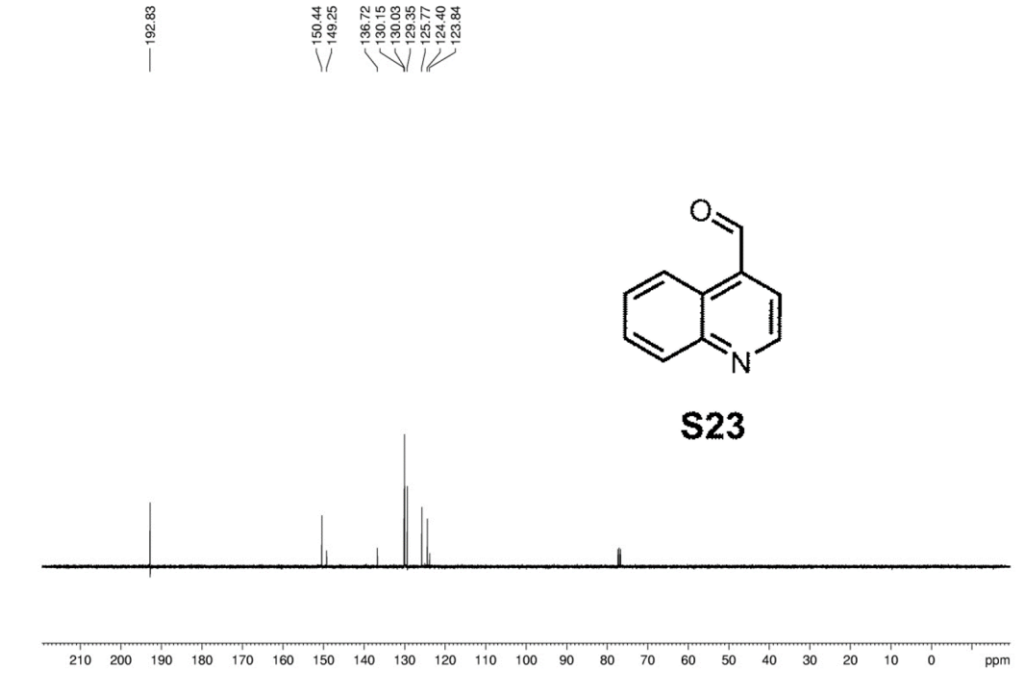
192.83
150.44
149.25
136.72
130.15
130.03
129.35
125.77
124.40
123.84
O
N
S23
210 200 190 180 170 160 150 140 130 120 110 100 90 80 70 60 50 40 30 20 10 0 ppm

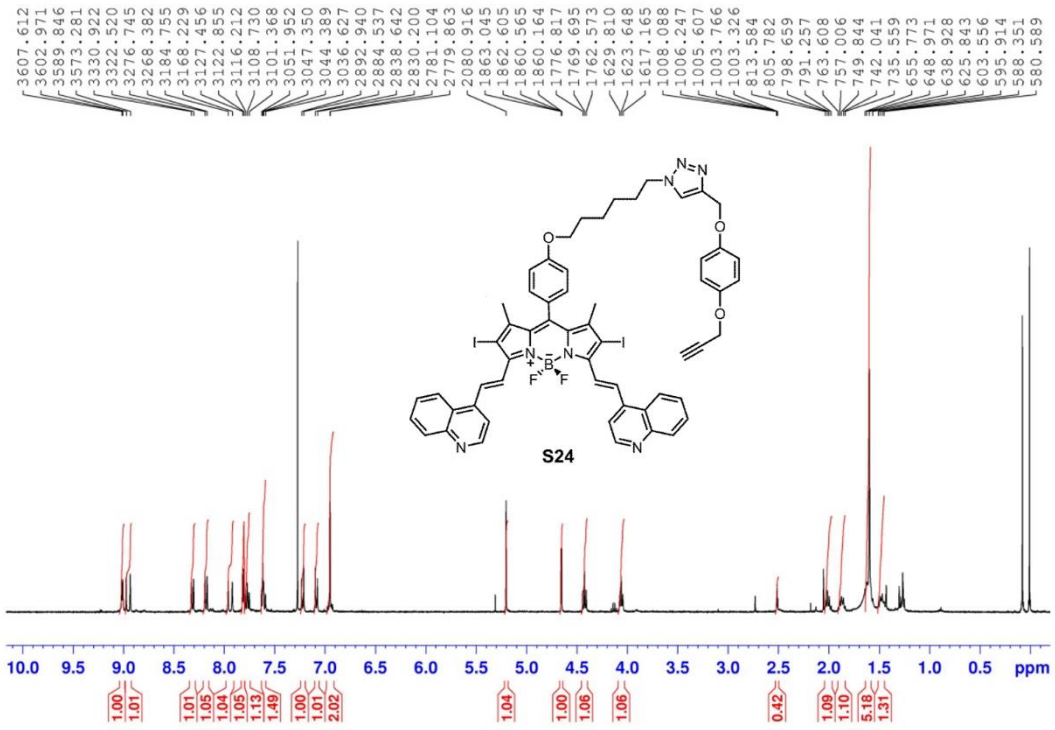
3607.612
3602.971
3589.846
3573.281
3330.922
3322.520
3276.745
3268.382
3184.755
3168.229
3127.456
3122.855
3116.212
3108.730
3101.368
3051.952
3047.350
3044.389
3036.627
2892.940
2884.537
2838.642
2830.200
2781.104
2779.863
2080.916
1863.045
1862.605
1860.565
1860.164
1776.817
1769.695
1762.573
1629.810
1623.648
1617.165
1008.088
1006.247
1005.607
1003.766
1003.326
813.584
805.782
798.659
791.257
763.608
757.006
749.844
742.041
735.559
655.773
648.971
638.928
625.843
603.556
595.914
588.351
580.589
S24
10.0 9.5 9.0 8.5 8.0 7.5 7.0 6.5 6.0 5.5 5.0 4.5 4.0 3.5 3.0 2.5 2.0 1.5 1.0 0.5 ppm
1.00 1.01 1.01 1.05 1.04 1.05 1.13 1.49 1.00 1.01 2.02 1.04 1.00 1.06 1.06 0.42 1.09 1.10 5.18 1.31

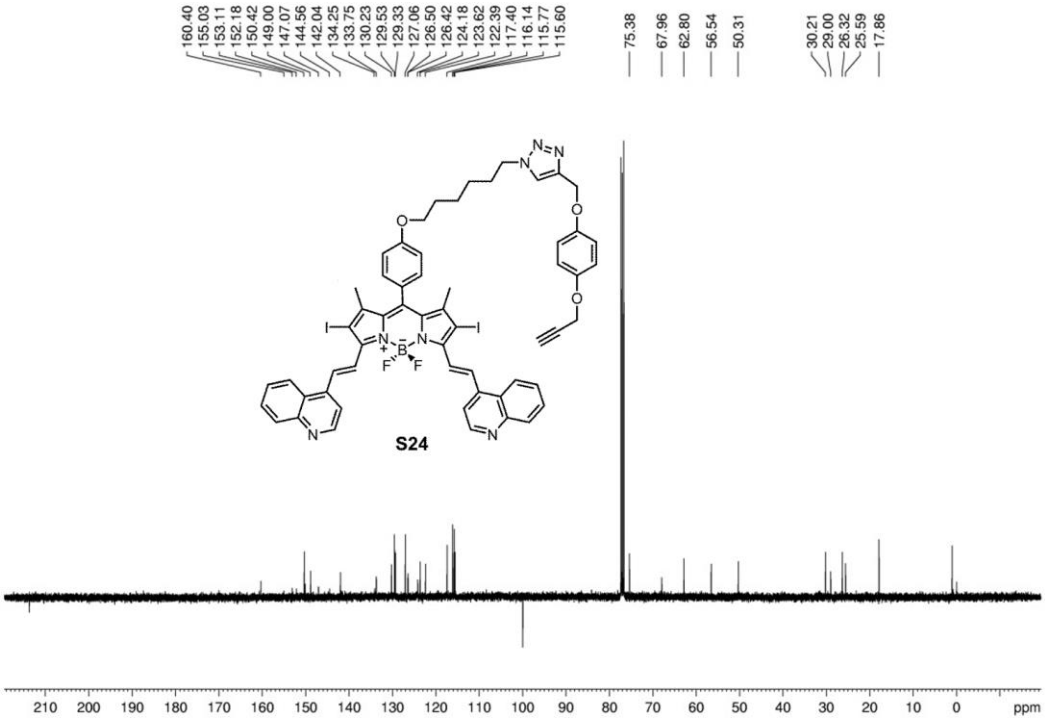
160.40
155.03
153.11
152.18
150.42
149.00
147.07
144.56
142.04
134.25
133.75
130.23
129.53
129.33
127.06
126.50
126.42
124.18
123.62
122.39
117.40
116.14
115.77
115.60
75.38
67.96
62.80
56.54
50.31
30.21
29.00
26.32
25.59
17.86
S24
210 200 190 180 170 160 150 140 130 120 110 100 90 80 70 60 50 40 30 20 10 0 ppm

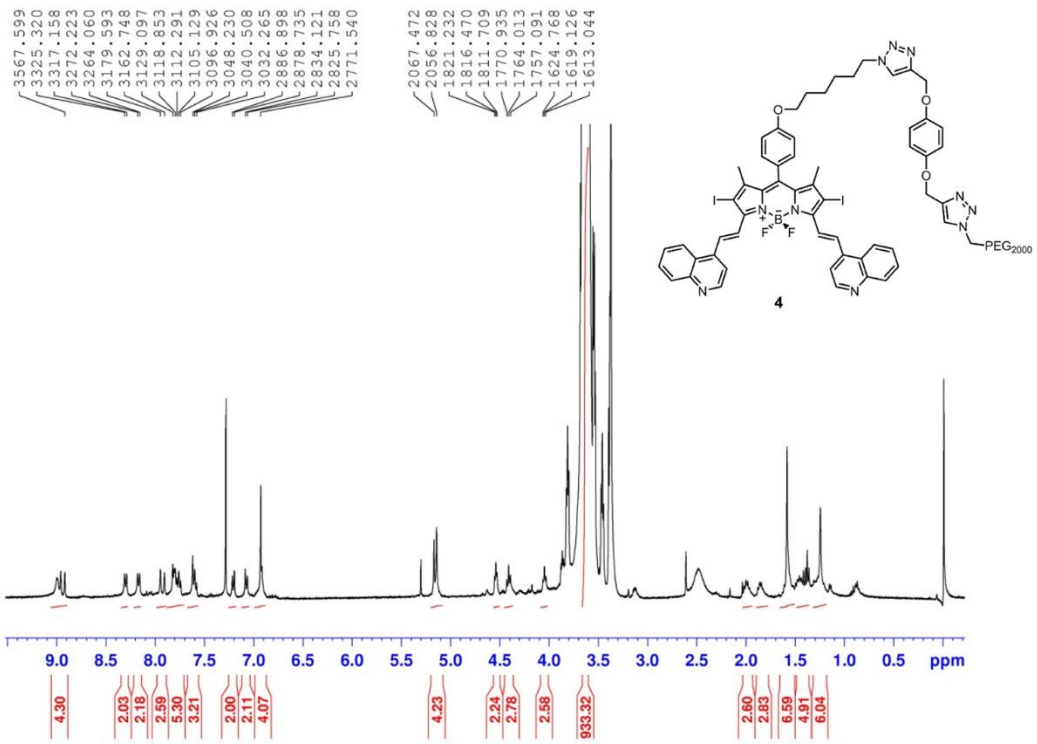
3567.599
3325.320
3317.158
3272.223
3264.060
3179.593
3162.748
3129.097
3118.853
3112.291
3105.129
3096.926
3048.230
3040.508
3032.265
2886.898
2878.735
2834.121
2825.758
2771.540
2067.472
2056.828
1821.232
1816.470
1811.709
1770.935
1764.013
1757.091
1624.768
1619.126
1613.044
PEG2000
4
9.0 8.5 8.0 7.5 7.0 6.5 6.0 5.5 5.0 4.5 4.0 3.5 3.0 2.5 2.0 1.5 1.0 0.5 ppm
4.30
2.03
2.18
2.59
5.30
3.21
2.00
2.11
4.07
4.23
2.24
2.78
2.58
933.32
2.60
2.83
6.59
4.91
6.04

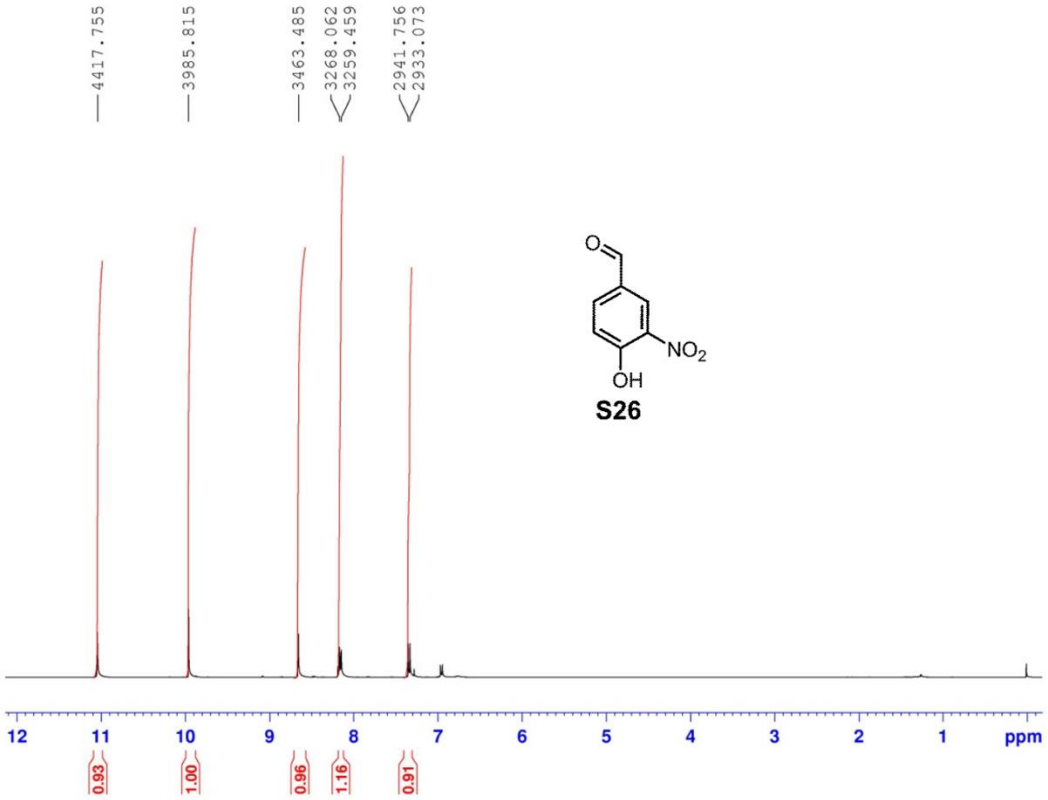
4417.755
3985.815
3463.485
3268.062
3259.459
2941.756
2933.073
O
NO2
OH
S26
12
11
10
9
8
7
6
5
4
3
2
1
ppm
0.93
1.00
0.96
1.16
0.91

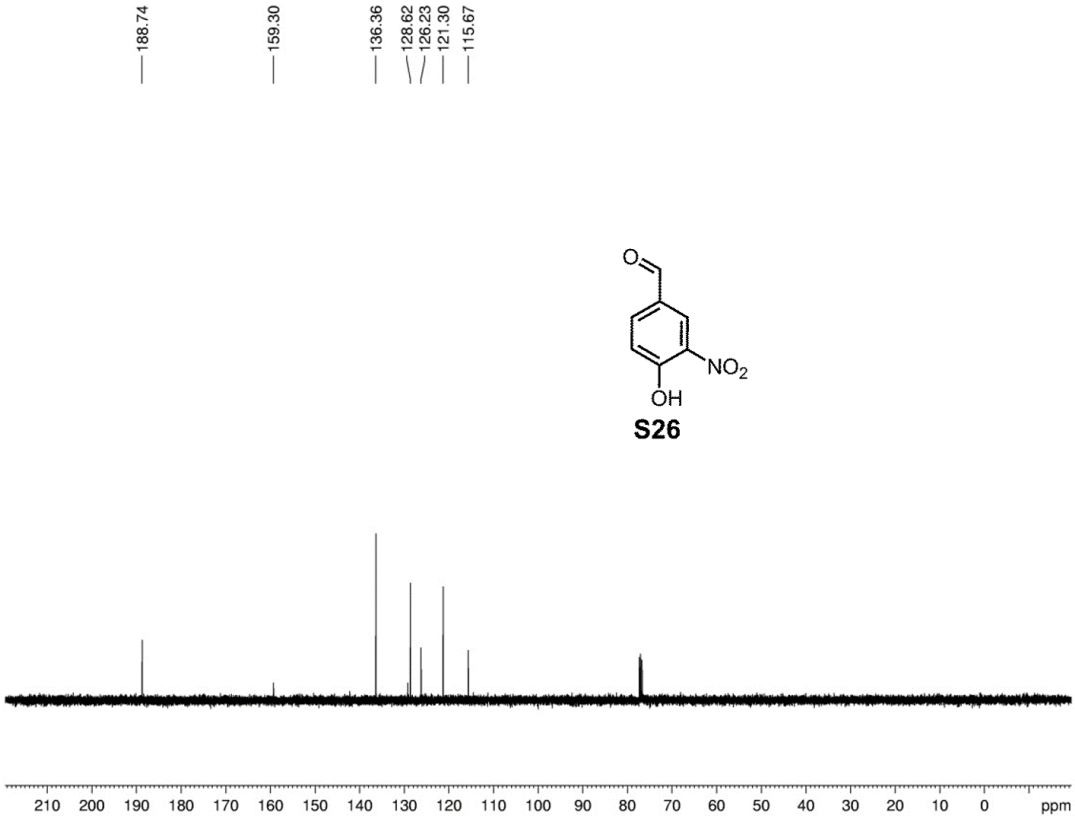
188.74
159.30
136.36
128.62
126.23
121.30
115.67
O
NO2
OH
S26
210
200
190
180
170
160
150
140
130
120
110
100
90
80
70
60
50
40
30
20
10
0
ppm

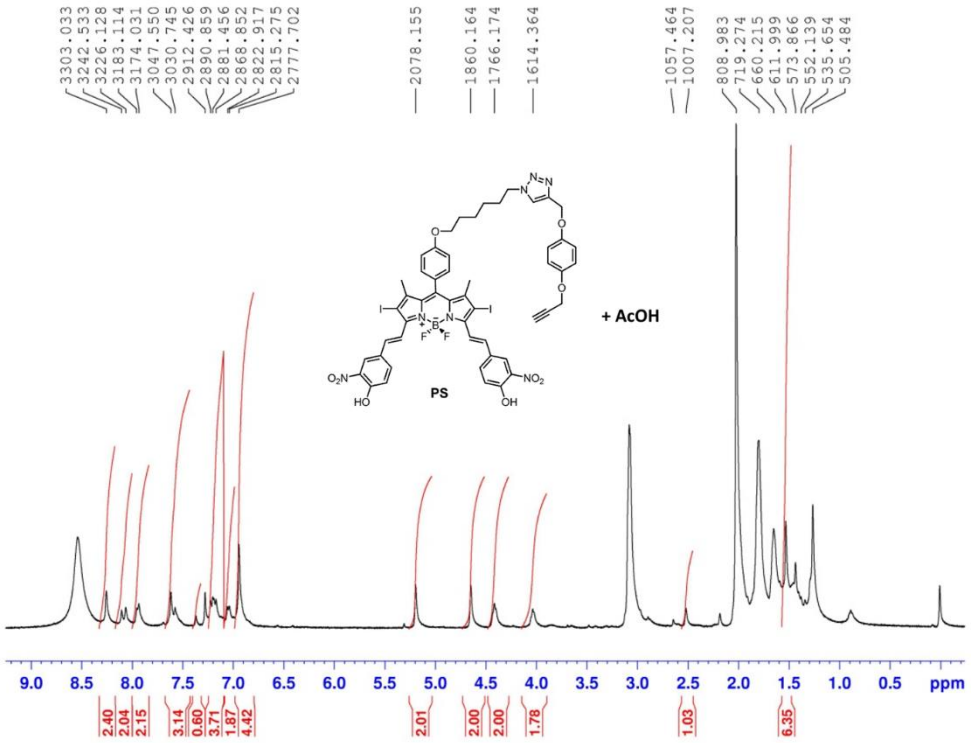
3303.033
3242.533
3226.128
3183.114
3174.031
3047.550
3030.745
2912.426
2890.859
2881.456
2868.852
2822.917
2815.275
2777.702
2078.155
1860.164
1766.174
1614.364
1057.464
1007.207
808.983
719.274
660.215
611.999
573.866
552.139
535.654
505.484
+ AcOH
PS
9.0 8.5 8.0 7.5 7.0 6.5 6.0 5.5 5.0 4.5 4.0 3.5 3.0 2.5 2.0 1.5 1.0 0.5 ppm
2.40 2.04 2.15 3.14 0.60 3.71 1.87 4.42 2.01 2.00 2.00 1.78 1.03 6.35

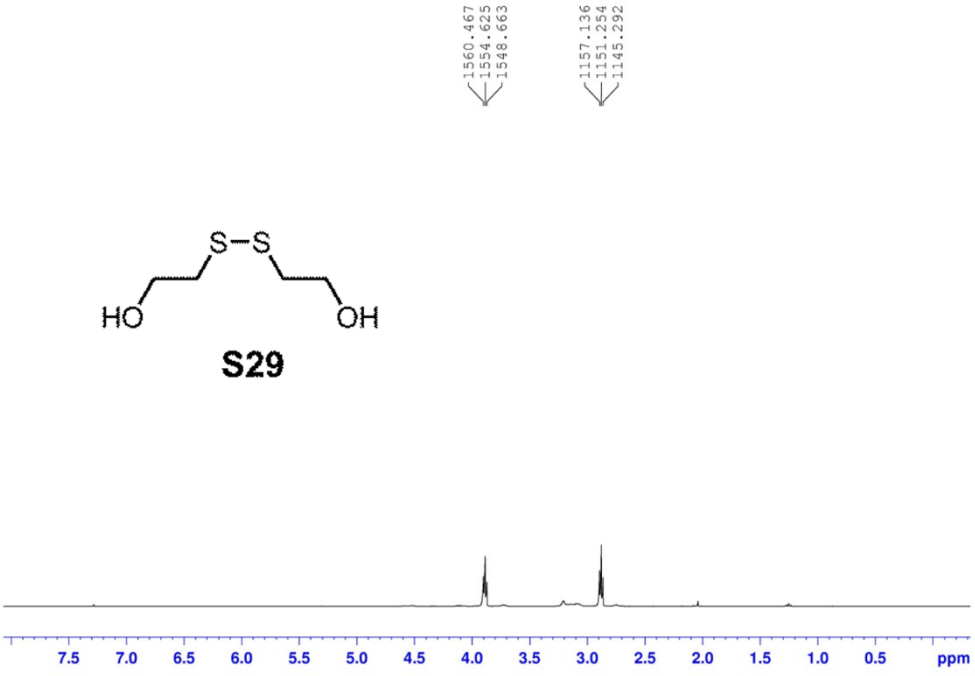
1560.467
1554.625
1548.663
1157.136
1151.254
1145.292
7.5 7.0 6.5 6.0 5.5 5.0 4.5 4.0 3.5 3.0 2.5 2.0 1.5 1.0 0.5 ppm

S–S
HO
OH

S29

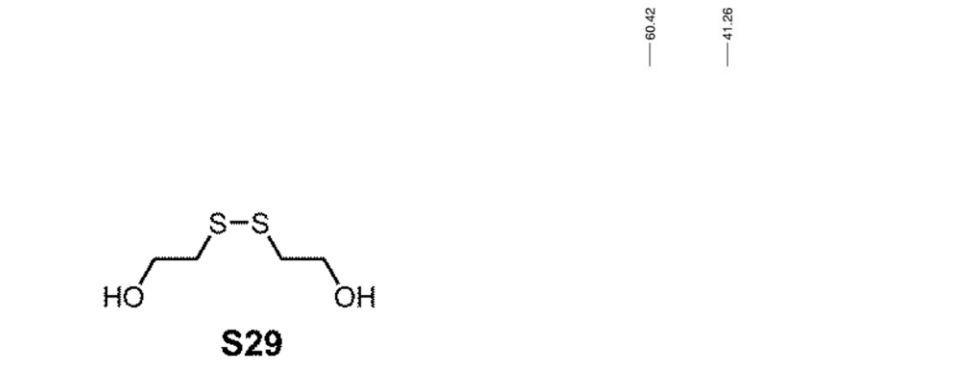
60.42
41.26
S–S
HO
OH
210 200 190 180 170 160 150 140 130 120 110 100 90 80 70 60 50 40 30 20 10 0 ppm

S29

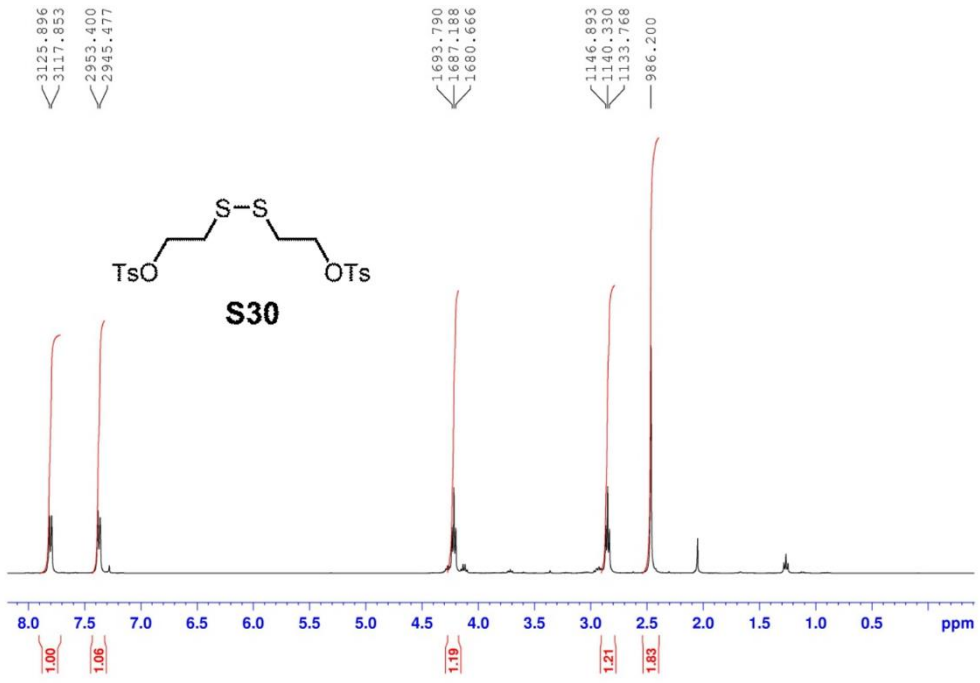
3125.896
3117.853
2953.400
2945.477
1693.790
1687.188
1680.666
1146.893
1140.330
1133.768
986.200
S–S
TsO
OTs
8.0 7.5 7.0 6.5 6.0 5.5 5.0 4.5 4.0 3.5 3.0 2.5 2.0 1.5 1.0 0.5 ppm
1.00
1.06
1.19
1.21
1.83

S30

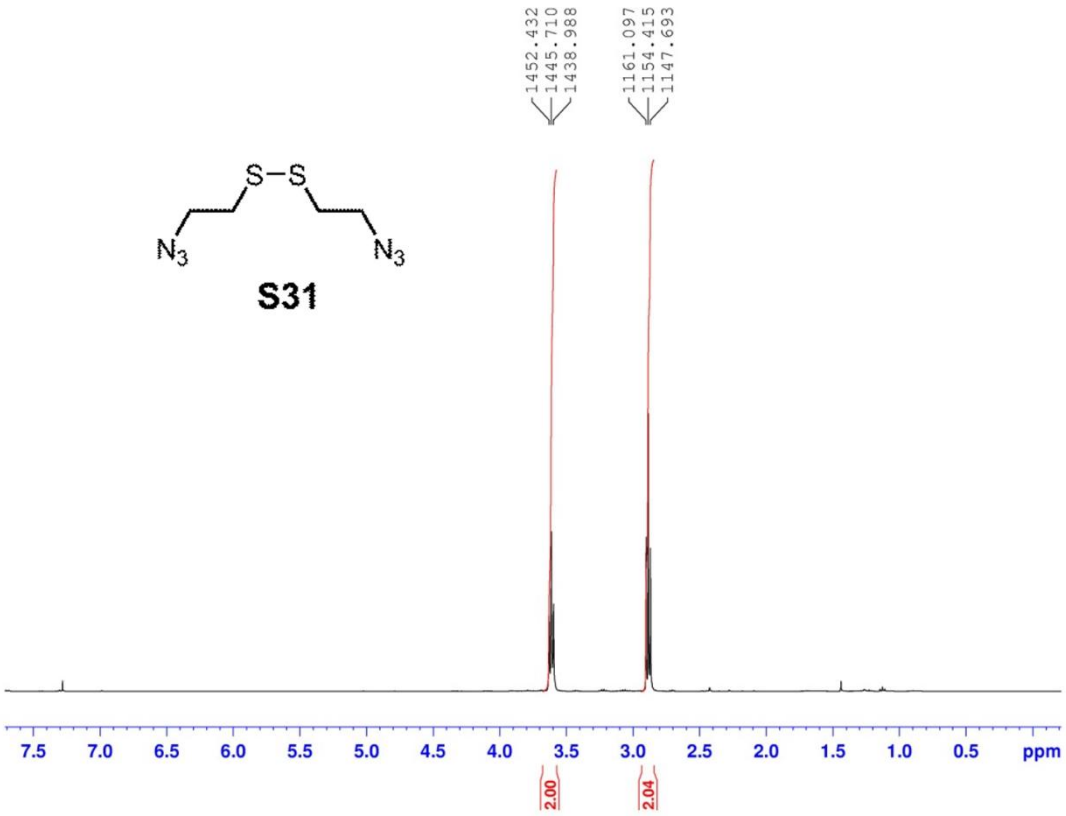
1452.432
1445.710
1438.988
1161.097
1154.415
1147.693
S−S
N3
N3
S31
7.5 7.0 6.5 6.0 5.5 5.0 4.5 4.0 3.5 3.0 2.5 2.0 1.5 1.0 0.5 ppm
2.00
2.04

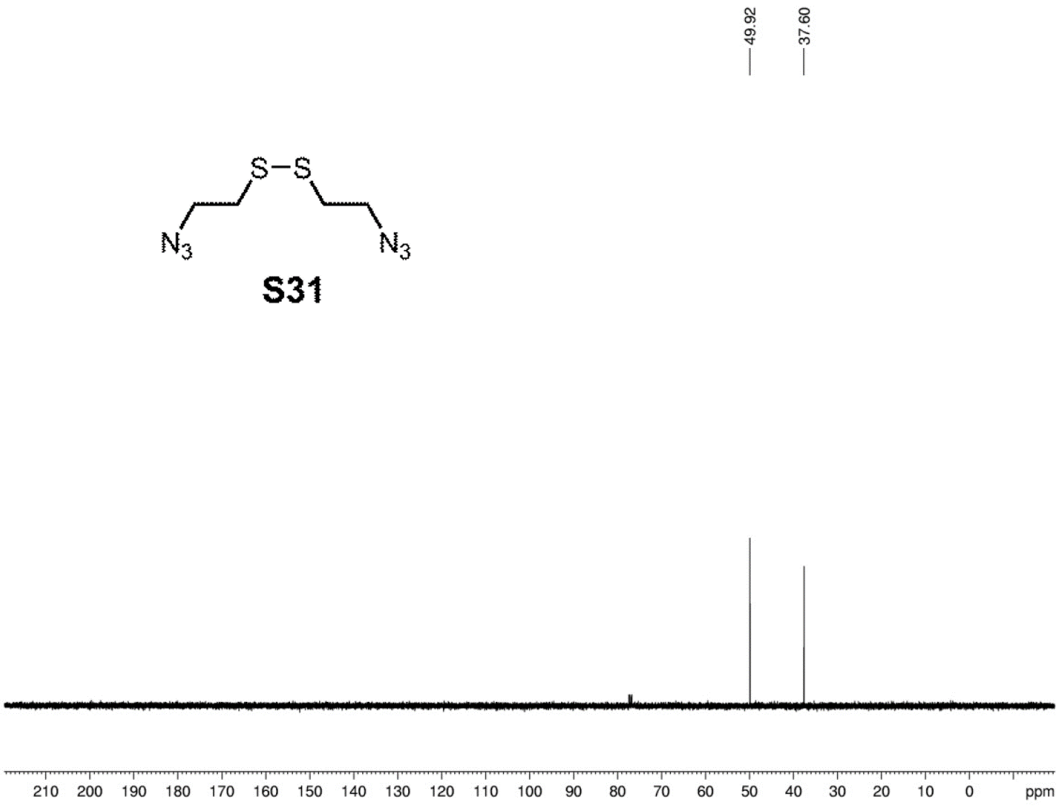
49.92
37.60
S−S
N3
N3
S31
210 200 190 180 170 160 150 140 130 120 110 100 90 80 70 60 50 40 30 20 10 0 ppm

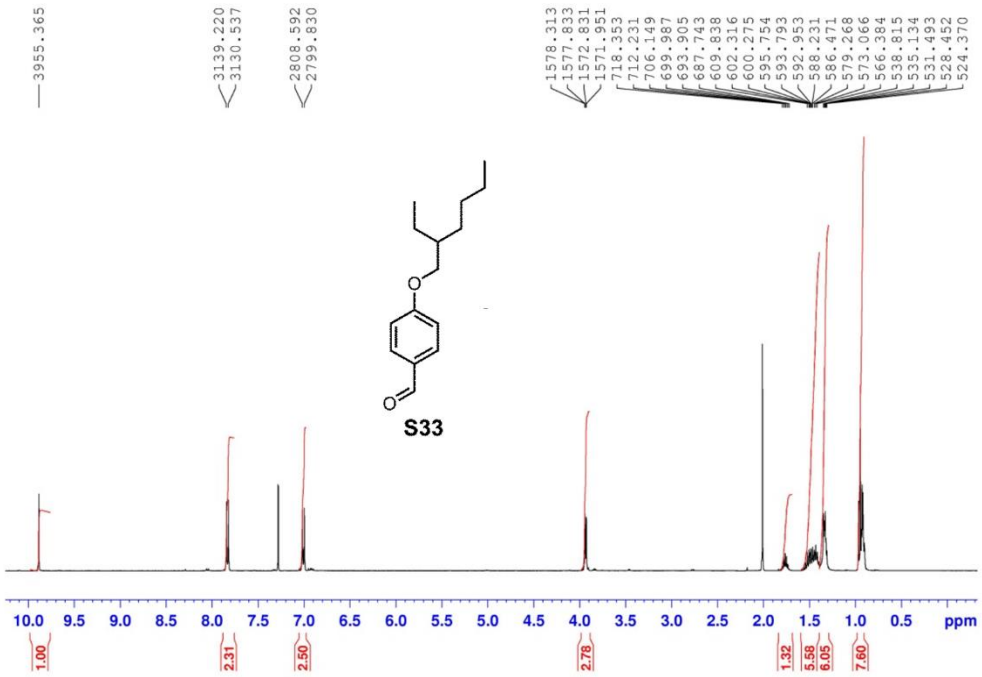
3955.365
3139.220
3130.537
2808.592
2799.830
1578.313
1577.833
1572.831
1571.951
718.353
712.231
706.149
699.987
693.905
687.743
609.838
602.316
600.275
595.754
593.793
592.953
588.231
586.471
579.268
573.066
566.384
538.815
535.134
531.493
528.452
524.370
S33
10.0 9.5 9.0 8.5 8.0 7.5 7.0 6.5 6.0 5.5 5.0 4.5 4.0 3.5 3.0 2.5 2.0 1.5 1.0 0.5 ppm
1.00
2.31
2.50
2.78
1.32
5.58
6.05
7.60

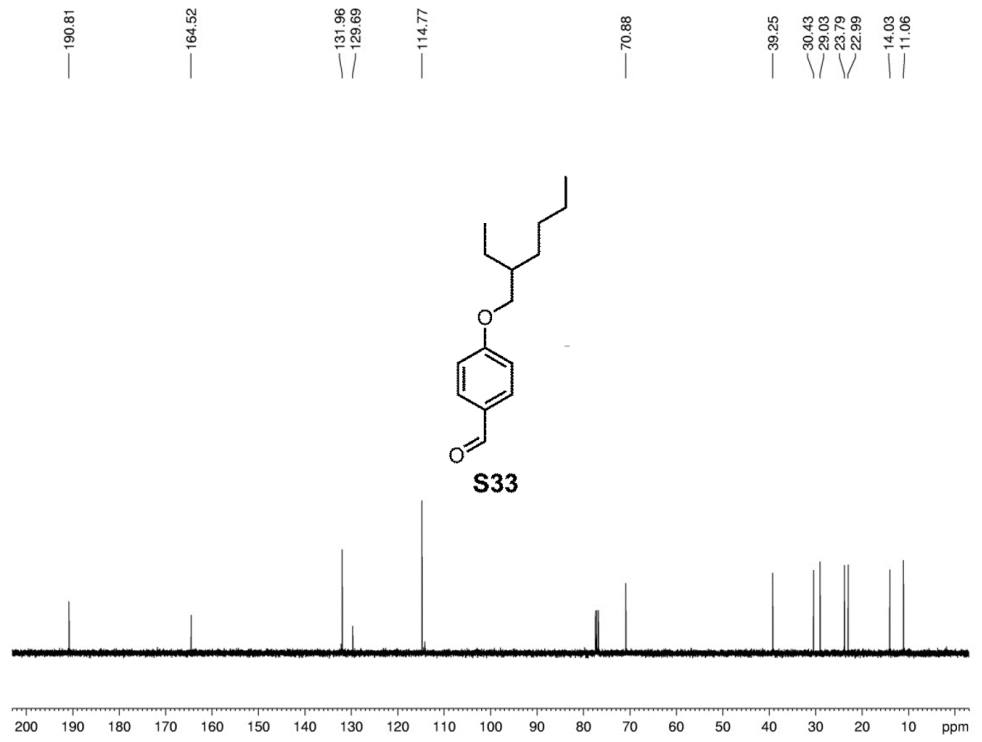
190.81
164.52
131.96
129.69
114.77
70.88
39.25
30.43
29.03
23.79
22.99
14.03
11.06
S33
200 190 180 170 160 150 140 130 120 110 100 90 80 70 60 50 40 30 20 10 ppm

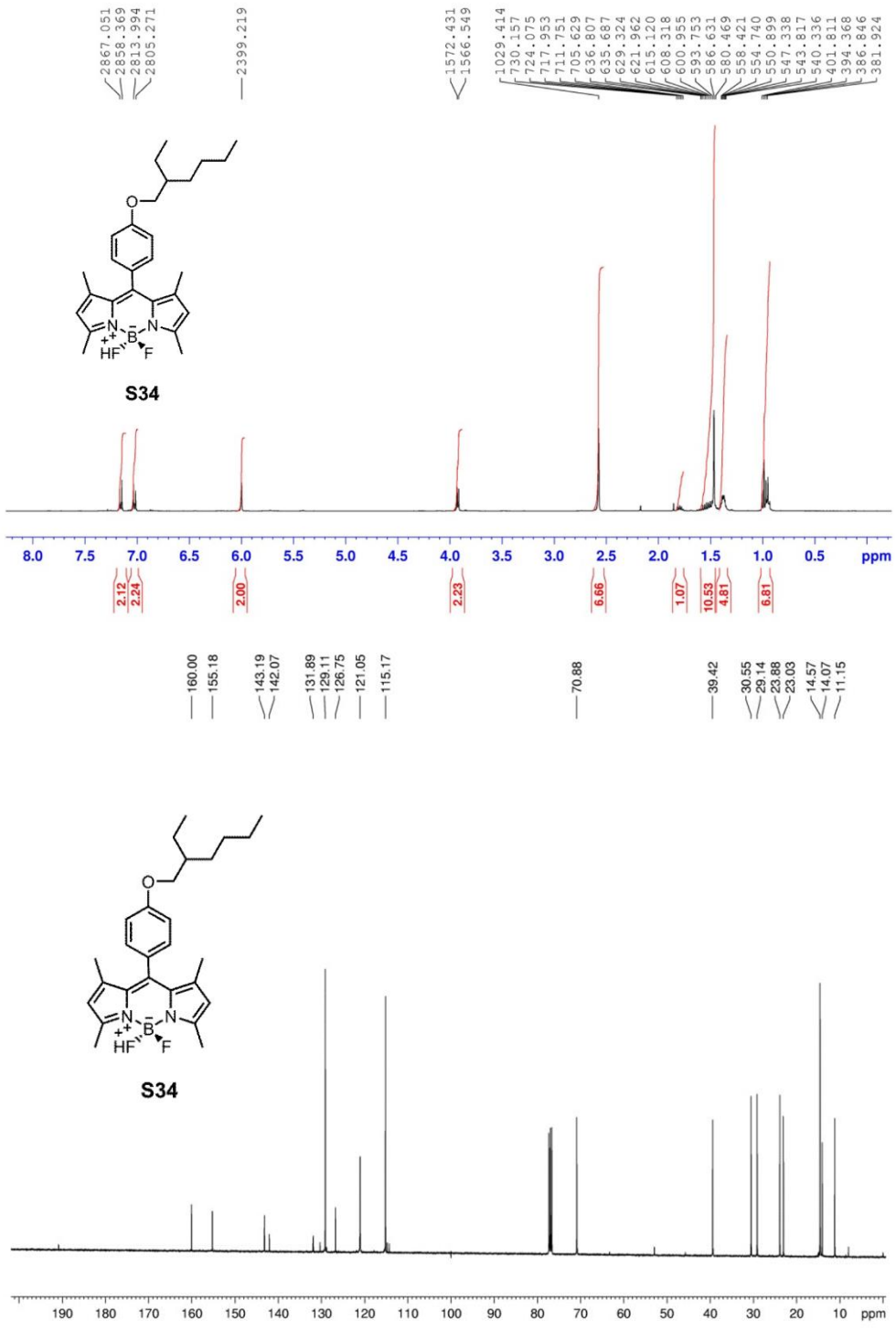
2867.051
2858.369
2813.994
2805.271
2399.219
1572.431
1566.549
1029.414
730.157
724.075
717.953
711.751
705.629
636.807
635.687
629.324
621.962
615.120
608.318
600.955
593.753
586.631
580.469
558.421
554.740
550.899
547.338
543.817
540.336
401.811
394.368
386.846
381.924
S34
8.0
7.5
7.0
6.5
6.0
5.5
5.0
4.5
4.0
3.5
3.0
2.5
2.0
1.5
1.0
0.5
ppm
2.12
2.24
2.00
2.23
6.66
1.07
10.53
4.81
6.81
160.00
155.18
143.19
142.07
131.89
129.11
126.75
121.05
115.17
70.88
39.42
30.55
29.14
23.88
23.03
14.57
14.07
11.15
S34
190
180
170
160
150
140
130
120
110
100
90
80
70
60
50
40
30
20
10
ppm

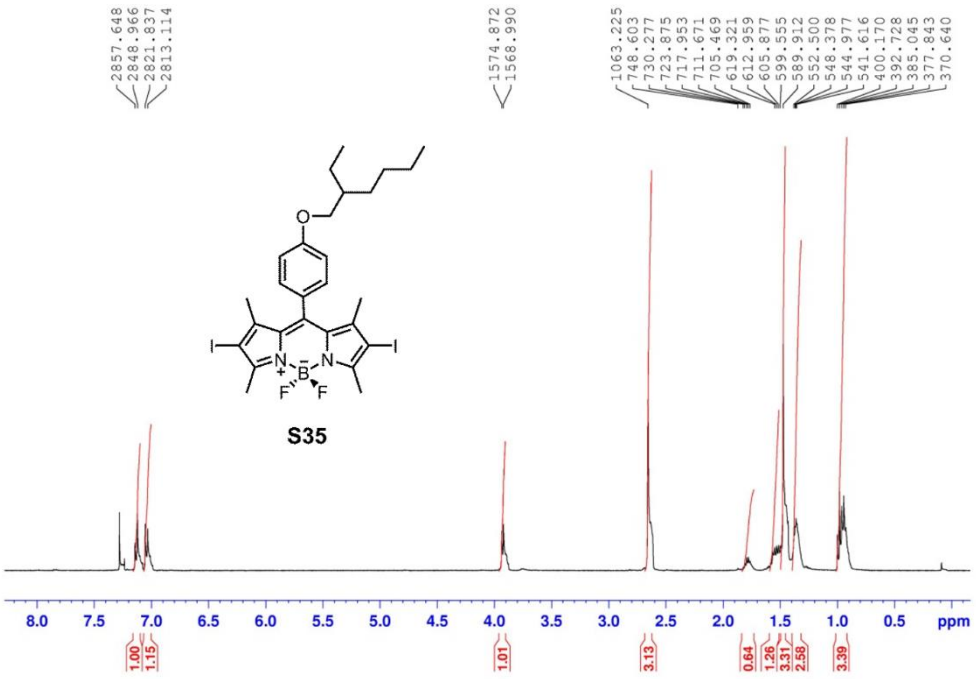
2857.648
2848.966
2821.837
2813.114
1574.872
1568.990
1063.225
748.603
730.277
723.875
717.953
711.671
705.469
619.321
612.959
605.877
599.555
589.912
552.500
548.378
544.977
541.616
400.170
392.728
385.045
377.843
370.640
S35
8.0
7.5
7.0
6.5
6.0
5.5
5.0
4.5
4.0
3.5
3.0
2.5
2.0
1.5
1.0
0.5
ppm
1.00
1.15
1.01
3.13
0.64
1.26
3.31
2.58
3.39

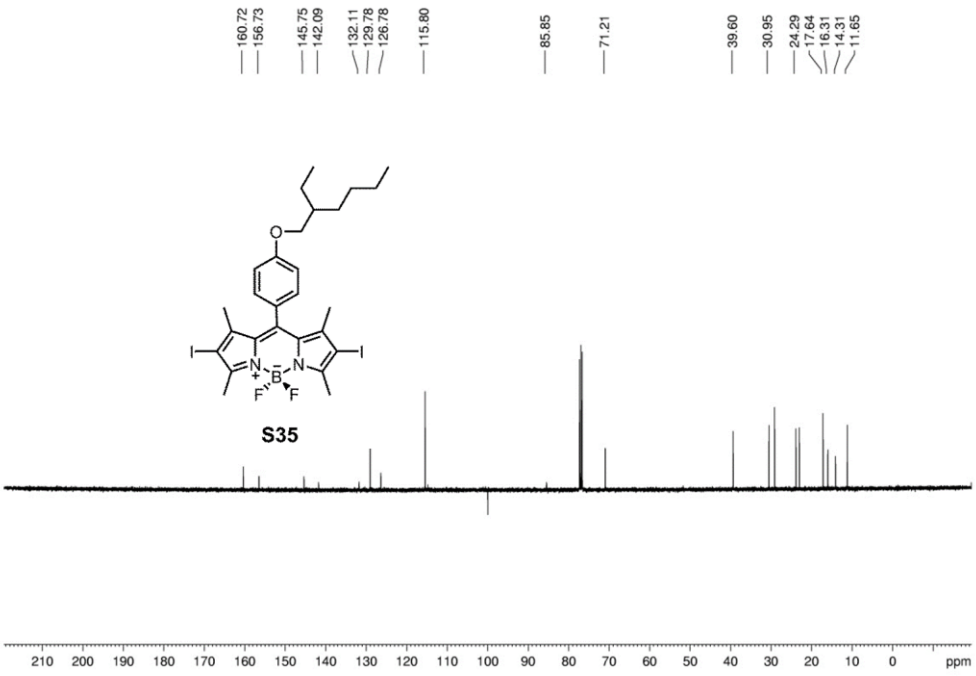
160.72
156.73
145.75
142.09
132.11
129.78
126.78
115.80
85.85
71.21
39.60
30.95
24.29
17.64
16.31
14.31
11.65
S35
210
200
190
180
170
160
150
140
130
120
110
100
90
80
70
60
50
40
30
20
10
0
ppm

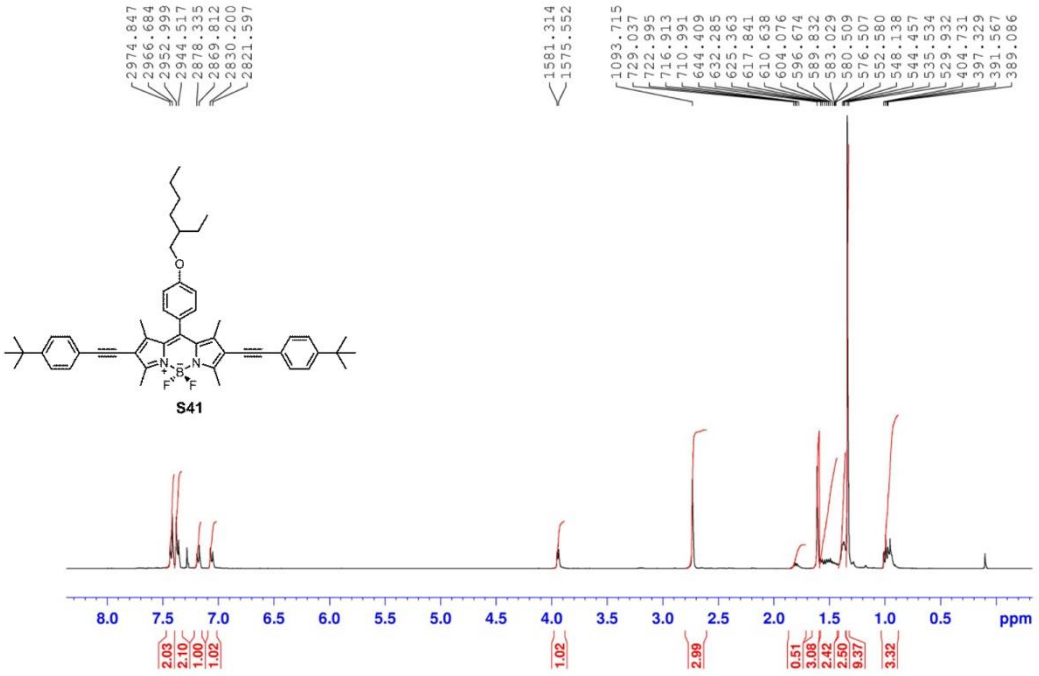
2974.847
2966.684
2952.999
2944.517
2878.335
2869.812
2830.200
2821.597
1581.314
1575.552
1093.715
729.037
722.995
716.913
710.991
644.409
632.285
625.363
617.841
610.638
604.076
596.674
589.832
583.029
580.509
576.507
552.580
548.138
544.457
535.534
529.932
404.731
397.329
391.567
389.086
S41
8.0
7.5
7.0
6.5
6.0
5.5
5.0
4.5
4.0
3.5
3.0
2.5
2.0
1.5
1.0
0.5
ppm
2.03
2.10
1.00
1.02
1.02
2.99
0.51
3.06
2.42
2.50
9.37
3.32

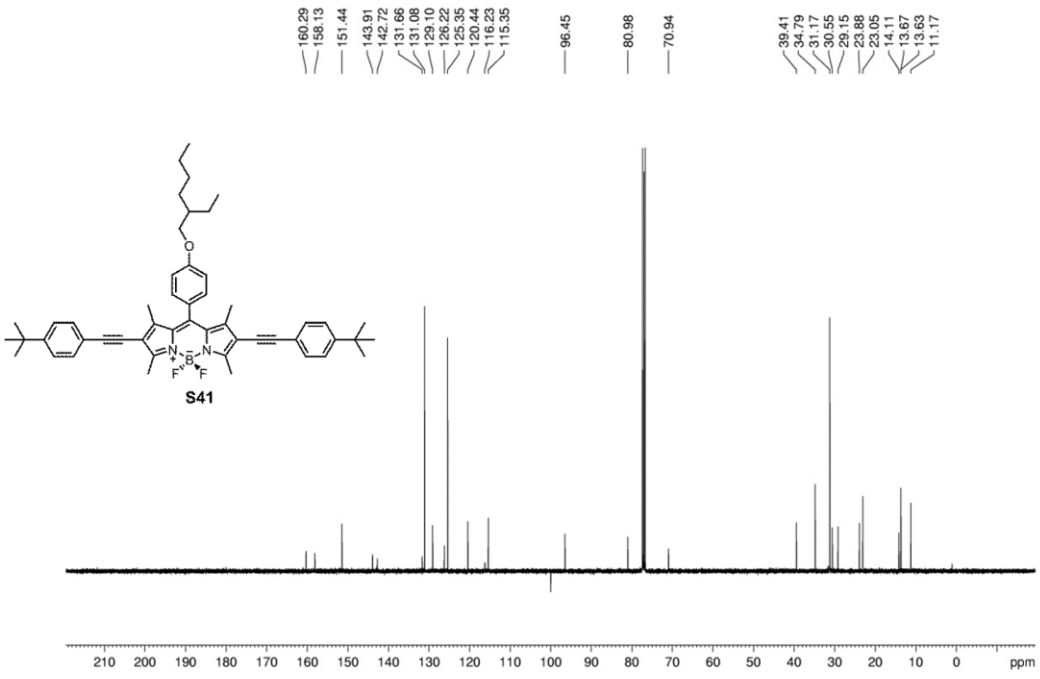
160.29
158.13
151.44
143.91
142.72
131.66
131.08
129.10
126.22
125.35
120.44
116.23
115.35
96.45
80.98
70.94
39.41
34.79
31.17
30.55
29.15
23.88
23.05
14.11
13.67
13.63
11.17
S41
210
200
190
180
170
160
150
140
130
120
110
100
90
80
70
60
50
40
30
20
10
0
ppm

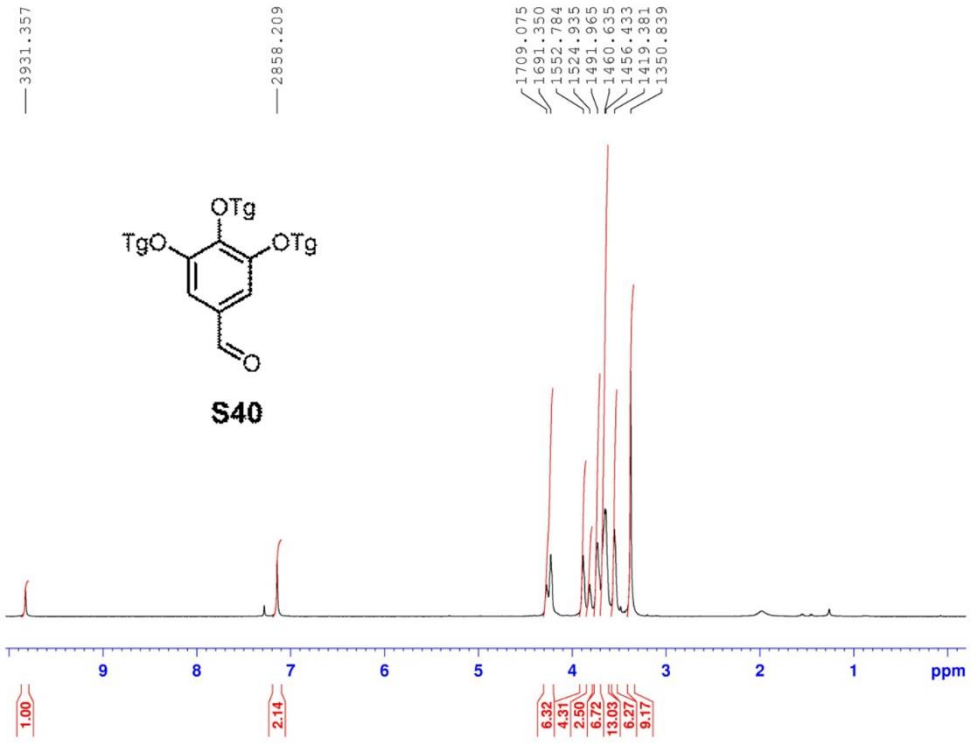
3931.357
2858.209
1709.075
1691.350
1552.784
1524.935
1491.965
1460.635
1456.433
1419.381
1350.839
OTg
TgO
OTg
O
S40
9
8
7
6
5
4
3
2
1
ppm
1.00
2.14
6.32
4.31
2.50
6.72
13.03
6.27
9.17

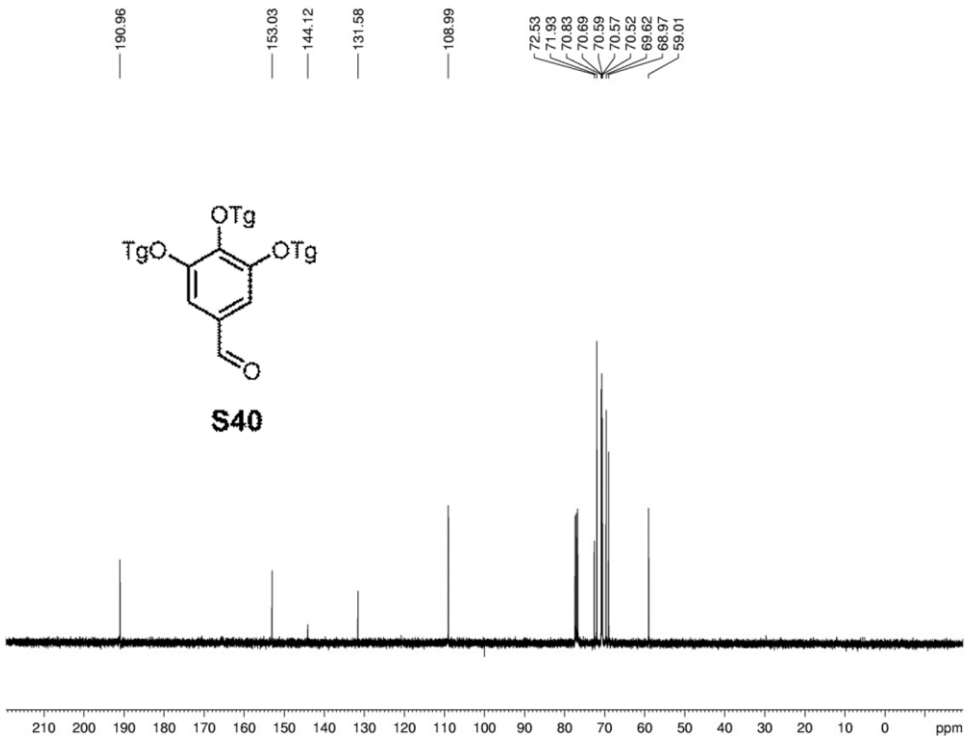
190.96
153.03
144.12
131.58
108.99
72.53
71.93
70.83
70.69
70.59
70.57
70.52
69.62
68.97
59.01
OTg
TgO
OTg
O
S40
210
200
190
180
170
160
150
140
130
120
110
100
90
80
70
60
50
40
30
20
10
0
ppm

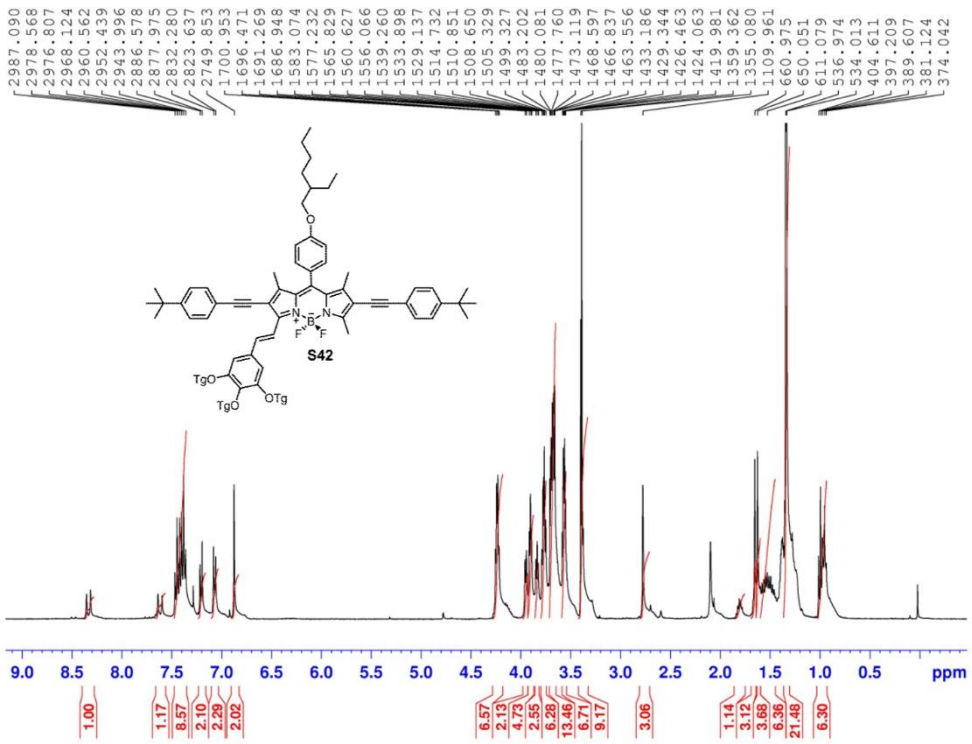
2987.090
2978.568
2976.807
2968.124
2960.562
2952.439
2943.996
2886.578
2877.975
2832.280
2823.637
2749.853
1700.953
1696.471
1691.269
1686.948
1583.074
1577.232
1565.829
1560.627
1556.066
1539.260
1533.898
1529.137
1514.732
1510.851
1508.650
1505.329
1499.327
1483.202
1480.081
1477.760
1473.119
1468.597
1466.837
1463.556
1433.186
1429.344
1426.463
1424.063
1419.981
1359.362
1355.080
1109.961
660.975
650.051
611.079
536.974
534.013
404.611
397.209
389.607
381.124
374.042
S42
TgO
TgO
OTg
9.0 8.5 8.0 7.5 7.0 6.5 6.0 5.5 5.0 4.5 4.0 3.5 3.0 2.5 2.0 1.5 1.0 0.5 ppm
1.00
1.17
8.57
2.10
2.29
2.02
6.57
2.13
4.73
2.55
6.28
13.46
6.71
9.17
3.06
1.14
3.12
3.68
6.36
21.48
6.30

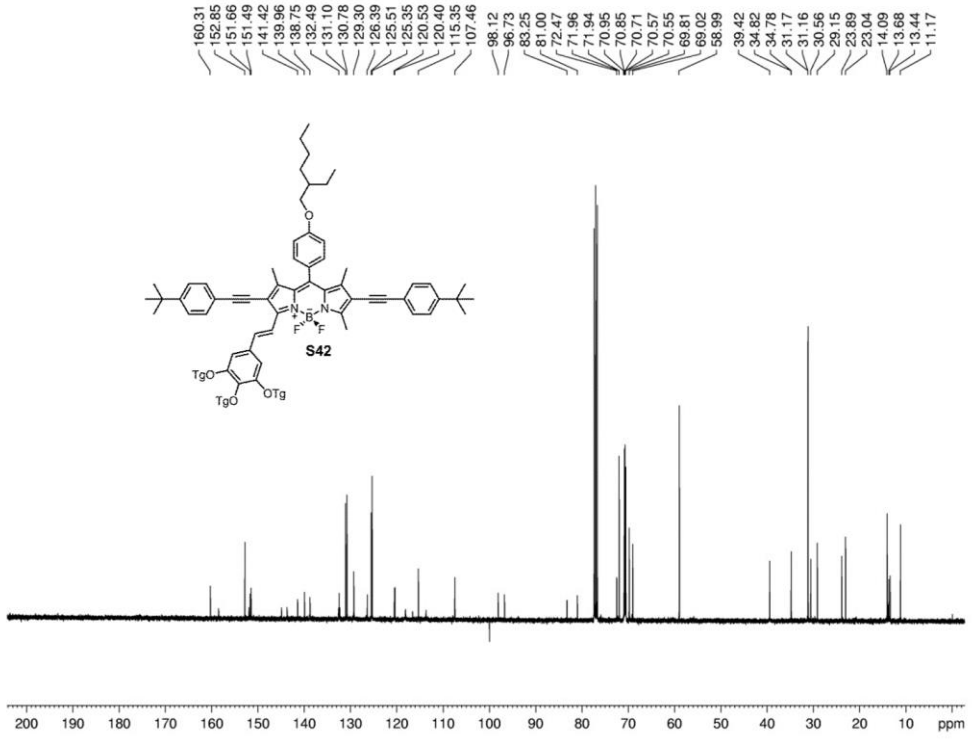
160.31
152.85
151.66
151.49
141.42
139.96
138.75
132.49
131.10
130.78
129.30
126.39
125.51
125.35
120.53
120.40
115.35
107.46
98.12
96.73
83.25
81.00
72.47
71.96
71.94
70.95
70.85
70.71
70.57
70.55
69.81
69.02
58.99
39.42
34.82
34.78
31.17
31.16
30.56
29.15
23.89
23.04
14.09
13.68
13.44
11.17
S42
TgO
TgO
OTg
200 190 180 170 160 150 140 130 120 110 100 90 80 70 60 50 40 30 20 10 ppm

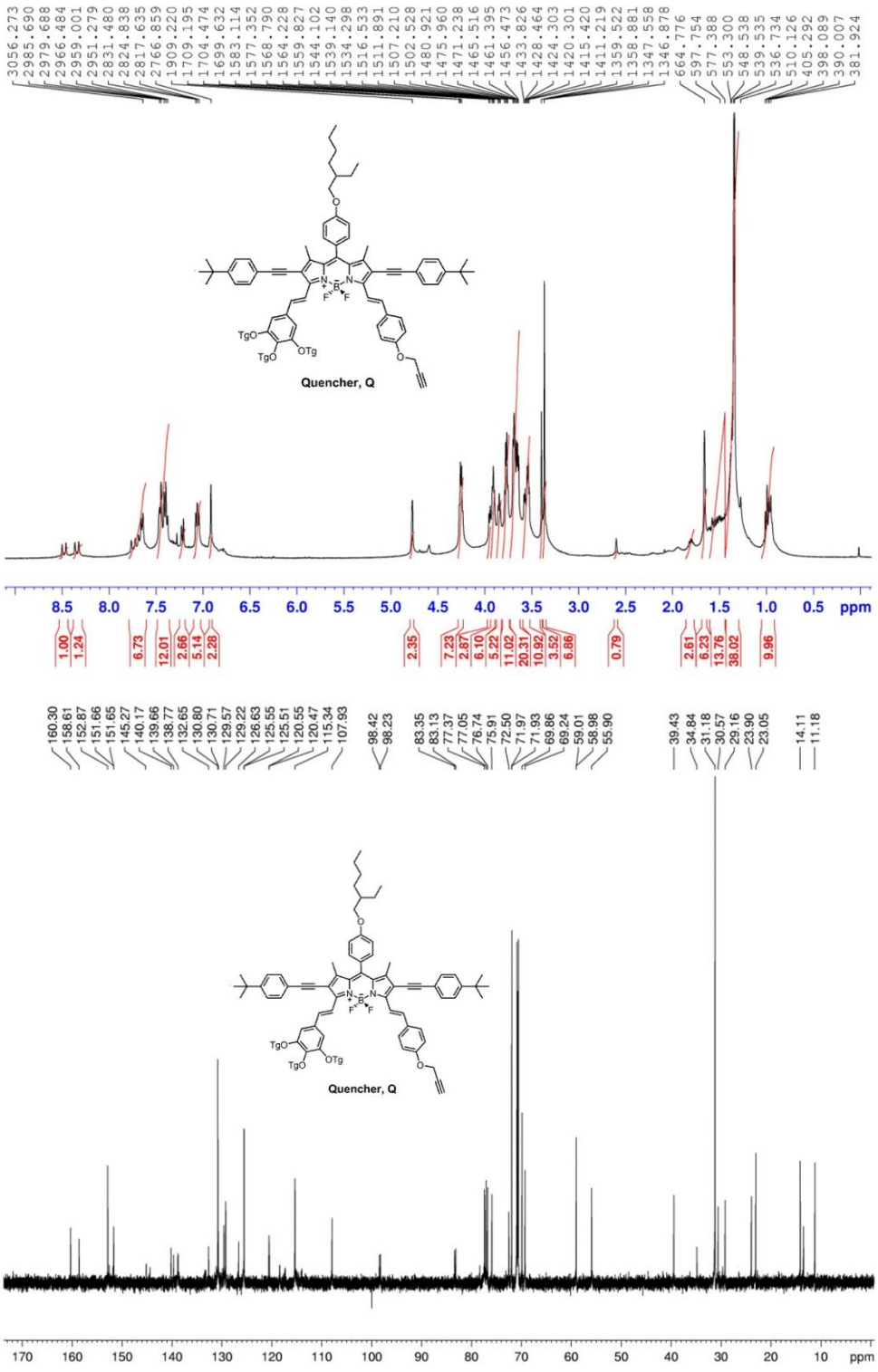
Quencher, Q
Quencher, Q
ppm
ppm

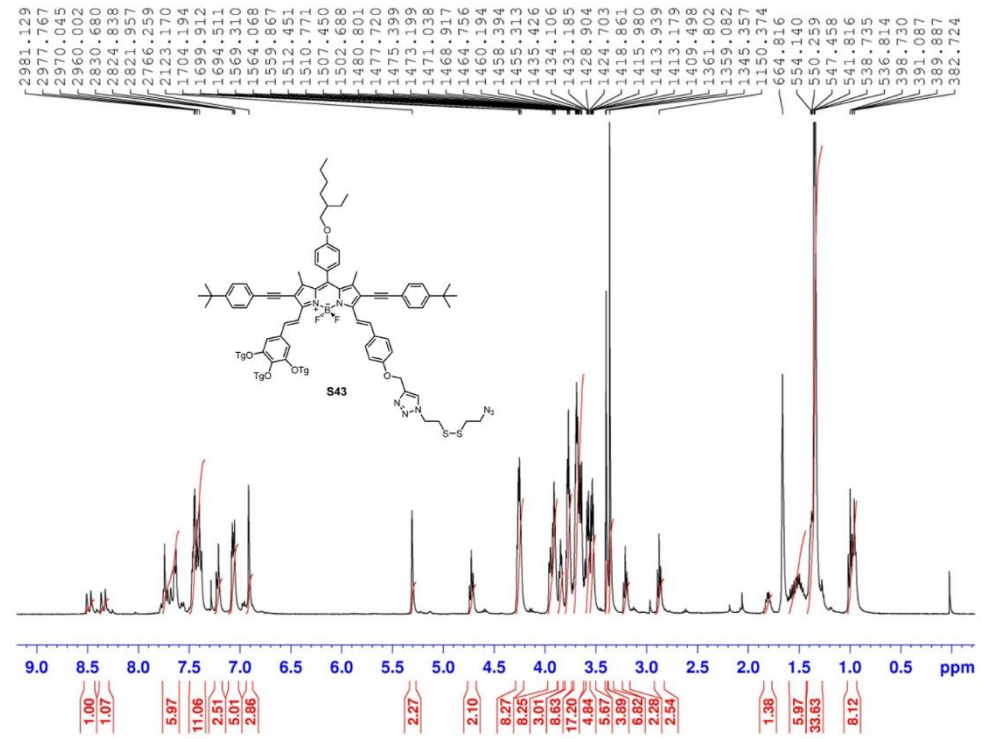
S43

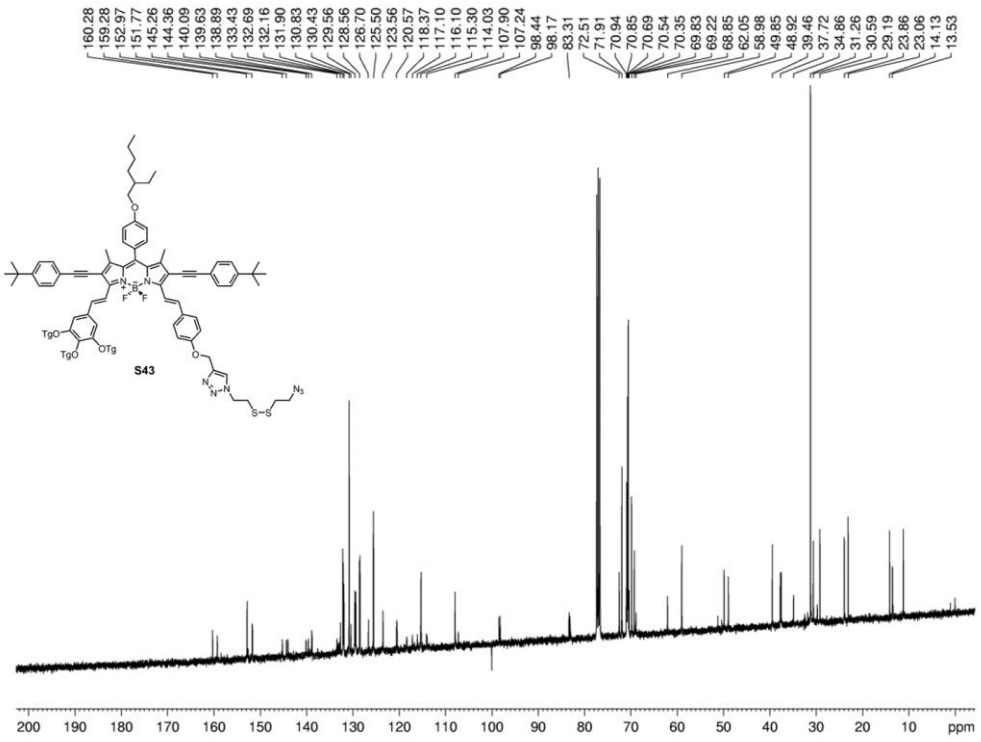
S43

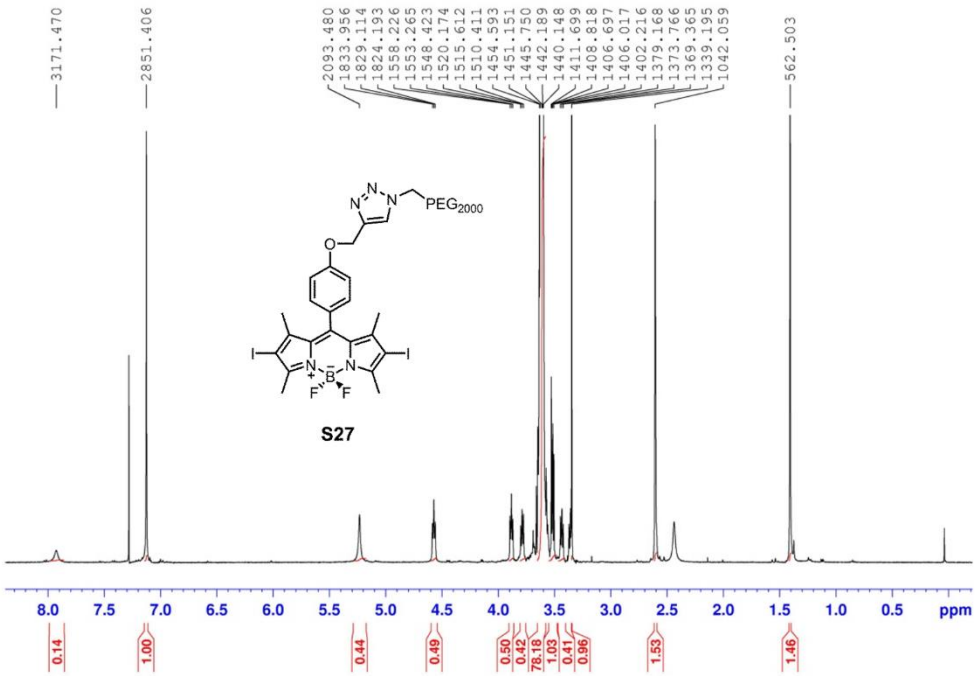
3171.470
2851.406
2093.480
1833.956
1829.114
1824.193
1558.226
1553.265
1548.423
1520.174
1515.612
1510.411
1454.593
1451.151
1445.750
1442.189
1440.148
1411.699
1408.818
1406.697
1406.017
1402.216
1379.168
1373.766
1369.365
1339.195
1042.059
562.503
PEG2000
S27
8.0 7.5 7.0 6.5 6.0 5.5 5.0 4.5 4.0 3.5 3.0 2.5 2.0 1.5 1.0 0.5 ppm
0.14
1.00
0.44
0.49
0.50
0.42
78.18
1.03
0.41
0.96
1.53
1.46

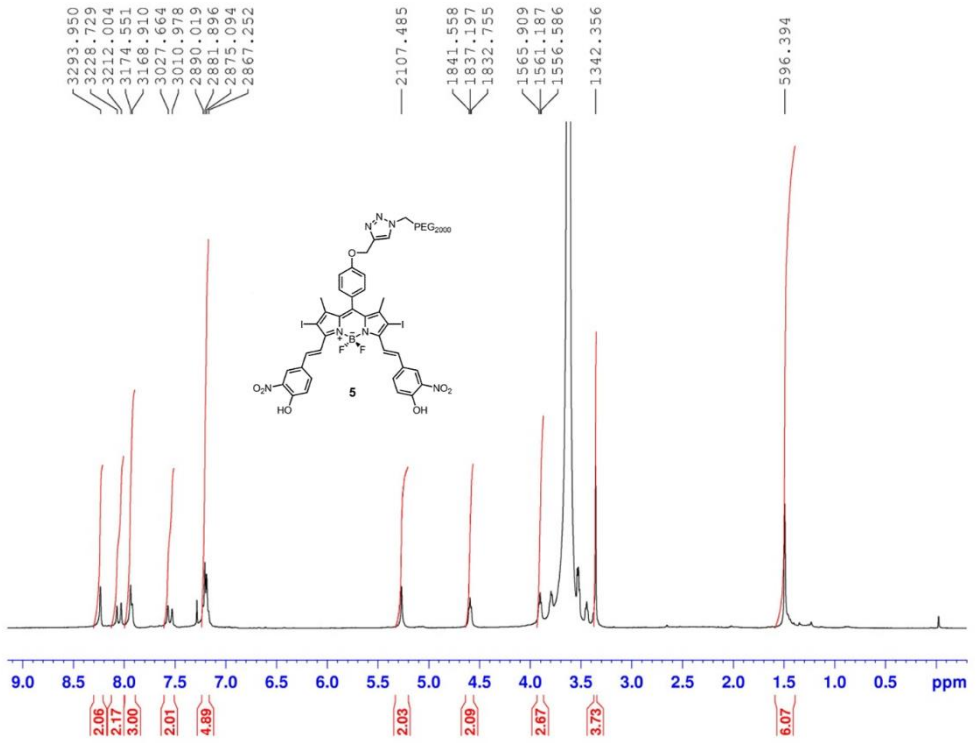
3293.950
3228.729
3212.004
3174.551
3168.910
3027.664
3010.978
2890.019
2881.896
2875.094
2867.252
2107.485
1841.558
1837.197
1832.755
1565.909
1561.187
1556.586
1342.356
596.394
PEG2000
5
9.0 8.5 8.0 7.5 7.0 6.5 6.0 5.5 5.0 4.5 4.0 3.5 3.0 2.5 2.0 1.5 1.0 0.5 ppm
2.06
2.17
3.00
2.01
4.89
2.03
2.09
2.67
3.73
6.07

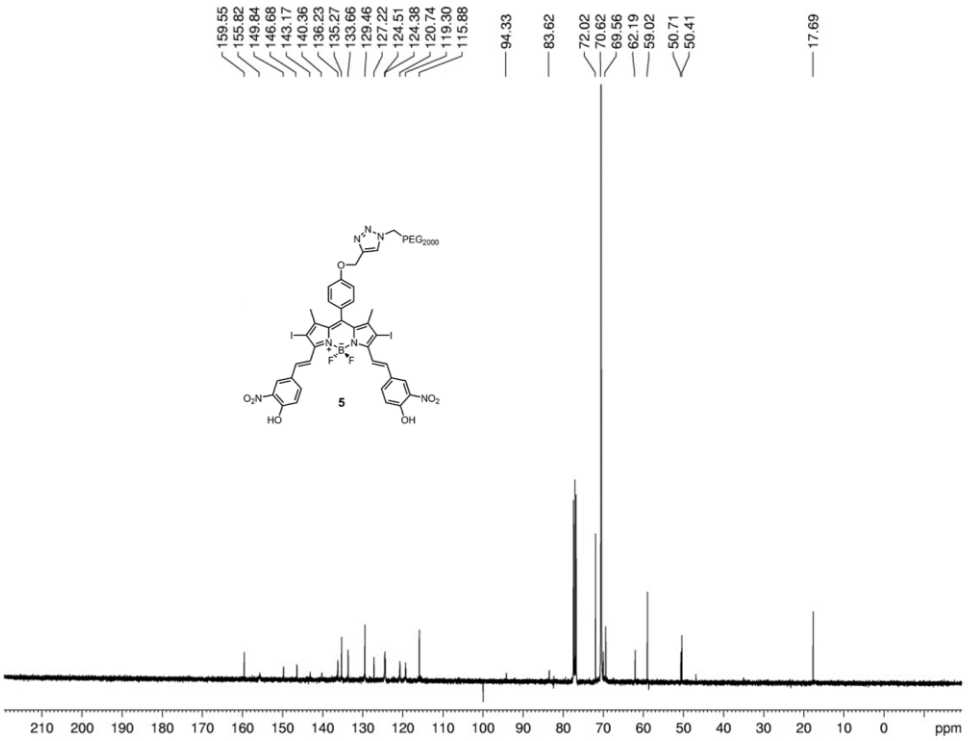
159.55
155.82
149.84
146.68
143.17
140.36
136.23
135.27
133.66
129.46
127.22
124.51
124.38
120.74
119.30
115.88
94.33
83.62
72.02
70.62
69.56
62.19
59.02
50.71
50.41
17.69
PEG2000
5
210 200 190 180 170 160 150 140 130 120 110 100 90 80 70 60 50 40 30 20 10 0 ppm

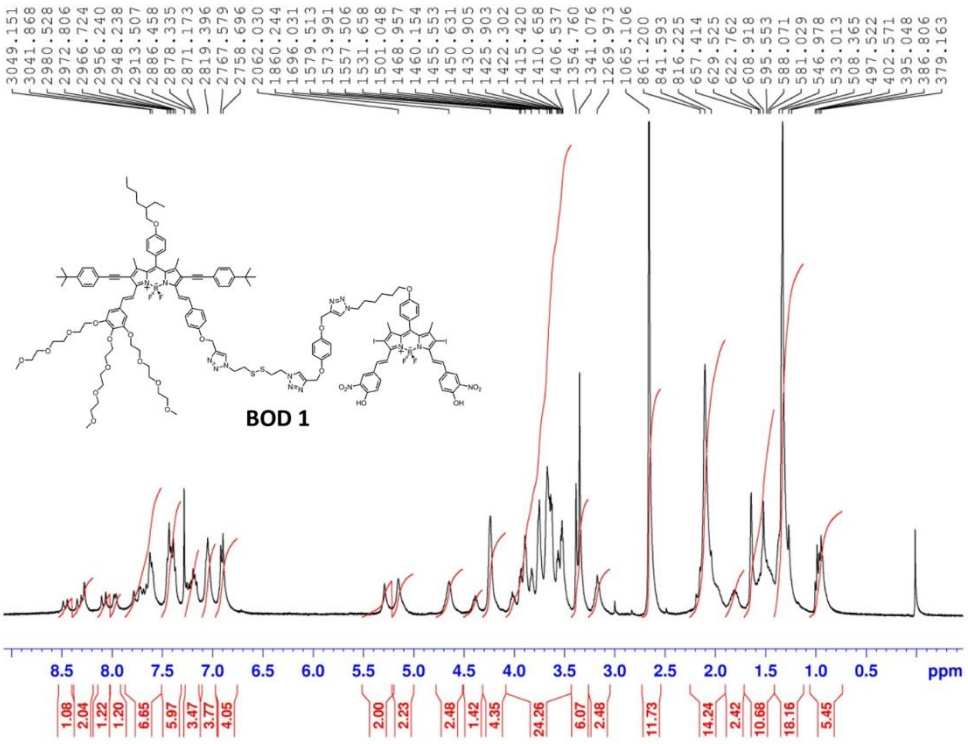
3049.151
3041.868
2980.528
2972.806
2966.724
2956.240
2948.238
2913.507
2886.458
2878.335
2871.173
2819.396
2767.579
2758.696
2062.030
1860.244
1696.031
1579.513
1573.991
1557.506
1531.658
1501.048
1468.957
1460.154
1455.553
1450.631
1430.905
1425.903
1422.302
1415.420
1410.658
1406.537
1354.760
1341.076
1269.973
1065.106
861.200
841.593
816.225
657.414
629.525
622.762
608.918
595.553
588.071
581.029
546.978
533.013
508.365
497.522
402.571
395.048
386.806
379.163
BOD 1
8.5 8.0 7.5 7.0 6.5 6.0 5.5 5.0 4.5 4.0 3.5 3.0 2.5 2.0 1.5 1.0 0.5 ppm
1.08
2.04
1.22
1.20
6.65
5.97
3.47
3.77
4.05
2.00
2.23
2.48
1.42
4.35
24.26
6.07
2.48
11.73
14.24
2.42
10.68
18.16
5.45

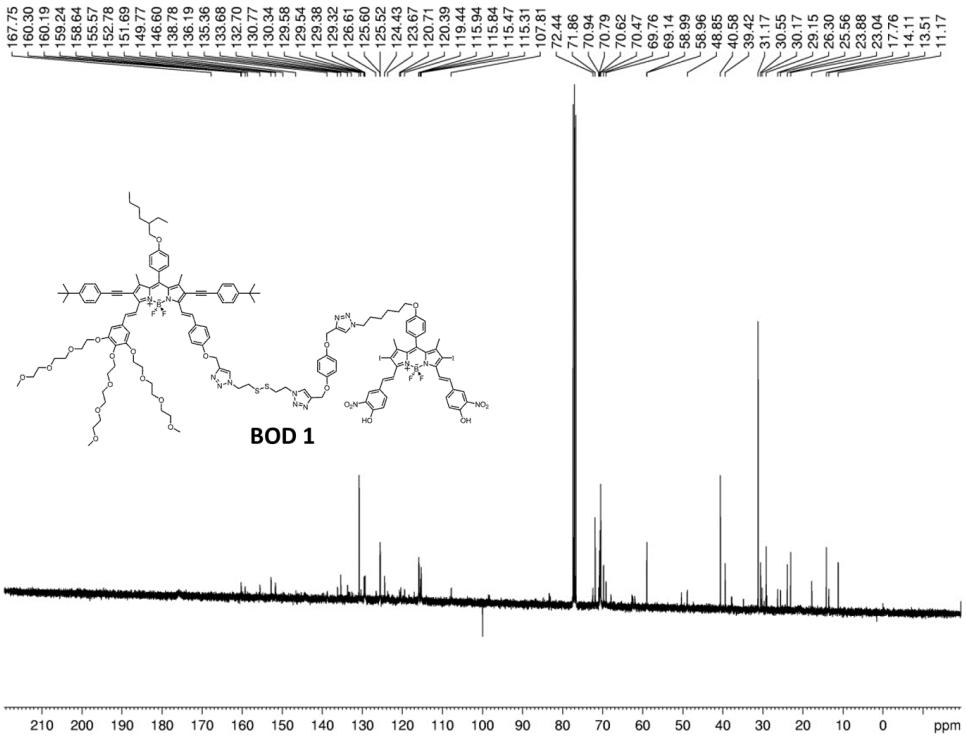
167.75
160.30
160.19
159.24
158.64
155.57
152.78
151.69
149.77
146.60
138.78
136.19
135.36
133.88
132.70
130.77
130.34
129.58
129.54
129.38
129.32
126.61
125.60
125.52
124.43
123.67
120.71
120.39
119.44
115.94
115.84
115.47
115.31
107.81
72.44
71.86
70.94
70.79
70.62
70.47
69.76
69.14
58.99
58.96
48.85
40.58
39.42
31.17
30.55
30.17
29.15
26.30
25.56
23.88
23.04
17.76
14.11
13.51
11.17
BOD 1
210 200 190 180 170 160 150 140 130 120 110 100 90 80 70 60 50 40 30 20 10 0 ppm

A4. BODIPY Assisted Dopamine Recognition (^{1}H, ^{13}C and Mass Spectra)

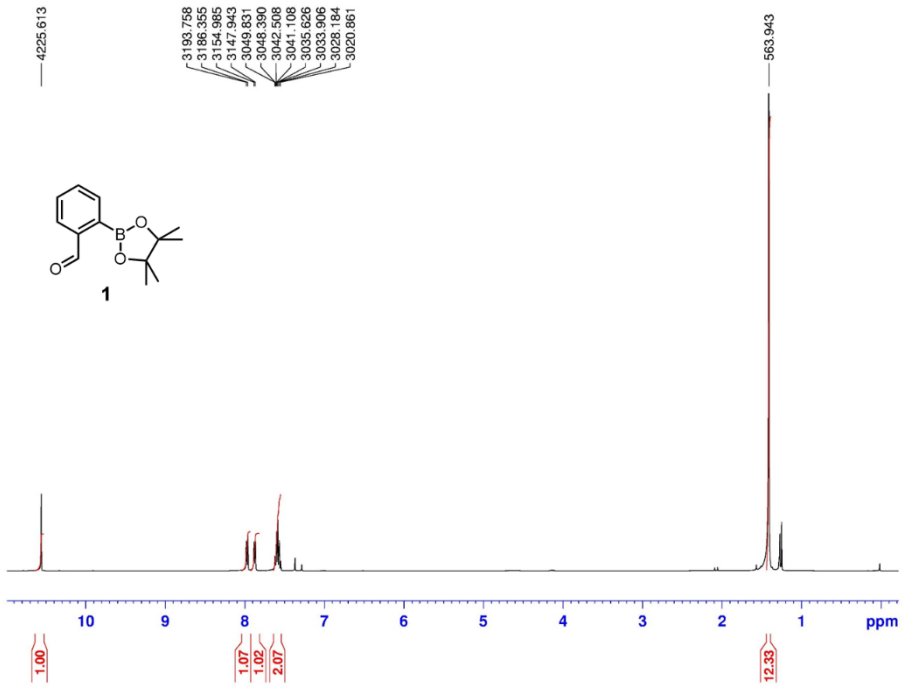

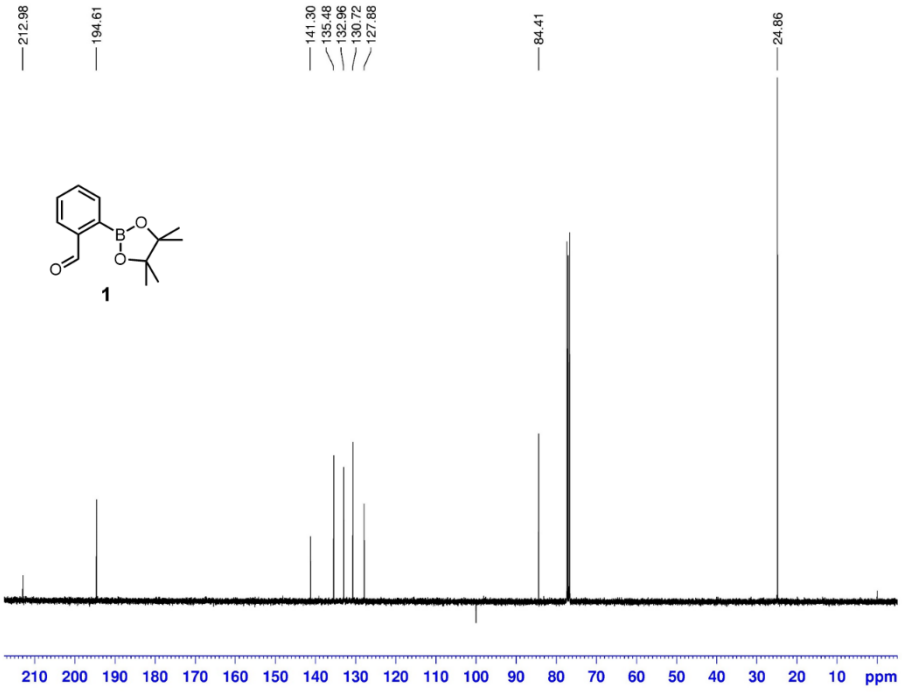

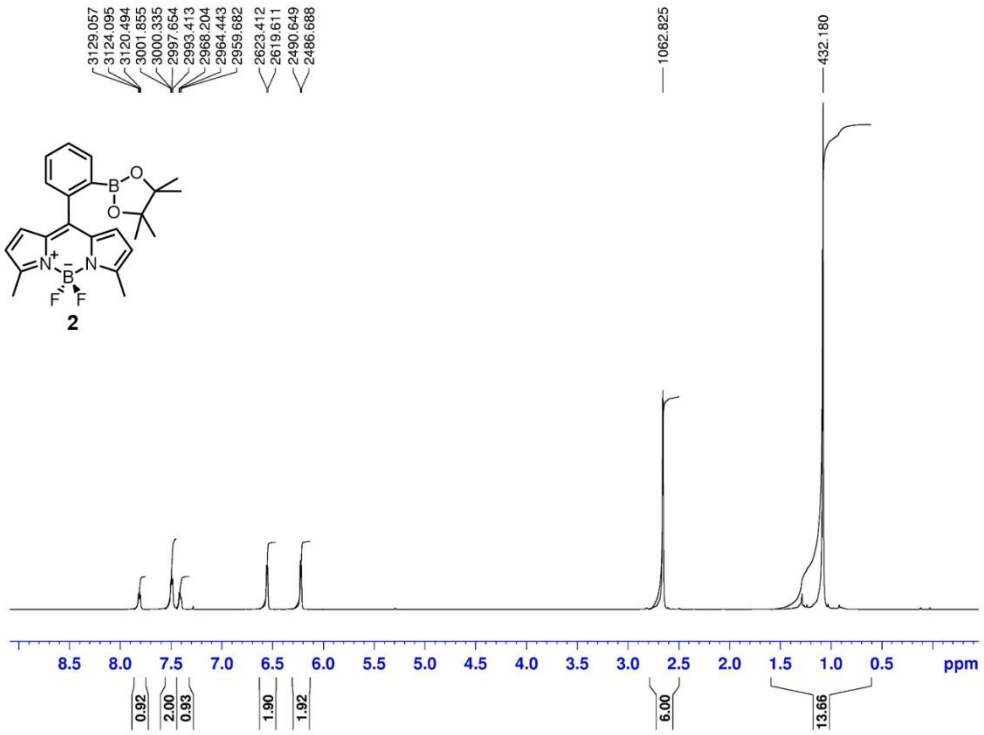
3129.057
3124.095
3120.494
3001.855
3000.335
2997.654
2993.413
2968.204
2964.443
2959.682
2623.412
2619.611
2490.649
2486.688
1062.825
432.180
2
8.5 8.0 7.5 7.0 6.5 6.0 5.5 5.0 4.5 4.0 3.5 3.0 2.5 2.0 1.5 1.0 0.5 ppm
0.92
2.00
0.93
1.90
1.92
6.00
13.66

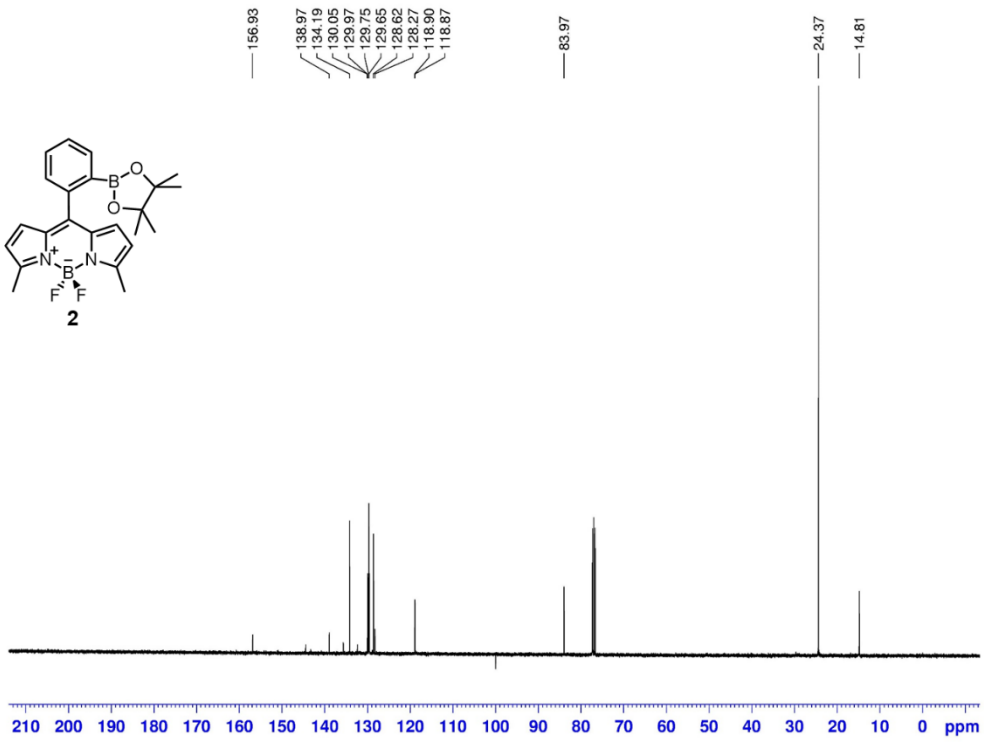
156.93
138.97
134.19
130.05
129.97
129.75
129.65
128.62
128.27
118.90
118.87
83.97
24.37
14.81
2
210 200 190 180 170 160 150 140 130 120 110 100 90 80 70 60 50 40 30 20 10 0 ppm

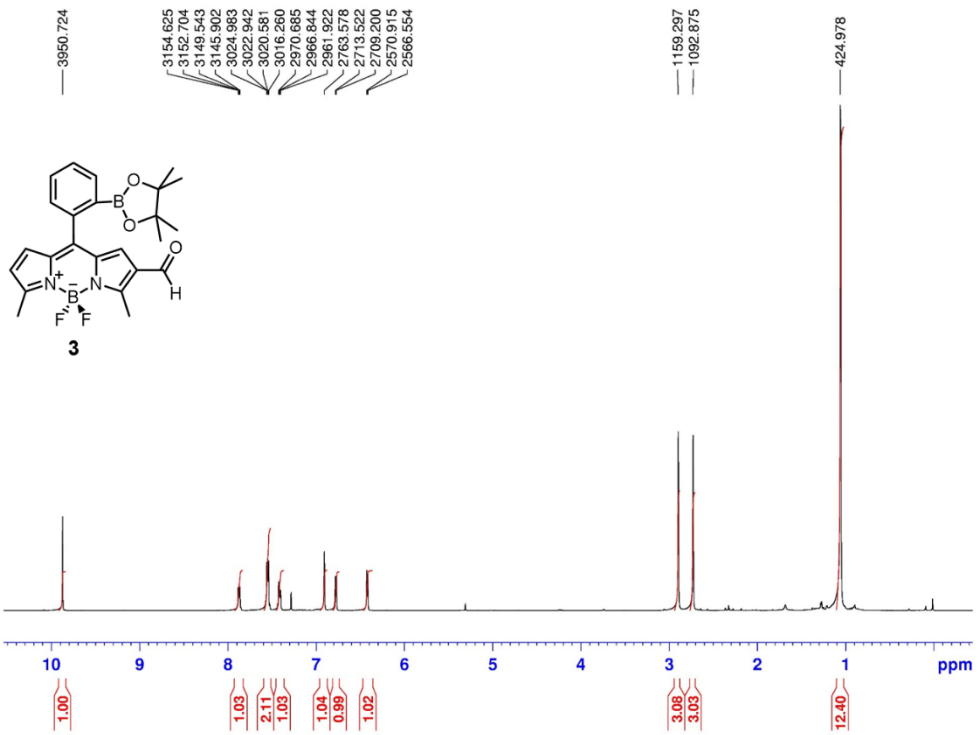
3950.724
3154.625
3152.704
3149.543
3145.902
3024.983
3022.942
3020.581
3016.260
2970.685
2966.844
2961.922
2763.578
2713.522
2709.200
2570.915
2566.554
1159.297
1092.875
424.978
3
10
9
8
7
6
5
4
3
2
1
ppm
1.00
1.03
2.11
1.03
1.04
0.99
1.02
3.08
3.03
12.40

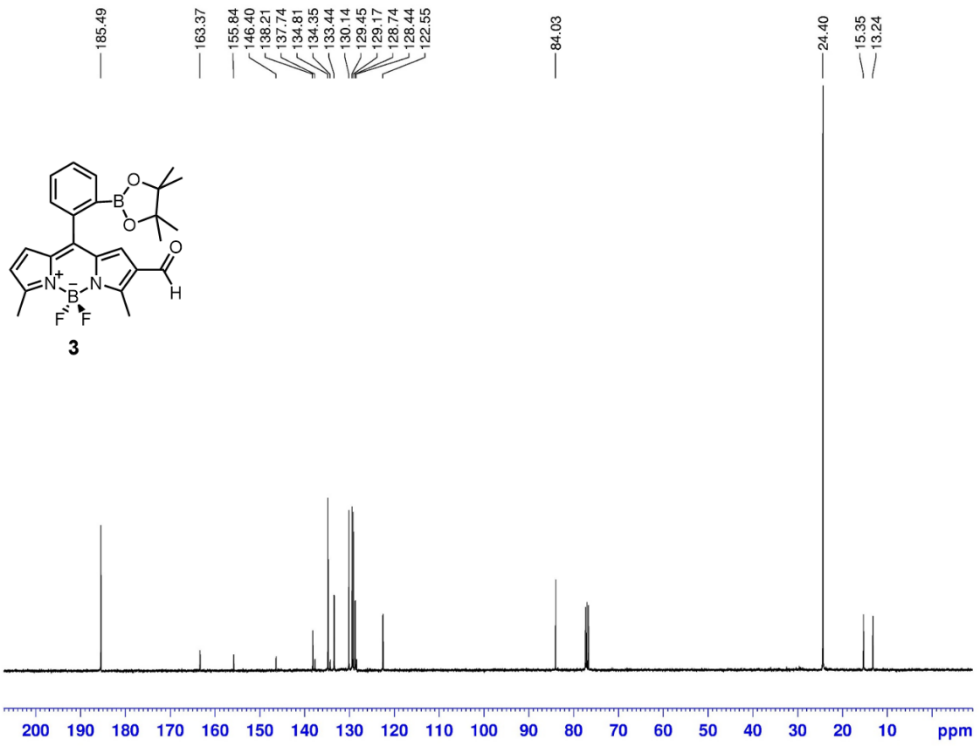
185.49
163.37
155.84
146.40
138.21
137.74
134.81
134.35
133.44
130.14
129.45
129.17
128.74
128.44
122.55
84.03
24.40
15.35
13.24
3
200
190
180
170
160
150
140
130
120
110
100
90
80
70
60
50
40
30
20
10
ppm

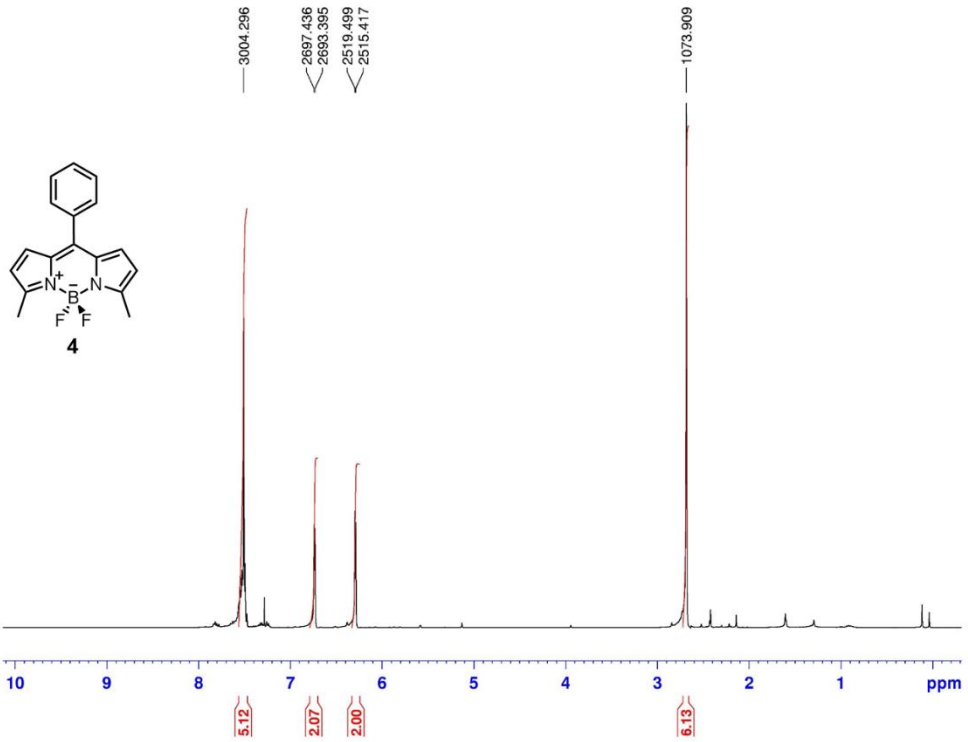
3004.296
2697.436
2693.395
2519.499
2515.417
1073.909
4
10
9
8
7
6
5
4
3
2
1
ppm
5.12
2.07
2.00
6.13

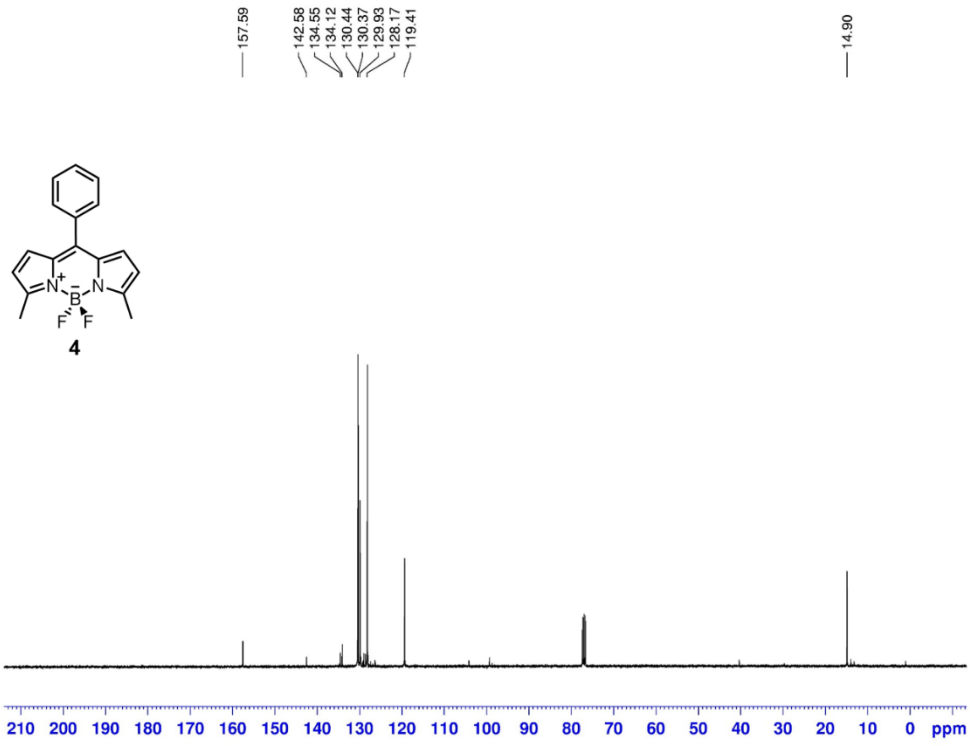
157.59
142.58
134.55
134.12
130.44
130.37
129.93
128.17
119.41
14.90
4
210
200
190
180
170
160
150
140
130
120
110
100
90
80
70
60
50
40
30
20
10
0
ppm

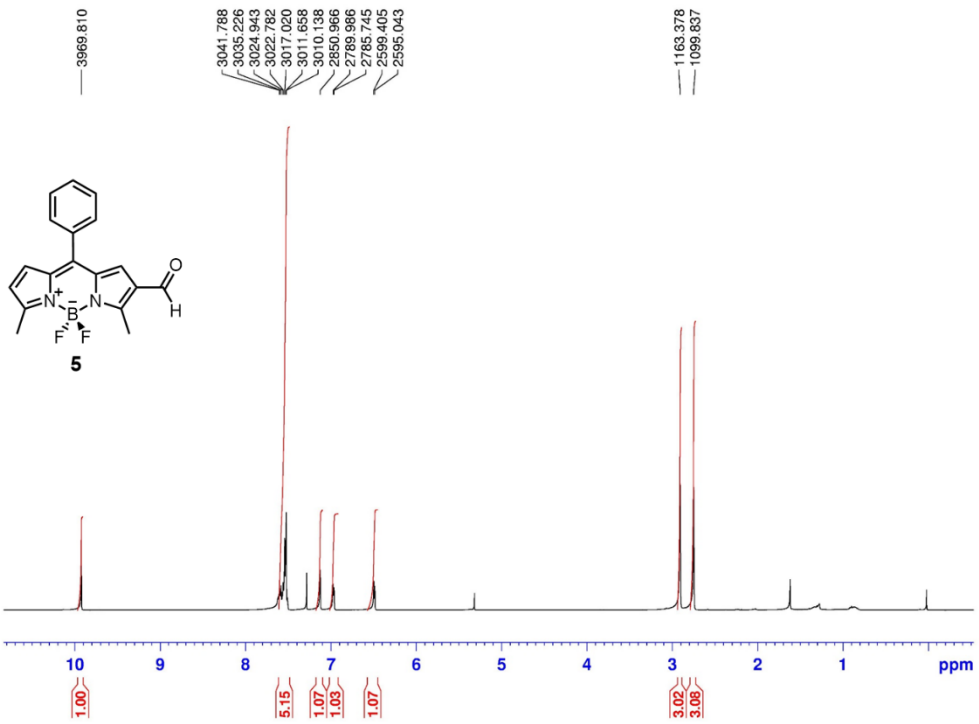
3969.810
3041.788
3035.226
3024.943
3022.782
3017.020
3011.658
3010.138
2850.966
2789.986
2785.745
2599.405
2595.043
1163.378
1099.837
5
10
9
8
7
6
5
4
3
2
1
ppm
1.00
5.15
1.07
1.03
1.07
3.02
3.08

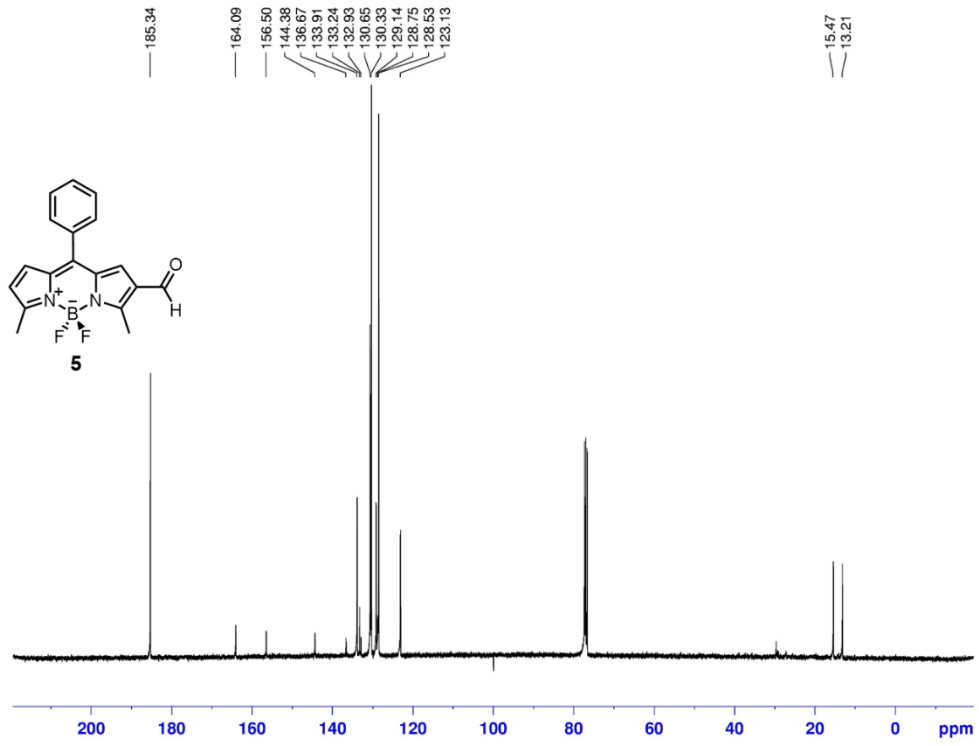
185.34
164.09
156.50
144.38
136.67
133.91
133.24
132.93
130.65
130.33
129.14
128.75
128.53
123.13
15.47
13.21
5
200
180
160
140
120
100
80
60
40
20
0
ppm

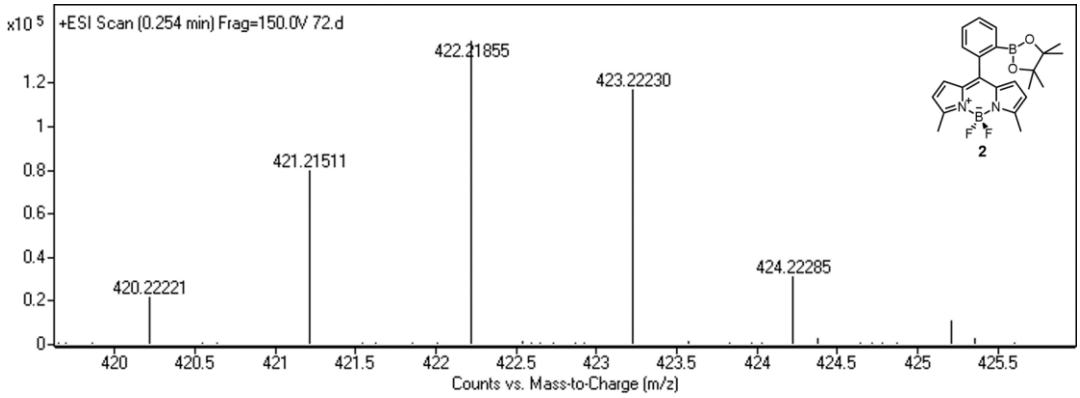
x10 5
+ESI Scan (0.254 min) Frag=150.0V 72.d
422.21855
423.22230
421.21511
424.22285
420.22221
Counts vs. Mass-to-Charge (m/z)
2

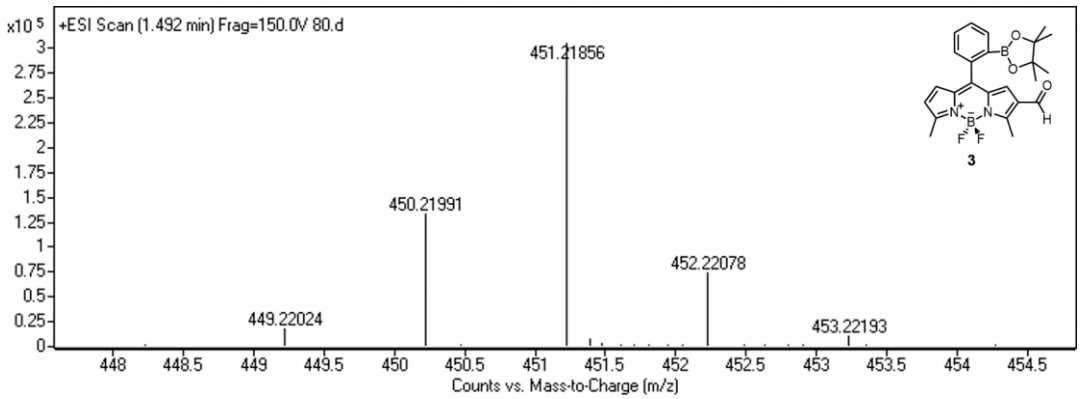
x10 5
+ESI Scan (1.492 min) Frag=150.0V 80.d
451.21856
450.21991
452.22078
449.22024
453.22193
Counts vs. Mass-to-Charge (m/z)
3

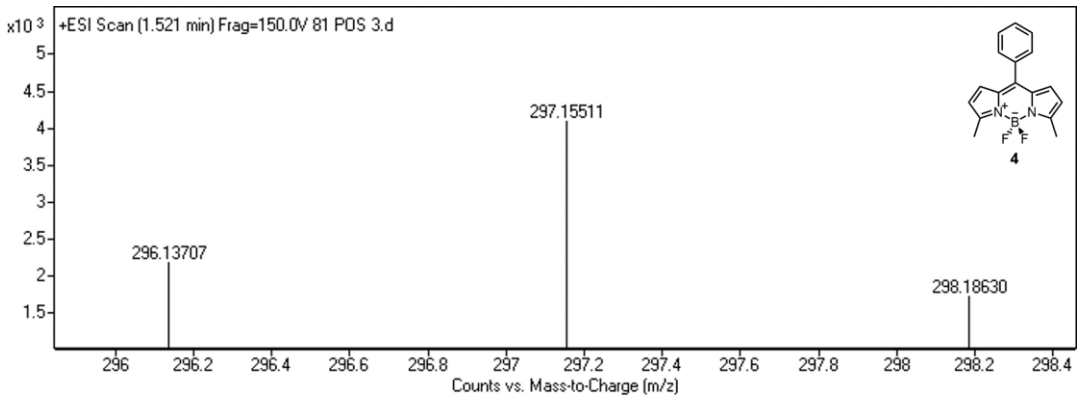
x10 3
+ESI Scan (1.521 min) Frag=150.0V 81 POS 3.d
297.15511
296.13707
298.18630
Counts vs. Mass-to-Charge (m/z)
4

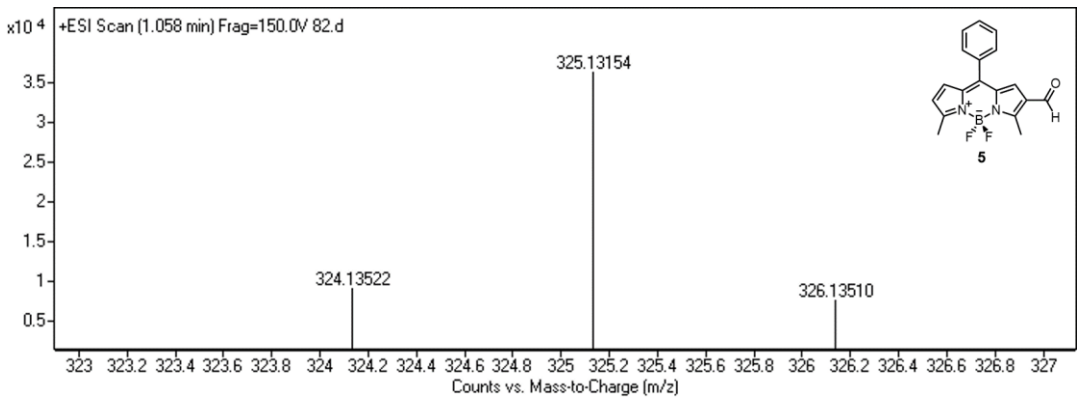
x10 4
+ESI Scan (1.058 min) Frag=150.0V 82.d
325.13154
324.13522
326.13510
Counts vs. Mass-to-Charge (m/z)
5